

UNIVERSIDADE FEDERAL DO PARANÁ

INGRID FATIMA ZATTONI



STUDY OF PORPHYRINS AND HETERODIMERS TARGETING ABCG2  
TRANSPORTER AND DEVELOPMENT OF A MULTIPLEXED FLOW CYTOMETRIC  
APPROACH FOR DETECTION OF ANTI SARS-CoV-2 IgG, IgM AND IgA

CURITIBA

2021

INGRID FATIMA ZATTONI

STUDY OF PORPHYRINS AND HETERODIMERS TARGETING ABCG2  
TRANSPORTER AND DEVELOPMENT OF A MULTIPLEXED FLOW CYTOMETRIC  
APPROACH FOR DETECTION OF ANTI SARS-CoV-2 IgG, IgM AND IgA

Tese apresentada ao Curso de Pós-Graduação em Ciências Farmacêuticas, Setor de Ciências da Saúde, Universidade Federal do Paraná, como requisito parcial à obtenção do título de Doutor em Ciências Farmacêuticas.

Orientador: Prof. Dr. Glaucio Valdameri

Coorientadores: Prof Dr. Alan Guilherme Gonçalves

Prof Dr. Ahcène Boumendjel

CURITIBA

2021

Zattoni, Ingrid Fatima

Study of porphyrins and heterodimers targeting ABCG2 transporter and development of a multiplexed flow cytometric approach for detection of anti Sars-CoV-2 IgG, IgM and IgA [recurso eletrônico] / Ingrid Fatima Zattoni – Curitiba, 2021.  
1 arquivo (120 p.):PDF

Tese (doutorado) – Programa de Pós-Graduação em Ciências Farmacêuticas.  
Setor de Ciências da Saúde, Universidade Federal do Paraná, 2021.

Orientador: Prof. Dr. Glaucio Valdameri  
Coorientador: Prof. Dr. Alan Guilherme Gonçalves  
Coorientador: Prof. Dr. Ahcène Boumendjel

1. Porfirina. 2. Covid-19. 3. Substratos. 4. Mitoxantrona. I. Valdameri, Glaucio.  
II. Gonçalves, Alan Guilherme. III. Boumendjel, Ahcène. IV. Universidade Federal do Paraná. V. Título.

CDD 547.593



MINISTÉRIO DA EDUCAÇÃO  
SETOR DE CIÊNCIAS DA SAÚDE  
UNIVERSIDADE FEDERAL DO PARANÁ  
PRÓ-REITORIA DE PESQUISA E PÓS-GRADUAÇÃO  
PROGRAMA DE PÓS-GRADUAÇÃO CIÊNCIAS  
FARMACÊUTICAS - 40001016042P8

## APPROVAL MINUTE

The Examining Board is designated by the Faculty of the Graduate Program of the Federal University of Paraná in CIÊNCIAS FARMACÊUTICAS where invited to argue the DISSERTATION of PHILOSOPHY DOCTOR by **INGRID FATIMA ZATTONI**, entitled: **STUDY OF PORPHYRINS AND HETERODIMERS TARGETING ABCG2 TRANSPORTER AND DEVELOPMENT OF A MULTIPLEXED FLOW CYTOMETRIC APPROACH FOR DETECTION OF ANTI SARS-CoV-2 IgG, IgM AND IgA**, under the supervision of Dr. GLAUCIO VALDAMERI, which and after assessment of the candidate and the work, the Examining Board decided for the approval in the present rite.

The granting of the title of philosophy doctor is contingent upon the fulfillment of all the requirements indicated by the Examining Board and terms determined in the regulation of the Graduate Program.

CURITIBA, November 17th, 2021.

GLAUCIO VALDAMERI  
President of the Examining Board

LIA SUMIE NAKAO  
External Member (UNIVERSIDADE FEDERAL DO PARANÁ)

AHCENE BOUMENDJEL  
External Member (UNIVERSITÉ GRENOBLE ALPES)

ROBERT WILLIAM ROBEY  
External Member (NATIONAL INSTITUTES OF HEALTH)

## ACKNOWLEDGMENTS

This work was supported by many hands in which I would like to specially thank.

Firstly, to my parents, Celia and Dejalma, for the education and unconditional support during all these years. To my brother Gleidiston that showed me the way to university and was my first mentor.

To my fiancée Thiago for the support and love when things were not right, for the excitement when things worked, for the encouragement during our period abroad and for turning everything meaningful.

To the lab's old guard, Diogo, Isadora, Gisele and Diego for the laughs and jokes. The lab was always a good place to be in.

To the lab's new guard, specially Manoela, Giovana, Julia, Melanie and Larissa for the help, support, and good moments.

To my friends outside the university for their friendship.

To my supervisor Glaucio for the opportunities and trust during this journey. Also to Professors Alan and Vivian for good talks and advice.

I'd like to thank Dr. Ahcène Boumendjel for welcoming me at UGA. Also, to Kim, Pascal and Mathieu for helping me during my period in France.

Thank you, Dr. Suresh Ambudkar, for thermostability assays, Dr. Marcos B Gonçalves and Dr. Thales Kronenberger for computational experiments.

To my colleagues and good friends Matheus and Lais for the porphyrin synthesis.

To Pharmaceutical Sciences Graduation Program (PPGCF) for the research opportunity.

To CAPES, Fundação Araucária and CNPq for the scholarship and for finance this project.

To CAPES/PRINT for providing the opportunity to research abroad in the Université Grenoble-Alpes.

It's a dangerous business going out your door.  
You step onto the road, and if you don't keep your feet,  
there's no knowing where you might be swept off to.

J. R. R Tolkien

## RESUMO

O transportador ABCG2 possui papel central na resistência a múltiplas drogas, porém, nenhum inibidor específico de ABCG2 foi testado em ensaios clínicos. A família de transportadores ABC transporta uma grande variedade de substratos, mas fotossensibilizadores baseados em estruturas porfirínicas são reconhecidos exclusivamente por ABCG2. No capítulo 1 foi descrita pela primeira vez uma porfirina (**4B**) capaz de inibir o transportador ABCG2 e de ressensibilizar células resistentes *in vitro*. A inibição foi dependente do tempo de incubação e **4B** não se comportou como substrato de ABCG2. A porfirina **4B** demonstrou IC<sub>50</sub> de 1.6 µM e tipo de inibição mista, independente do substrato. **4B** inibiu a atividade ATPásica e aumentou a ligação do anticorpo conformacional 5D3. O ensaio de termo-estabilidade confirmou as alterações alostéricas na proteína desencadeadas pela ligação da porfirina. Simulações de dinâmica molecular revelaram um comportamento distinto entre porfirina **4B** e o substrato Pheophorbide a. Pheophorbide a foi capaz de ligar-se em três regiões diferentes da proteína enquanto **4B** apresentou apenas região de interação na proteína, apresentando forte interação iônica com aminoácido GLU446. A inibição foi seletiva já que não foi observada inibição em P-gP nem em MRP1. Porfirina **4B** foi capaz de ressensibilizar células que superexpressam o transportador ABCG2. Estes achados reforçam a ideia de que substratos podem ser uma fonte privilegiada de estruturas para identificação de novos inibidores para transportadores ABC associados a resistência à múltiplas drogas. Baseados nos resultados mostrados no capítulo 1, outras macromoléculas foram sintetizadas para avaliar os efeitos de heterodímeros construídos a partir de moléculas conhecidamente bioativas. Quatro heterodímeros foram propostos, mas apenas dois foram sintetizados com sucesso (BODIPY-colesterol e Chalcona-colesterol). Resultados preliminares sugerem que BODIPY-colesterol não se comporta como substrato de ABCG2 e que o colesterol não alterou o efluxo de mitoxantrona e hoechst 33342 mediado por ABCG2. Por sua vez, o colesterol anula o efeito da chalcona já que o heterodímero chalcona-colesterol modificou o perfil inibitório quando comparado à chalcona sozinha. Estes resultados trazem novas ideias sobre o papel do colesterol sobre ABCG2. Esta tese foi desenvolvida num contexto de pandemia do COVID-19 que trouxe a necessidade urgente do desenvolvimento rápido de novas metodologias para detecção de anticorpos anti-SARS-CoV-2. No capítulo 3 está descrita uma estratégia inovadora para detecção simultânea das imunoglobulinas IgG, IgM e IgA em pacientes com COVID-19. A proteína Nucleopcapsídeo foi covalentemente ligada à superfície de beads funcionalizadas através do linker sulfo-SMCC. Anti – IgG BUV395, anti-IgM BB515, anti-IgA1/IgA2 biotinilado e streptavidina BV421 foram usados como anticorpos secundários. As condições de incubação e diluição do soro foram otimizadas para detecção de cada isotipo de anticorpo e o ensaio multiplex foi então desenvolvido. Este novo ensaio livre de células foi capaz de diferenciar de maneira eficiente amostras positivas e negativas para COVID-19. A detecção simultânea de IgG, IgM e IgA apresentou sensibilidade de 88.5 – 96.2% e especificidade de 100%. Esta estratégia nova abre um novo caminho para diagnósticos baseados em citometria de fluxo.

Palavras-Chave: ABCG2; porfirina; ensaio Multiplex; COVID-19; heterodímeros.

## ABSTRACT

The ABCG2 transporter plays a pivotal role in multidrug resistance (MDR), however, none inhibitor selective toward ABCG2 was evaluated in clinical trials. Although ABC transporters actively extrude a wide variety of substrates, photodynamic therapeutic agents with porphyrinic scaffolds are exclusively transported by ABCG2. In Chapter 1, we described for the first time a porphyrin derivative (**4B**), which plays as inhibitor of ABCG2 and capable to overcome MDR *in vitro*. The inhibition was time-dependent and **4B** was not itself transported by ABCG2. Independently of the substrate, the porphyrin **4B** showed an IC<sub>50</sub> value of 1.6 μM and a mixed type of inhibition. This compound inhibited the ATPase activity and increased the binding of the conformational-sensitive antibody 5D3. A thermostability assay confirmed allosteric protein changes triggered by the porphyrin. Long-timescale molecular dynamics simulations revealed a different behavior between the ABCG2 porphyrinic substrate pheophorbide *a* and the porphyrin **4B**. Pheophorbide *a* was able to bind in three different protein sites. In contrast, **4B** was able to bind in an unique protein site, showing a strong ionic interaction with GLU446. The inhibition was selective toward ABCG2, since no inhibition was observed for P-glycoprotein and MRP1. Finally, this compound successfully chemosensitized cells that overexpress ABCG2. These findings reinforce that substrates of ABC proteins may be a privileged source of chemical scaffolds for identification of new inhibitors of MDR-linked to ABC transporters. Based on Chapter 1 data, other macromolecules were synthesized and the biological effects evaluated against ABCG2 transporter. Based on known bioactive molecules, four heterodimers were proposed, however, only two were successfully synthesized (BODIPY – cholesterol and chalcone – cholesterol). The results suggest that cholesterol is not an ABCG2 substrate, since BODIPY - cholesterol was not transported by ABCG2. In addition, cholesterol alone does not affect the ABCG2-mediated transport of mitoxantrone and hoechst 33342. Interestingly, cholesterol abrogate the inhibitory effect of chalcone, since the chalcone – cholesterol modified the inhibition profile of chalcone alone. Those results provide new insights about the role of cholesterol on ABCG2 transporter. This thesis was developed during the pandemic of coronavirus disease 2019 (COVID-19). The pandemic brought the urgent necessity of the rapid development of assays for detection of antibodies anti-SARS-CoV-2. In Chapter 3, we described an innovative strategy for simultaneous detection of immunoglobulin G (IgG), IgM and IgA in COVID-19 patients. The SARS-CoV-2 nucleocapsid protein was covalently bound to functional beads surface applying sulfo-SMCC chemistry. BUV395 anti-IgG, BB515 anti-IgM, biotinylated anti-IgA1/IgA2 and BV421 streptavidin were used as fluorophore conjugated secondary antibodies. Serum and antibodies reaction conditions were optimized for each antibody isotype detection and a multiplexed detection assay was developed. This new cell-free assay efficiently discriminate COVID-19 negative and positive samples. The simultaneous detection of IgG, IgM and IgA showed a sensibility of 88.5-96.2% and specificity of 100%. This novel strategy opens a new avenue for flow cytometry-based diagnosis.

Keywords: ABCG2; porphyrin; Multiplex assay; COVID-19; heterodimers



## LIST OF FIGURES

### Introduction

**Figure 1:** Main approaches for identification of new ABCG2 inhibitors and characterization of the biochemical and molecular mechanism of inhibition.....17

### Chapter 1

**Figure 1:** Results overview..... 30

**Figure 2:** Intracellular accumulation of porphyrin **4D** along the time using HEK293-wild type cells.....35

**Figure 3:** Inhibition curves of porphyrin **4B** and intracellular accumulation.....37

**Figure 4:** Cell viability assay performed using the MTT method.....38

**Figure 5:** Kinetic behavior of ABCG2 with mitoxantrone and hoechst 33342.....39

**Figure 6:** Allosteric changes triggered by **4B**.....40

**Figure 7:** Frequency of hydrogen bonding interactions and hydrophobic interactions observed along with the molecular dynamic simulation.....41

**Figure 8:** Selectivity assay using stably transfected cell lineages for MRP1, P-gp and ABCG2.....42

### Chapter 2

**Figure 1:** Difference on Porphyrin and chlorine structure.....51

**Figure 2:** <sup>1</sup>H NMR comparison between chalcone 1 and 2.....58

**Figure 3:** Schematic reaction between Porphyrin 4B and Chalcone 2.....59

**Figure 4:** Modifications on Pheophytin.....60

**Figure 5:** Coupling reaction on pheophorbide a and the representation of possible side reactions.....61

**Figure 6:** Mass spectroscopy of compound 5 and the calculated mass of formic acid adduct.....62

**Figure 7:** Adduct formation of compound 6 with formic acid and monoisotopic mass.....63

**Figure 8:** Comparison of the <sup>1</sup>H NMR spectra from Pheophorbide a derivatives. ....64

**Figure 9:** Comparison of the <sup>1</sup>H NMR spectra from BODIPY, Cholesterol and heterodimer.....66

**Figure 10:** Energetic rotamer hypothesis.....67

**Figure 11:** Comparison of the <sup>1</sup>H NMR spectra from chalcone 1, cholesterol 7 and heterodimer.....68

**Figure 12:** Fluorescence shift according to concentrations used for BODIPY and BODIPY – cholesterol.....69

**Figure 13:** Histograms overlay of HEK293-WT and HEK293-ABCG2 treated with BODIPY-cholesterol.....70

**Figure 14:** Efflux profile of Mitoxantrone and Pheophorbide a in the presence and absence of cholesterol.....71

**Figure 15:** Influence of cholesterol in Chalcone 1 inhibition profile.....71

### Chapter 3

**Figure 1:** Rational strategy overview.....80

**Figure 2:** Serum and antibody dilution.....82

**Figure 3:** Receiver operating characteristic (ROC) curves and Venn diagram.....83

## LIST OF TABLES

### Chapter 1

**Table 1.** Porphyrin structures and the percentage of inhibition of ABCG2 transport activity .....35

### Chapter 2

**Table 1:** Chalcone – porphyrin reaction attempts.....59

**Table 2:** Attempted reactions for compound 5 formation.....61

**Table 3:** Attempted reactions for compound 6 formation.....62

**Table 4:** Attempted reactions for Pheophorbide – Chalcone binding.....65

**Table 5:** Attempted conditions for Cholesterol – Bodipy heterodimer formation.....65

**Table 6:** Attempted conditions for Cholesterol – chalcone heterodimer formation.....66

**Table 7:** Raw data of BODIPY fluorescence screening.....69

## LIST OF ABBREVIATIONS

<b>ABC</b>	ATP binding cassette
<b>ACE2</b>	Angiotensin Converting Enzyme 2
<b>ATP</b>	Adenosine Triphosphate
<b>BCRP</b>	Breast Cancer Resistance Protein
<b>CS</b>	Collateral Sensitivity
<b>DCM</b>	Dichloromethane
<b>DDQ</b>	2,3-Dichloro-5,6-dicyano-p-benzoquinone
<b>DIPEA</b>	N,N-Diisopropylethylamine
<b>DMAP</b>	4-Dimethylaminopyridine
<b>DMF</b>	Dimethylformamide
<b>DMSO</b>	Dimethyl sulfoxide
<b>DTT</b>	Dithiothreitol
<b>EDC</b>	1-ethyl-3-(3-dimethylaminopropyl)carbodiimide hydrochloride
<b>EGTA</b>	Ethylene glycol-bis(2-aminoethylether)-N,N,N',N'-tetra acetic acid
<b>FBS</b>	Fetal bovine serum
<b>HOBT</b>	1-Hydroxybenzotriazole
<b>IC<sub>50</sub></b>	Concentration that inhibits 50% of maximum inhibition
<b>IG<sub>50</sub></b>	Concentration that 50% of population survive
<b>K<sub>m</sub></b>	Michaelis Menten constant
<b>M.W</b>	Microwave
<b>MD</b>	Molecular Dynamics
<b>MDR</b>	Multidrug Resistance
<b>MRP1</b>	Multidrug Resistance Protein 1
<b>NBD</b>	Nucleotide Binding Domain
<b>O.N</b>	Overnight
<b>PBS</b>	Phosphate Buffer Solution
<b>PCA</b>	Principal Component Analysis
<b>PDB</b>	Protein Data Bank
<b>P-gp</b>	P-glycoprotein
<b>PHEO</b>	Pheophorbide a
<b>R.T</b>	Room temperature
<b>RBD</b>	Receptor Binding Domain
<b>SDS</b>	Sodium Dodecyl Sulfate
<b>TEA</b>	Triethylamine
<b>TFA</b>	Trifluoroacetic acid
<b>TKI</b>	Tyrosine Kinase inhibitor
<b>TLC</b>	Thin layer chromatography
<b>TMD</b>	Transmembrane Binding Domain
<b>V<sub>max</sub></b>	Maximum efflux at saturation

## SUMMARY

<b>THESIS OVERVIEW .....</b>	<b>14</b>
<b>1. INTRODUCTION .....</b>	<b>15</b>
1.1 TARGETING ABCG2 BY INHIBITORS .....	15
1.2 SCREENING OF DIFFERENT CLASSES .....	16
1.3 IN VITRO AND IN SILICO STRATEGIES FOR IDENTIFICATION OF INHIBITORS.....	17
1.4 MINIMAL REQUIREMENTS FOR A DESIRABLE INHIBITOR .....	20
<b>2. REFERENCES .....</b>	<b>22</b>
<b>RESEARCH OBJECTIVES.....</b>	<b>28</b>
<b>CHAPTER 1 - A NEW PORPHYRIN AS SELECTIVE SUBSTRATE-BASED INHIBITOR OF BREAST CANCER RESISTANCE PROTEIN(BCRP/ABCG2) .....</b>	<b>29</b>
<b>1. INTRODUCTION.....</b>	<b>29</b>
<b>2. MATERIAL AND METHODS .....</b>	<b>31</b>
2.1 CHEMICALS.....	31
2.2 CELL CULTURE.....	31
2.3 ACCUMULATION ASSAY .....	31
2.4 INHIBITION ASSAY .....	31
2.5 CONFOCAL MICROSCOPY .....	32
2.6 CELL VIABILITY ASSAY.....	32
2.7 ATPASE ASSAY .....	32
2.8 CONFORMATIONAL ANTIBODY BINDING (5D3) .....	33
2.9 THERMOSTABILITY ASSAY .....	33
2.10 MOLECULAR MODELLING.....	33
<b>3. RESULTS .....</b>	<b>34</b>
3.1 SCREENING OF PORPHYRINS AS INHIBITORS OF ABCG2 TRANSPORT ACTIVITY.....	34
3.2 IC <sub>50</sub> OF ABCG2 INHIBITION AND ABSENCE OF TRANSPORT .....	36
3.3 MECHANISM OF INHIBITION.....	38
3.4 DOCKING AND MOLECULAR DYNAMICS SIMULATIONS .....	40
3.5 SELECTIVITY TOWARD ABCG2 AND CHEMOSENSITIZATION .....	41
<b>4. DISCUSSION.....</b>	<b>42</b>
<b>5. REFERENCES.....</b>	<b>44</b>
<b>CHAPTER 2 - SYNTHESIS AND BIOLOGICAL EVALUATION OF HETERODIMERS ON ABCG2 ACTIVITY .....</b>	<b>50</b>
<b>INTRODUCTION.....</b>	<b>50</b>
<b>2. MATERIALS AND METHODS .....</b>	<b>51</b>
2.1 GENERAL METHODS .....	51
2.2 CHALCONE SYNTHESIS .....	51
2.3 CHALCONE ALKYLATION WITH 1,4 DIBROMOBUTANE.....	52
2.4 PHEOPHYTIN EXTRACTION .....	52
2.5 PHEOPHORBIDE A SYNTHESIS .....	53
2.6 PHEOPHORBIDE A AMINE COUPLING .....	53
2.7 PHEOPHORBIDE A AMINE DEPROTECTION.....	54
2.8 BODIPY SYNTHESIS .....	54
2.9 CHOLESTEROL O-ALKYLATION .....	55
2.10 CHOLESTEROL-BODIPY HETERODIMER DIMER SYNTHESIS .....	55
2.11 CHOLESTEROL-CHALCONE HETERODIMER SYNTHESIS.....	56
2.12 INTRACELLULAR ACCUMULATION AND ABCG2-MEDIATED TRANSPORT OF BODIPY .....	57

2.13 CHOLESTEROL INFLUENCE ON ABCG2-MEDIATED TRANSPORT OF SUBSTRATES.....	57
2.14 EFFECT OF CHALCONE – CHOLESTEROL HETERODIMER ON ABCG2-MEDIATED TRANSPORT .....	57
<b>3. RESULTS .....</b>	<b>58</b>
3.1 CHALCONE – PORPHYRIN HETERODIMER .....	58
3.2 PHEOPHORBIDE A – CHALCONE .....	60
3.3 CHOLESTEROL – BODIPY HETERODIMER .....	65
3.4 CHOLESTEROL – CHALCONE HETERODIMER.....	66
3.5 BIOLOGICAL EVALUATION OF CHOLESTEROL AND HETERODIMERS ON ABCG2 .....	69
3.5.1 Cholesterol effect on drug transport ABCG2-mediated.....	69
3.5.2 BODIPY – cholesterol .....	69
3.5.3 Chalcone – cholesterol.....	71
<b>4. DISCUSSION .....</b>	<b>72</b>
<b>5. REFERENCES.....</b>	<b>72</b>
<b>CHAPTER 3 - MULTIPLEXED FLOW CYTOMETRIC APPROACH FOR DETECTION OF ANTI-SARS-COV-2 IGG, IGM AND IGA USING BEADS COVALENTLY COUPLED TO THE NUCLEOCAPSID PROTEIN .....</b>	<b>74</b>
<b>SIGNIFICANCE AND IMPACT OF THE STUDY.....</b>	<b>74</b>
<b>1. INTRODUCTION .....</b>	<b>74</b>
1.1 IMMUNOLOGICAL CHARACTERISTICS OF SARS-CoV-2 INFECTION .....	75
1.2 COVID-19 ANTIBODY DETECTION METHODS .....	76
1.3 CELL BASED SYSTEMS .....	76
1.4 CELL FREE SYSTEMS .....	77
<b>2. MATERIALS AND METHODS .....</b>	<b>77</b>
2.1 CHEMICALS AND ANTIBODIES .....	77
2.2 ANTIGEN PREPARATION AND BEADS CONJUGATION .....	78
2.3 SAMPLES.....	78
2.4 STAINING AND ANALYSIS .....	78
<b>3. RESULTS AND DISCUSSION .....</b>	<b>79</b>
3.1 STRATEGY AT A GLANCE .....	79
3.2 OPTIMIZATION OF CONDITIONS .....	80
3.3 PROOF OF CONCEPT.....	82
<b>4. FINAL REMARKS.....</b>	<b>84</b>
<b>5. REFERENCES.....</b>	<b>85</b>
<b>THESIS CONCLUSION .....</b>	<b>88</b>
<b>REFERENCES.....</b>	<b>88</b>
<b>PHD SCIENTIFIC PRODUCTION .....</b>	<b>101</b>
<b>SUPPLEMENTARY DATA.....</b>	<b>102</b>
<b>CHAPTER 1 - A NEW PORPHYRIN AS SELECTIVE SUBSTRATE-BASED INHIBITOR OF BREAST CANCER RESISTANCE PROTEIN (BCRP/ABCG2) .....</b>	<b>102</b>
<b>CHAPTER 2 - SYNTHESIS AND BIOLOGICAL EVALUATION OF HETERODIMERS ON ABCG2 ACTIVITY .....</b>	<b>106</b>
<b>CHAPTER 3 - MULTIPLEXED FLOW CYTOMETRIC APPROACH FOR DETECTION OF ANTI-SARS-COV-2 IGG, IGM AND IGA USING BEADS COVALENTLY COUPLED TO THE NUCLEOCAPSID PROTEIN .....</b>	<b>119</b>

## THESIS OVERVIEW

The findings described on this thesis bring new insights about the ABCG2 transporter and the use of flow cytometry for diagnosis of infectious diseases. This document was conceived as described below:

- An introduction about the general aspects of ABCG2, including strategies for overcome MDR and an overview about ABCG2 inhibitors.
- Chapter 1 shows the identification and characterization of porphyrin **4B** as a new ABCG2 inhibitor.
- Chapter 2 describes the synthesis of heterodimers and the biological effect against ABCG2.
- Chapter 3 presents the development of a cell-free flow cytometric approach for simultaneous identification of three immunoglobulins in COVID-19 patients.

## 1. INTRODUCTION

Multidrug resistance (MDR) is the main cause of treatment failures of many cancers. Different mechanisms promote the MDR phenotype, such as: apoptosis failure, activation of detoxifying systems, increased DNA repair, drug compartmentalization, changes of molecular drug targets and overexpression of ATP-binding cassette (ABC) transporters [1–4].

The human genome contains 48 genes that encode ABC proteins, organized in seven subfamilies (ABCA-ABCG) [5,6]. The overexpression of ABC transporters on cancer cells probably is the most relevant MDR mechanism [1,7]. These transporters can efflux a myriad of compounds with unrelated chemical structures, leading to a decrease on intracellular drug accumulation and impairing the cell response to drug-induced cell death [8,9]. In addition, many ABC transporters share a physiological role by exporting xenobiotics, proteins, metabolic products and lipids in tissues like liver, gut, kidney, placenta and blood brain barrier [9–11]. Among the 48 ABC proteins, three are closely related to MDR: glycoprotein-P (P-gp/ABCB1), multidrug resistance protein 1 (MRP1/ABCC1) and breast cancer resistance protein (BCRP/ABCG2) [12].

P-gp was discovered in 1976, corresponding to the first identified ABC transporter responsible for MDR [13]. This transporter is also known as multidrug resistance protein 1 (MDR1), being firstly described in a chinese ovary tissue culture cells (CHO cells) resistant to colchicine with cross-resistance to other chemotherapeutics [13]. In 1992 the second ABC transporter associated with MDR was discovered. MRP1 was described in lung cancer cell line H69AR by doxorubicin selection [14]. The ABCG2 transporter was identified simultaneously in 1998 by three different laboratories [15]. The ABCG2 transporter had its role in a MDR breast cancer subline verified in 1998, receiving the name of breast cancer resistance protein (BCRP) [16]. The overexpression of this protein was also verified on mitoxantrone resistant S1-M1-80 cells cDNA [17] and placenta tissue [18].

The ABC transporter structure is formed by two NBDs (Nucleotide-binding Domain) and two TMDs (Transmembrane-binding Domain). The catalytic cycle is based on the recognition of substrates by the TMD. Then, two molecules of ATP binds on the NBD. When the first ATP is hydrolyzed, the substrate is released. Then, the second ATP is hydrolyzed to return the protein to the basal conformation [19,20].

Different strategies can be applied on drug-design and development of new ABCG2 inhibitors. We present and discuss the most useful approaches cell- and membrane-based for identification and characterization of the mechanism of inhibition, as well the *in silico* methods. A table containing the ABCG2 inhibitors is presented, and the critical features of promising inhibitors is discussed. Finally, the use of ABCG2 inhibitors targeting cancer stem cells (CSC) is introduced and an overview about compounds the modulate the expression levels is presented.

### 1.1 Targeting ABCG2 by inhibitors

Different strategies were developed to overcome multidrug resistance. The first is the development of chemotherapeutics not effluxed by ABC transporters. Some taxenes derivarives were described as more active in P-gp overexpressing cells when compared with paclitaxel and docetaxel. Altstadt (2001) described a potent paclitaxel derivative by modifying C-7 motif on paclitaxel molecule to prevent P-gp binding. The molecule BMS-184476 was very active against HOC79 cell line [21]. Distefano (1997) also reported paclitaxel derivatives. Modifications on C-1, C-3 and C14 of taxenes

scaffold were responsible for the activity, however, the authors did not show if the result was due to absence of P-gp transport. [22]. Another interesting molecule is DJ-927, another taxene derivative with increased toxicity even on P-gp overexpressing cell lines. The authors assumed that the effects were due the reduced efflux by P-gp [23]. Besides being an interesting strategy, it is very difficult to apply on rational synthesis. ABC transporters are known as promiscuous transporters meaning that they can efflux a variety of unrelated compounds so is quite hard to find a logical structure-activity relationship on substrates [24].

The second strategy is to induce Collateral Sensitivity (CS) on ABC overexpressing cell lines. Collateral sensitivity is the hypersensitivity showed by MDR cell lines to a compound that do not sensitize the parental cell line [25]. This mechanism is not exclusive for cancer cells since it was firstly identified in *E coli* strains in 1952 [26]. In 1976, Bech-Hansen identified cancer cells resistant to colchicine that presented increased sensitivity to local anesthetics and steroids hormones [27]. Later, in 1982, it was demonstrated that colchicine resistant cell lines showed increased sensitivity to Taxol, verapamil and other calcium channel blockers [28–30]. This sensitivity was dependent on P-gp overexpression in a mechanism unrelated to inhibition [31]. Only in 2003 the mechanism of CS triggered by verapamil was described as the stimulation of ATPase activity on P-gp, leading to low ATP levels and triggering apoptosis [32]. For ABCG2, few compounds are known to induce CS in a clear way. Kuete (2013) described that natural benzophenones were capable to induce CS resistant cell lines overexpressing ABCG2 (isogarcinol in MDA-MB-231 and MDA-MB-231 *BCRP*) probably by inducing apoptosis but it is not clear the participation of ABCG2 in the process [33]. To induce collateral sensitivity is an interesting strategy but very difficult to explore due the variety of mechanisms that may be involved, hampering the synthesis of new compounds.

The more feasible strategy to overcome MDR is by inhibiting the transporter. The publication of ABCG2 high resolution protein is an advantage in this strategy since the interactions between protein-inhibitor can be explored and bring insights about important amino acids and regions for inhibitors [34]. This strategy can also direct for rational design of new molecules, leading to generations of compounds with improvement of their characteristics [35]. Different strategies can be used to prospect for new inhibitors. The first aims to test molecules that act as inhibitors to other transporters, like P-gp and MRP1. The literature shows inhibitors that were first identified for P-gp that also worked in ABCG2 like GF120918 [36]. The opposite is also true. Ko143 was firstly described as a specific inhibitor of ABCG2 but could inhibit P-gp and MRP1 at higher concentrations [37,38]. Another approach is based on testing different classes of drugs that presents a set of structural characteristics known to be beneficial for inhibition as a guide to prospection like hydrophobicity, aromaticity, planar structure and, generally, methoxy groups [39]. Drug repurposing is another way to prospect for new inhibitors with the advantage of shortening the development steps [40]. In this case, drugs used for unrelated diseases can represent an alternative for drug discovery with known pharmacokinetics, pharmacodynamics, and therapeutic index [40]. Drugs like calcium channel blockers, anti-HIV and xanthine oxidase inhibitors were identified as ABCG2 inhibitors [41–44].

## 1.2 Screening of different classes

Before the publication of ABCG2 structure, in 2017, the most used strategy for discovery of new inhibitors of ABCG2 was to identify chemical features among



different classes of molecules that interact with other ABC transporters [45,46]. The inhibitors of P-gp worked as a starting point for the discovery of ABCG2 inhibitors. GF120918 (Elacridar) is classified as the second generation of P-gp inhibitors [47]. This compound is also able to inhibit ABCG2 transport activity, but with lower potency compared with the effect observed for P-gp [36]. Based on these findings, GF120918 scaffold was used for the synthesis of many compounds with improved activity toward ABCG2 [48].

Considering the biochemical characteristics of the drug-binding sites on ABCG2, several classes of hydrophobic compounds were screened as inhibitors of ABCG2, as TKIs. As an attempt to verify the interactions with ABC transporters, Hegeus and co-workers demonstrated that some TKIs strongly interact with P-gp and MRP1. These compounds showed a dual behavior, being described as substrates or inhibitors [49]. Later, many TKIs were described as inhibitors of ABCG2 [50].

Natural products are a great source of chemical scaffolds for new drugs and constitute a privileged source for inhibitors of ABCG2. Flavonoids [51], botryllamides [52], polyphenols [53] are among the natural compounds identified as inhibitors of ABCG2 that were later modified to improve their activity. It is interesting to notice that those classes share some characteristics as hydrophobicity, aromaticity and planar structure.

### 1.3 *In vitro* and *in silico* strategies for identification of inhibitors

Several approaches can be used for identification of new ABCG2 inhibitors. As represented in the figure 1, most of them are cell-based assays. Nevertheless, membrane-based assays and *in silico* approaches are also useful tools for the study of the mechanism of inhibition.

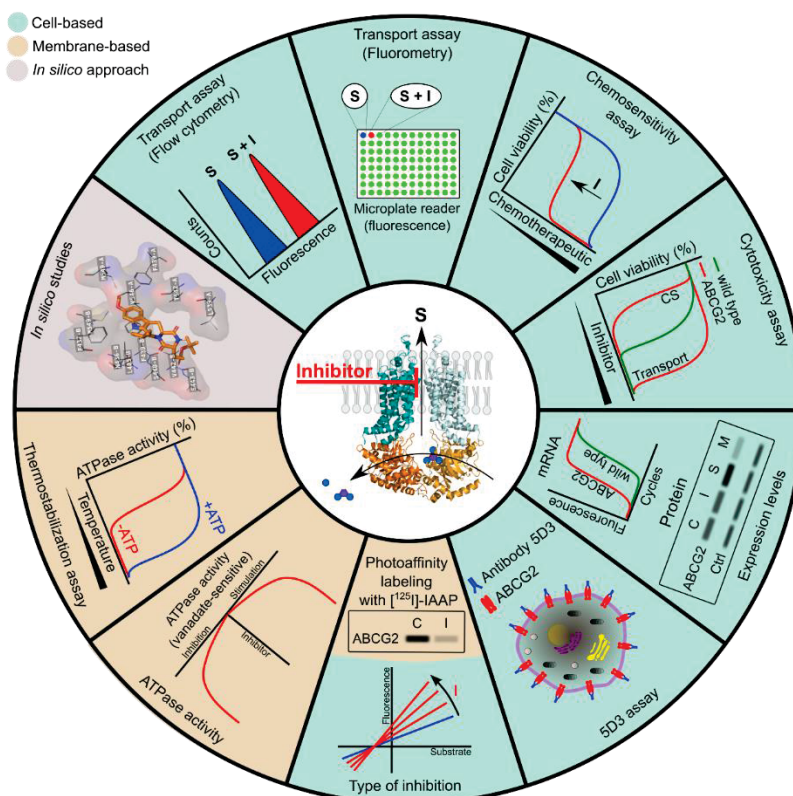


**Figure 1:** Main approaches for identification of new ABCG2 inhibitors and characterization of the biochemical and molecular mechanism of inhibition. S – substrate, I – inhibitor, CS – collateral sensitivity, C – control, M – modulator of protein expression levels.

Fluorescent substrates constitute a powerful tool for studies of ABCG2-mediated efflux. The most used fluorescent dyes are mitoxantrone, hoechst 33342, bodipy prazosin and pheophorbide *a*. The choice of the appropriate substrate is associated with the aim of the study and the equipment available. Among these ABCG2 substrates, only mitoxantrone is a chemotherapeutic agent, that is also transported by others ABC transporters [54]. The unique fluorescent substrate specific for ABCG2 is pheophorbide *a* [55]. Some common fluorescent dyes can also be applied for specific studies, as rhodamine 123, that is not a substrate of ABCG2 wild-type but is well transported by R482T ABCG2 mutant [56]. In contrast to the other ABCG2 substrates, hoechst 33342 is a fluorescent dye that require an ultraviolet laser for excitation, rarely found in flow cytometers.

In cell-based approaches, the flow cytometry is considered the gold standard for studies of ABCG2 transport activity. Two cell-based models are commonly used: (i) transfected and (ii) drug-selected cells. Differently of drug-selected cells, transiently or stable-transfected cells only overexpress the protein of interest, in this case ABCG2, becoming the best biological model for identification of new inhibitors without bias of additional MDR mechanisms or even the presence of other ABC transporters. The intracellular fluorescence detected by flow cytometry is dependent of the ABCG2 transport activity. Two differentials of flow cytometry are the easy discrimination of viable cells and cellular debris and the detection of subpopulations, that can impact the analysis. The inhibition can be reported as a percentage relative to control, since the ABCG2 inhibitor will increase the fluorescence signal when compared with the condition without the inhibitor. Intracellular accumulation controls that indicate 100% of inhibition can be achieved by reference inhibitors, such as Ko143 or using wild-type cells (or cell transfected with the empty vector), that do not express ABCG2 [57].

Microplates readers can also be useful to access intracellular accumulation or efflux of fluorescent dyes, similarly to flow cytometry. As a fluorescent ABCG2 substrate is used, the intracellular fluorescence intensity is directly proportional to the transporter activity [58]. The advantages of microplate readers over the flow cytometry are the intuitive user interface and the equipment cost. Nevertheless, the microplate readers are not capable to discriminate the fluorescence of cellular subpopulations or even of viable cells from the background noise [58–61]. Another drawback are the extensive washing steps before the analysis in a microplate reader [62].

The chemosensitivity approach is widely used method for the screening of new ABCG2 inhibitors. This approach is based on the cytotoxicity triggered by chemotherapeutic agents transported by ABCG2, such as mitoxantrone and SN-38. Usually, parental and cells overexpressing ABCG2 are exposed to increasing concentrations of the cytotoxic agent, allowing the determination of  $IG_{50}$  values (concentration that produces 50% growth inhibition). Cells overexpressing ABCG2 show a higher  $IG_{50}$  values compared to parental cells, indicating that the drug was pumped out of the cell. The association of ABCG2 inhibitors with the cytotoxic agents in cells overexpressing ABCG2 decrease the  $IG_{50}$  values. A complete inhibition of the ABCG2-mediated transport is observed when the  $IG_{50}$  value of the association of inhibitor and cytotoxic agent in resistant cells is similar to the  $IG_{50}$  value observed on parental cells treated with the cytotoxic agent [63]. MTT colorimetric assay is commonly used for indirect quantification of drug cytotoxicity. This method measures cellular metabolic activity as an indicator of cell viability and is suitable for early stages of drug screening *in vitro* [64,65]. The advantage of this method includes the low cost, although there are some interferences, mostly associated with compounds targeting mitochondria, which can interfere on cytotoxic effect [66].

The intrinsic cytotoxicity of ABCG2 inhibitors is an undesirable feature, however, the cytotoxic profile of these inhibitors comparing parental and cells overexpressing ABCG2 can provide a valuable information and should be addressed. The results obtained by this approach can suggest: (i) cross-resistance, (ii) absence of transport and (iii) CS. A cross-resistance is observed when the  $IG_{50}$  value obtained for cells overexpressing ABCG2 is higher than for parental cells. This result suggests that the ABCG2 inhibitor is transported by ABCG2, as observed with some TKIs, that inhibit ABCG2 by are also described to be transported [67]. The same cytotoxic profile in both cell lines, suggests an absence of transport mediated by ABCG2. Finally, some compounds can preferentially promote the cell death on cells overexpressing ABCG2, indicating that this inhibitor also trigger CS [68].

Additionally, it is important to evaluate the effect of new ABCG2 inhibitors on mRNA and protein levels. In the section 11 of this review, we present some inhibitors of the ABCG2 transport activity that also modulate the expression levels. The most used technique for investigation of the effect of compounds at transcriptional levels is qPCR (real-time PCR), while western blot analysis remains the gold standard for investigation of the effect on protein level. Flow cytometry and immunofluorescence microscopy can also be used for detection of protein levels, or even to check the correct addressing of the protein on membrane. However, the extracellular epitope of ABCG2 recognized by antibodies can be affected by conformational changes induced by the binding of inhibitors at TMDs. This interesting feature is explored by flow cytometry using the conformational antibody 5D3. Generally, ABCG2 substrates do not change the 5D3 immunoreactivity, however, ABCG2 inhibitors are described to increase the 5D3 binding. Thus, this approach based on binding shift of 5D3 was proposed for investigation of drug interactions with ABCG2 [69]. One important drawback is that the antibody 5D3 itself inhibits the ABCG2 transport activity due to the capability to hold the ABCG2 monomers together, avoiding the formation of an outward-facing conformation, which is fundamental for the drug efflux [70].

The type of inhibition can be investigated using cell-based assays, as well using membrane preparations. The kinetic parameters  $K_m$  and  $V_{max}$  can be obtained measuring the transport activity of ABCG2 using several substrate concentrations and some fixed concentrations of inhibitors. The kinetic analysis can suggest the type of inhibition by interpretation of the effects on  $K_m$  and  $V_{max}$ . Since the initial reaction rate is determined by intracellular substrate accumulation, increased inhibitor concentrations led to higher intracellular fluorescence, resulting in increased  $V_{max}$  values. The type of inhibition can also be investigated by a membrane-based assay. This method requires the use of photoaffinity-labeled compounds, generally iodorylazidoprazosin (IAAP), with membranes prepared from ABCG2 transfected insect cells (or membranes prepared from ABCG2-overexpressing human cells). A possible competition for the same binding site between the ABCG2 inhibitor with [ $^{125}I$ ]-IAAP can be quantified by autoradiography [63,71,72].

The effect of inhibitors on the ATPase activity can be measured in the crude membranes of mammalian or insect cells [73,74]. As the drug efflux mediated by ABC transporters is driven by ATP binding and hydrolysis, this assay can indirectly to predict if compounds are substrates of ABC transporters or not. Substrates are described to stimulate the ATPase activity, in contrast to inhibitors of the transport activity, that inhibit the ATPase activity. However, this premise should be carefully used for ABCG2. Some compounds that inhibit the ABCG2 transport activity also are stronger inhibitors of the ATPase activity, such as Ko143 [37]. However, some inhibitors of the transport activity can produce either a mild inhibition effect on the ATPase activity, as observed

by porphyrin 4B [75], or none effect, as described for ketonic indeno[1,2-*b*]indoles [76]. Interestingly, many potent ABCG2 inhibitors of the transport activity stimulate the ATPase activity, such as methoxy stilbenes and curcumin analogs [56,71].

The transport of substrates involves orchestrated protein conformational changes. Thus, a thermostabilization assay was recently proposed to assess how the binding of substrates or inhibitors affect the thermostability of ABC transporters in a membrane environment [77]. This assay is based on measurements of the ATPase activity using total membranes prepared from insect cells overexpressing the ABC transporter. A temperature range is applied to identify the  $IT_{50}$  value (temperature that reduces 50% of the ATPase activity). It was demonstrated that some indeno[1,2-*b*]indole derivatives produce a complete (100%) inhibition of ABCG2 transport activity, while others are partial inhibitors [78]. The thermostabilization assay revealed that these inhibitors triggered ABCG2 conformational changes stabilizing the protein structure. In addition, the partial inhibitors showed a moderate effect compared to complete inhibitors.

Finally, *in silico* approaches constitute a powerful tool for identification of the binding site of new ABCG2 inhibitors. Molecular docking is a technique used to identify and optimize promising drugs, by generating acceptable bonding conformations between the target protein and the ligand. Therefore, each ligand is docked into the active site of the protein and then scored -according to geometric, chemical, and energetic criteria - to establish which conformation is the most stable [79,80]. Likewise, molecular dynamics (MD) can be used to explore the protein's function and dynamics at an atomic level, providing the identification of their physiological conformations. It is also used on structural adjustments of postdocking complexes. Docking and molecular dynamics depends on 3D protein knowledge. [80,81]. Docking studies on indeno[1,2-*b*]indole derivatives showed that PHE439 seems to be related to inhibitors recognition [78] which is in accordance to Crio-EM studies, suggesting that inhibitors and substrates stays between PHE439 sidechains [82]. Interestingly, Pheophorbide a was also demonstrated by molecular dynamics as assuming different positions on ABCG2, differing from inhibitor 4B which assumes a more rigid conformation [75]. The same behavior was observed by Crio-EM where substrates bound were more flexible than inhibitors [83]. These observations show the good accordance between experimental methods (Crio-EM) and *in silico* methods.

#### 1.4 Minimal requirements for a desirable inhibitor

Small molecules that inhibit ABCG2 are often judged by its potency of inhibition, cytotoxicity and selectivity toward this ABC transporter. The primary concern of the development of new ABCG2 inhibitors is to assure a high potency of transport activity inhibition, targeting nanomolar concentrations, as described for Febuxostat, an ABCG2 inhibitor identified by the strategy of drug repurposing [42,84]. Thus, the screening of new inhibitors should focus on the identification of  $IC_{50}$  values of inhibition, that indirectly reflects the affinity of the inhibitor. Importantly, some ABCG2 inhibitors promote a partial inhibition, such as methoxy stilbenes and 6-prenylchrysin, that present a maximal inhibition around 70% [56,85]. Even compounds from the same chemical class can trigger complete or partial effects [86]. Interestingly, we recently demonstrated that partial inhibitors can completely reverse the MDR phenotype [78]. The partial inhibition can also be explored on bi-modulation assays, that consists in the association of two inhibitors for studies of the mechanism of inhibition [56,78]. For a

more precise comparison among different inhibitors, we recommend the authors to include the maximal inhibition percentage ( $I_{MAX}$  values) or the  $IC_{50}$  curves of inhibition.

A lower cytotoxicity or preferentially the absence of cytotoxicity is mandatory for development of new ABCG2 inhibitors. Many potent ABCG2 inhibitors identified using *in vitro* approaches failed in pre-clinical animal models, due its intrinsic toxicity [87]. We proposed the identification of a therapeutic ratio (TR) as an index that combines the potency of inhibition and the intrinsic cytotoxicity of inhibitors. This index is the ratio between  $IG_{50}/IC_{50}$  (intrinsic cytotoxicity/potency of inhibition), that allows a simplified comparison among different inhibitors, providing some guidance for selection of compounds that can follow for *in vivo* studies [83,84]. This concept was already successfully applied during the screening of chromones. The MBL-II-141 showed a very high TR, around 2000 [89]. This inhibitor was selected for *in vivo* studies, showing excellent results [90].

The selectivity toward ABCG2 is generally evaluated testing the new inhibitor against the other two human ABC transporters well known to have a clinical role in MDR: P-gp and MRP1. Despite the limited information about the real selectivity, this approach is valuable since these ABC transporters share several ligands. The selectivity could be relative to the concentration, as evidenced by the reference inhibitor Ko143, that in higher concentrations shows a promiscuous behavior, inhibiting the transport of substrates mediated by P-gp and MRP1 [37]. The concern about potency, cytotoxicity, and selectivity arose from clinical trials with P-gp inhibitors. Some of these studies were interrupted because the potency of inhibition was insufficient, either interfered on chemotherapeutic pharmacokinetics or were also cytotoxic [91]. For this reason, the association of these three parameters are critical and desired to minimize side effects as consequence of blocking physiological roles, avoid drug-drug interactions and distribution [35].

An important step is to confirm if ABCG2 inhibitors identified by transport activity assays also successfully sensitize resistant cells. The chemosensitization assays are based on the cytotoxic effect of chemotherapeutic agents transported by ABCG2. Usually, this assay is performed on parental and ABCG2 overexpressing cells after 72 hours of drug exposure. The chemosensitization assay is compatible with non-fluorescent drugs, increasing the range of ABCG2 substrates that can be employed. Considering that the values of ABCG2 inhibition were obtained by a transport activity assay performed in transfected cells overexpressing ABCG2, the chemosensitization assays provide additional information when performed with drug-selected ABCG2 overexpressing cancer cells. This *in vitro* investigation of the capacity of ABCG2 inhibitors in reverse the MDR phenotype is recommended before *in vivo* studies, however, the results should be carefully interpreted. Since the chemosensitization assays are evaluated after 72 hours of exposure with the inhibitors, the effect on mRNA and protein levels should be also explored and correlated [92].

After identification of new ABCG2 inhibitors, different approaches can be used for studies of the mechanism of inhibition, as represented in figure 1. The most widely used are the investigation of the effect of inhibitors on the ATPase activity and on the shift of 5D3 conformational antibody [93,94]. However, many reports describe the type of inhibition through kinetic analysis or using [ $^{125}I$ ]-IAAP [95]. After the publication of the protein structure, several papers performed *in silico* studies, contributing enormously for the identification of the drug binding site on ABCG2 [78,96]. Recently, the thermostabilization assay was introduced targeting the investigation of protein conformational changes triggered by inhibitors [77]. Finally, to confirm the transport or the absence of transport mediated by ABCG2, we proposed a “washing assay” [78].

This approach consists in the removal of the inhibitor from the culture media for long periods before the substrate addition on transport activity assays. This assay can be easily applied for non-cytotoxic inhibitors at laboratories that do not have access to LC-MS/MS platforms. Finally, *in vivo* validation for the lead compounds and studies of plasma stability and pharmacokinetic parameters will speed the development of ABCG2 inhibitors in clinical trials [97,98].

In summary, the minimal characteristics of a robust ABCG2 inhibitor are: (i) high potency of inhibition, (ii) low cytotoxicity and (iii) selectivity. However, we suggest to the authors to perform the maximal set of experiments to improve the available information about the ABCG2 inhibitors.

## 2. REFERENCES

- [1] Y.A. Luqmani, Mechanisms of Drug Resistance in Cancer Chemotherapy, *Med. Princ. Pract.* 14(suppl 1 (2005) 35–48. <https://doi.org/10.1159/000086183>.
- [2] K. Bukowski, M. Kciuk, R. Kontek, Mechanisms of Multidrug Resistance in Cancer Chemotherapy, *Int. J. Mol. Sci.* 21 (2020). <https://doi.org/10.3390/ijms21093233>.
- [3] Q. Wu, Z. Yang, Y. Nie, Y. Shi, D. Fan, Multi-drug resistance in cancer chemotherapeutics: Mechanisms and lab approaches, *Cancer Lett.* 347 (2014) 159–166. <https://doi.org/https://doi.org/10.1016/j.canlet.2014.03.013>.
- [4] S.M. Simon, M. Schindler, Cell biological mechanisms of multidrug resistance in tumors, *Proc. Natl. Acad. Sci.* 91 (1994) 3497 LP – 3504. <https://doi.org/10.1073/pnas.91.9.3497>.
- [5] M. Dean, The genetics of ATP-binding cassette transporters., *Methods Enzymol.* 400 (2005) 409–429. [https://doi.org/10.1016/S0076-6879\(05\)00024-8](https://doi.org/10.1016/S0076-6879(05)00024-8).
- [6] M. Dean, A. Rzhetsky, R. Allikmets, The human ATP-binding cassette (ABC) transporter superfamily, *Genome Res.* 11 (2001) 1156–1166. <https://doi.org/10.1101/gr.184901>.
- [7] M.M. Gottesman, I. Pastan, Biochemistry of Multidrug Resistance mediated by the Multidrug transporter, *Annu. Rev. Biochem.* 62 (1993) 385–427.
- [8] R.W. Robey, S. Shukla, E.M. Finley, R.K. Oldham, D. Barnett, S. V Ambudkar, T. Fojo, S.E. Bates, Inhibition of P-glycoprotein (ABCB1)- and multidrug resistance-associated protein 1 (ABCC1)-mediated transport by the orally administered inhibitor, CBT-1((R)), *Biochem. Pharmacol.* 75 (2008) 1302–1312. <https://doi.org/10.1016/j.bcp.2007.12.001>.
- [9] I.S. Mohammad, W. He, L. Yin, Understanding of human ATP binding cassette superfamily and novel multidrug resistance modulators to overcome MDR., *Biomed. Pharmacother.* 100 (2018) 335–348. <https://doi.org/10.1016/j.biopha.2018.02.038>.
- [10] K.J. Linton, Structure and Function of ABC Transporters, *Physiology.* 22 (2007) 122–130. <https://doi.org/10.1152/physiol.00046.2006>.
- [11] I.B. Holland, ABC transporters, mechanisms and biology: an overview, *Essays Biochem.* 50 (2011) 1–17. <https://doi.org/10.1042/bse0500001>.
- [12] Y.H. Choi, A. Yu, ABC Transporters in Multidrug Resistance and Pharmacokinetics , and Strategies for Drug Development, *Curr. Pharm. Des.* 20 (2014) 793–807.
- [13] R.L. Juliano, V. Ling, A surface glycoprotein modulating drug permeability in Chinese hamster ovary cell mutants, *Biochim. Biophys. Acta - Biomembr.* 455 (1976) 152–162. [https://doi.org/https://doi.org/10.1016/0005-2736\(76\)90160-7](https://doi.org/https://doi.org/10.1016/0005-2736(76)90160-7).
- [14] S.P.C. Cole, G. Bhardwaj, J.H. Gerlach, J.E. Mackie, C.E. Grant, K.C. Almquist, A.J. Stewart, E.U. Kurz, A.M. V Duncan, R.G. Deeley, Overexpression of a Transporter Gene in a Multidrug-Resistant Human Lung Cancer Cell Line, *Science* (80-. ). 258 (1992) 1650–1654. <https://doi.org/10.1126/science.1360704>.
- [15] K. Natarajan, Y. Xie, M.R. Baer, D.D. Ross, Role of breast cancer resistance protein (BCRP/ABCG2) in cancer drug resistance, *Biochem. Pharmacol.* 83 (2012) 1084–1103. <https://doi.org/https://doi.org/10.1016/j.bcp.2012.01.002>.
- [16] L.A. Doyle, W. Yang, L. V Abruzzo, T. Krogmann, Y. Gao, A.K. Rishi, D.D. Ross, A multidrug resistance transporter from human MCF-7 breast cancer cells., *Proc. Natl. Acad. Sci. U. S. A.* 95 (1998) 15665–15670. <https://doi.org/10.1073/pnas.95.26.15665>.
- [17] K. Miyake, L. Mickley, T. Litman, Z. Zhan, R. Robey, B. Cristensen, M. Brangi, L. Greenberger, M. Dean, T. Fojo, S.E. Bates, Molecular Cloning of cDNAs Which Are Highly Overexpressed in Mitoxantrone-resistant Cells, *Cancer Res.* 59 (1999) 8–13. <http://cancerres.aacrjournals.org/content/59/1/8.abstract>.

- [18] R. Allikmets, L.M. Schriml, A. Hutchinson, V. Romano-Spica, M. Dean, A human placenta-specific ATP-binding cassette gene (ABCP) on chromosome 4q22 that is involved in multidrug resistance., *Cancer Res.* 58 (1998) 5337–5339.
- [19] M.M. Gottesman, S. V Ambudkar, D. Xia, Structure of a multidrug transporter, *Nat. Biotechnol.* 27 (2009) 546–547. <https://doi.org/10.1038/nbt0609-546>.
- [20] J.-P. Becker, G. Depret, F. Van Bambeke, P.M. Tulkens, M. Prévost, Molecular models of human P-glycoprotein in two different catalytic states., *BMC Struct. Biol.* 9 (2009) 3. <https://doi.org/10.1186/1472-6807-9-3>.
- [21] T.J. Altstadt, C.R. Fairchild, J. Golik, K.A. Johnston, J.F. Kadow, F.Y. Lee, B.H. Long, W.C. Rose, D.M. Vyas, H. Wong, M.-J. Wu, M.D. Wittman, Synthesis and Antitumor Activity of Novel C-7 Paclitaxel Ethers: Discovery of BMS-184476, *J. Med. Chem.* 44 (2001) 4577–4583. <https://doi.org/10.1021/jm0102607>.
- [22] M. Distefano, G. Scambia, C. Ferlini, C. Gaggini, R. De Vincenzo, A. Riva, E. Bombardelli, I. Ojima, A. Fattorossi, P.B. Panici, S. Mancuso, Anti-proliferative activity of a new class of taxanes (14 $\beta$ -hydroxy-10-deacetylbaicatin III derivatives) on multidrug-resistance-positive human cancer cells, *Int. J. Cancer.* 72 (1997) 844–850. [https://doi.org/https://doi.org/10.1002/\(SICI\)1097-0215\(19970904\)72:5<844::AID-IJC22>3.0.CO;2-7](https://doi.org/https://doi.org/10.1002/(SICI)1097-0215(19970904)72:5<844::AID-IJC22>3.0.CO;2-7).
- [23] M. Shionoya, T. Jimbo, M. Kitagawa, T. Soga, A. Tohgo, DJ-927, a novel oral taxane, overcomes P-glycoprotein-mediated multidrug resistance in vitro and in vivo, *Cancer Sci.* 94 (2003) 459–466. <https://doi.org/https://doi.org/10.1111/j.1349-7006.2003.tb01465.x>.
- [24] H. Glavinas, P. Krajcsi, J. Cserepes, B. Sarkadi, The Role of ABC Transporters in Drug Resistance, *Metabolism and Toxicity, Curr. Drug Deliv.* 1 (2004) 27–42.
- [25] G. Szakács, M.D. Hall, M.M. Gottesman, A. Boumendjel, R. Kachadourian, B.J. Day, H. Cortay-Baubichon, A. Di Pietro, Targeting the Achilles Heel of Multidrug-Resistant Cancer by Exploiting the Fitness Cost of Resistance Gergely Szaka c, (2014).
- [26] W. Szybaski, V. Bryson, Genetic studies on microbial cross resistance to toxic agents. I. Cross resistance of *Escherichia coli* to fifteen antibiotics, *J. Bacteriol.* 64 (1952) 489–499. <https://doi.org/10.1128/jb.64.4.489-499.1952>.
- [27] N.T. Bech-Hansen, J.E. Till, V. Ling, Pleiotropic phenotype of colchicine-resistant CHO cells: cross-resistance and collateral sensitivity., *J. Cell. Physiol.* 88 (1976) 23–31. <https://doi.org/10.1002/jcp.1040880104>.
- [28] J.R. Warr, D.J. Flanagan, M. Anderson, Mutants of Chinese hamster ovary cells with altered sensitivity to taxol and benzimidazole carbamates, *Cell Biol. Int. Rep.* 6 (1982) 455–460. [https://doi.org/https://doi.org/10.1016/0309-1651\(82\)90117-5](https://doi.org/https://doi.org/10.1016/0309-1651(82)90117-5).
- [29] J.R. Warr, F. Brewer, M. Anderson, J. Fergusson, Verapamil hypersensitivity of vincristine resistant Chinese hamster ovary cell lines., *Cell Biol. Int. Rep.* 10 (1986) 389–399. [https://doi.org/10.1016/0309-1651\(86\)90011-1](https://doi.org/10.1016/0309-1651(86)90011-1).
- [30] J.R. Warr, M. Anderson, J. Fergusson, Properties of verapamil-hypersensitive multidrug-resistant Chinese hamster ovary cells., *Cancer Res.* 48 (1988) 4477–4483.
- [31] D.F. Cano-Gauci, J.R. Riordan, Action of calcium antagonists on multidrug resistant cells. Specific cytotoxicity independent of increased cancer drug accumulation., *Biochem. Pharmacol.* 36 (1987) 2115–2123. [https://doi.org/10.1016/0006-2952\(87\)90139-0](https://doi.org/10.1016/0006-2952(87)90139-0).
- [32] J. Karwatsky, M.C. Lincoln, E. Georges, A Mechanism for P-Glycoprotein-Mediated Apoptosis As Revealed by Verapamil Hypersensitivity, *Biochemistry.* 42 (2003) 12163–12173. <https://doi.org/10.1021/bi034149+>.
- [33] V. Kuete, P.D. Tchakam, B. Wiench, B. Ngameni, H.K. Wabo, M.F. Tala, M.L. MOUNGANG, B.T. Ngadjui, T. Murayama, T. Efferth, Cytotoxicity and modes of action of four naturally occurring benzophenones: 2,2',5,6'-tetrahydroxybenzophenone, guttiferone E, isogarcinol and isoxanthochymol., *Phytomedicine.* 20 (2013) 528–536. <https://doi.org/10.1016/j.phymed.2013.02.003>.
- [34] S.M. Jackson, I. Manolaridis, J. Kowal, M. Zechner, N.M.I. Taylor, M. Bause, S. Bauer, R. Bartholomaeus, G. Bernhardt, B. Koenig, A. Buschauer, H. Stahlberg, K.H. Altmann, K.P. Locher, Structural basis of small-molecule inhibition of human multidrug transporter ABCG2, *Nat. Struct. Mol. Biol.* 25 (2018) 333–340. <https://doi.org/10.1038/s41594-018-0049-1>.
- [35] D. Peña-Solórzano, S.A. Stark, B. König, C.A. Sierra, C. Ochoa-Puentes, ABCG2/BCRP: Specific and Nonspecific Modulators, *Med. Res. Rev.* 37 (2017) 987–1050. <https://doi.org/https://doi.org/10.1002/med.21428>.
- [36] M. de Bruin, K. Miyake, T. Litman, R. Robey, S.E. Bates, Reversal of resistance by GF120918 in cell lines expressing the ABC half-transporter, MXR, *Cancer Lett.* 146 (1999) 117–126.

- [https://doi.org/https://doi.org/10.1016/S0304-3835\(99\)00182-2](https://doi.org/https://doi.org/10.1016/S0304-3835(99)00182-2).
- [37] L.D. Weidner, S.S. Zoghbi, S. Lu, S. Shukla, S. V. Ambudkar, V.W. Pike, J. Mulder, M.M. Gottesman, R.B. Innis, M.D. Hall, The inhibitor Ko143 is not specific for ABCG2, *J. Pharmacol. Exp. Ther.* 354 (2015) 384–393. <https://doi.org/10.1124/jpet.115.225482>.
- [38] J.D. Allen, A. van Loevezijn, J.M. Lakhai, M. van der Valk, O. van Tellingen, G. Reid, J.H.M. Schellens, G.-J. Koomen, A.H. Schinkel, Potent and Specific Inhibition of the Breast Cancer Resistance Protein Multidrug Transporter *in Vitro* and in Mouse Intestine by a Novel Analogue of Fumitremorgin C 1 This work was supported in part by grant NKI 97-1433 from the Dutch Cancer Socie, *Mol. Cancer Ther.* 1 (2002) 417 LP – 425. <http://mct.aacrjournals.org/content/1/6/417.abstract>.
- [39] Y.A. Gandhi, M.E. Morris, Structure–Activity Relationships and Quantitative Structure–Activity Relationships for Breast Cancer Resistance Protein (ABCG2), *AAPS J.* 11 (2009) 541. <https://doi.org/10.1208/s12248-009-9132-1>.
- [40] J.S. Shim, J.O. Liu, Recent Advances in Drug Repositioning for the Discovery of New Anticancer Drugs, *Int J Biol Sci.* 10 (2014) 654–663. <https://doi.org/10.7150/ijbs.9224>.
- [41] Y. Zhang, A. Gupta, H. Wang, L. Zhou, R.R. Vethanayagam, J.D. Unadkat, Q. Mao, BCRP Transports Dipyridamole and is Inhibited by Calcium Channel Blockers, *Pharm. Res.* 22 (2005) 2023–2034. <https://doi.org/10.1007/s11095-005-8384-4>.
- [42] Y. Toyoda, T. Takada, H. Suzuki, Inhibitors of Human ABCG2: From Technical Background to Recent Updates With Clinical Implications, *Front. Pharmacol.* 10 (2019) 208. <https://doi.org/10.3389/fphar.2019.00208>.
- [43] J. Weiss, W.E. Haefeli, Potential of the novel antiretroviral drug rilpivirine to modulate the expression and function of drug transporters and drug-metabolising enzymes *in vitro.*, *Int. J. Antimicrob. Agents.* 41 (2013) 484–487. <https://doi.org/10.1016/j.ijantimicag.2013.01.004>.
- [44] A. Gupta, Y. Zhang, J.D. Unadkat, Q. Mao, HIV Protease Inhibitors Are Inhibitors but Not Substrates of the Human Breast Cancer Resistance Protein (BCRP/ABCG2), *J. Pharmacol. Exp. Ther.* 310 (2004) 334 LP – 341. <https://doi.org/10.1124/jpet.104.065342>.
- [45] T.J. Raub, P-Glycoprotein Recognition of Substrates and Circumvention through Rational Drug Design, *Mol. Pharm.* 3 (2006) 3–25. <https://doi.org/10.1021/mp0500871>.
- [46] E. Nicolle, A. Boumendjel, S. Macalou, E. Genoux, A. Ahmed-Belkacem, P.A. Carrupt, A. Di Pietro, QSAR analysis and molecular modeling of ABCG2-specific inhibitors, *Adv. Drug Deliv. Rev.* 61 (2009) 34–46. <https://doi.org/10.1016/j.addr.2008.10.004>.
- [47] G. Szakács, J.K. Paterson, J.A. Ludwig, C. Booth-Genthe, M.M. Gottesman, Targeting multidrug resistance in cancer, *Nat. Rev. Drug Discov.* 5 (2006) 219–234. <https://doi.org/10.1038/nrd1984>.
- [48] A. Boumendjel, S. Macalou, A. Ahmed-Belkacem, M. Blanc, A. Di Pietro, Acridone derivatives: Design, synthesis, and inhibition of breast cancer resistance protein ABCG2, *Bioorg. Med. Chem.* 15 (2007) 2892–2897. <https://doi.org/https://doi.org/10.1016/j.bmc.2007.02.017>.
- [49] T. Hegedűs, L. Órfi, A. Seprődi, A. Váradi, B. Sarkadi, G. Kéri, Interaction of tyrosine kinase inhibitors with the human multidrug transporter proteins, MDR1 and MRP1, *Biochim. Biophys. Acta - Mol. Basis Dis.* 1587 (2002) 318–325. [https://doi.org/https://doi.org/10.1016/S0925-4439\(02\)00095-9](https://doi.org/https://doi.org/10.1016/S0925-4439(02)00095-9).
- [50] C. Özvegy-Laczka, T. Hegedűs, G. Várady, O. Ujhelly, J.D. Schuetz, A. Váradi, G. Kéri, L. Órfi, K. Németh, B. Sarkadi, High-Affinity Interaction of Tyrosine Kinase Inhibitors with the ABCG2 Multidrug Transporter, *Mol. Pharmacol.* 65 (2004) 1485 LP – 1495. <https://doi.org/10.1124/mol.65.6.1485>.
- [51] S. Zhang, X. Yang, M.E. Morris, Flavonoids Are Inhibitors of Breast Cancer Resistance Protein (ABCG2)-Mediated Transport, *Mol. Pharmacol.* 65 (2004) 1208 LP – 1216. <https://doi.org/10.1124/mol.65.5.1208>.
- [52] C.J. Henrich, R.W. Robey, K. Takada, H.R. Bokesch, S.E. Bates, S. Shukla, S. V Ambudkar, J.B. McMahon, K.R. Gustafson, Botryllamides: Natural Product Inhibitors of ABCG2, *ACS Chem. Biol.* 4 (2009) 637–647. <https://doi.org/10.1021/cb900134c>.
- [53] S. Shukla, H. Zaher, A. Hartz, B. Bauer, J.A. Ware, S. V Ambudkar, Curcumin Inhibits the Activity of ABCG2/BCRP1, a Multidrug Resistance-Linked ABC Drug Transporter in Mice, *Pharm. Res.* 26 (2009) 480–487. <https://doi.org/10.1007/s11095-008-9735-8>.
- [54] L. Homolya, T.I. Orbán, L. Csanády, B. Sarkadi, Mitoxantrone is expelled by the ABCG2 multidrug transporter directly from the plasma membrane, *Biochim. Biophys. Acta - Biomembr.* 1808 (2011) 154–163. <https://doi.org/https://doi.org/10.1016/j.bbamem.2010.07.031>.
- [55] R.W. Robey, K. Steadman, O. Polgar, K. Morisaki, M. Blayney, P. Mistry, S.E. Bates, Pheophorbide a Is a Specific Probe for ABCG2 Function and Inhibition, *Cancer Res.* 64 (2004) 1242–1246. <https://doi.org/10.1158/0008-5472.CAN-03-3298>.



- [56] G. Valdameri, L. Pereira Rangel, C. Spatafora, J. Guitton, C. Gauthier, O. Arnaud, A. Ferreira-Pereira, P. Falson, S.M.B. Winnischofer, M.E.M. Rocha, C. Tringali, A. Di Pietro, Methoxy Stilbenes as Potent, Specific, Untransported, and Noncytotoxic Inhibitors of Breast Cancer Resistance Protein, *ACS Chem. Biol.* 7 (2012) 322–330. <https://doi.org/10.1021/cb200435y>.
- [57] E. Wang, C.N. Casciano, R.P. Clement, W.W. Johnson, Cholesterol Interaction with the Daunorubicin Binding Site of P-Glycoprotein, *Biochem. Biophys. Res. Commun.* 276 (2000) 909–916. <https://doi.org/https://doi.org/10.1006/bbrc.2000.3554>.
- [58] G.P. Tegos, A.M. Evangelisti, J.J. Strouse, O. Ursu, C. Bologna, L.A. Sklar, A high throughput flow cytometric assay platform targeting transporter inhibition, *Drug Discov. Today Technol.* 12 (2014) e95–e103. <https://doi.org/https://doi.org/10.1016/j.ddtec.2014.03.010>.
- [59] F. Förster, A. Volz, G. Fricker, Compound profiling for ABCG2 (MRP2) using a fluorescent microplate assay system, *Eur. J. Pharm. Biopharm.* 69 (2008) 396–403. <https://doi.org/https://doi.org/10.1016/j.ejpb.2007.10.003>.
- [60] B. Bauer, D.S. Miller, G. Fricker, Compound Profiling for P-Glycoprotein at the Blood–Brain Barrier Using a Microplate Screening System, *Pharm. Res.* 20 (2003) 1170–1176. <https://doi.org/10.1023/A:1025040712857>.
- [61] T. Frgala, O. Kalous, R.T. Proffitt, C.P. Reynolds, A fluorescence microplate cytotoxicity assay with a 4-log dynamic range that identifies synergistic drug combinations, *Mol. Cancer Ther.* 6 (2007) 886–897. <https://doi.org/10.1158/1535-7163.MCT-04-0331>.
- [62] H. Glavinas, P. Krajcsi, J. Cserepes, B. Sarkadi, The Role of ABC Transporters in Drug Resistance, Metabolism and Toxicity, *Curr. Drug Deliv.* 1 (2004).
- [63] G. Szakács, A. Váradi, C. Özvegy-Laczka, B. Sarkadi, The role of ABC transporters in drug absorption, distribution, metabolism, excretion and toxicity (ADME–Tox), *Drug Discov. Today.* 13 (2008) 379–393. <https://doi.org/https://doi.org/10.1016/j.drudis.2007.12.010>.
- [64] E. Ulukaya, M. Colakogullari, E.J. Wood, Interference by Anti-Cancer Chemotherapeutic Agents in the MTT-Tumor Chemosensitivity Assay, *Chemotherapy.* 50 (2004) 43–50. <https://doi.org/10.1159/000077285>.
- [65] M.C. Alley, D.A. Scudiero, A. Monks, M.L. Hursey, M.J. Czerwinski, D.L. Fine, B.J. Abbott, J.G. Mayo, R.H. Shoemaker, M.R. Boyd, Feasibility of Drug Screening with Panels of Human Tumor Cell Lines Using a Microculture Tetrazolium Assay, *Cancer Res.* 48 (1988) 589–601. <https://cancerres.aacrjournals.org/content/48/3/589>.
- [66] H. Mueller, M.U. Kassack, M. Wiese, Comparison of the Usefulness of the MTT, ATP, and Calcein Assays to Predict the Potency of Cytotoxic Agents in Various Human Cancer Cell Lines, *J. Biomol. Screen.* 9 (2004) 506–515. <https://doi.org/10.1177/1087057104265386>.
- [67] R. Sen, K. Natarajan, J. Bhullar, S. Shukla, H.-B. Fang, L. Cai, Z.-S. Chen, S. V Ambudkar, M.R. Baer, The Novel BCR-ABL and FLT3 Inhibitor Ponatinib Is a Potent Inhibitor of the MDR-Associated ATP-Binding Cassette Transporter ABCG2, *Mol. Cancer Ther.* 11 (2012) 2033–2044. <https://doi.org/10.1158/1535-7163.MCT-12-0302>.
- [68] M.D. Hall, M.D. Handley, M.M. Gottesman, Is resistance useless? Multidrug resistance and collateral sensitivity, *Trends Pharmacol. Sci.* 30 (2009) 546–556. <https://doi.org/https://doi.org/10.1016/j.tips.2009.07.003>.
- [69] Á. Telbisz, C. Hegedüs, C. Özvegy-Laczka, K. Goda, G. Várady, Z. Takáts, E. Szabó, B.P. Sorrentino, A. Váradi, B. Sarkadi, Antibody binding shift assay for rapid screening of drug interactions with the human ABCG2 multidrug transporter, *Eur. J. Pharm. Sci.* 45 (2012) 101–109. <https://doi.org/https://doi.org/10.1016/j.ejps.2011.10.021>.
- [70] N.M.I. Taylor, I. Manolaridis, S.M. Jackson, J. Kowal, H. Stahlberg, K.P. Locher, Structure of the human multidrug transporter ABCG2., *Nature.* 546 (2017) 504–509. <https://doi.org/10.1038/nature22345>.
- [71] M. Murakami, S. Ohnuma, M. Fukuda, E.E. Chufan, K. Kudoh, K. Kanehara, N. Sugisawa, M. Ishida, T. Naitoh, H. Shibata, Y. Iwabuchi, S. V Ambudkar, M. Unno, Synthetic Analogs of Curcumin Modulate the Function of Multidrug Resistance-Linked ATP-Binding Cassette Transporter ABCG2, *Drug Metab. Dispos.* 45 (2017) 1166–1177. <https://doi.org/10.1124/dmd.117.076000>.
- [72] P.-R. Ding, A.K. Tiwari, S. Ohnuma, J.W.K.K. Lee, X. An, C.-L. Dai, Q.-S. Lu, S. Singh, D.-H. Yang, T.T. Talele, S. V Ambudkar, Z.-S. Chen, The Phosphodiesterase-5 Inhibitor Vardenafil Is a Potent Inhibitor of ABCB1/P-Glycoprotein Transporter, *PLoS One.* 6 (2011) e19329. <https://doi.org/10.1371/journal.pone.0019329>.
- [73] A. Pozza, J.M. Préz-Victoria, A. Di Pietro, Overexpression of homogeneous and active ABCG2 in insect cells, *Protein Expr. Purif.* 63 (2009) 75–83. <https://doi.org/https://doi.org/10.1016/j.pep.2008.09.021>.

- [74] S. V Ambudkar, Drug-stimulatable ATPase activity in crude membranes of human MDR1-transfected mammalian cells, in: *ABC Transp. Biochem. Cell. Mol. Asp.*, Academic Press, 1998: pp. 504–514. [https://doi.org/https://doi.org/10.1016/S0076-6879\(98\)92039-0](https://doi.org/https://doi.org/10.1016/S0076-6879(98)92039-0).
- [75] I.F. Zattoni, T. Kronenberger, D.H. Kita, L.D. Guanaes, M.M. Guimarães, L. de O. Prado, M. Ziasch, L.C. Vesga, F.G. de M. Rego, G. Picheth, M.B. Gonçalves, M.D. Nosedá, D.R.B. Ducatti, A. Poso, R.W. Robey, S. V Ambudkar, V.R. Moure, A.G. Gonçalves, G. Valdameri, A new porphyrin as selective-based inhibitor of breast cancer resistance protein (BCRP/ABCG2), *Chem. Biol. Interact.* In press (2021).
- [76] G.J. Gozzi, Z. Bouaziz, E. Winter, N. Daflon-Yunes, M. Honorat, N. Guragossian, C. Marminon, G. Valdameri, A. Bollacke, J. Guillon, N. Pinaud, M. Marchivie, S.M. Cadena, J. Jose, M. Le Borgne, A. Di Pietro, Phenolic indeno[1,2-b]indoles as ABCG2-selective potent and non-toxic inhibitors stimulating basal ATPase activity., *Drug Des. Devel. Ther.* 9 (2015) 3481–3495. <https://doi.org/10.2147/DDDT.S84982>.
- [77] S. Lusvarghi, S. V Ambudkar, ATP-dependent thermostabilization of human P-glycoprotein (ABCB1) is blocked by modulators, *Biochem. J.* 476 (2019) 3737–3750. <https://doi.org/10.1042/BCJ20190736>.
- [78] D.H. Kita, N. Guragossian, I.F. Zattoni, V.R. Moure, F.G. de M. Rego, S. Lusvarghi, T. Moulenat, B. Belhani, G. Picheth, S. Bouacida, Z. Bouaziz, C. Marminon, M. Berredjem, J. Jose, M.B. Gonçalves, S. V Ambudkar, G. Valdameri, M. Le Borgne, Mechanistic basis of breast cancer resistance protein inhibition by new indeno[1,2-b]indoles, *Sci. Rep.* 11 (2021) 1788. <https://doi.org/10.1038/s41598-020-79892-w>.
- [79] A. Wadood, N. Ahmed, L. Shah, A. Ahmad, H. Hassan, S. Shams, In-silico drug design: An approach which revolutionarised the drug discovery process, *Drug Des. Deliv.* 1 (2013).
- [80] A. Ganesan, M.L. Coote, K. Barakat, Molecular dynamics-driven drug discovery: leaping forward with confidence, *Drug Discov. Today.* 22 (2017) 249–269. <https://doi.org/https://doi.org/10.1016/j.drudis.2016.11.001>.
- [81] G.F. Ecker, T. Stockner, P. Chiba, Computational models for prediction of interactions with ABC-transporters, *Drug Discov. Today.* 13 (2008) 311–317. <https://doi.org/https://doi.org/10.1016/j.drudis.2007.12.012>.
- [82] B.J. Orlando, M. Liao, ABCG2 transports anticancer drugs via a closed-to-open switch, *Nat. Commun.* 11 (2020) 1–11. <https://doi.org/10.1038/s41467-020-16155-2>.
- [83] J. Kowal, D. Ni, S.M. Jackson, I. Manolaridis, H. Stahlberg, K.P. Locher, Structural Basis of Drug Recognition by the Multidrug Transporter ABCG2, *J. Mol. Biol.* 433 (2021) 166980. <https://doi.org/https://doi.org/10.1016/j.jmb.2021.166980>.
- [84] H. Miyata, T. Takada, Y. Toyoda, H. Matsuo, K. Ichida, H. Suzuki, Identification of Febuxostat as a New Strong ABCG2 Inhibitor: Potential Applications and Risks in Clinical Situations, *Front. Pharmacol.* 7 (2016) 518. <https://doi.org/10.3389/fphar.2016.00518>.
- [85] A. Ahmed-Belkacem, A. Pozza, F. Muñoz-Martínez, S.E. Bates, S. Castanys, F. Gamarro, A. Di Pietro, J.M. Pérez-Victoria, Flavonoid structure-activity studies identify 6-prenylchrysin and tectochrysin as potent and specific inhibitors of breast cancer resistance protein ABCG2., *Cancer Res.* 65 (2005) 4852–4860. <https://doi.org/10.1158/0008-5472.CAN-04-1817>.
- [86] G. Valdameri, C. Gauthier, R. Terreux, R. Kachadourian, B.J. Day, S.M. Winnischofer, M.E. Rocha, V. Frachet, X. Ronot, A. Di Pietro, A. Boumendjel, Investigation of chalcones as selective inhibitors of the breast cancer resistance protein: critical role of methoxylation in both inhibition potency and cytotoxicity, *J Med Chem.* 55 (2012) 3193–3200. <https://doi.org/10.1021/jm2016528>.
- [87] M. Nishiyama, T. Kuga, Central Effects of the Neurotropic Mycotoxin Fumitremorgin A in the Rabbit (I) Effects on the Spinal Cord, *Jpn. J. Pharmacol.* 50 (1989) 167–173. [https://doi.org/https://doi.org/10.1016/S0021-5198\(19\)42469-4](https://doi.org/https://doi.org/10.1016/S0021-5198(19)42469-4).
- [88] G. Valdameri, C. Gauthier, R. Terreux, R. Kachadourian, B.J. Day, S.M.B. Winnischofer, M.E.M. Rocha, V. Frachet, X. Ronot, A. Di Pietro, A. Boumendjel, Investigation of Chalcones as Selective Inhibitors of the Breast Cancer Resistance Protein: Critical Role of Methoxylation in both Inhibition Potency and Cytotoxicity, *J. Med. Chem.* 55 (2012) 3193–3200. <https://doi.org/10.1021/jm2016528>.
- [89] G. Valdameri, E. Genoux-Bastide, B. Peres, C. Gauthier, J. Guitton, R. Terreux, S.M.B. Winnischofer, M.E.M. Rocha, A. Boumendjel, A. Di Pietro, Substituted chromones as highly-potent nontoxic inhibitors, specific for the breast cancer resistance protein., *J. Med. Chem.* (2011). <https://doi.org/10.1021/jm201404w>.
- [90] M.M. Honorat, L.L. Payen, J.J. Guitton, C. Gauthier, C. Bouard, F. Lecerf-Schmidt, B. Peres, R.R. Terreux, H.H. Gervot, C. Rioufol, A.A. Boumendjel, A. Puisieux, A. di Pietro, MBL-II-141, a

- chromone derivative, enhances irinotecan (CPT-11) anticancer efficiency in ABCG2-positive xenografts, *Oncotarget*. 5 (2014) 11957–11970.
- [91] A. Tamaki, C. Ierano, G. Szakacs, R.W. Robey, S.E. Bates, The controversial role of ABC transporters in clinical oncology, *Essays Biochem.* 50 (2011) 209–232. <https://doi.org/10.1042/bse0500209>.
- [92] A. Pick, M. Wiese, Tyrosine Kinase Inhibitors Influence ABCG2 Expression in EGFR-Positive MDCK BCRP Cells via the PI3K/Akt Signaling Pathway, *ChemMedChem*. 7 (2012) 650–662. <https://doi.org/https://doi.org/10.1002/cmdc.201100543>.
- [93] C. Özvegy-Laczka, G. Várady, G. Köblös, O. Ujhelly, J. Cervenak, J.D. Schuetz, B.P. Sorrentino, G.J. Koomen, A. Váradi, K. Német, B. Sarkadi, Function-dependent conformational changes of the ABCG2 multidrug transporter modify its interaction with a monoclonal antibody on the cell surface, *J. Biol. Chem.* 280 (2005) 4219–4227. <https://doi.org/10.1074/jbc.M411338200>.
- [94] C. Özvegy, T. Litman, G. Szakács, Z. Nagy, S. Bates, A. Váradi, B. Sarkadi, Functional Characterization of the Human Multidrug Transporter, ABCG2, Expressed in Insect Cells, *Biochem. Biophys. Res. Commun.* 285 (2001) 111–117. <https://doi.org/https://doi.org/10.1006/bbrc.2001.5130>.
- [95] K.F.K. Ejendal, N.K. Diop, L.C. Schweiger, C.A. Hrycyna, The nature of amino acid 482 of human ABCG2 affects substrate transport and ATP hydrolysis but not substrate binding, *Protein Sci.* 15 (2006) 1597–1607. <https://doi.org/https://doi.org/10.1110/ps.051998406>.
- [96] L.C. Vesga, T. Kronenberger, A.K. Tonduru, D.H. Kita, I.F. Zattoni, C.C. Bernal, A.R.R. Bohórquez, S.C. Mendez-Sánchez, S. V Ambudkar, G. Valdameri, A. Poso, Tetrahydroquinoline/4,5-dihydroisoxazole molecular hybrids as novel inhibitors of Breast Cancer Resistance Protein (BCRP/ABCG2)., *ChemMedChem*. (2021). <https://doi.org/10.1002/cmdc.202100188>.
- [97] F. Antoni, M. Bause, M. Scholler, S. Bauer, S.A. Stark, S.M. Jackson, I. Manolaridis, K.P. Locher, B. König, A. Buschauer, G. Bernhardt, Tariquidar-related triazoles as potent, selective and stable inhibitors of ABCG2 (BCRP), *Eur. J. Med. Chem.* 191 (2020) 1–16. <https://doi.org/10.1016/j.ejmech.2020.112133>.
- [98] B. Poller, D. Iusuf, R.W. Sparidans, E. Wagenaar, J.H. Beijnen, A.H. Schinkel, Differential Impact of P-Glycoprotein (ABCB1) and Breast Cancer Resistance Protein (ABCG2) on Axitinib Brain Accumulation and Oral Plasma Pharmacokinetics, *Drug Metab. Dispos.* 39 (2011) 729–735. <https://doi.org/10.1124/dmd.110.037317>.

## RESEARCH OBJECTIVES

- Study of porphyrins as ABCG2 inhibitors.
  - Screenin of porphyrins as ABCG2 inhibitors on stably transfected cell line;
  - Determination of IC<sub>50</sub> by flow cytometry;
  - Determination of IG<sub>50</sub> by MTT cytotoxicity assay;
  - Verification of porphyrin transport by ABCG2;
  - Determination of type of inhibition;
  - Verification of conformational changes using 5D3 binding, thermostability assay and ATPase hydrolysis.
  - Verification of interactions between porphyrin and ABCG2 by docking and Molecular dynamics;
  - Verification of selectivity of porphyrin in P-gp and MRP1.
  - Verification of ability of chemosensitization on transfected cell line and cancer selected cell lines.
- Study of heterodimers containing porphyrins or cholesterol on ABCG2
  - Synthesis and characterization of heterodimers Porphyrin – chalcone; Pheophorbide a – chalcone; BODIPY – cholesterol and Chalcone – cholesterol.
  - Evaluation of heterodimers on stably transfected cell line overexpressing ABCG2 as inhibitors or substrates.
- Development of flow cytometry-based methodology for identification of IgG, IgA and IgM on SARS-CoV-2 infected patients.
  - Promote the binding of nucleocapsid protein on CBA beads using sulfo-SMCC chemistry
  - Optimization of serum dilution individually for IgG, IgM and IgA;
  - Optimization of antibody dilution individually for IgG, IgM and IgA;
  - Optimization of Streptavidin dilution for IgA;
  - Development of a multiplex assay based on serum and antibody dilution previously determined;
  - Validate the assay using COVI-19 patient's serum.

## CHAPTER 1 - A NEW PORPHYRIN AS SELECTIVE SUBSTRATE-BASED INHIBITOR OF BREAST CANCER RESISTANCE PROTEIN(BCRP/ABCG2)

This chapter was based on the article published in the journal “Chemico-Biological Interactions” with the following authors:

DOI: 10.1016/j.cbi.2021.109718

Ingrid Fatima Zattoni<sup>1</sup>, Thales Kronenberger<sup>2,3</sup>, Diogo Henrique Kita<sup>1,4</sup>, Lais Danciguer Guanaes<sup>5</sup>, Matheus Murrel Guimarães<sup>5</sup>, Larissa de Oliveira Prado<sup>6</sup>, Melanie Ziasch<sup>6</sup>, Luis C. Vesga<sup>2,7,8</sup>, Fabiane Gomes de Moraes Rego<sup>6</sup>, Geraldo Picheth<sup>6</sup>, Marcos Brown Gonçalves<sup>9</sup>, Miguel D. Nosedá<sup>10</sup>, Diogo R. B. Ducatti<sup>10</sup>, Antti Poso<sup>2,3</sup>, Robert W. Robey<sup>4</sup>, Suresh V. Ambudkar<sup>4</sup>, Vivian Rotuno Moure<sup>1,6</sup>, Alan Guilherme Gonçalves<sup>5\*</sup>, Glaucio Valdameri<sup>1,6\*</sup>.

<sup>1</sup>Pharmaceutical Sciences Graduate Program, Laboratory of Cancer Drug Resistance, Federal University of Paraná, Curitiba, PR, Brazil.

<sup>2</sup>School of Pharmacy, University of Eastern Finland, Faculty of Health Sciences, Kuopio, 70211, Finland.

<sup>3</sup>Department of Medical Oncology and Pneumology, Internal Medicine VIII, University Hospital of Tübingen, Otfried-Müller-Strasse 14, 72076, Tübingen, Germany.

<sup>4</sup>Laboratory of Cell Biology, Center for Cancer Research, National Cancer Institute, National Institutes of Health, Bethesda, Maryland, USA.

<sup>5</sup>Department of Pharmacy, Federal University of Paraná, Curitiba, PR, Brazil.

<sup>6</sup>Department of Clinical Analysis, Federal University of Paraná, Curitiba, PR, Brazil

<sup>7</sup>Grupo de Investigación en Bioquímica y Microbiología GIBIM, Escuela de Química, Universidad Industrial de Santander, A.A. 678, Bucaramanga (Colombia).

<sup>8</sup>Grupo de Investigación en Compuestos Orgánicos de Interés Medicinal CODEIM, Parque Tecnológico Guatiguará, Universidad Industrial de Santander, A. A. 678, Piedecuesta, (Colombia)

<sup>9</sup>Department of Physics, Federal Technological University of Paraná, 80230-901 Curitiba, Parana, Brazil

<sup>10</sup>Department of Biochemistry and Molecular Biology, Federal University of Paraná, Curitiba, Paraná, Brazil.

\*Correspondence and requests for materials should be addressed to Alan Guilherme Gonçalves (alan.goncalves@ufpr.br) or Glaucio Valdameri (gvaldameri@ufpr.br).

Full postal address

### 1. INTRODUCTION

Multidrug resistance (MDR) mediated by ATP-binding cassette transporters (ABC transporters) is the most prevalent mechanism of resistance clinically observed [1]. Among the 48 genes in the human genome that encode ABC proteins, three ABC transporters are closely related to MDR: P-glycoprotein (P-gp/*ABCB1*), multidrug resistance protein 1 (MRP1/*ABCC1*) and breast cancer resistance protein (BCRP/*ABCG2*)[2]. *ABCG2* was discovered in 1998 by three laboratories simultaneously using different cell sources (breast cancer cell line MCF-7, colon carcinoma cell line S1-M1 and placenta tissue). For this reason, *ABCG2* is also named as BCRP (Breast Cancer Resistance protein), MXR (Mitoxantrone Resistance protein) and ABCP (Placenta-specific ABC transporter) [3–5].

The *ABCG2* transporter exerts physiological roles related to cellular detoxification, usually found in healthy tissues such as the liver, blood-brain barrier and placenta [6,7]. In cancer cells, *ABCG2* is responsible for the efflux of chemotherapeutics with unrelated chemical structures, such as mitoxantrone[8], methotrexate[9], topotecan, SN-38[10] and photosensitizers, such as pheophorbide a [7,11]. *ABCG2* is also highly expressed in cancer stem cells (CSC) called Side population (SP) [12,13] which is defined by the ability to exclude hoescht 33342 [14]. The presence of *ABCG2* in CSC is very intriguing since it can protect those cells from

chemotherapeutic agents [15]. This context suggests that ABCG2 inhibition may represent a way to avoid cancer recurrence.

The relationship between porphyrins and the ABCG2 transporter is well documented. ABCG2 seems to play a role in the heme biosynthesis pathway, actively transporting porphyrinic intermediates [16,17]. This interaction was first reported by Jonker (2002), which showed the protective activity of ABCG2 with dietary porphyrins, most specifically pheophorbide *a* [18]. Since then, pheophorbide *a* and other porphyrin-based photodynamic therapy (PDT) agents were reported as specific substrates of ABCG2 [11,19–23].

Some substrates of ABC transporters can also act as inhibitors. For instance, tyrosine kinase inhibitors (TKI's) [24–26], stilbenes [27–29] and tariquidar [30–36] are substrates with intrinsic inhibitory capacity. Specifically, TKIs are known as both ABCG2/P-gp inhibitors and substrates depending on the employed concentration, where higher concentrations lead to competitive inhibition in the substrate binding site [24–26]. Tariquidar is an ABCG2 substrate at low concentrations (~100 nM), which at higher concentrations (1  $\mu$ M) can compete with the substrate mitoxantrone [30,31]. Further studies reported selective and potent ABCG2 inhibitors obtained from tariquidar derivatives [32,33,35,36], with emphasis on XR9577, which showed noncompetitive behavior with pheophorbide *a* [34]. Another example is resveratrol, a substrate with inhibition capacity at high concentrations (30  $\mu$ M). The resveratrol inhibitory potency was increased by the insertion of methoxy groups to produce analogs, making stilbenes a new class of ABCG2 selective inhibitors [27–29].

The study of substrate derivatives as potential inhibitors might be an effective strategy for the development of highly potent optimized inhibitors, taking advantages of their chemical scaffold. Porphyrins are well characterized ABCG2 substrates, and to the best of our knowledge, no previous work has screened this class of compounds as ABCG2 inhibitors. This paper describes a new porphyrin derivative as a specific ABCG2 inhibitor and characterizes its mechanism of inhibition.

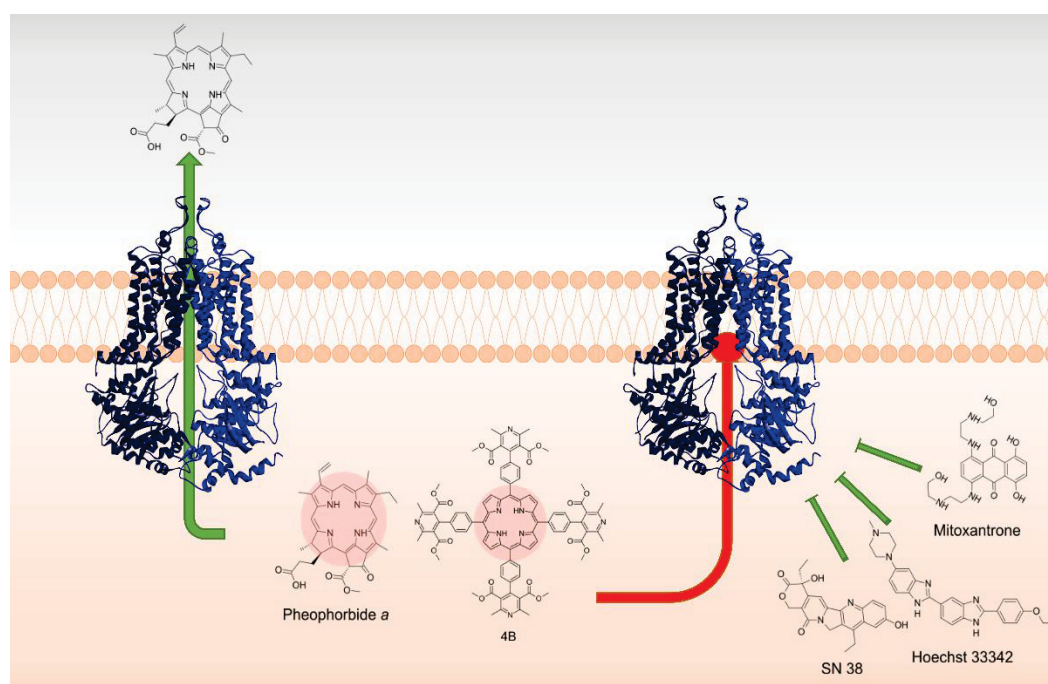


**Figure 1:** Results overview

## 2. MATERIAL AND METHODS

### 2.1 Chemicals

The porphyrins tested in this work were synthesized in the Laboratory of Heterocycles and Glycoconjugates at Federal University of Paraná (Brazil). The full synthesis and characterization were described in previous publications [37–41].

All chemotherapeutics, substrates and reference inhibitors were purchased from Sigma-Aldrich, Abcam and Invitrogen. Cell culture supplies were purchased from Gibco and Sigma-Aldrich. MTT reagent (3-(4,5-dimethylthiazol-2-yl)-2,5-diphenyltetrazolium bromide) was purchased from VWR life sciences. Antibodies for flow cytometry Mouse anti-human CD338 Clone 5D3 and Goat anti-mouse conjugated with Phycoerythrin were purchased from BD Pharmingen (New Jersey, USA).

### 2.2 Cell culture

HEK293, NIH3T3, BHK21 and H460 wild type cells were cultivated in Dulbecco's modified eagle medium high glucose supplemented with 10% of bovine fetal serum (FBS) and 50 µg/mL of gentamicin. PANC-1 wild type was cultivated in RPMI medium supplemented with 10% of FBS, 1% of penicillin and 0.25 µg/mL of amphotericin. The cells were cultivated until 80–90% of confluence and then used for experimentation. Stably transfected cells, HEK293-*ABCG2*, NIH3T3-*ABCB1*, BHK21-*ABCC1* were additionally supplemented with 0.75 mg/mL of G418, 60 ng/mL of colchicine and 0.1 mg/mL of methotrexate for *ABCG2*, *ABCB1* and *ABCC1*, respectively. H460MX20 and PANC-1MX100 cells were cultivated under mitoxantrone pressure (20 nM and 100 nM respectively). The cells HEK293, NIH3T3, BHK21 and transfected cell lines were kindly provided by Dr. Attilio Di Pietro (IBCP, Lyon, France). Wild type H460, H460MX20, PANC-1 and PANC-1MX100 were provided by Dr. Attilio Di Pietro (IBCP, Lyon, France) and Dr. Susan Bates laboratory (HIH, Bethesda, MD, USA).

### 2.3 Accumulation assay

HEK293-wild type cells were seeded in a 24 wells plate ( $2.0 \times 10^5$  cells/well) and incubated for 24 h to attach. Then, cells were treated with porphyrin **4D** for 1, 2, 4, 18, 22 and 28 h. After this period, cells were washed with PBS (300 µL), detached with trypsin and the intracellular accumulation of porphyrin **4D** was analyzed by flow cytometry using a FACS Calibur (FL-3 filter) (BD Biosciences, New Jersey, USA).

### 2.4 Inhibition assay

The inhibition capacity was measured by flow cytometry. HEK293-*ABCG2* and HEK293-wild type cells were seeded into a 24 wells plate ( $2.0 \times 10^5$  cells/well). After 24 h, cells were treated with porphyrins (10 µM) for 30 min and 24 h. The fluorescent substrates (mitoxantrone 10 µM or hoechst 33342 3 µM) were added as follow: for the 30 min treatment, the fluorescent substrate and porphyrin were added at the same time. For the 24 h of porphyrin treatment, the fluorescent substrate was added in the last 30 min of the treatment. After treatment, cells were washed with PBS (300 µL), detached with trypsin and analyzed by flow cytometry using FACS Calibur (BD

Biosciences) Red Laser and FL-4 filter for mitoxantrone and FACS Celesta (BD Biosciences) Ultraviolet Laser and the Band-Pass 450-50 filter for hoechst 33342.

The IC<sub>50</sub> curves were obtained with increasing concentrations of **4B** (0.09 μM to 10 μM, 24 h of incubation) using mitoxantrone and hoechst 33342 as substrates. Selectivity assay was performed using 10 μM of **4B** incubated for 24 h and rhodamine 123 (5 μM for ABCB1) or daunorubicin (10 μM for ABCC1) as fluorescent substrates.

For the washing assay, HEK293-ABCG2 cells were treated with **4B** at 10 μM for 24 h. Cells were then washed with PBS (300 μL) and kept in culture medium without **4B** (300 μL) for 1, 3 and 24 h. After that, the medium was removed and mitoxantrone at 10 μM (dissolved in cell culture media) was added for 30 min, then, the cells were washed with PBS (300 μL) and detached with trypsin to perform the flow cytometry, as previously described.

The inhibition mechanism was determined by treating the cells with **4B** (10, 1.65 and 0.5 μM) for 24 h. After this period, the treatment was removed and the substrate was added for 30 min (hoechst 33342 at concentrations 6, 3, 1.5 and 0.75 μM and mitoxantrone at concentrations 20, 10, 5 and 2.5 μM). The cells were washed with PBS (300 μL), detached with trypsin and analyzed by flow cytometry.

## 2.5 Confocal microscopy

HEK293-ABCG2 were seeded into 24 well plates (1.0x10<sup>5</sup> cells/well) with coverslips on the bottom and incubated for 48 h. After cell adhesion, the cells were treated with **4B** (10 μM for 24 h) and hoechst 33342 (1 μM for 30 min). The coverslips were recovered, washed, and placed on microscopy slides with Glycerin. The images were taken with Confocal microscopy Nikon A1R MP + (NIKON, Tokyo, Japan) at 40x objective. The fluorescence was reached using 405 nm laser for excitation and the emission was detected using 425-475 nm filter. The images were visualized with software Nis Elements 4.20 (NIKON, Tokyo, Japan).

## 2.6 Cell viability assay

Cells were seeded (2.0x10<sup>4</sup> cell/well) into a 96 wells plate and incubated for 24 h to attachment. To evaluate the cell cytotoxicity, cells were treated with increasing concentrations of **4B** (0.09 μM to 100 μM) and incubated for 72 h. For chemosensitivity assay, cells were treated with **4B** (10 μM) for 24 h and then SN-38 was added for additional 48 h (0.1 nm to 20 μM for HEK293 cell lines, 0.5 μM and 5.0 μM for H460 and PANC-1 cell lines). After this period, the medium was removed, cells were washed with PBS (100 μL) and incubated with MTT solution (100 μL of solution 0.5 mg/mL in PBS) for 4 h. Then, the solution was removed, and the formazan crystals were dissolved with 100 μL of ethanol/DMSO (1:1). The absorbance was measured using a microplate reader at 595 nm (Bio-Rad iMark).

## 2.7 ATPase assay

ATPase activity was determined as previously described by Ambudkar (1998) [42]. Total membranes of High five cells overexpressing ABCG2 were used (5 μg protein/tube, final volume 100 μL). The membranes were mixed with assay buffer (50 mM Tris-HCl pH 6.8, 150 mM *N*-methyl-D-glucamine (NMDG)-Cl, 5 mM sodium azide, 1 mM EGTA, 1 mM ouabain, 2mM DTT and 10 mM MgCl<sub>2</sub>) in the presence or absence of sodium orthovanadate at 0.3 mM. The membranes were treated with **4B** in a range



of 0.1 to 2.5  $\mu\text{M}$  and incubated for 20 min at 37°C with ATP (5 mM). After this period, 100  $\mu\text{L}$  of 5% SDS, 400  $\mu\text{L}$  of  $\text{P}_i$  solution (sulfuric acid 36.2 N, water, ammonium molybdate and antimony potassium tartarate) and 200  $\mu\text{L}$  of 1% ascorbic acid were added. After 10 min, the absorbance was measured at 880 nm using Ultrospec 3100 pro spectrophotometer (Amersham Biosciences, UK).

## 2.8 Conformational antibody binding (5D3)

HEK293-ABCG2 were seeded at a density of  $2.0 \times 10^5$  cells/well into a 24 wells plate and, after 24 h, cells were treated with 10  $\mu\text{M}$  of porphyrin **4B** for 10, 30 min and 24 h. Then, cells were detached with trypsin, collected with 300  $\mu\text{M}$  of PBS and centrifuged (1000 x g for 3 min). The pellet was resuspended in 100  $\mu\text{L}$  of PBS/BSA (40  $\mu\text{g}/\text{mL}$  of BSA) and the primary antibody (Mouse anti-human CD338 Clone 5D3, BD Pharmigen) was added (1:100) for 30 min at 37°C. The cells were centrifuged (1000 x g, 3 min), the supernatant removed and resuspended with 100  $\mu\text{L}$  of PBS with the secondary antibody (Goat anti-mouse conjugated with Phycoerythrin, BD Pharmigen) 1:200 for 30 min at 37°C. Then, the cells were centrifuged, the supernatant removed, and the cell pellet was resuspended in 300  $\mu\text{L}$  of PBS. The analysis was performed using FACS Calibur using the blue laser (488 nm) and FL-2 filter.

## 2.9 Thermostability assay

Membranes from High Five insect cells overexpressing ABCG2 were incubated with assay buffer at 3  $\mu\text{g}$  protein/tube in the presence or absence of 0.3 mM orthovanadate, reaching 50  $\mu\text{L}$  as final volume (Assay buffer: 50 mM Tris-HCl pH 6.8, 150 mM *N*-methyl-*D*-glucamine (NMDG)-Cl, 5 mM sodium azide, 1 mM ouabain, 2 mM DTT). Then, the tests were prepared with 12.5 mM  $\text{MgCl}_2$  or 6.25 mM ATP and incubated with a temperature range from 37 to 61°C for 10 min using a thermocycler C1000 Touch (Bio-Rad, Hercules, CA).

After this period, 10  $\mu\text{L}$  of 25 mM ATP or 50 mM  $\text{MgCl}_2$  was added (final concentration of 5 and 10 mM respectively) followed by incubation at 37°C for 20 min. Then, the reaction was stopped with 50  $\mu\text{L}$   $\text{P}_i$  reagent (1% ammonium molybdate, 2.5 N  $\text{H}_2\text{SO}_4$  and 0.014% potassium-antimony tartarate). The tests were transferred to a 96 well plate (50  $\mu\text{L}/\text{well}$ ), 150  $\mu\text{L}$  of 0.33% sodium ascorbate solution was added. After 15 min, the absorbance was measured using a microplate reader Spectramax iD3 (Molecular devices, San Jose, CA, USA). The sensitive activity to vanadate was calculated as the difference between the activity value in the absence and presence of vanadate at each temperature.

## 2.10 Molecular modelling

The system preparation and docking calculations were performed using the Schrödinger Drug Discovery suite for molecular modelling (version 2019.4). The ABCG2 crystal structure (PDB ID: 6FFC, resolution 3.56 Å [43]) was obtained from the Protein Data Bank (PDB; www.rcsb.org). The structure was chosen since it is one of the cryo-EM structures with high-resolution reported. ABCG2 structure was prepared with the Protein preparation wizard [44] to fix protonation states of amino acids residues, adding hydrogens and also fixing missing side-chain atoms. Missing loops between Asp301 – Leu328 and Gly354 – Tyr369 were generated and optimized using Prime [45]. Compounds **4B** and PHEO were drawn using maestro and prepared

using LigPrep [46] to generate the three-dimensional conformation, adjust protonation state to physiological pH (7.4), and calculate the partial atomic charges, with the force field OPLS3e [47].

Docking studies with the prepared ligands were performed using Glide [48,49] (Glide V7.7), with the flexible modality of Induced-fit docking with extra precision (XP), followed by a side-chain minimization step using Prime [50]. Ligands were docked within a grid around 12 Å from the centroid of the residue Glu446(A), to represent Site 1 in between the subunits. For each ligand 10 docking poses were generated. Selected docking poses were further validated by molecular dynamics simulation, where ligand stability within the proposed pocket and its interactions were evaluated. MD simulations were carried out using Desmond [51] engine with the OPLS3e force-field [48,52], which leads to improved performance in predicting protein-ligand binding affinities. Protein was embedded within a DMPC lipid pre-generated from Maestro, using the System Builder, where the membrane positioning was controlled by the orientation of the alpha-helices based on the transmembrane sequences.

The protein-membrane system was placed in a cubic box with 15 Å from the box edges to any atom of the protein, using PBC conditions, and, filled with TIP3P [53] water. Then, all systems were equilibrated by short simulations under the NPT ensemble for 5 ns implementing the Berendsen thermostat and Barostat methods. A constant temperature of 310 K and 1atm of pressure throughout the simulation using the Nose-Hoover thermostat algorithm and Martyna-Tobias-Klein Barostat algorithm, respectively. After minimization and relaxing steps, we proceeded with the production step of at least 1 μs. All MD simulations were performed at least three independent runs with randomly generated seeds. Trajectories and interaction data are available on Zenodo repository (MZ29 trajectories were previously published elsewhere [54] and can be found under the code: 10.5281/zenodo.3746123, while additional PHEO and **4B** trajectory simulations are reported in 10.5281/zenodo.3988214).

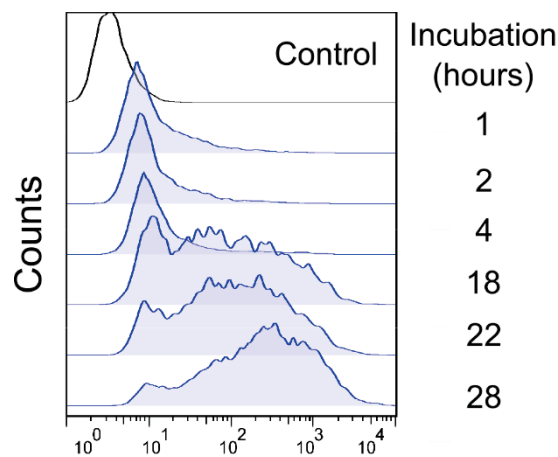
For principal component analyses, the backbone of each frame was extracted and aligned using `trj_selection_dl.py` and `trj_align.py` scripts from Schrodinger. Individual simulations from all the runs were merged using `trj_merge.py` into a final trajectory and CMS file which was further used for the generation of the principal components. Principal components of protein C-alpha atoms were calculated using `trj_essential_dynamics.py` script. Most of the large moments were captured in the first two components with the first component having 32.5% and the second component having 11.10% of the total motion. Protein-ligand interactions and protein conformational changes were analyzed using the Simulation Interaction Diagram (SID) tool with standard options.

Molecular dynamics trajectories were visualized, and figures were produced using PyMol (Schrödinger LCC, version 2.2.3). The stability of the MD simulations was monitored by looking specifically at the root mean square deviation (RMSD) (Supporting information Fig. S5, represents RMSD variation along with the simulation), root mean square fluctuation (RMSF, supporting information Fig. S3) of the ligand and protein along the simulation time, our simulations were compared against ABCG2 – MZ29 previously published.

### 3. RESULTS

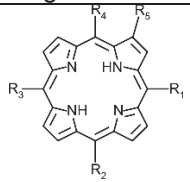
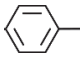
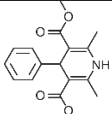
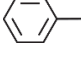
#### 3.1 Screening of porphyrins as inhibitors of ABCG2 transport activity

A total of 19 porphyrin derivatives (Fig. S1 and Table 1) were evaluated as potential inhibitors of ABCG2 transporter by examining their effect on mitoxantrone efflux. Stably transfected cells overexpressing ABCG2 (HEK293-ABCG2) were incubated with 10  $\mu$ M of the porphyrins for 30 minutes. Four porphyrins showed a mild inhibition (10 to 30% of inhibition) of mitoxantrone efflux, and only the porphyrin **4B** showed an inhibition higher than 40% (Table 1). Considering the intrinsic fluorescent property of some porphyrins, a screening with this set of compounds was performed in HEK293-wild type cells to evaluate the intracellular accumulation. The best fluorescent signal was observed with porphyrin **4D**, which showed a time-dependent accumulation (Fig. 2), no other porphyrin showed relevant fluorescence (Table S2). Thus, the potential of ABCG2 inhibition for the 19 porphyrins was reevaluated after 24 h of incubation. A clear improvement on the potency of inhibition was observed to compound **4B**, increasing the inhibition effect at 10  $\mu$ M from 44 to 78%, confirming the time-dependent intracellular accumulation of porphyrins and consequently the inhibition effect (Table 1).



**Figure 2:** Intracellular accumulation of porphyrin **4D** along the time using HEK293-wild type cells. Cells were analyzed by flow cytometry using the blue laser (488 nm) and FL-3 filter (670 nm long pass).

**Table 1.** Porphyrin structures and the percentage of inhibition of ABCG2 transport activity.

 Common scaffold						
Porphyrin	R <sub>1</sub>	R <sub>2</sub> =R <sub>3</sub> =R <sub>4</sub>	R <sub>5</sub>	Reference	ABCG2 inhibition (%) $\pm$ SD	
					30 min	24 h
Core				[32]	14.07 $\pm$ 12.22	-20.63 $\pm$ 3.68
<b>1A</b>			-H	[41]	6.95 $\pm$ 8.4	51.89 $\pm$ 4.75

<b>1B</b>				[41]	-16.43 ± 8.74	1.34 ± 12.36
<b>1C</b>				[31, 32]	-3.51 ± 3.47	-24.65 ± 4.55
<b>1C*</b>			-NO <sub>2</sub>	[33]	-0.62 ± 5.67	7.61 ± 3.13
<b>1D</b>			-H	[30]	9.83 ± 13.59	-6.00 ± 16.33
<b>1E</b>					7.37 ± 5.82	9.49 ± 17.20
<b>1F</b>				[30, 31]	-4.45 ± 7.76	-31.01 ± 9.60
<b>1G</b>				[30]	23.69 ± 18.35	-18.75 ± 0.37
<b>1H</b>					-7.90 ± 0.84	-5.20 ± 0.21
<b>4A</b>				[41]	-7.49 ± 11.81	-12.20 ± 1.77
<b>4B</b>				[41]	43.99 ± 8.07	78.30 ± 9.33
<b>4D</b>				[32]	19.08 ± 2.38	-16.11 ± 0.79
<b>4E</b>				[31]	0.50 ± 3.91	-15.58 ± 17.37
<b>4I</b>					1.51 ± 6.12	-14.86 ± 10.48
<b>4J</b>			9.31 ± 5.51		0.71 ± 4.96	
<b>4K</b>			9.27 ± 0.12		-20.46 ± 1.37	
<b>4L</b>			-15.48 ± 5.67		18.87 ± 8.56	
<b>4M</b>			-19.78 ± 0.03		-4.46 ± 3.17	

The inhibition of ABCG2-mediated efflux of mitoxantrone (5  $\mu$ M) was assayed in HEK293-ABCG2 cells. Cells were exposed to porphyrins at 10  $\mu$ M for 30 min or 24 h. The percent inhibition of ABCG2 transport was determined by flow cytometry using the reference inhibitor Ko143 (0.5  $\mu$ M) as a control, which produces 100% inhibition. The data are the mean  $\pm$  SD of, at least, two independent experiments.

The tested porphyrins can be divided in two groups: mono and tetrasubstituted. Among the monosubstituted porphyrins, the **1A** structure can be highlighted since it showed 51% of inhibition after 24 h of incubation, despite the low inhibition at 30 min (around 6%). Porphyrin **1A** is closely related to **1B**, which bears a pyridine ring as substituent, instead of a dihydropyridine ring. However, **1B** did not display considerable inhibition. In this case, the ring aromatization seems to be detrimental for the inhibition.

On the tetrasubstituted porphyrins group, porphyrin **4B** showed higher inhibition than other structures at 30 min (44%) and 24 h (78% of inhibition). The related structure, **4A**, did not show quantifiable inhibition.

Interestingly, on monosubstituted porphyrins, aromatization was detrimental for inhibition effect but was favorable on the tetrasubstituted structure. The opposite was observed with dihydropyridine rings, where it was favorable on monosubstituted structures and unfavorable on the tetrasubstituted scaffold.

### 3.2 IC<sub>50</sub> of ABCG2 inhibition and absence of transport

The effect of porphyrin **4B** on ABCG2 function after 24 h of exposure was explored by different approaches. Porphyrin **4B** was able to inhibit, with the same potency, the transport of different substrates of ABCG2, showing an  $IC_{50}$  of 1.63 and 1.65  $\mu\text{M}$  for mitoxantrone and hoechst 33342, respectively (Fig. 3A and C). In addition, a saturating concentration of porphyrin **4B** (10  $\mu\text{M}$ ) resulted in intracellular accumulation of mitoxantrone and hoechst 33342 similar to the reference inhibitor Ko143 (Fig. 3B and D). The intracellular accumulation of hoechst 33342 on cells treated with porphyrin **4B** was also confirmed by confocal microscopy (Fig. 3E). In cells incubated only with hoechst 33342, the fluorescence was diffuse, and do not concentrate in the nucleus. However, in the presence of Ko143, the intracellular fluorescence of hoechst 33342 was higher and localized in the nucleus. The treatment of cells with **4B** increased the accumulation of hoechst 33342, much like the known ABCG2 reference inhibitor Ko143, confirming that porphyrin **4B** inhibits the ABCG2 transport activity independently of the substrate.

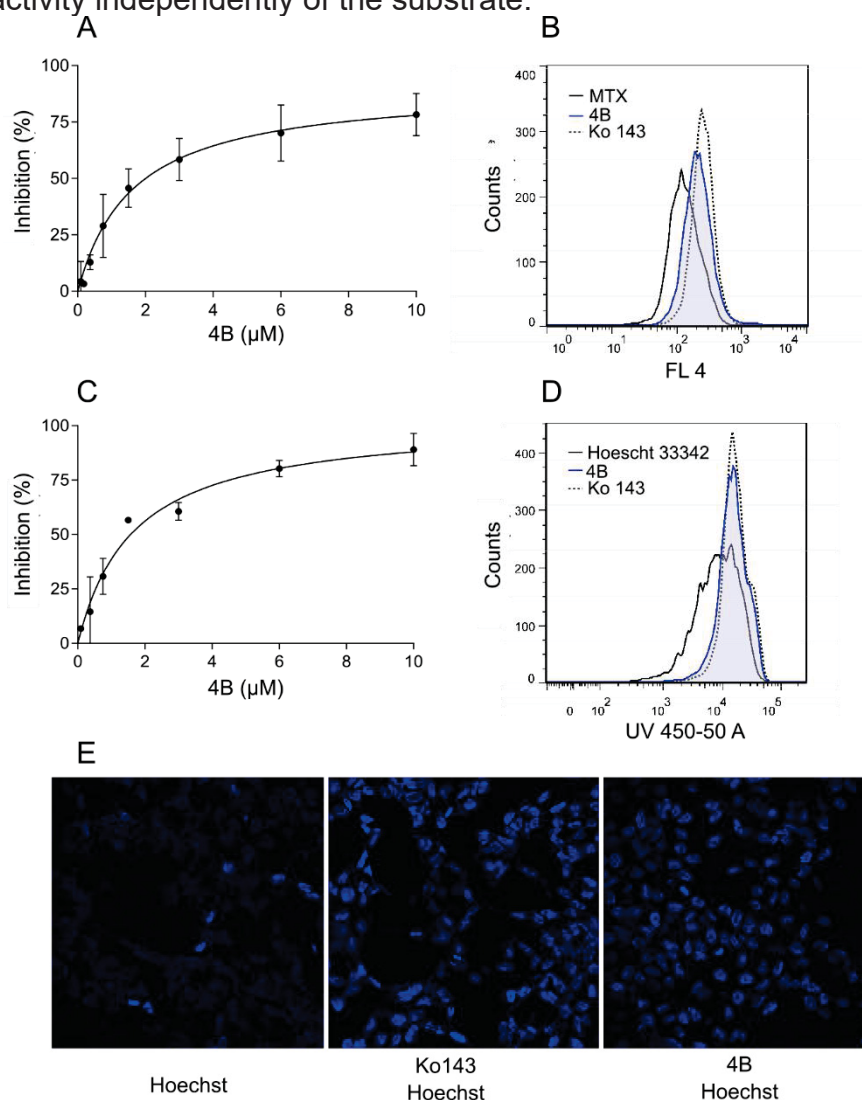


**Figure 3:** Inhibition curves of porphyrin **4B** and intracellular accumulation. (A) Mitoxantrone as substrate. (B) Histogram with mitoxantrone (MTX) 10  $\mu\text{M}$  (full line), Ko143 0.5  $\mu\text{M}$  (dotted line) and **4B** 10  $\mu\text{M}$  (blue histogram). (C) hoechst 33342 as substrate. (D) Histogram with hoechst 33342 3  $\mu\text{M}$  (full line), Ko143 0.5  $\mu\text{M}$  (dotted line) and **4B** 10  $\mu\text{M}$  (blue histogram). (E) Confocal microscopy using hoechst 33342 1  $\mu\text{M}$  as substrate and Ko143 0.5  $\mu\text{M}$  as reference inhibitor and **4B** at 10  $\mu\text{M}$ . The data represent at least two independent experiments.

The cytotoxicity profile comparing the effect of drugs in parental cells and cells overexpressing ABC transporters can provide valuable information about ABCG2-mediated cross-resistance. Also, this simple approach can also demonstrate a possible collateral sensitivity effect [55]. Considering that porphyrins are classic ABCG2 substrates, potential cross-resistance to **4B** was investigated using HEK293-wild type and HEK293-ABCG2 cells (Fig. 4A). The porphyrin **4B** was cytotoxic at high concentrations, which allowed to verify a cross-resistance effect. The cytotoxicity pattern was similar after 72 h of treatment for both the parental and ABCG2-overexpressing cell lines, demonstrating an absence of cross-resistance (Fig. 4A). This finding suggests that porphyrin **4B** is not transported by ABCG2.

To confirm the absence of transport, a cell washing assay was performed. HEK293-ABCG2 cells were exposed to mitoxantrone and **4B** at a saturating concentration (10  $\mu$ M) for 24 h. After the treatment, cells were washed with PBS to remove the porphyrin and mitoxantrone from the culture medium, and the transport assay was performed by flow cytometry after 1, 3 and 24 h. As shown in Fig. 3B, even after the removal of **4B** from culture medium for 24 h, the potency of inhibition was similar to reference inhibitor Ko143, supporting the hypothesis that **4B** is not transported by ABCG2 and also presents high affinity for ABCG2 (Fig. 4B).

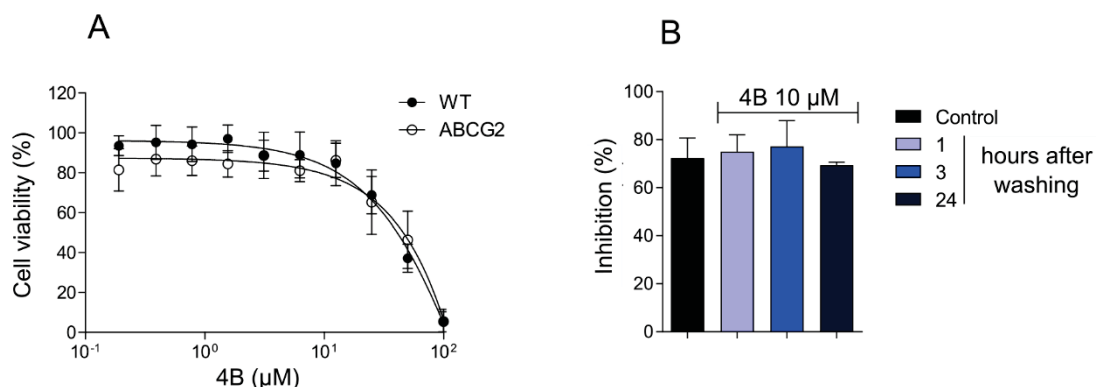


**Figure 4:** (A) Cell viability assay performed using the MTT method. HEK293-ABCG2 and Wild type were submitted to a long-term treatment (72 h) with an increasing concentration of **4B**. (B) Treatment with Ko143 (control – 30 min) porphyrin **4B** (blue bars - 24 h) followed by a washing step with PBS and incubation of the cells in absence of the porphyrin for 1, 3 and 24 h. Mitoxantrone was used as substrate. The data represent at least two independent experiments.

### 3.3 Mechanism of inhibition

The fact that we did not find evidence of ABCG2-mediated transport of **4B** suggests that the porphyrin binds to another region or site compared to hoechst 33342. To pursue this hypothesis, the type of inhibition was investigated using different concentrations of mitoxantrone or hoechst 33342 in combination with a dose response of **4B**. The data showed an increasing of  $V_{max}$  and  $K_m$  while inhibitor concentration increased (Fig. 5A-D), suggesting a mixed type of inhibition for both substrates, which was confirmed through Hanes-Woolf plot (Fig. S2).

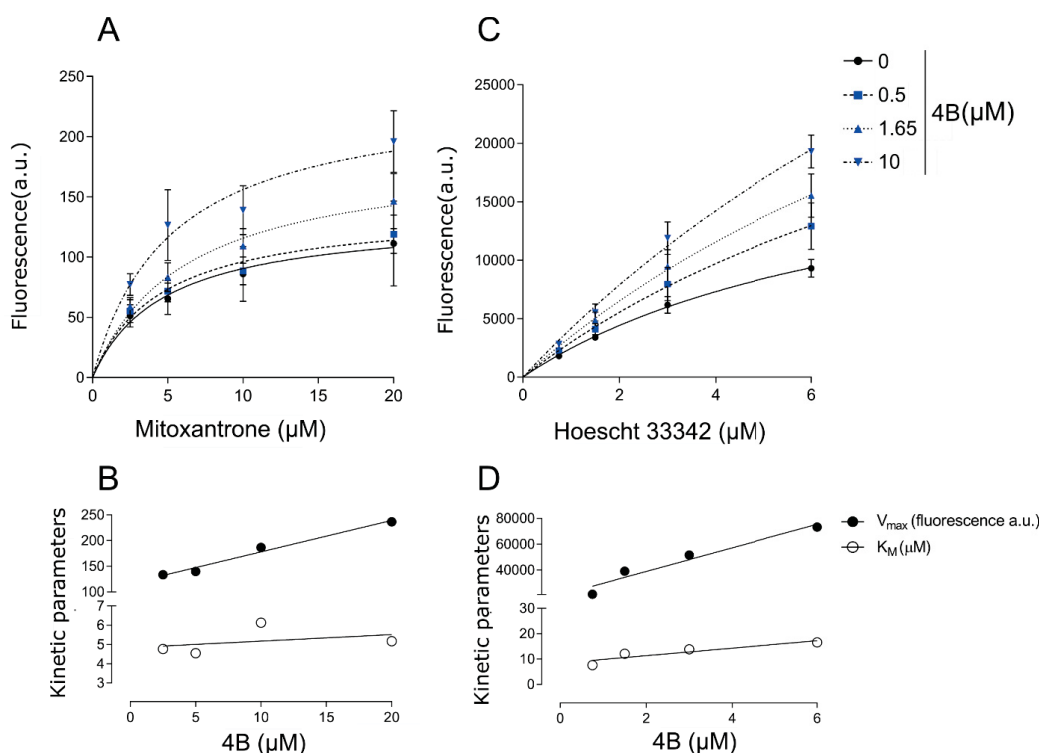


**Figure 5:** Kinetic behavior of ABCG2 with mitoxantrone (A) and hoechst 33342 (C). Comparison of  $V_{max}$  and  $K_m$  with different concentrations of **4B** with mitoxantrone (B) and hoechst 33342 (D).  $K_m$  and  $V_{max}$  were obtained from nonlinear regression from graphs A and C using GraphPad Prism v8.0.

The ATPase activity of ABC transporters is commonly stimulated by substrates and decreased by compounds that inhibit activity [56,57]. ATPase activity was evaluated after treatment with increasing concentrations of **4B** using total membranes from ABCG2-overexpressing High-Five insect cells. As shown in Fig. 6A, porphyrin **4B** produced a mild inhibition of the ATPase activity of ABCG2 (~20%). Another common feature of ABCG2 inhibitors is increased binding of the conformation-sensitive antibody 5D3, which recognizes an epitope in the extracellular loop of ABCG2. Porphyrin **4B** triggered a time-dependent increase of 5D3 binding (Fig. 6B). This increase was higher than the reference inhibitor Ko143 after 24 h of incubation (Fig. 6C and D). These data are in accordance with the time dependent inhibition observed in the initial screening (Table 1). Considering that the maximum inhibition was visualized only after 24 h of incubation, this result suggests that the porphyrin interaction causes important conformational changes to the transporter.

To confirm allosteric conformational changes induced by **4B**, a thermostability assay using total membranes from ABCG2-overexpressing High-Five insect cells was performed. In the absence of ATP, **4B** does not promote significant changes on  $IT_{50}$  values (Fig. 6E, F). On the other hand, in the presence of ATP, porphyrin **4B** decreased the  $IT_{50}$  value around 7°C compared to the control (DMSO), suggesting increased ABCG2 thermostability induced by conformational changes by **4B** binding.

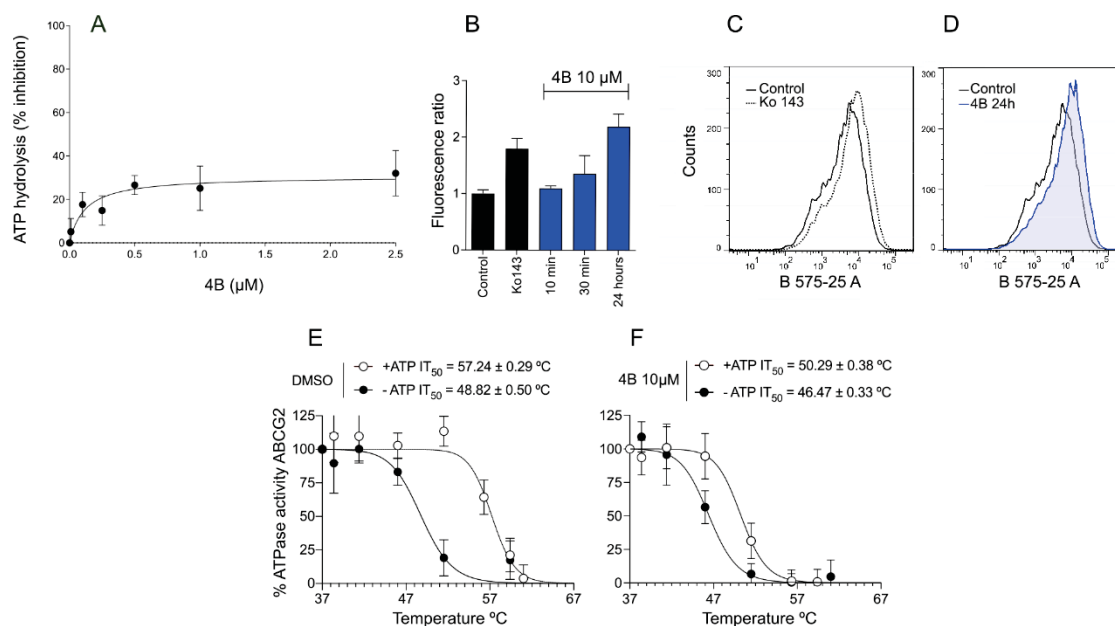


**Figure 6:** Allosteric changes triggered by **4B**. (A) ATPase activity performed with membranes of High-Five insect cells in the presence of porphyrin **4B**. (B) Conformational antibody binding in three different incubation times: 10, 30 min and 24 h with **4B** at 10 μM. The data was normalized by the untreated control. (C) Histogram from the conformational antibody showing the fluorescent shift between the untreated control and cells treated with Ko143 2 μM. (D) Histogram from conformational antibody showing the untreated control and 24 h in the presence of porphyrin **4B** (10 μM). (E) Thermostability assay in the absence of **4B** (F) and the presence of **4B**. The data represent at least two independent experiments.

### 3.4 Docking and molecular dynamics simulations

To explore potential binding modes of the porphyrin **4B** and compared with the substrate Pheophorbide *a* (PHEO), we performed molecular docking calculations in the cavity between subunits of the ABCG2 cryo-EM structure followed by long-timescale molecular dynamics (MD) simulations. Principal component analyses of our MD simulation trajectories (Fig. S3A) grouped the **4B** conformations into two closely related states, in contrast to PHEO, that showed three independent states. PCA suggests a single conformational state for the inhibitor previously analyzed MZ29, however, this could be a result of shorter sampling (Fig. S3A).

Upon simulation, compound **4B** has little change in position, being stabilized by the hydrogen bond interaction with Glu446(A) and water-mediated contacts with Asn436 (Fig. 7A, B and Fig. S3B). However, PHEO occupies different sites in the protein with an intermittent interaction with Glu446's from both chains and short contacts with Arg184 (Fig. 7A, C). Porphyrin **4B** and PHEO can occupy the space in between subunits establishing several different hydrophobic contacts (Fig. 7A). Interestingly, the substrate PHEO can fit in the site between subunits, near residues such as Phe439 (Fig. S3B, Fig. S4). The binding of **4B** and PHEO induces conformational changes in the TMD closing the gap between subunits as observed by the smaller average distance between Phe439 and increased per residue mobility in that region, as well as the connective linker between the TMD and NBD (Fig. S3B-D).



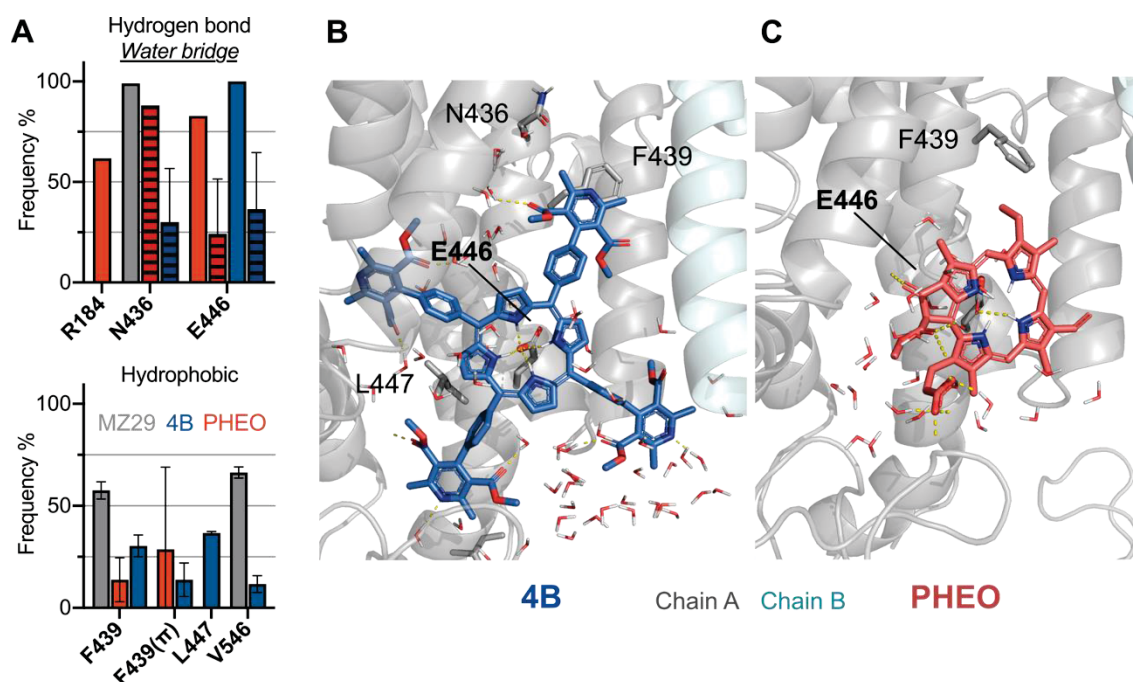


**Figure 7:** Frequency of hydrogen bonding interactions and hydrophobic interactions (A) observed along with the molecular dynamic simulation. Each bar represents the standard error of at least three independent simulations (1  $\mu$ s each, for 4B and PHEO, and 500 ns for MZ29). Snapshots of the last frames for molecular dynamic simulations of the (B) 4B inhibitor (blue) and the (C) PHEO substrate (red). ABCG2's residues are colored according to the atom type of the interacting amino-acid residues (protein's carbon, light grey (chain A) and pale green (chain B); oxygen, red; nitrogen, blue). Hydrogen bond interactions are represented by dashed yellow lines. MZ29 interaction profile was retrieved from the previous publication for comparison purposes.

### 3.5 Selectivity toward ABCG2 and chemosensitization

Despite the selectivity of porphyrins as ABCG2 substrates, the inhibition selectivity was evaluated comparing the effect of porphyrin **4B** on P-gp and MRP1, using rhodamine 123 and daunorubicin as substrates, respectively. Stably transfected cells overexpressing each one of these ABC transporters were used. As shown in Fig. 8A-D, **4B** selectively inhibited ABCG2 activity as it did not show any inhibition of P-gp and MRP1. This confirms that porphyrins are a class of compounds that exclusively affects the activity of ABCG2 transporter.

Finally, to verify the potential use of porphyrins as inhibitors in future pre-clinical models, an *in vitro* chemosensitization assay using transfected cells overexpressing ABCG2 was performed. Cells were treated with porphyrin **4B** and the active metabolite of irinotecan (SN-38), a chemotherapeutic transported by ABCG2. Cells overexpressing ABCG2 co-treated with **4B** and SN-38 displayed a  $EC_{50}$  value 7-fold lower than the resistant cells treated only with SN-38 (Fig. 8E and S3). In addition, the pattern observed of ABCG2 cells co-treated with **4B** and SN-38 was similar to wild-type cells treated only with SN-38, demonstrating a complete phenotype reversion (Fig. 8E).

The chemosensitization effect was additionally investigated in selected cancer cell lines that overexpresses ABCG2. The mitoxantrone selected H460-MX20 lung cancer and PANC-1MX100 pancreatic cancer cell lines were treated with SN-38 alone or in association with porphyrin **4B**. Cell viability were compared with parental cell lines H460 and PANC-1, also treated with SN-38. Co-treatment of H460-MX20 and PANC-1MX100 cells with porphyrin **4B** and SN-38 chemosensitized the cells to the same

level as observed with parental H460 and PANC-1 cells (Fig. 8F-G), confirming the results obtained using stably transfected cells and validating the use of **4B** in cancer cells.

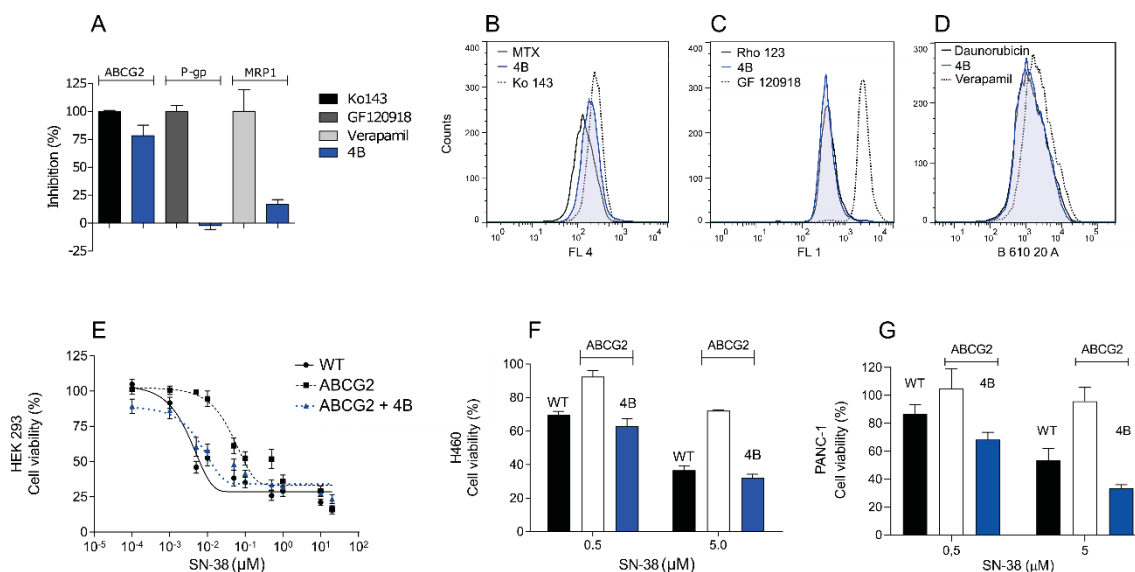


**Figure 8:** (A) Selectivity assay using stably transfected cell lineages for MRP1 (BHK21-*ABCC1*), P-gp (NIH3T3-*ABCB1*) and ABCG2 (HEK293-*ABCG2*). The cells were seeded in a 24 wells plate and treated with the porphyrin at 10  $\mu\text{M}$  for 24 hours. The substrates/inhibitors used for each lineage were mitoxantrone (MTX) 10  $\mu\text{M}$ /Ko143 0.5  $\mu\text{M}$  (ABCG2), rhodamine 123 5  $\mu\text{M}$ /GF120918 1  $\mu\text{M}$  (P-gp) and daunorubicin 10  $\mu\text{M}$ /verapamil 30  $\mu\text{M}$  (MRP1). The histogram of each condition is represented on figures B, C and D. (E) Chemo sensitization evaluation performed using HEK293-Wild type, HEK293-*ABCG2* (F) lung tumor cell lineage H460-Wild type and H460-MX20 (cultivated in the presence of Mitoxantrone) (G) and pancreatic tumor cell lineage PANC-1-Wild type and PANC-1-MX100 (cultivated in the presence of Mitoxantrone). The cells were seeded and treated with the porphyrin for 24 hours, following the addition of SN-38 as chemotherapy for more 48 hours in increasing concentrations. The evaluation of cell viability was made by MTT assay. The data represent at least two independent experiments.

## 4. DISCUSSION

Porphyrins and related compounds (like chlorins) have been recognized as specific ABCG2 substrates [19]. For this reason, the presence of ABCG2 in cancer cells does not impair only classical chemotherapy, but play an important role in another cancer treatment approach, the photodynamic therapy [58,59]. Here, we screened 19 porphyrins to verify their potential as specific inhibitors of ABCG2. Regarding porphyrinic substituents, the number and type displayed a counter-intuitive behavior: on the one hand, the presence of four pyridinic rings was favorable for inhibition, but a single pyridinic ring did not have any effect on ABCG2 activity. In contrast, four dihydropyridinic rings were unfavorable, and the presence of only one did promote inhibition. Considering the two best cases, the presence of four pyridinic rings was superior in inhibition than only one dihydropyridinic ring.

Porphyrin **4B** inhibited the ABCG2-mediated substrate transport with an  $\text{IC}_{50}$  value of 1.6  $\mu\text{M}$  using two different substrates, demonstrating a substrate independent inhibition (Fig. 3). Interestingly, **4B** contradicts the idea of porphyrins behaving as substrates, since **4B** was not transported by ABCG2 (Fig. 4A). This was also confirmed in a washout assay where no loss in transport inhibition was observed even 24 h after the removal of the inhibitor (Fig. 4B). This latter piece of data supports the idea that porphyrin **4B** seems to have a high affinity toward ABCG2.

To better understand the type of inhibition produced by porphyrin **4B**, a kinetic experiment was conducted. Using two different substrates, **4B** showed a mixed type of inhibition (Fig. 5 and S3). The porphyrin **4B** binds on the apo (substrate-free) protein and may produce conformational changes in the substrate binding site, decreasing the substrate affinity. The same type of inhibition was observed with pyridopyrimidines [43]. In contrast with some recently described ABCG2 inhibitors that stimulate the ATPase activity, such as indeno[1,2-*b*]indoles [60], pyridopyrimidines [43], Ulixertinib [61] acryloylphenylcarboxylates [62] and EGFR inhibitor Rociletinib [63], porphyrin **4B** mildly inhibited the ATPase activity (around 20%), when compared to Ko143 and MZ29, which completely inhibits the ATPase activity of ABCG2 [44,64].

In general, ABCG2 inhibitors increase the binding of the conformation-sensitive antibody 5D3 [65–67]. Porphyrin **4B** followed the same pattern, but in a time-dependent manner. This finding is in accordance with the transport inhibition results, which was also time-dependent, suggesting that conformational changes occur due to **4B** binding. The thermostability assay showed a significant decrease of protein stability in the presence of **4B** and ATP, since the  $IT_{50}$  decreased by approximately 7°C. This is similar to the effect triggered by the indeno[1,2-*b*]indoles on ABCG2, where a decrease of  $IT_{50}$  around 5°C was observed [60]. This result demonstrates that structural protein changes are induced by **4B** binding.

Molecular modelling was then employed to compare the potential binding mode of a porphyrinic substrate, pheophorbide *a* (PHEO), and the porphyrinic inhibitor identified in this work. Molecular docking suggests that PHEO could bind in three different regions in the ABCG2's central cavity (Fig. S3,4), while **4B** displayed one single conformation. Molecular dynamics simulations, in the timescale of few microseconds (Fig. S5), supported the stability of these binding modes, showing a strong ionic interaction between the charged nitrogen atom in the center of the porphyrinic ring and the Glu446. It is noteworthy that residue Glu446 is the only negatively charged residue facing the central cavity from TMH2.

The work from Khunweeraphong *et al.*, 2017 [68], suggests a mechanism where drugs entering the central cavity would be trapped by the interaction with Glu446. They also observed that E446K/A/D mutations disrupts the efflux of mitoxantrone, rhodamine 123 and hoechst 33342 [68,69], while retaining normal expression and membrane localization. Interestingly, the transport-incompetent E446D variant retains ATPase activity, which suggests that the side-chain size and potential interaction distances are relevant for the recognition. Our simulation data (Fig. 7 and S2,3B) suggests that **4B** closely interacts with Glu446, where PHEO has a larger variation in the distance interaction, which supports its substrate behavior. Recently, Kowal *et al.*, (2021) showed that substrate binding is more flexible than inhibitors, shifting in the binding cavity, using Cryo-EM structures [70].

When binding substrates, this increased flexibility was extended to the nucleotide-binding domains (NBDs), where multiple conformations could be observed [70]. The conformational change required for ATP hydrolysis occur in the NBDs and are conveyed to the TMDs via intracellular loop 1 (ICL1). Recent work proposes that while TMH2-E446 is involved in the trapping and recognition of inhibitors, the conformational changes in the NBDs are mediated by the Glu451 (localized in the ICL1) and therefore independent [71]. Additionally, our compounds showed an interaction with Arg184 (Fig. S4), which was more prominent with the **4B** inhibitor than in the PHEO substrate. Arg184 stabilizes the ATP in closed ABCG2 conformation, as observed in the CryoEM structure (PDB ID 6HBU) [72].

Transporter selectivity is a desirable feature in the design of new inhibitors [6,73]. Selectivity can mitigate collateral effects due to the interference on physiological processes and the pharmacokinetics of other drugs [74]. Porphyrin **4B** was selective toward ABCG2 (Fig. 8), confirming the selective interaction of porphyrins with ABCG2. In addition, the co-treatment of stably transfected cells and drug-selected resistant cells with **4B** and SN-38 successfully chemosensitized the cells to levels comparable to the parental cells, proving that porphyrin **4B** is an efficient inhibitor to circumvent multidrug resistance mediated by ABCG2.

In addition to playing a role in drug resistance, ABCG2 is expressed at various barrier sites such as the gut and has been shown to limit the oral bioavailability of substrate drugs [6,73]. In mouse models, coadministration of ABCG2 inhibitors such as elacridar has been shown to increase oral bioavailability of the ABCG2 substrate topotecan [75]. Additionally, coadministration of elacridar and topotecan has been shown to increase oral bioavailability of topotecan in humans in a clinical trial [76]. Thus, ABCG2 inhibitors such as **4B** may also be useful in increasing the oral bioavailability of chemotherapy agents in patients.

In summary, the conversion of substrate scaffold into inhibitors was already successfully employed; however, to the best of our knowledge, this is the first report that used a ABCG2 specific substrate core structure, the porphyrins, to identify new specific inhibitors. Interestingly, the best inhibitor, porphyrin **4B** was not transported by ABCG2 and successfully reversed the MDR phenotype. These findings will support and guide the development of new ABCG2 inhibitors based on porphyrinic scaffold for future pre-clinical studies.

**Acknowledgments:** The authors acknowledge CENAPD at UNICAMP, Brazil, and the CSC – IT Center for Science, Finland, for the generous computational resources. We also thank Attilio Di Pietro from IBCP and Dr. Susan Bates from NCI, NIH for having provided the cell lines.

**Funding:** This work was supported by CNPq (grant number 400953/2016-1) and Coordenação de Aperfeiçoamento de Pessoal de Nível Superior – Brasil (CAPES) (Finance code 001). RWR and SVA were supported by the Intramural Research Program of the National Institutes of Health, the national Cancer Institute, Center for Cancer Research.

## 5. REFERENCES

- [1] W. Li, H. Zhang, Y.G. Assaraf, K. Zhao, X. Xu, J. Xie, D.-H.H. Yang, Z.-S.S. Chen, Overcoming ABC transporter-mediated multidrug resistance: Molecular mechanisms and novel therapeutic drug strategies, *Drug Resist. Updat.* 27 (2016) 14–29. <https://doi.org/https://doi.org/10.1016/j.drug.2016.05.001>.
- [2] S.M. Stefan, Multi-target ABC transporter modulators: what next and where to go?, *Future Med. Chem.* 11 (2019) 2353–2358. <https://doi.org/10.4155/fmc-2019-0185>.
- [3] K. Miyake, L. Mickley, T. Litman, Z. Zhan, R. Robey, B. Cristensen, M. Brangi, L. Greenberger, M. Dean, T. Fojo, S.E. Bates, Molecular Cloning of cDNAs Which Are Highly Overexpressed in Mitoxantrone-resistant Cells, *Cancer Res.* 59 (1999) 8–13. <http://cancerres.aacrjournals.org/content/59/1/8.abstract>.
- [4] R. Allikmets, L.M. Schriml, A. Hutchinson, V. Romano-Spica, M. Dean, A human placenta-specific ATP-binding cassette gene (ABCP) on chromosome 4q22 that is involved in multidrug resistance, *Cancer Res.* 58 (1998) 5337–5339.
- [5] L.A. Doyle, W. Yang, L. V Abruzzo, T. Krogmann, Y. Gao, A.K. Rishi, D.D. Ross, A multidrug resistance transporter from human MCF-7 breast cancer cells., *Proc. Natl. Acad. Sci. U. S. A.* 95 (1998) 15665–15670. <https://doi.org/10.1073/pnas.95.26.15665>.

- [6] R.W. Robey, K.K.K. To, O. Polgar, M. Dohse, P. Fetsch, M. Dean, S.E. Bates, ABCG2: A perspective, *Adv. Drug Deliv. Rev.* 61 (2009) 3–13. <https://doi.org/10.1016/j.addr.2008.11.003>.
- [7] D. Hira, T. Terada, BCRP/ABCG2 and high-alert medications: Biochemical, pharmacokinetic, pharmacogenetic, and clinical implications, *Biochem. Pharmacol.* 147 (2018) 201–210. <https://doi.org/10.1016/j.bcp.2017.10.004>.
- [8] T. Litman, M. Brangi, E. Hudson, P. Fetsch, A. Abati, D.D. Ross, K. Miyake, J.H. Resau, S.E. Bates, The multidrug-resistant phenotype associated with overexpression of the new ABC half-transporter, MXR (ABCG2), *J. Cell Sci.* 113 (2000) 2011–2021. <https://doi.org/10.1242/jcs.113.11.2011>.
- [9] E.L. Volk, K.M. Farley, Y. Wu, F. Li, R.W. Robey, E. Schneider, Overexpression of Wild-Type Breast Cancer Resistance Protein Mediates Methotrexate Resistance, *Cancer Res.* 62 (2002) 5035–5040.
- [10] K. Nakatomi, M. Yoshikawa, M. Oka, Y. Ikegami, S. Hayasaka, K. Sano, K. Shiozawa, S. Kawabata, H. Soda, T. Ishikawa, S. Tanabe, S. Kohno, Transport of 7-Ethyl-10-hydroxycamptothecin (SN-38) by Breast Cancer Resistance Protein ABCG2 in Human Lung Cancer Cells, *Biochem. Biophys. Res. Commun.* 288 (2001) 827–832. <https://doi.org/https://doi.org/10.1006/bbrc.2001.5850>.
- [11] R.W. Robey, K. Steadman, O. Polgar, K. Morisaki, M. Blayney, P. Mistry, S.E. Bates, Pheophorbide a is a Specific Probe for ABCG2 Function and Inhibition, *Cancer Res.* 64 (2004) 1242–1246. <https://doi.org/10.1158/0008-5472.CAN-03-3298>.
- [12] S. Zhou, J.D. Schuetz, K.D. Bunting, A.M. Colapietro, J. Sampath, J.J. Morris, I. Lagutina, G.C. Grosveld, M. Osawa, H. Nakauchi, B.P. Sorrentino, The ABC transporter Bcrp1/ABCG2 is expressed in a wide variety of stem cells and is a molecular determinant of the side-population phenotype., *Nat. Med.* 7 (2001) 1028–1034. <https://doi.org/10.1038/nm0901-1028>.
- [13] L. Yang, P. Shi, G. Zhao, J. Xu, W. Peng, J. Zhang, G. Zhang, X. Wang, Z. Dong, F. Chen, H. Cui, Targeting cancer stem cell pathways for cancer therapy, *Signal Transduct. Target. Ther.* 5 (2020) 8. <https://doi.org/10.1038/s41392-020-0110-5>.
- [14] M.A. Goodell, K. Brose, G. Paradis, A.S. Conner, R.C. Mulligan, Isolation and functional properties of murine hematopoietic stem cells that are replicating in vivo., *J. Exp. Med.* 183 (1996) 1797–1806. <https://doi.org/10.1084/jem.183.4.1797>.
- [15] J. Zhao, Cancer stem cells and chemoresistance: The smartest survives the raid, *Pharmacol. Ther.* 160 (2016) 145–158. <https://doi.org/https://doi.org/10.1016/j.pharmthera.2016.02.008>.
- [16] E. Desuzinges-Mandon, O. Arnaud, L. Martinez, F. Huché, A. Di Pietro, P. Falson, ABCG2 transports and transfers heme to albumin through its large extracellular loop, *J. Biol. Chem.* 285 (2010) 33123–33133. <https://doi.org/10.1074/jbc.M110.139170>.
- [17] P. Wang, M. Sachar, J. Lu, A.I. Shehu, J. Zhu, J. Chen, K. Liu, K.E. Anderson, W. Xie, F.J. Gonzalez, C.D. Klaassen, X. Ma, The essential role of the transporter ABCG2 in the pathophysiology of erythropoietic protoporphyria, *Sci. Adv.* 5 (2019) 1–9. <https://doi.org/10.1126/sciadv.aaw6127>.
- [18] J.W. Jonker, M. Buitelaar, E. Wagenaar, M.A. Van der Valk, G.L. Scheffer, R.J. Scheper, T. Plösch, F. Kuipers, R.P.J. Oude Elferink, H. Rosing, J.H. Beijnen, A.H. Schinkel, T. Plosch, F. Kuipers, R.P.J.O. Elferink, H. Rosing, J.H. Beijnen, A.H. Schinkel, The breast cancer resistance protein protects against a major chlorophyll-derived dietary phototoxin and protoporphyria, *Proc. Natl. Acad. Sci. U. S. A.* 99 (2002) 15649–15654. <https://doi.org/10.1073/pnas.202607599>.
- [19] R.W. Robey, K. Steadman, O. Polgar, S.E. Bates, ABCG2-mediated transport of photosensitizers: Potential impact on photodynamic therapy, *Cancer Biol. Ther.* 4 (2005) 187–194. <https://doi.org/10.4161/cbt.4.2.1440>.
- [20] J. Usuda, Y. Tsunoda, S. Ichinose, T. Ishizumi, K. Ohtani, Lung Cancer Breast cancer resistant protein (BCRP) is a molecular determinant of the outcome of photodynamic therapy (PDT) for centrally located early lung cancer, 67 (2010) 198–204. <https://doi.org/10.1016/j.lungcan.2009.04.002>.
- [21] N. Kawai, Y. Hirohashi, Y. Ebihara, T. Saito, A. Murai, T. Saito, T. Shirotsuki, T. Kubo, M. Nakatsugawa, T. Kanaseki, T. Tsukahara, T. Shichinohe, L. Li, S. Hirano, T. Torigoe, ABCG2 expression is related to low 5-ALA photodynamic diagnosis (PDD) efficacy and cancer stem cell phenotype, and suppression of ABCG2 improves the efficacy of PDD, *PLoS One.* 14 (2019) 1–15. <https://doi.org/10.1371/journal.pone.0216503>.
- [22] Z.Y. Xu, K. Wang, X.Q. Li, S. Chen, J.M. Deng, Y. Cheng, Z.G. Wang, The ABCG2 transporter is a key molecular determinant of the efficacy of sonodynamic therapy with Photofrin in glioma stem-like cells, *Ultrasonics.* 53 (2013) 232–238. <https://doi.org/10.1016/j.ultras.2012.06.005>.
- [23] J. Usuda, S. Ichinose, T. Ishizumi, K. Ohtani, T. Inoue, S. Maehara, K. Imai, K. Shima, T. Ohira,

- H. Kato, N. Ikeda, A.S. Ichinose, T. Ishizumi, K. Ohtani, T. Inoue, S. Maehara, Molecular determinants of photodynamic therapy for lung cancers, *Lasers Surg. Med.* 599 (2011) 591–599. <https://doi.org/10.1002/lsm.21097>.
- [24] L.N. Eadie, T.P. Hughes, D.L. White, Interaction of the Efflux Transporters ABCB1 and ABCG2 With Imatinib, Nilotinib, and Dasatinib, *Clin. Pharmacol. Ther.* 95 (2014) 294–306. <https://doi.org/10.1038/clpt.2013.208>.
- [25] S. Shukla, A.P. Skoumbourdis, M.J. Walsh, A.M.S. Hartz, K.L. Fung, C. Wu, M.M. Gottesman, C.J. Thomas, S. V. Ambudkar, Synthesis and Characterization of a BODIPY Conjugate of the BCR-ABL Kinase Inhibitor Tassigna (Nilotinib): Evidence for Transport of Tassigna and Its Fluorescent Derivative by ABC Drug Transporters, *Mol. Pharm.* (2011) 1292–1302. <https://doi.org/10.1021/mp2001022>.
- [26] Y. Inoue, T. Morita, M. Onozuka, K.-I. Saito, K. Sano, K. Hanada, M. Kondo, Y. Nakamura, T. Kishino, H. Nakagawa, Y. Ikegami, Impact of Q141K on the Transport of Epidermal Growth Factor Receptor Tyrosine Kinase Inhibitors by ABCG2., *Cells.* 8 (2019) 1–12. <https://doi.org/10.3390/cells8070763>.
- [27] G. Valdameri, L. Pereira Rangel, C. Spatafora, J. Guitton, C. Gauthier, O. Arnaud, A. Ferreira-Pereira, P. Falson, S.M.B. Winnischofer, M.E.M. Rocha, C. Tringali, A. Di Pietro, Methoxy Stilbenes as Potent, Specific, Untransported, and Noncytotoxic Inhibitors of Breast Cancer Resistance Protein, *ACS Chem. Biol.* 7 (2012) 322–330. <https://doi.org/10.1021/cb200435y>.
- [28] P. Breedveld, D. Pluim, G. Cipriani, F. Dahlhaus, M.A.J. van Eijndhoven, C.J.F. de Wolf, A. Kuil, J.H. Beijnen, G.L. Scheffer, G. Jansen, P. Borst, J.H.M. Schellens, The Effect of Low pH on Breast Cancer Resistance Protein (ABCG2)-Mediated Transport of Methotrexate, 7-Hydroxymethotrexate, Methotrexate Diglutamate, Folic Acid, Mitoxantrone, Topotecan, and Resveratrol in In Vitro Drug Transport Models, *Mol. Pharmacol.* 71 (2007) 240 LP – 249. <https://doi.org/10.1124/mol.106.028167>.
- [29] H.C. Cooray, T. Janvilisri, H.W. van Veen, S.B. Hladky, M.A. Barrand, Interaction of the breast cancer resistance protein with plant polyphenols., *Biochem. Biophys. Res. Commun.* 317 (2004) 269–275. <https://doi.org/10.1016/j.bbrc.2004.03.040>.
- [30] P. Kannan, S. Telu, S. Shukla, S. V. Ambudkar, V.W. Pike, C. Halldin, M.M. Gottesman, R.B. Innis, M.D. Hall, The “specific” P-glycoprotein inhibitor tariquidar is also a substrate and an inhibitor for Breast Cancer Resistance Protein (BCRP/ABCG2), *ACS Chem. Neurosci.* 2 (2011) 82–89. <https://doi.org/10.1021/cn100078a>.
- [31] R.W. Robey, K. Steadman, O. Polgar, K. Morisaki, M. Blayney, P. Mistry, S.E. Bates, Pheophorbide a is a Specific Probe for ABCG2 Function and Inhibition, *Cancer Res.* 64 (2004) 1242–1246. <https://doi.org/10.1158/0008-5472.CAN-03-3298>.
- [32] S. Bauer, C. Ochoa-Puentes, Q. Sun, M. Bause, G. Bernhardt, B. König, A. Buschauer, Quinoline carboxamide-type ABCG2 modulators: Indole and quinoline moieties as anilide replacements, *ChemMedChem.* 8 (2013) 1773–1778. <https://doi.org/10.1002/cmdc.201300319>.
- [33] C. Ochoa-Puentes, S. Bauer, M. Kühnle, G.G. Bernhardt, A. Buschauer, B. König, M. Kühnle, G.G. Bernhardt, A. Buschauer, B. König, Benzanilide-biphenyl replacement: A bioisosteric approach to quinoline carboxamide-type ABCG2 modulators, *ACS Med. Chem. Lett.* 4 (2013) 393–396. <https://doi.org/10.1021/ml4000832>.
- [34] A. Pick, W. Klinkhammer, M. Wiese, Specific inhibitors of the breast cancer resistance protein (BCRP), *ChemMedChem.* 5 (2010) 1498–1505. <https://doi.org/10.1002/cmdc.201000216>.
- [35] M. Kühnle, M. Egger, C. Müller, A. Mahringer, G. Bernhardt, G. Fricker, B. König, A. Buschauer, Potent and selective inhibitors of breast cancer resistance protein (ABCG2) derived from the p-glycoprotein (ABCB1) modulator tariquidar, *J. Med. Chem.* 52 (2009) 1190–1197. <https://doi.org/10.1021/jm8013822>.
- [36] C.O. Puentes, P. Höcherl, M. Kühnle, S. Bauer, K. Bürger, G. Bernhardt, A. Buschauer, B. König, Solid phase synthesis of tariquidar-related modulators of ABC transporters preferring breast cancer resistance protein (ABCG2), *Bioorganic Med. Chem. Lett.* 21 (2011) 3654–3657. <https://doi.org/10.1016/j.bmcl.2011.04.094>.
- [37] J.C.C. Dallagnol, D.R.B. Ducatti, S.M.W. Barreira, M.D. Nosedá, M.E.R. Duarte, A.G. Gonçalves, Synthesis of porphyrin glycoconjugates bearing thiourea, thiocarbamate and carbamate connecting groups: Influence of the linker on chemical and photophysical properties, *Dye. Pigment.* 107 (2014) 69–80. <https://doi.org/10.1016/j.dyepig.2014.03.029>.
- [38] A.M. Slomp, S.M.W. Barreira, L.Z.B. Carrenho, C.C. Vandresen, I.F. Zattoni, S.M.S. Ló, J.C.C. Dallagnol, D.R.B. Ducatti, A. Orsato, M.E.R. Duarte, M.D. Nosedá, M.F. Otuki, A.G. Gonçalves, Photodynamic effect of meso - (aryl) porphyrins and meso - (1-methyl-4-pyridinium) porphyrins on HaCaT keratinocytes, *Bioorg. Med. Chem. Lett.* 27 (2017) 156–161.

- <https://doi.org/10.1016/j.bmcl.2016.11.094>.
- [39] S.M.S. Ló, D.R.B. Ducatti, M.E.R. Duarte, S.M.W. Barreira, M.D. Nosedá, A.G. Gonçalves, Synthesis of meso-tetraarylporphyrins using SeO<sub>2</sub> as oxidant, *Tetrahedron Lett.* 52 (2011) 1441–1443. <https://doi.org/10.1016/j.tetlet.2011.01.044>.
- [40] C.M.A. Alonso, M.G.P.M.S. Neves, A.C. Tomé, A.M.S. Silva, J.A.S. Cavaleiro, Reaction of (2-amino-5,10,15,20-tetraphenylporphyrinato)nickel(II) with quinones, *Tetrahedron.* 61 (2005) 11866–11872. <https://doi.org/10.1016/j.tet.2005.09.080>.
- [41] L.D. Guanaes, M.M. Guimarães, D.R.B. Ducatti, M.E.R. Duarte, S.M.W. Barreira, M.D. Nosedá, A.G. Gonçalves, Synthesis and photophysical evaluation of meso-phenyl-1,4-dihydropyridine and pyridine-porphyrin hybrids, *Chem. Heterocycl. Compd.* In press (2021).
- [42] S. V Ambudkar, Drug-stimulatable ATPase activity in crude membranes of human MDR1-transfected mammalian cells., *Methods Enzymol.* 292 (1998) 504–514. [https://doi.org/10.1016/s0076-6879\(98\)92039-0](https://doi.org/10.1016/s0076-6879(98)92039-0).
- [43] M.K. Krapf, J. Gallus, S. Vahdati, M. Wiese, New Inhibitors of Breast Cancer Resistance Protein (ABCG2) Containing a 2,4-Disubstituted Pyridopyrimidine Scaffold, *J. Med. Chem.* 61 (2018) 3389–3408. <https://doi.org/10.1021/acs.jmedchem.7b01012>.
- [44] S.M. Jackson, I. Manolaridis, J. Kowal, M. Zechner, N.M.I. Taylor, M. Bause, S. Bauer, R. Bartholomaeus, G. Bernhardt, B. Koenig, A. Buschauer, H. Stahlberg, K.H. Altmann, K.P. Locher, Structural basis of small-molecule inhibition of human multidrug transporter ABCG2, *Nat. Struct. Mol. Biol.* 25 (2018) 333–340. <https://doi.org/10.1038/s41594-018-0049-1>.
- [45] G.M. Sastry, M. Adzhigirey, T. Day, R. Annabhimoju, W. Sherman, Protein and ligand preparation: parameters, protocols, and influence on virtual screening enrichments., *J. Comput. Aided. Mol. Des.* 27 (2013) 221–234. <https://doi.org/10.1007/s10822-013-9644-8>.
- [46] M.P. Jacobson, D.L. Pincus, C.S. Rapp, T.J.F. Day, B. Honig, D.E. Shaw, R.A. Friesner, A hierarchical approach to all-atom protein loop prediction., *Proteins.* 55 (2004) 351–367. <https://doi.org/10.1002/prot.10613>.
- [47] J.C. Shelley, A. Cholleti, L.L. Frye, J.R. Greenwood, M.R. Timlin, M. Uchimaya, Epik: a software program for pK( a ) prediction and protonation state generation for drug-like molecules., *J. Comput. Aided. Mol. Des.* 21 (2007) 681–691. <https://doi.org/10.1007/s10822-007-9133-z>.
- [48] K. Roos, C. Wu, W. Damm, M. Reboul, J.M. Stevenson, C. Lu, M.K. Dahlgren, S. Mondal, W. Chen, L. Wang, R. Abel, R.A. Friesner, E.D. Harder, OPLS3e: Extending Force Field Coverage for Drug-Like Small Molecules, *J. Chem. Theory Comput.* 15 (2019) 1863–1874. <https://doi.org/10.1021/acs.jctc.8b01026>.
- [49] R.A. Friesner, J.L. Banks, R.B. Murphy, T.A. Halgren, J.J. Klicic, D.T. Mainz, M.P. Repasky, E.H. Knoll, M. Shelley, J.K. Perry, D.E. Shaw, P. Francis, P.S. Shenkin, Glide: A New Approach for Rapid, Accurate Docking and Scoring. 1. Method and Assessment of Docking Accuracy, *J. Med. Chem.* 47 (2004) 1739–1749. <https://doi.org/10.1021/jm0306430>.
- [50] T.A. Halgren, R.B. Murphy, R.A. Friesner, H.S. Beard, L.L. Frye, W.T. Pollard, J.L. Banks, Glide: a new approach for rapid, accurate docking and scoring. 2. Enrichment factors in database screening., *J. Med. Chem.* 47 (2004) 1750–1759. <https://doi.org/10.1021/jm030644s>.
- [51] W. Sherman, T. Day, M.P. Jacobson, R.A. Friesner, R. Farid, Novel Procedure for Modeling Ligand/Receptor Induced Fit Effects, *J. Med. Chem.* 49 (2006) 534–553. <https://doi.org/10.1021/jm050540c>.
- [52] K.J. Bowers, E. Chow, H. Xu, R.O. Dror, M.P. Eastwood, B.A. Gregersen, J.L. Klepeis, I. Kolossvary, M.A. Moraes, F.D. Sacerdoti, J.K. Salmon, Y. Shan, D.E. Shaw, Scalable Algorithms for Molecular Dynamics Simulations on Commodity Clusters, in: *Proc. 2006 ACM/IEEE Conf. Supercomput.*, Association for Computing Machinery, New York, NY, USA, 2006: pp. 84–es. <https://doi.org/10.1145/1188455.1188544>.
- [53] E. Harder, W. Damm, J. Maple, C. Wu, M. Reboul, J.Y. Xiang, L. Wang, D. Lupyán, M.K. Dahlgren, J.L. Knight, J.W. Kaus, D.S. Cerutti, G. Krilov, W.L. Jorgensen, R. Abel, R.A. Friesner, OPLS3: A Force Field Providing Broad Coverage of Drug-like Small Molecules and Proteins, *J. Chem. Theory Comput.* 12 (2016) 281–296. <https://doi.org/10.1021/acs.jctc.5b00864>.
- [54] L.C. Vesga, T. Kronenberger, A.K. Tonduru, D.H. Kita, I.F. Zattoni, C.C. Bernal, A.R.R. Bohórquez, S.C. Mendez-Sánchez, S. V Ambudkar, G. Valdameri, A. Poso, Tetrahydroquinoline/4,5-dihydroisoxazole molecular hybrids as novel inhibitors of Breast Cancer Resistance Protein (BCRP/ABCG2)., *ChemMedChem.* (2021). <https://doi.org/10.1002/cmdc.202100188>.
- [55] M.D. Hall, M.D. Handley, M.M. Gottesman, Is resistance useless? Multidrug resistance and collateral sensitivity, *Trends Pharmacol. Sci.* 30 (2009) 546–556. <https://doi.org/10.1016/j.tips.2009.07.003>.

- [56] H. Glavinas, E. Kis, Á. Pál, R. Kovács, M. Jani, E. Vági, É. Molnár, S. Bánsághi, Z. Kele, T. Janáky, G. Báthori, O. von Richter, G.-J.J. Koomen, P. Krajcsi, ABCG2 (Breast Cancer Resistance Protein/Mitoxantrone Resistance-Associated Protein) ATPase Assay: A Useful Tool to Detect Drug-Transporter Interactions, *Drug Metab. Dispos.* 35 (2007) 1533–1542. <https://doi.org/10.1124/dmd.106.014605>.
- [57] C. Özvegy, T. Litman, G. Szakács, Z. Nagy, S. Bates, A. Váradi, B. Sarkadi, Functional Characterization of the Human Multidrug Transporter, ABCG2, Expressed in Insect Cells, *Biochem. Biophys. Res. Commun.* 285 (2001) 111–117. <https://doi.org/https://doi.org/10.1006/bbrc.2001.5130>.
- [58] P. Müller, S.A. Abdel, W. Zimmermann, R. Wittig, H. Stepp, S.A. Abdel Gaber, W. Zimmermann, R. Wittig, H. Stepp, ABCG2 influence on the efficiency of photodynamic therapy in glioblastoma cells, *J. Photochem. Photobiol. B Biol.* 210 (2020) 111963. <https://doi.org/10.1016/j.jphotobiol.2020.111963>.
- [59] J.H. Kim, J.M. Park, Y.J. Roh, I.W. Kim, T. Hasan, M.G. Choi, Enhanced efficacy of photodynamic therapy by inhibiting ABCG2 in colon cancers, *BMC Cancer.* 15 (2015) 1–9. <https://doi.org/10.1186/s12885-015-1514-4>.
- [60] D.H. Kita, N. Guragossian, I.F. Zattoni, V.R. Moure, F.G. de M. Rego, S. Lusvardi, T. Moulenat, B. Belhani, G. Picheth, S. Bouacida, Z. Bouaziz, C. Marminon, M. Berredjem, J. Jose, M.B. Gonçalves, S. V. Ambudkar, G. Valdameri, M. Le Borgne, Mechanistic basis of breast cancer resistance protein inhibition by new indeno[1,2-b]indoles, *Sci. Rep.* 11 (2021) 1788. <https://doi.org/10.1038/s41598-020-79892-w>.
- [61] N. Ji, Y. Yang, Z. Lei, C. Cai, J. Wang, P. Gupta, Ulixertinib ( BVD-523 ) antagonizes ABCB1- and ABCG2-mediated chemotherapeutic drug resistance, *Biochem. Pharmacol.* 158 (2018) 274–285. <https://doi.org/10.1016/j.bcp.2018.10.028>.
- [62] S. Kraege, K. Stefan, S.C. Köhler, M. Wiese, Optimization of Acryloylphenylcarboxamides as Inhibitors of ABCG2 and Comparison with Acryloylphenylcarboxylates, *ChemMedChem.* 11 (2016) 2547–2558. <https://doi.org/10.1002/cmdc.201600455>.
- [63] F. Zeng, F. Wang, Z. Zheng, Z. Chen, K.K. Wah To, H. Zhang, Q. Han, L. Fu, Rociletinib (CO-1686) enhanced the efficacy of chemotherapeutic agents in ABCG2-overexpressing cancer cells in vitro and in vivo, *Acta Pharm. Sin. B.* 10 (2020) 799–811. <https://doi.org/https://doi.org/10.1016/j.apsb.2020.01.008>.
- [64] L.D. Weidner, S.S. Zoghbi, S. Lu, S. Shukla, S. V. Ambudkar, V.W. Pike, J. Mulder, M.M. Gottesman, R.B. Innis, M.D. Hall, The inhibitor Ko143 is not specific for ABCG2, *J. Pharmacol. Exp. Ther.* 354 (2015) 384–393. <https://doi.org/10.1124/jpet.115.225482>.
- [65] Á. Telbisz, C. Hegedüs, C. Özvegy-Laczka, K. Goda, G. Várady, Z. Takáts, E. Szabó, B.P. Sorrentino, A. Váradi, B. Sarkadi, Antibody binding shift assay for rapid screening of drug interactions with the human ABCG2 multidrug transporter, *Eur. J. Pharm. Sci.* 45 (2012) 101–109. <https://doi.org/https://doi.org/10.1016/j.ejps.2011.10.021>.
- [66] C. Özvegy-Laczka, G. Várady, G. Köblös, O. Ujhelly, J. Cervenak, J.D. Schuetz, B.P. Sorrentino, G.J. Koomen, A. Váradi, K. Német, B. Sarkadi, Function-dependent conformational changes of the ABCG2 multidrug transporter modify its interaction with a monoclonal antibody on the cell surface, *J. Biol. Chem.* 280 (2005) 4219–4227. <https://doi.org/10.1074/jbc.M411338200>.
- [67] C.J. Henrich, R.W. Robey, H.R. Bokesch, S.E. Bates, S. Shukla, S. V. Ambudkar, M. Dean, J.B. McMahon, New inhibitors of ABCG2 identified by high-throughput screening, *Mol. Cancer Ther.* 6 (2007) 3271–3278. <https://doi.org/10.1158/1535-7163.MCT-07-0352>.
- [68] N. Khunweeraphong, T. Stockner, K. Kuchler, The structure of the human ABC transporter ABCG2 reveals a novel mechanism for drug extrusion, *Sci. Rep.* 7 (2017) 13767. <https://doi.org/10.1038/s41598-017-11794-w>.
- [69] M. Miwa, S. Tsukahara, E. Ishikawa, S. Asada, Y. Imai, Y. Sugimoto, Single amino acid substitutions in the transmembrane domains of breast cancer resistance protein (BCRP) alter cross resistance patterns in transfectants., *Int. J. Cancer.* 107 (2003) 757–763. <https://doi.org/10.1002/ijc.11484>.
- [70] J. Kowal, D. Ni, S.M. Jackson, I. Manolaridis, H. Stahlberg, K.P. Locher, Structural Basis of Drug Recognition by the Multidrug Transporter ABCG2, *J. Mol. Biol.* 433 (2021) 166980. <https://doi.org/https://doi.org/10.1016/j.jmb.2021.166980>.
- [71] N. Khunweeraphong, K. Kuchler, The first intracellular loop is essential for the catalytic cycle of the human ABCG2 multidrug resistance transporter, *FEBS Lett.* 594 (2020) 4059–4075. <https://doi.org/10.1002/1873-3468.13994>.
- [72] I. Manolaridis, S.M. Jackson, N.M.I. Taylor, J. Kowal, H. Stahlberg, K.P. Locher, Cryo-EM structures of a human ABCG2 mutant trapped in ATP-bound and substrate-bound states, *Nature.*



- 563 (2018) 426–430. <https://doi.org/10.1038/s41586-018-0680-3>.
- [73] M.L.H. Vlaming, J.S. Lagas, A.H. Schinkel, Physiological and pharmacological roles of ABCG2 (BCRP): Recent findings in Abcg2 knockout mice, *Adv. Drug Deliv. Rev.* 61 (2009) 14–25. <https://doi.org/https://doi.org/10.1016/j.addr.2008.08.007>.
- [74] E. Teodori, S. Dei, C. Martelli, S. Scapecchi, F. Gualtieri, The Functions and Structure of ABC Transporters: Implications for the Design of New Inhibitors of Pgp and MRP1 to Control Multidrug Resistance (MDR), *Curr. Drug Targets.* 7 (2006) 893–909. <https://doi.org/10.2174/138945006777709520>.
- [75] J.W. Jonker, J.W. Smit, R.F. Brinkhuis, M. Maliepaard, J.H. Beijnen, J.H. Schellens, A.H. Schinkel, Role of breast cancer resistance protein in the bioavailability and fetal penetration of topotecan., *J. Natl. Cancer Inst.* 92 (2000) 1651–1656. <https://doi.org/10.1093/jnci/92.20.1651>.
- [76] C.M.F. Kruijtzter, J.H. Beijnen, H. Rosing, W.W. ten Bokkel Huinink, M. Schot, R.C. Jewell, E.M. Paul, J.H.M. Schellens, Increased oral bioavailability of topotecan in combination with the breast cancer resistance protein and P-glycoprotein inhibitor GF120918., *J. Clin. Oncol. Off. J. Am. Soc. Clin. Oncol.* 20 (2002) 2943–2950. <https://doi.org/10.1200/JCO.2002.12.116>.

## CHAPTER 2 - SYNTHESIS AND BIOLOGICAL EVALUATION OF HETERODIMERS ON ABCG2 ACTIVITY

This chapter describes the work developed during PhD exchange period on Université Grenoble-Alpes – France during November/2019 – October/2020 under the supervision of Prof<sup>o</sup> Dr. Ahcène Boumendjel on chemical synthesis. The biological experiments were performed in Brazil under the supervision of Prof<sup>o</sup> Dr. Glaucio Valdameri.

### INTRODUCTION

Pheophorbide *a* is a chlorin known as a specific ABCG2 substrate and the synthesis is well described [1,2]. The chemical structure of this compound is related to porphyrins, differing only on the absence of one insaturation at pyrrolic ring (figure 1) [3]. This class of compounds is called chlorins, present on natural compounds, such as chlorophyll [4,5]. Similarly to pheophorbide *a*, the porphyrinic heme group also showed important interactions with ABCG2, more specifically with ECL3 loop, located on extracellular domains of ABCG2 [6]. Because of these interactions, new porphyrin-related compounds were tested and the results are shown on Chapter 1, where porphyrin **4B** was described as the first porphyrin-based ABCG2 inhibitor.

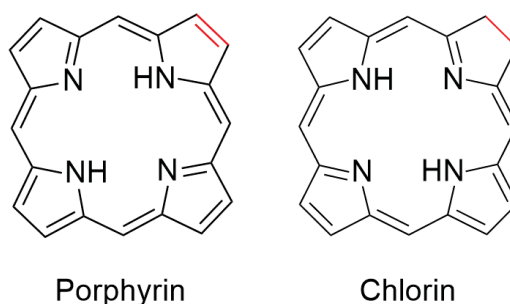


**Figure 1:** Difference on Porphyrin and chlorine structure.

To improve **4B** potency on ABCG2, we decided to combine the **4B** structure with another potent ABCG2 inhibitor from a different chemical class, forming a heterodimer. A chalcone derivative, chalcone 38, previously published by Valdameri et al (2012) was chosen for this purpose, due their high affinity toward ABCG2 and the high therapeutic ratio [7]. Additionally, to explore the effect of heterodimers containing porphyrins on ABCG2, we also proposed the combination between the ABCG2 substrate pheophorbide *a* and chalcone 38. Thus, synthetic routes were proposed to bind porphyrin **4B** and pheophorbide *a* to chalcone 38.

Another important molecule that interacts with ABCG2 is cholesterol. In placental tissue, ABCG2 can be found on lipid rafts, a region on cellular membrane rich on cholesterol [8]. ABCG2 efflux depends on lipid rafts integrity since the decrease of cholesterol on cellular environment decreases substantially ABCG2 activity. However, the precise mechanism of this influence is not clear [8,9]. Regarding ATPase activity on ABCG2, cholesterol plays a major role. ATPase activity is directly related with cholesterol concentration on cell membrane, since an increase of the ATPase

activity is observed with cholesterol enrichment. The opposite is found with low levels of cholesterol [10,11].

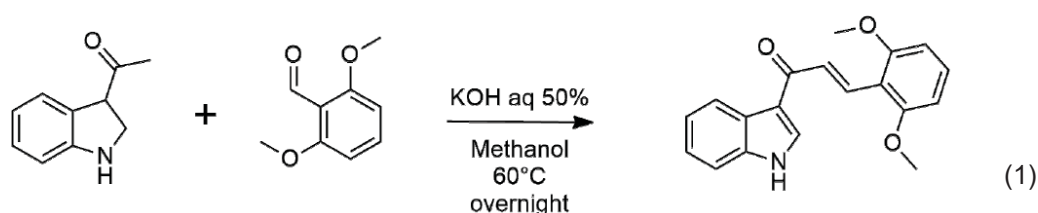
Considering that the subfamily G of ABC transporters is related to cholesterol metabolism and associated to spermatozoa maturation [12,13], some authors proposed the use of commercial Cholesterol – BODIPY dimers as a probe for cholesterol efflux in spermatozoa maturation [14]. However, it is blurred the association of cholesterol efflux mediated by ABCG2 [12,13, 14]. Another proposed function of cholesterol is the “fill-in” model for substrate recognition, in which cholesterol would help the transport of small substrates by filling spaces on protein binding sites [15]. Here, we proposed the synthesis of two heterodimers: BODIPY – cholesterol, to evaluate a possible efflux mediated by ABCG2, and Chalcone – cholesterol, to explore the effect of an ABCG2 inhibitor covalently bound to cholesterol.

## 2. MATERIALS AND METHODS

### 2.1 General methods

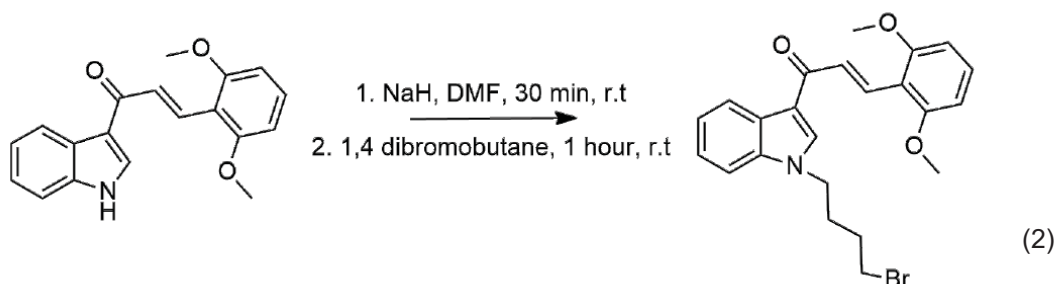
All reagents and solvents were reagent grade and used without previous purification. The chromatography was performed using a pre-coated TLC sheets ALUGRAM Xtra SIL G/UV 254 with 0.2 mm silica gel 60 layer with fluorescent indicator UV 254. The elution was performed using the mixture of solvents indicated for each reaction and revealed with UV light or TLC revealing solution as indicated. The NMR1H and NMR13C were acquired using a Bruker Avance 400 MHz and Bruker Avance III 500 MHz spectrometers. The samples were dissolved on the adequate deuterium solvent and the respective solvent signal was used as internal standard. The spectra interpretation was performed using MestReNova software (version 6.0.2-5475, Mastrelab Research S.L). The mass spectrometry was performed on a BRUKER amaZon speed and Thermo Scientific LTQ Orbitrap XL for high resolution spectra, both with electrospray as ionization source. A CEM Discovery microwave was used for microwave assisted synthesis. Porphyrin **4B** was kindly provided by Prof Dr<sup>o</sup> Alan Guilherme Gonçalves and Lais Guanaes.

### 2.2 Chalcone synthesis



321.9 mg (2 mmol) of 3 acetyl indole and 334.0 mg (2 mmol) of 2,6 dimethoxy benzaldehyde were dissolved in 20 mL of methanol, then, 2 mL of KOH 50% aqueous were added to the mixture. The reaction was stirred overnight at 60°C. The solvent was dried under reduced pressure and ethyl acetate was added to allow precipitation. 66% of yield. Monoisotopic mass: calculated [M+H]<sup>+</sup> 308.12812, found 308.12771. [16] <sup>1</sup>H NMR (400 MHz, DMSO) δ 8.42 (s, 1H), 8.39 – 8.34 (m, 1H), 8.07 (d, *J* = 15.9 Hz, 1H), 7.95 (d, *J* = 15.9 Hz, 1H), 7.59 – 7.54 (m, 1H), 7.38 (t, *J* = 8.4 Hz, 1H), 7.29 – 7.20 (m, 2H), 6.78 (d, *J* = 8.4 Hz, 2H), 3.97 (s, 6H). <sup>13</sup>C NMR (101 MHz, DMSO) δ 184.84, 173.89, 159.62, 137.20, 133.87, 131.17, 130.46, 126.49, 126.06, 122.77, 121.67, 121.55, 117.68, 112.40, 111.95, 104.13, 55.96, 25.63.

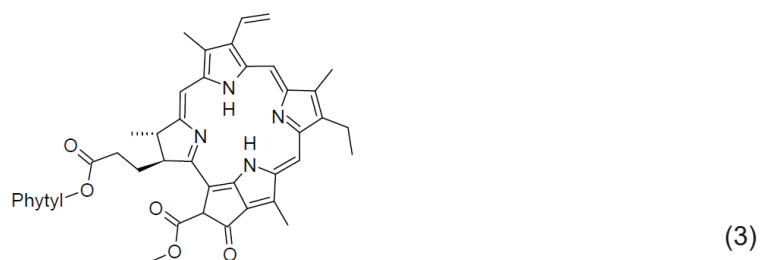
### 2.3 Chalcone alkylation with 1,4 dibromobutane



110 mg of chalcone were dissolved in 5 mL of anhydrous DMF with 30 mg of NaH (60% in mineral oil) and the mixture was stirred for 30 minutes. In parallel, 50  $\mu$ L of 1.4 dibromobutane was dissolved in 5 mL of anhydrous DMF. Then, the reaction was added dropwise in the 1.4 dibromo butane mixture (around 30 minutes). After the addition was complete, the reaction was stirred for more 30 minutes. The solvent was dried under reduced pressure, 5 mL of dichloromethane was added and formed a white precipitate that was removed by filtration. The organic phase was purified by chromatographic column using dichloromethane as eluent. The band visualization was performed using UV light. 43% of yield. Monoisotopic mass: calculated  $[M+H]^+$  442.1012, found 442.10.

$^1\text{H}$  NMR (400 MHz,  $\text{CDCl}_3$ )  $\delta$  8.58 – 8.51 (m, 1H), 8.25 (d,  $J$  = 15.9 Hz, 1H), 7.89 – 7.82 (m, 2H), 7.37 – 7.23 (m, 4H), 6.59 (d,  $J$  = 8.4 Hz, 2H), 4.20 (t,  $J$  = 7.0 Hz, 2H), 3.92 (s, 6H), 3.39 (t,  $J$  = 6.4 Hz, 2H), 2.12 – 2.00 (m, 2H), 1.94 – 1.82 (m, 2H).  $^{13}\text{C}$  NMR (101 MHz,  $\text{CDCl}_3$ )  $\delta$  186.56, 160.17, 136.84, 134.05, 132.28, 130.77, 127.16, 123.36, 123.20, 122.41, 118.31, 113.30, 109.69, 103.91, 55.95, 46.22, 32.78, 29.78, 28.56.

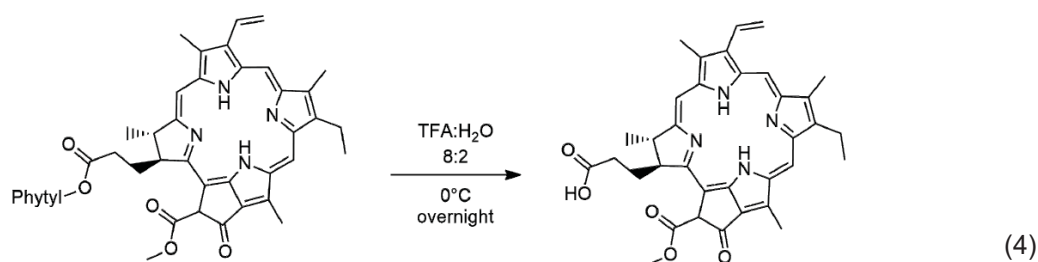
### 2.4 Pheophytin extraction



25 g of dried *Spirulina maxima* were mixed with 250 mL of acetone and stirred under reflux at 60°C for three hours. Then, the extract was filtered to separate the organic phase and the powder was extracted two more times with the same amount of acetone. After, the extracts were combined and dried under reduced pressure, resulting in 1.7 g of dried extract. A chromatographic column was carried out using dichloromethane as eluent to remove the carotenoids (orange fraction) and dichloromethane: acetone (95:5) to elute the pheophytin. The product is a dark green solid (21% of yield). Monoisotopic mass calculated  $[M+H]^+$  871.57320, found 871.57185. [2].

$^1\text{H}$  NMR (400 MHz,  $\text{CDCl}_3$ )  $\delta$  9.48 (s, 1H), 9.33 (s, 1H), 8.55 (s, 1H), 7.96 (dd,  $J$  = 17.8, 11.5 Hz, 1H), 6.31 – 6.23 (m, 2H), 6.19 – 6.14 (m, 1H), 5.41 – 5.32 (m, 2H), 5.22 – 5.08 (m,  $J$  = 8.3, 7.1 Hz, 1H), 4.54 – 4.40 (m,  $J$  = 19.5, 12.5, 7.0 Hz, 3H), 4.25 – 4.18 (m, 1H), 3.90 (s, 3H), 3.69 – 3.60 (m, 5H), 3.39 (s, 3H), 3.19 (s, 3H), 2.41 – 2.30 (m, 2H), 2.26 – 2.14 (m,  $J$  = 20.7, 10.3, 5.3 Hz, 2H), 1.92 – 1.85 (m,  $J$  = 12.1, 7.0 Hz, 2H), 1.82 (d,  $J$  = 7.3 Hz, 3H), 1.68 (t,  $J$  = 6.3 Hz, 3H), 1.58 (s, 3H), 0.85 (d,  $J$  = 6.6 Hz, 6H), 0.83 – 0.77 (m, 6H), -1.64 (s, 1H).

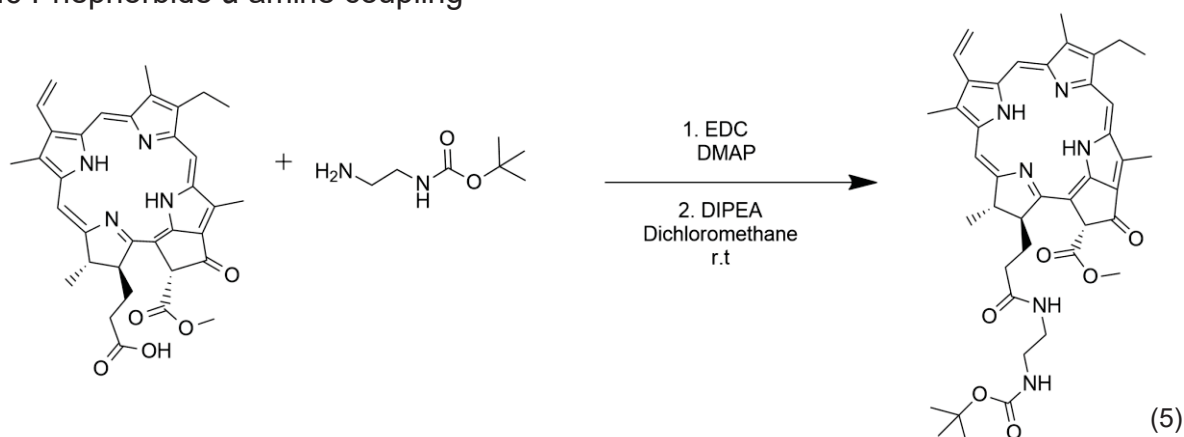
## 2.5 Pheophorbide a synthesis



100 mg of purified Pheophytin were mixed with 10 mL TFA: H<sub>2</sub>O (8:2 previously degassed with argon for 30 minutes). The reaction was stirred overnight in ice bath and protected from light. Then, 60 mL of distilled water and 60 mL of dichloromethane were added to the reaction to extract the product. The organic layer was separated and washed 3 times with water and one time with a NaHCO<sub>3</sub> 10% (60 mL each time) and it will form a precipitate. Then, 60 mL of citric acid 10% was added carefully to wash the organic layer until the precipitate disappear. Then, the dichloromethane was filtered in MgSO<sub>4</sub> anhydrous and removed under reduced pressure. The chromatographic column was performed using dichloromethane: ethyl acetate (1:1) as eluent to remove the starting material, then, dichloromethane : methanol (95:5) was added to elute the product. The product was collected as a black solid (75% of yield). Monoisotopic mass: calculated [M+H]<sup>+</sup> 593.2785, found 593.2759. [2].

<sup>1</sup>H NMR (400 MHz, CDCl<sub>3</sub>) δ 9.35 (s, 1H), 9.20 (s, 1H), 8.45 (s, 1H), 7.89 – 7.74 (m, 1H), 6.20 – 5.99 (m, 3H), 4.35 (dd, *J* = 7.3, 1.8 Hz, 1H), 4.11 (d, *J* = 8.7 Hz, 1H), 3.77 (s, 3H), 3.58 – 3.44 (m, 5H), 3.27 (s, 3H), 3.07 (s, 3H), 2.60 – 2.40 (m, 2H), 2.25 – 2.11 (m, 2H), 1.72 (d, *J* = 7.3 Hz, 3H), 1.56 (t, *J* = 7.6 Hz, 3H), -1.77 (s, 1H).

## 2.6 Phephorbide a amine coupling

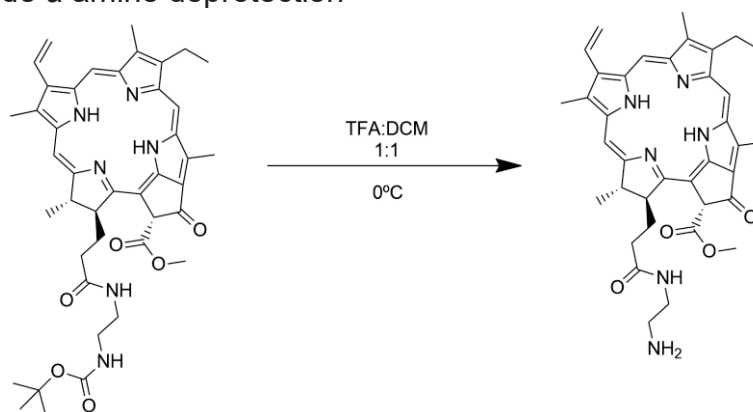


18.3 mg of Pheophorbide a (0.03 mmol), 11 mg of EDC (0.057 mmol) and 10 mg of DMAP (0.081 mmol) were dissolved in 5 mL of dried dichloromethane and stirred for 1 hour. Then 25 μL of DIPEA (0.143 mmol) and 400 μL (2.52 mmol) of N-Boc ethylenediamine were added with a syringe and stirred for 30 hours at room temperature. The reaction was washed two times with brine, filtered on MgSO<sub>4</sub> anhydrous and dried under reduced pressure and purified by column using dichloromethane: acetone (9:1) as eluent. The product was collected as a dark green solid (63% of yield). Monoisotopic mass: calculated [M+H]<sup>+</sup> 735.38, found 781.39 [2]

<sup>1</sup>H NMR (400 MHz, CDCl<sub>3</sub>) δ 9.67 (s, 1H), 9.61 (s, 1H), 8.80 (s, 1H), 8.06 (dd, *J* = 17.8, 11.5 Hz, 1H), 6.33 (dd, *J* = 17.8, 1.3 Hz, 1H), 6.12 (dd, *J* = 11.5, 1.3 Hz, 1H), 5.58 – 5.18 (m, 3H), 4.48 (q, *J* = 7.2 Hz,

1H), 4.40 (dd,  $J = 9.7, 2.2$  Hz, 1H), 4.13 – 3.97 (m, 2H), 3.82 – 3.77 (m, 2H), 3.75 (s, 3H), 3.53 (s, 3H), 3.48 (s, 3H), 3.29 (s, 3H), 2.50 (dt,  $J = 15.8, 8.0$  Hz, 1H), 2.23 (dt,  $J = 16.2, 8.0$  Hz, 1H), 2.10 (ddd,  $J = 15.6, 7.9, 4.7$  Hz, 1H), 1.88 – 1.76 (m, 1H), 1.71 (dt,  $J = 7.6, 4.0$  Hz, 5H), 1.42 (s, 9H), 1.13 (t,  $J = 7.1$  Hz, 3H), -1.78 (s, 1H).  $^{13}\text{C}$  NMR (101 MHz,  $\text{CDCl}_3$ )  $\delta$  173.86, 173.19, 168.94, 166.80, 156.55, 154.21, 149.04, 144.70, 138.92, 136.09, 134.95, 134.81, 134.77, 134.51, 130.18, 129.81, 129.35, 128.00, 121.55, 102.29, 101.35, 98.79, 93.72, 79.50, 60.54, 53.14, 52.22, 49.26, 40.69, 37.89, 31.39, 29.79, 29.27, 28.42, 23.12, 19.65, 17.73, 14.18, 12.13, 11.80, 11.25.

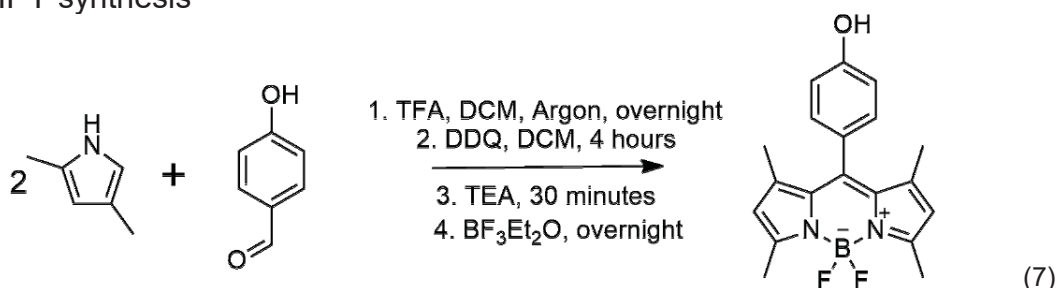
## 2.7 Pheophorbide a amine deprotection



14.4 mg of Pheophorbide a N-Boc ethylene diamine (0.019 mmol) were dissolved in 10 mL of TFA:DCM (1:1) and kept in ice bath for 24 hours. Then, 10 mL of dichloromethane were added to the reaction and the mixture was washed 3 times with water and 1 time with a solution of  $\text{NaHCO}_3$  5%. The organic phase was dried with  $\text{MgSO}_4$ . The purification was performed by chromatographic column with methanol as eluent (37% of yield). Monoisotopic mass: calculated  $[\text{M}+\text{H}]^+$  635.3340, found 681.3391 (adduct with formic acid). Synthesis based on [17]

$^1\text{H}$  NMR (500 MHz,  $\text{CDCl}_3$ )  $\delta$  9.67 (s, 1H), 9.61 (s, 1H), 8.82 (s, 1H), 8.04 (dd,  $J = 17.8, 11.6$  Hz, 1H), 6.84 (s, 1H), 6.32 (d,  $J = 17.8$  Hz, 1H), 6.10 (d,  $J = 11.5$  Hz, 1H), 5.54 (d,  $J = 19.0$  Hz, 1H), 5.26 (d,  $J = 18.9$  Hz, 1H), 4.49 (dd,  $J = 13.8, 6.6$  Hz, 1H), 4.39 (d,  $J = 8.6$  Hz, 1H), 4.15 – 3.98 (m, 2H), 3.81 – 3.71 (m, 5H), 3.51 (s, 2H), 3.48 (s, 3H), 3.27 (s, 3H), 2.58 – 2.43 (m, 1H), 2.31 – 2.18 (m, 1H), 2.17 – 2.07 (m, 1H), 1.77 – 1.66 (m, 6H), 1.15 (t,  $J = 7.0$  Hz, 3H), -1.64 (d,  $J = 46.4$  Hz, 1H), -1.81 (s, 1H).  $^{13}\text{C}$  NMR (126 MHz,  $\text{CDCl}_3$ )  $\delta$  207.03, 173.92, 173.17, 169.63, 168.84, 166.77, 154.16, 149.08, 144.71, 138.85, 136.10, 135.01, 134.77, 134.50, 130.13, 129.90, 129.44, 128.33, 121.58, 102.24, 101.33, 98.82, 93.69, 60.51, 53.11, 52.14, 49.22, 41.31, 37.91, 31.36, 30.92, 29.74, 23.10, 19.68, 17.73, 14.15, 12.17, 11.93, 11.31.

## 2.8 BODIPY synthesis

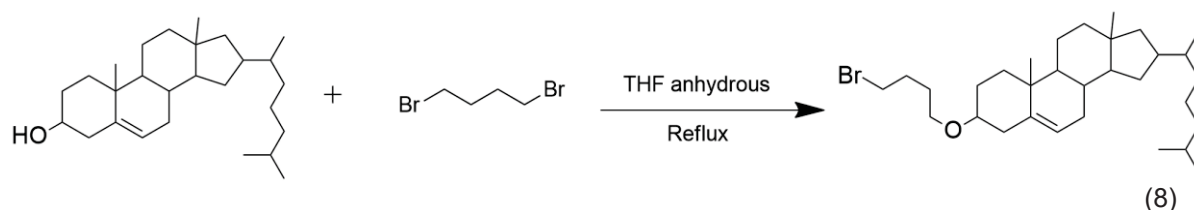


300 mg of 4 hydroxy benzaldehyde (2.45 mmol) and 500  $\mu\text{L}$  of 2,4 dimethyl pyrrol (4.85 mmol) were dissolved in 70 mL of dichloromethane under argon atmosphere. 60  $\mu\text{L}$  of TFA (0.8 mmol) were added and reacted overnight. After this period, 600 mg of DDQ (2.64 mmol) were dissolved in 30 mL of dichloromethane and mixed to the reaction for

additional 4 hours. 15 mL of triethylamine (179 mmol) were added for more 30 minutes and then 15 mL of  $\text{BF}_3\text{Et}_2\text{O}$  (121 mmol) were mixed. The reaction was stirred overnight (all steps were performed at room temperature). After the reaction was completed, it was filtered by a celite pad to remove DDQ and washed with  $\text{NaHCO}_3$  10%, water and brine (one time each). The reaction was dried under reduced pressure forming a dark purple solid. The chromatographic column was made using dichloromethane as eluent (the reaction was adsorbed on silica for a better chromatography). The band visualization was performed using UV light. The product was recovered as an orange solid bright under UV light. (15% of yield). Synthesis based on [18]

$^1\text{H}$  NMR (400 MHz,  $\text{CDCl}_3$ )  $\delta$  7.13 – 7.09 (m, 2H), 6.97 – 6.93 (m, 2H), 5.97 (s, 2H), 5.65 (s, 1H), 2.54 (s, 6H), 1.44 (s, 6H).  $^{13}\text{C}$  NMR (101 MHz,  $\text{CDCl}_3$ )  $\delta$  156.62, 155.43, 143.33, 141.98, 132.00, 129.51, 127.20, 121.26, 116.27, 14.70.

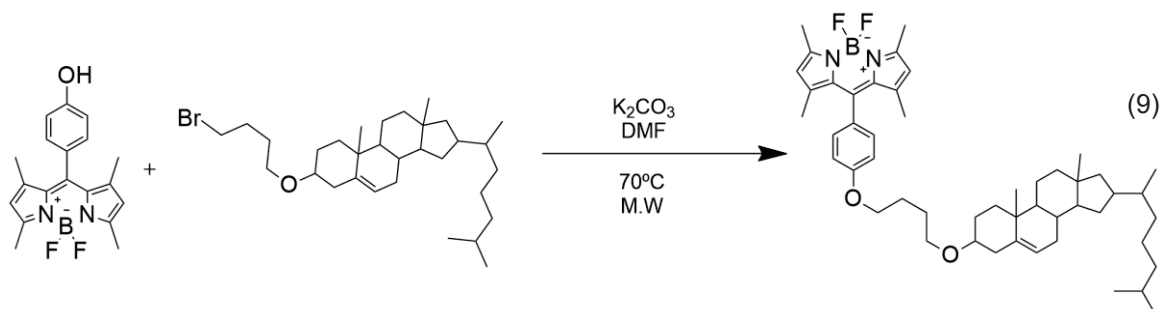
## 2.9 Cholesterol O-alkylation



Cholesterol (1.93g, 5 mmol), NaH (800 mg, 20 mmol) and 1,4 dibromobutane (2.4 mL, 20 mmol) were dissolved in 25 mL of dried THF. The reaction was stirred under reflux for 2 days. After this, distilled water was carefully added to the reaction (around 25 mL) and then the reaction was extracted with ethyl acetate (3x 25 mL). The ethyl acetate was collected, dried with  $\text{MgSO}_4$  and removed under reduced pressure. The purification was performed using cyclohexane: ethyl acetate 1:1 as eluent to separate the product from the starting material. A second column was performed using cyclohexane: dichloromethane 99:1 to remove the 1,4 dibromobutane and then, the final product was removed from silica using ethyl acetate. The band visualization was performed using solution of  $\text{H}_2\text{SO}_4$  10% in methanol. 16% off yield. [19]

$^1\text{H}$  NMR (400 MHz,  $\text{CDCl}_3$ )  $\delta$  5.34 (d,  $J$  = 5.3 Hz, 1H), 3.48 (t,  $J$  = 5.9 Hz, 2H), 3.44 (t,  $J$  = 6.8 Hz, 2H), 3.17 – 3.07 (m, 1H), 2.34 (ddd,  $J$  = 13.2, 4.7, 2.2 Hz, 1H), 2.23 – 2.11 (m, 1H), 2.06 – 1.76 (m, 8H), 1.74 – 1.00 (m, 24H), 0.99 (s, 4H), 0.91 (d,  $J$  = 6.6 Hz, 4H), 0.86 (dd,  $J$  = 6.6, 1.7 Hz, 6H), 0.67 (s, 3H).  $^{13}\text{C}$  NMR (101 MHz,  $\text{CDCl}_3$ )  $\delta$  141.02, 121.57, 79.11, 66.91, 56.82, 56.21, 50.25, 42.36, 39.83, 39.56, 39.20, 37.30, 36.93, 36.23, 35.82, 33.81, 31.99, 31.93, 29.84, 28.83, 28.49, 28.27, 28.04, 24.33, 23.87, 22.85, 22.59, 21.11, 19.41, 18.76, 11.89.

## 2.10 Cholesterol-BODIPY heterodimer dimer synthesis

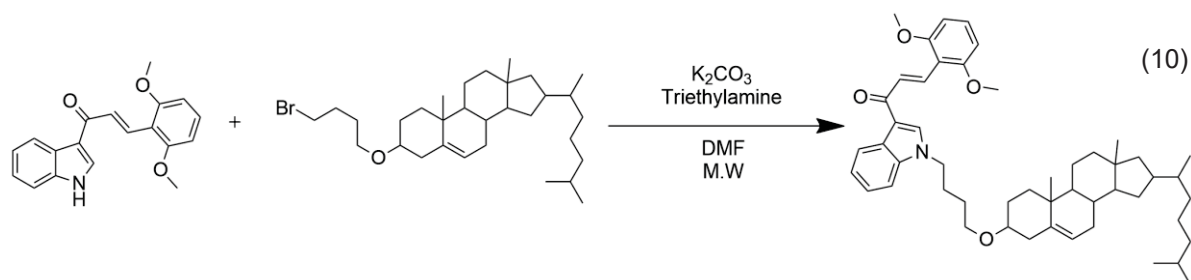


A solution of  $\text{K}_2\text{CO}_3$  (53 mg; 0.38 mmol) was mixed in 2 mL of dried DMF and heated to  $100^\circ\text{C}$  under agitation for 1 hour. This step helps the solubilization of the potassium carbonate but the dissolution is not complete. In a proper microwave flask, 10 mg of

BODIPY (0.029 mmol), 16.5 mg of Cholesterol bromide (0.031 mmol) and the mixture of DMF and K<sub>2</sub>CO<sub>3</sub> were added. The flask was placed on the microwave platform and heated at 70°C for 1 hour. After that, the solvent was removed and the reaction was purified by chromatographic column using dichloromethane as eluent. The band visualization was performed using solution of H<sub>2</sub>SO<sub>4</sub> 10% in methanol and UV light. 7% of yield. Monoisotopic mass: calculated [M+H]<sup>+</sup> 781.56579, found 781.56464

<sup>1</sup>H NMR (400 MHz, CDCl<sub>3</sub>) δ 7.76 – 7.66 (m, 1H), 7.59 – 7.47 (m, 1H), 7.15 (d, *J* = 8.7 Hz, 2H), 6.99 (d, *J* = 8.7 Hz, 2H), 5.97 (s, 2H), 5.35 (d, *J* = 5.3 Hz, 1H), 4.26 (dt, *J* = 12.0, 6.4 Hz, 2H), 4.09 (d, *J* = 6.7 Hz, 1H), 4.04 (t, *J* = 6.4 Hz, 2H), 3.56 (t, *J* = 6.4 Hz, 2H), 3.16 (td, *J* = 11.2, 5.6 Hz, 1H), 2.55 (s, 6H), 2.38 (ddd, *J* = 13.0, 4.5, 1.9 Hz, 1H), 2.25 – 2.19 (m, 1H), 2.02 (dd, *J* = 13.1, 4.1 Hz, 2H), 1.90 (dd, *J* = 14.8, 6.1 Hz, 4H), 1.43 (s, 6H), 1.25 (s, 7H), 1.18 – 1.04 (m, 10H), 1.01 (s, 3H), 0.99 – 0.88 (m, 12H), 0.86 (dd, *J* = 6.6, 1.7 Hz, 8H), 0.68 (s, 3H). <sup>13</sup>C NMR (126 MHz, CDCl<sub>3</sub>) δ 167.77, 159.65, 155.22, 143.19, 141.98, 141.05, 131.88, 130.91, 129.83, 129.16, 128.83, 126.88, 121.56, 121.08, 115.07, 79.09, 71.81, 68.17, 67.90, 67.55, 65.58, 63.13, 56.81, 56.18, 50.24, 42.34, 39.81, 39.53, 39.23, 38.74, 37.29, 36.94, 36.20, 35.80, 32.82, 31.97, 31.94, 31.92, 30.58, 30.37, 29.71, 29.67, 29.63, 29.53, 29.51, 29.45, 29.41, 29.37, 29.33, 29.24, 29.09, 28.94, 28.52, 28.24, 28.03, 27.73, 27.23, 26.77, 26.23, 25.75, 24.76, 24.30, 23.83, 23.76, 22.99, 22.83, 22.70, 22.57, 21.09, 19.40, 19.19, 19.17, 18.73, 14.59, 14.13, 14.06, 13.74, 11.87, 10.97.

## 2.11 Cholesterol-chalcone heterodimer synthesis



17.8 mg of chalcone, 27 mg of cholesterol bromide, 16.2 mg of K<sub>2</sub>CO<sub>3</sub> and 50 μL of triethylamine were dissolved in 2 mL of dried DMF and poured in a microwave flask. The flask was placed on a microwave platform and allowed to react during 1 hour at 70°C. Then, the solvent was removed and the reaction was purified using dichloromethane/acetone 198:2 as eluent. When necessary, another purification was performed using cyclohexane: ethyl acetate 3:1 as eluent to remove side products. The band visualization was performed using solution of H<sub>2</sub>SO<sub>4</sub> 10% in methanol. 7% yield. Monoisotopic mass: calculated [M+H]<sup>+</sup> 748.52994, found 748.52881.

<sup>1</sup>H NMR (400 MHz, CDCl<sub>3</sub>) δ 8.46 (dd, *J* = 6.1, 2.7 Hz, 0.67H), 8.37 (dd, *J* = 6.2, 2.9 Hz, 0.41H), 8.17 (d, *J* = 16.0 Hz, 0.62H), 7.80 (s, 0.5H), 7.78 (d, *J* = 16.0 Hz, 1.19H), 7.42 (s, 0.32H), 7.28 (ddd, *J* = 32.3, 6.1, 2.9 Hz, 2.58H), 7.18 – 7.13 (m, 0.88H), 6.79 (d, *J* = 12.7 Hz, 0.37H), 6.53 (d, *J* = 8.4 Hz, 1.14H), 6.49 (d, *J* = 12.7 Hz, 0.4H), 6.30 (d, *J* = 8.4 Hz, 0.67H), 5.30 – 5.23 (m, 1H), 4.17 (t, *J* = 7.2 Hz, 1H), 3.93 (t, *J* = 7.1 Hz, 1H), 3.71 (d, *J* = 120.2 Hz, 6H), 3.41 (t, *J* = 6.1 Hz, 1H), 3.33 (t, *J* = 6.3 Hz, 1H), 3.10 – 2.96 (m, 1H), 2.26 (dd, *J* = 11.3, 4.6 Hz, 1H), 2.15 – 2.05 (m, 1H), 1.99 – 1.84 (m, 4H), 1.78 (t, *J* = 10.1 Hz, 3H), 1.60 – 1.33 (m, 13H), 1.33 – 1.24 (m, 5H), 1.12 – 0.99 (m, 6H), 0.84 (dd, *J* = 6.5, 1.4 Hz, 4H), 0.79 (dd, *J* = 6.6, 1.7 Hz, 7H), 0.60 (d, *J* = 3.5 Hz, 3H). <sup>13</sup>C NMR (126 MHz, CDCl<sub>3</sub>) δ 188.95, 171.37, 161.30, 160.26, 157.60, 141.18, 141.14, 141.01, 136.82, 135.89, 130.20, 129.37, 127.56, 126.80, 122.98, 122.92, 122.18, 121.81, 121.65, 116.28, 114.69, 109.70, 104.00, 103.57, 79.29, 79.22, 77.41, 77.36, 77.16, 76.91, 71.95, 67.49, 67.36, 67.30, 64.52, 64.02, 56.93, 56.30, 56.04, 55.54, 53.56, 50.36, 50.11, 46.80, 42.47, 39.93, 39.66, 39.31, 37.41, 37.04, 36.64, 36.33, 35.92, 33.95, 32.09, 32.07, 32.04, 31.80, 31.58, 30.33, 30.22, 29.84, 29.80, 29.76, 29.71, 29.65, 29.58, 29.50, 29.46, 29.41, 29.37, 29.30, 29.09, 28.92, 28.60, 28.37, 28.15, 27.37, 27.01, 26.77, 26.66, 25.88, 25.66, 24.43, 23.96, 22.96, 22.83, 22.70, 21.21, 21.14, 19.52, 19.30, 19.01, 18.86, 14.26, 12.11, 12.00.



## 2.12 Intracellular accumulation and ABCG2-mediated transport of BODIPY

To evaluate the intracellular accumulation of compounds, the fluorescence of BODIPY was quantified by flow cytometry in HEK293-wild type cells. Cells were seeded on 24 well plates ( $2.5 \times 10^5$ ) and incubated for 24 hours for adhesion. Then, cells were treated with increasing concentrations of BODIPY (0.25; 0.5; 1; 2 and 4  $\mu\text{M}$ ) or BODIPY – cholesterol (0.25; 0.5; 1; 2; 4; 8; 10; 20 and 40  $\mu\text{M}$ ) for 30 minutes at 37°C. After incubation, the supernatant was removed and attached cells were washed with PBS prior to detachment with trypsin. Cells were resuspended on cold PBS and analyzed by flow cytometry using filter B 530 – 30 (FACS Celesta).

For efflux assay, HEK293-*ABCG2* cells were seeded on 24 well plates ( $2.5 \times 10^5$ ) and incubated for 24 hours for adhesion. Then, cells were treated with BODIPY – cholesterol (8  $\mu\text{M}$ ) for 30 minutes and 24 hours in the presence or absence of Ko143 (0.5  $\mu\text{M}$ ) at 37°C. Ko143 and Hoechst 33342 were used as experimental controls (0.5/3.0  $\mu\text{M}$ , respectively). Cells were washed, detached, and analyzed by flow cytometry as mentioned above.

## 2.13 Cholesterol influence on ABCG2-mediated transport of substrates

HEK293-*ABCG2* cells were seeded on 24 well plates ( $2.5 \times 10^5$ ) and incubated for 24 hours for adhesion. Then, cells were treated as follows:

- Mitoxantrone (0.15 to 20  $\mu\text{M}$ ) or Hoechst 33342 (0.09 to 12  $\mu\text{M}$ ).
- Mitoxantrone (0.15 to 20  $\mu\text{M}$ ) or Hoechst 33342 (0.09 to 12  $\mu\text{M}$ ) and cholesterol (50  $\mu\text{M}$ ).

Experimental control conditions were performed using mitoxantrone (7.5  $\mu\text{M}$ ) or Hoechst 33342 (3  $\mu\text{M}$ ) and Ko143 (0,5  $\mu\text{M}$ ). The assay was analyzed by flow cytometry (FACS Celesta) using V780 – 60 filter for mitoxantrone and UV 450 – 50 filter for hoechst 33342.

## 2.14 Effect of Chalcone – Cholesterol heterodimer on ABCG2-mediated transport

HEK293-*ABCG2* cells were seeded on 24 well plates ( $2.5 \times 10^5$ ) and incubated for 24 hours for adhesion. Cells were treated as follow:

- Chalcone (1) (0.25; 1; 5; 10 and 20  $\mu\text{M}$ ) and hoescht 33342 (3  $\mu\text{M}$ ).
- Chalcone – cholesterol dimer (10) (0.25; 1; 5; 10 and 20  $\mu\text{M}$ ) and hoescht 33342 (3  $\mu\text{M}$ ).
- Chalcone (1) (0.25; 1; 5; 10 and 20  $\mu\text{M}$ ), cholesterol (50  $\mu\text{M}$ ) and hoescht 33342 (3  $\mu\text{M}$ ).
- Chalcone (1) (0.25; 1; 5; 10 and 20  $\mu\text{M}$ ), cholesterol (0.25; 1; 5; 10 and 20  $\mu\text{M}$ ) and hoescht 33342 (3  $\mu\text{M}$ ).

Cells were treated for 30 minutes at 37°C. Then, the supernatant was removed and cells detached and resuspended in cold PBS. The analysis was performed by flow cytometry (FACS Celesta) using UV 450 – 50 filter.

### 3. RESULTS

#### 3.1 Chalcone – Porphyrin heterodimer

Chalcone 1 was synthesized by condensation of acetyl indole and dimethoxy benzaldehyde in the presence of potassium hydroxide (50% aqueous) using methanol as solvent [16]. Then, chalcone 1 was alkylated on indole nitrogen to prepare for further reactions. The alkylating agent 1,4 dibromo butane was added dropwise to avoid chalcone dimerization, forming chalcone 2 in the presence of sodium hydride as base to remove the acidic hydrogen from indole group. In contrast of the expected, a chalcone dimer was not detected on reaction system, probably because the alkylating agent was added dropwise. The  $^1\text{H}$  NMR comparison showed new multiplets between 4.5 to 1.5 ppm corresponding to the new alkyl chain (Fig. 2).

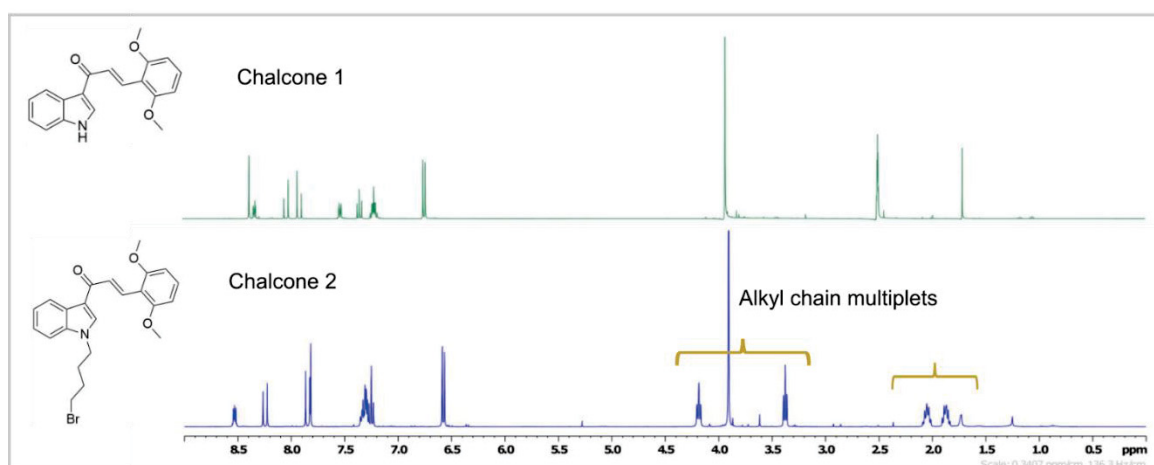


**Figure 2:**  $^1\text{H}$  NMR comparison between chalcone 1 and 2.

Porphyrin 4B was provided as previously described [20]. The proposed strategy for synthesis of the chalcone – porphyrin heterodimer was taking advantage on the presence of pyridinic nitrogen present on porphyrin 4B. The pyridinic nitrogen presents strong nucleophilicity due the presence of a free electronic pair and can be alkylated [21,22]. Thus, the next step was to promote the reaction between porphyrin 4B and chalcone 2 (Fig. 3). Three different reaction conditions

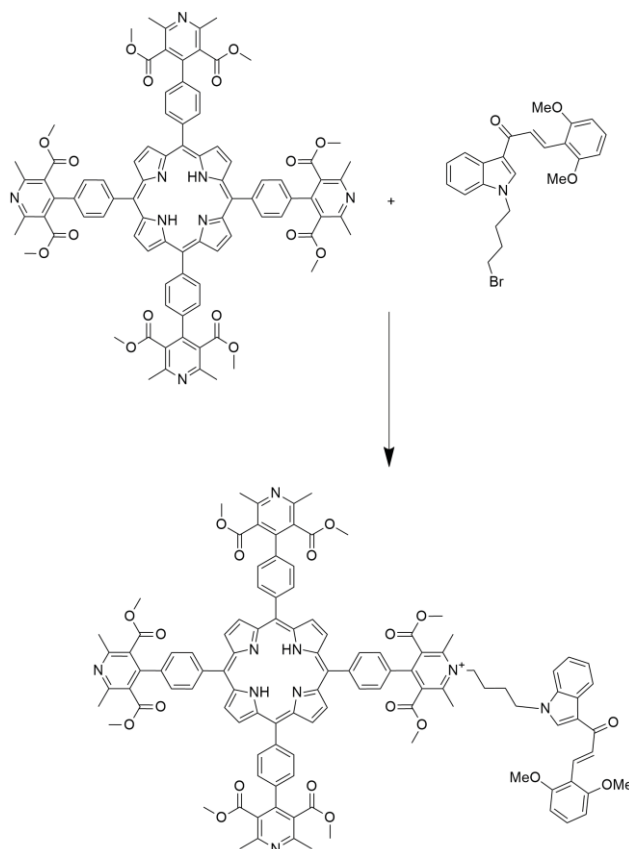


**Figure 3:** Schematic reaction between Porphyrin 4B and Chalcone 2.

**Table 1:** Chalcone – porphyrin reaction attempts.

Porphyrin 4B (eq)	Chalcone 2 (eq)	Solvent	Temperature	Time (hours)	Method	Yield (%)
4	1	DMF	R.T	24	Stirring	0
4	1	DMF	70°C	24	M.W	0
1	10	DMF	70°C	24	Stirring	0
4 (N)	10					

R.T: Room temperature

M.W: Microwave

DMF: dimethylformamide

Unfortunately, the tested conditions did not promote the dimerization. To explain the results, we hypothesized that: (i) Porphyrin 4B is a macromolecule and, since reactions are based on chemical approach and collision, it is quite difficult to promote the shock between the small chalcone 2 and pyridine region on large Porphyrin 4B, and (ii) besides the presence of pyridines as nucleophiles, the literatures shows that alkylation of pyridinic rings on porphyrins are made with large excess of alkylating agents [22]. However, this condition promotes the alkylation of all pyridines on porphyrin molecule and our attempt was to bind the chalcone in only one ring.

The synthesis of complex porphyrins is made with many steps, especially for asymmetric porphyrins. In this case, this porphyrin may be easily produced by dipyrromethane intermediates. This method proposes the synthesis of substituted aldehydes to be used for dipyrromethane intermediate construction, followed by porphyrin condensation.

### 3.2 Pheophorbide a – Chalcone

Structural modifications were performed on Pheophorbide a to allow the heterodimer formation. Figure 4 summarizes the attempted reactions.

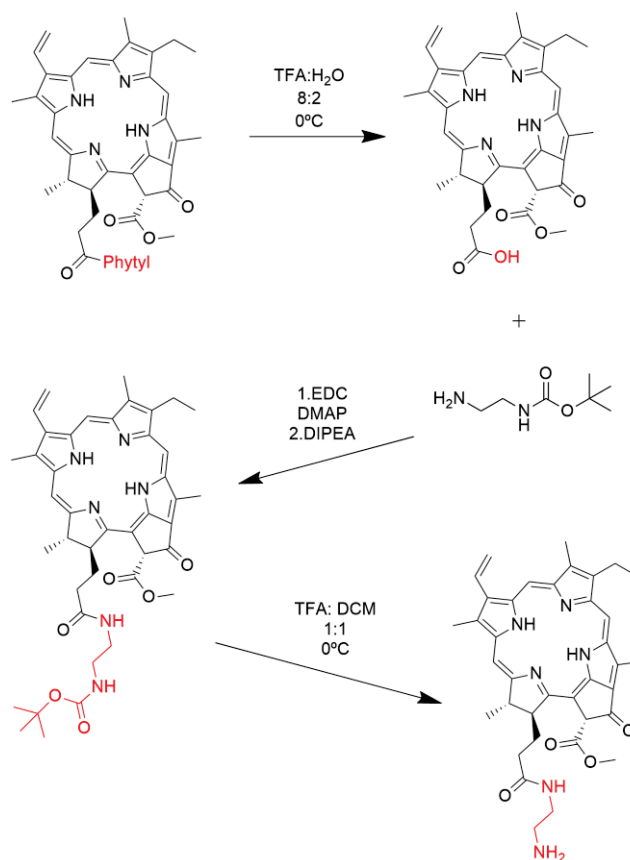


**Figure 4:** Modifications on Pheophytin.

The first step was to extract Pheophytin (3), an electron carrier intermediate on Photosynthesis [23]. The extraction was performed on acetone reflux for 3 hours using *Spirulina maxima* as Pheophytin source [2]. The solvent was filtered, and the extraction was repeated two more times. The purification was performed by chromatographic column followed by <sup>1</sup>H NMR characterization. The extraction yield was considered good for a natural product (around 20%). After characterization, Pheophytin was submitted to hydrolysis with TFA and distilled water to remove phytol group, leaving a free carboxylic acid on the structure, generating Pheophorbide a (4). This compound characterization was compared with literature based on <sup>1</sup>H NMR [2].

The next step was to introduce a diamine group on Pheophorbide a carboxylic acid, forming an amide with a N-Boc ethylene diamine protected tail (compound 5). The reaction was performed using EDC as coupling agent as described by Jinadasa (2011) [2]. Amide bonds formation require activation of carboxylic acid to improve the nucleophilic attack by amine on carbonyl group. This activation is performed by coupling agents like EDC and DCC that creates a more favorable leaving group and facilitates amide bond formation [24].

The reaction was performed using different bases, solvent and time reactions but coupling agent was maintained due the easiness to remove. The main problem found on this reaction was the formation of anhydride as side product (bis pheophorbide a) formed due to reaction between the activated acid and another

Pheophorbide a as shown on figure 5. To avoid anhydride formation, the volume of solvent was increased (dilutions may favor the amide formation), activation time was added (to facilitate the amine nucleophilic attack on activated acid) and with N-boc ethylenediamine excess (anhydride can suffer nucleophilic attack from amine, forming the desired product). The absence of water is crucial for reaction success and the maintenance of anhydrous conditions was also a problem. Table 2 summarizes the optimization conditions and reaction 10 was chosen due reproducibility and good yield.

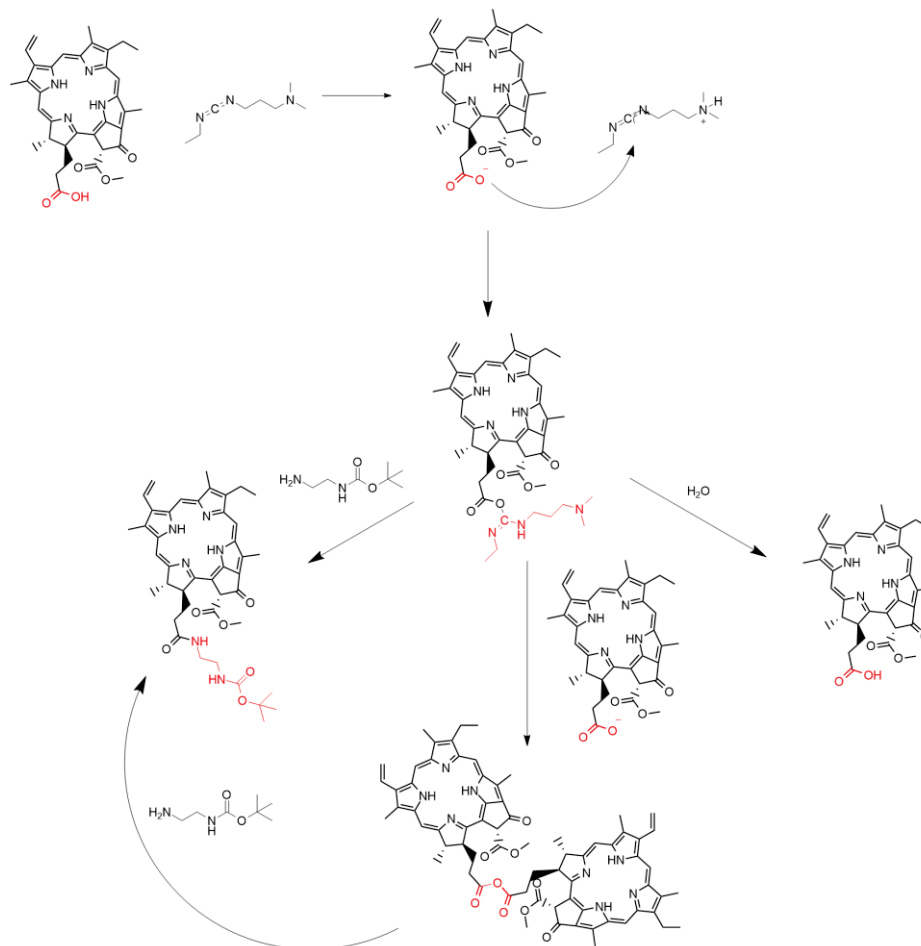


**Figure 5:** Coupling reaction on pheophorbide a and the representation of possible side reactions.

**Table 2:** Attempted reactions for compound 5 formation.

Reaction	Pheo (eq)	EDC (eq)	DMAP (eq)	DIPEA (eq)	HOBt (eq)	TEA (eq)	N-Boc (eq)	Solvent	Vol (mL)	Activation time (h)	Time (total h)	Yield
1	1	1,2	1	2,3	-	-	2,4	DCM	5	15 min	4	83
2	1	1,2	1	2,3	-	-	2,4	DCM	20	1 h	24	63
3	1	1,5	1,4	4	-	-	4,5	DMF	30	-		trace
4	1	1	-	-	1,2	-	1	DCM	6	-		trace
5	1	1,2	1,2	2,5	1,2	-	3	DCM	20	1h	24	trace
6	1	1	1	5	1,4	-	5,5	DCM	15	1h	24	trace
7	1	1	1	5	-	-	22	DCM	5	1h	6	40
8	1	1,5	1,2	4	-	-	4	DMF	15	-	24	trace
9	1	3	-	-	-	3	2,5	DCM		-		trace
10	1	2	2,5	4,5	-	-	81	DCM	5	1h	30	63

TEA: triethylamine

N-BOC: N-Boc ethylenediamine

The characterization was performed by  $^1\text{H}$  NMR,  $^{13}\text{C}$  NMR and mass spectrometry. The interpretation of  $^1\text{H}$  NMR allows the identification of a new signal

between 2.0 to 1.0 ppm. This region is characteristic of hydrogens bounded to methyl and ethyl groups. The presence of a singlet on 1.42 ppm integrating to 9 hydrogens is a strong indicative of amide formation since those 9 hydrogens corresponds to N-Boc group, however, the mass spectrometry showed an intriguing result. The exact mass expected for the product was 734.37 Da on positive mode ( $[M+H]^+$  734.37 Da) and the found mass was 781.39 Da. The difference of 46 Da corresponds exactly to a formiate anion and the formation of an adduct with formic acid (an additive for positive mode analysis) could explain the discrepancy on mass spectrometry as shows figure 6.

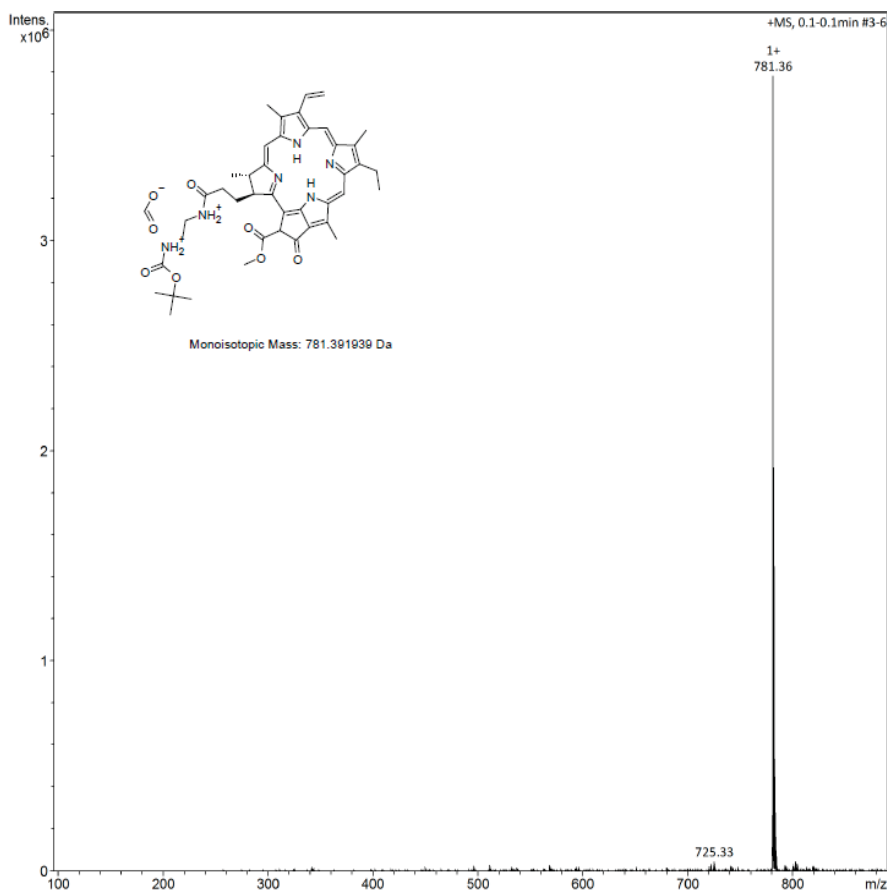


**Figure 6:** Mass spectroscopy of compound 5 and the calculated mass of formic acid adduct.

The next step was the removal of N-Boc protecting group (compound 6). For this reaction, Pheophorbide *a* was stirred with TFA:DCM at 0° for 24 hours. Purification was hampered due adducts formations and lack of reaction control which also made characterization challenging. Table 3 summarizes the attempted reactions.

**Table 3:** Attempted reactions for compound 6 formation.

Reaction	Pheophorbide (eq)	Thianisol (30 mM)	TFA (mL)	Solvent	Volume (mL)	Yield (%)
1	1	yes	1	DMF	4	Trace
2	1	yes	1	DCM	4	Trace
3	2	yes	2	DCM	8	25
4	0.8	no	1	DCM	4	9
5	0.2	no	4	DCM	4	14
6	0.5	no	1	DCM	4	Trace
7	0.3	no	5	DCM	5	37

TFA: trifluoroacetic acid

All conditions were performed with large excess of TFA on dried solvent (dichloromethane or dimethylformamide), in the presence or absence of thioanysole, and different TFA: solvent proportion. Thioanysole is used as scavenger on acidolytic cleavages, specially on peptide synthesis, preventing side reactions [25]. The reaction varied a lot regarding its reproducibility in all cases and thioanysole removal from reaction product was difficult. The removal of thioanysole from reaction set was not detrimental and the product yield was increased when TFA:solvent proportion was changed from 1:4 to 1:1 (entry 5 and 7). In this case, entry 7 was considered the best condition for deprotection of amine group on compound 6. The comparison of  $^1\text{H}$  NMR with compound 5 shows the absence of N-Boc singlet on 1.42 ppm, suggesting the removal of protecting group (figure 7). The mass spectroscopy also presented the same problem observed on compound 5 where the exact mass was not found. The calculated mass was 635.33 Da on positive mode ( $[\text{M}+\text{H}]^+$  635.3340 Da) but was found 681,33 Da. The difference corresponds to the same 46 Da from compound 5 and adduct formation with formic acid could also explain this situation. The figure 7 shows the mass spectroscopy considering the adduct formation and figure 8 shows the comparison of  $^1\text{H}$  NMR since Pheophytin until the last product.

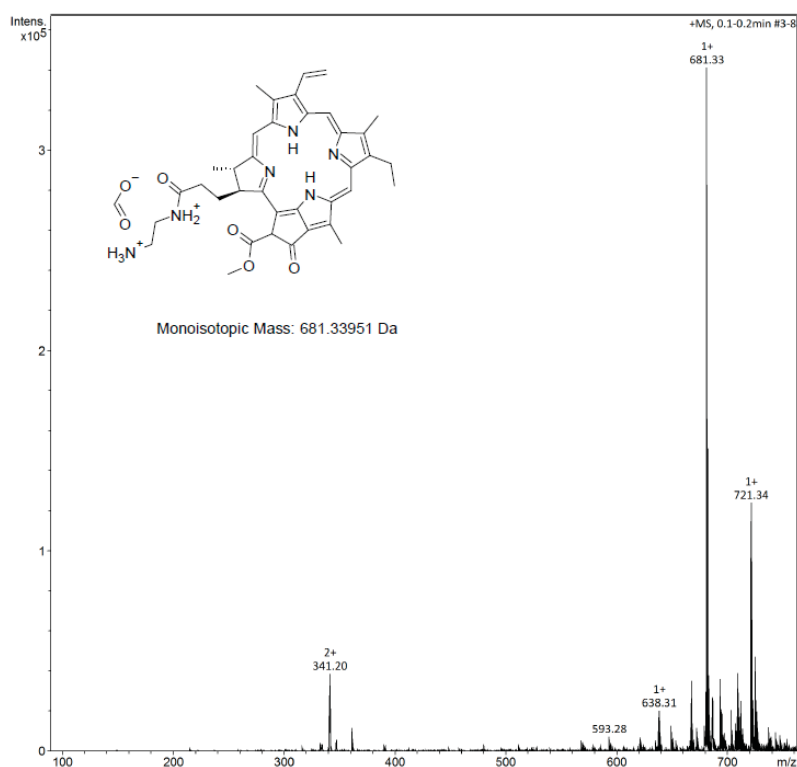


**Figure 7:** Adduct formation of compound 6 with formic acid and monoisotopic mass.

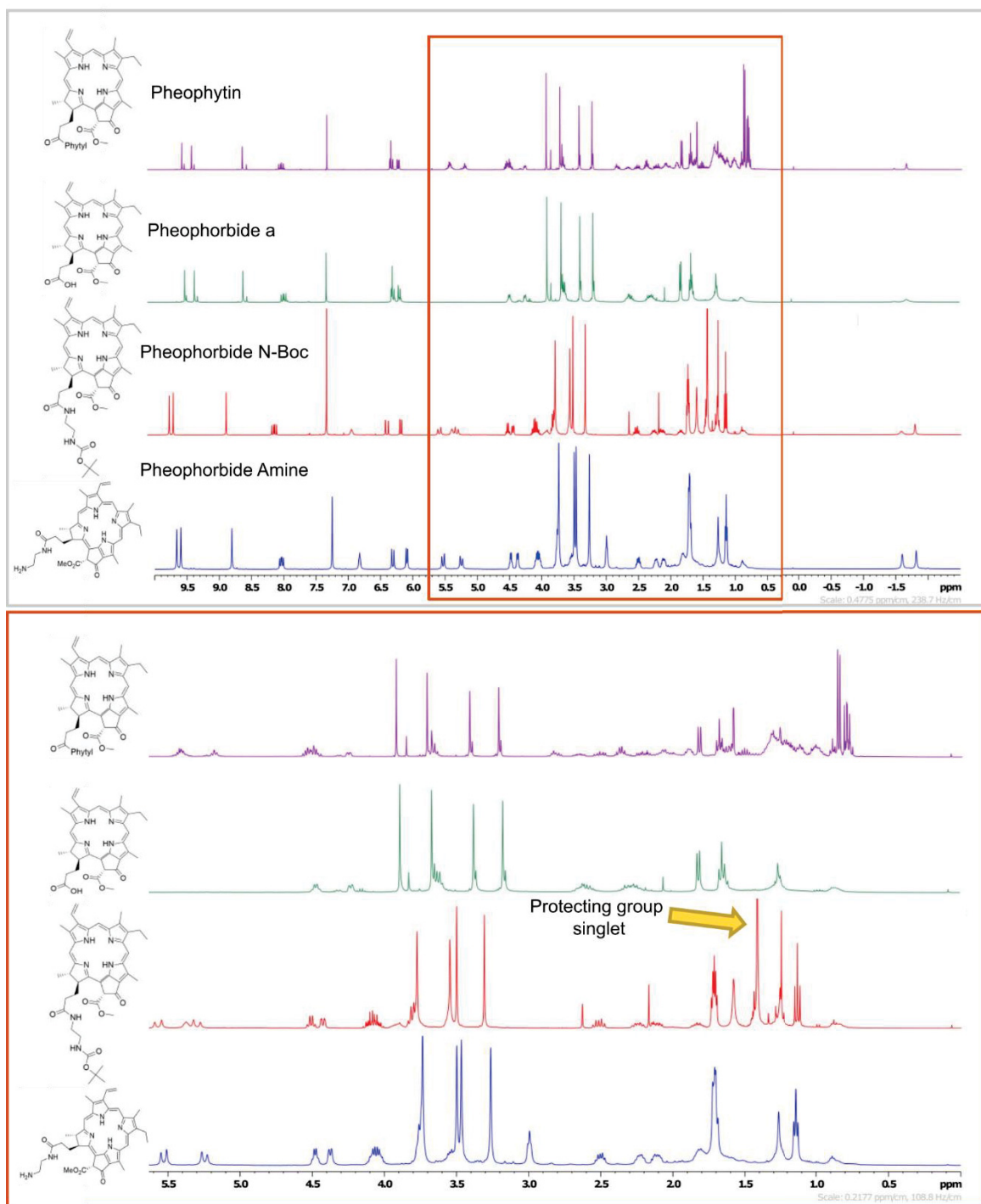


**Figure 8:** Comparison of the  $^1\text{H}$  NMR spectra from Phrophorbide a derivatives. The arrow indicates the singlet corresponding to protecting group and the lack of this signal on the last product.

The next reaction was binding compound 6 to chalcone 2. The reaction was performed under anhydrous system to avoid the nucleophilic attack from water on bromide moiety on chalcone. Also, a basic condition was chosen to avoid protonation on amine moiety, letting the compound 6 as a free base. Unfortunately, none of the attempted reactions were sufficient to promote the heterodimer formation. Table 4 summarizes the attempted reactions.



**Table 4:** Attempted reactions for Pheophorbide – Chalcone binding.

Reaction	Base	Solvent	Temp	Time	Method	Yield
1	K <sub>2</sub> CO <sub>3</sub>	DMF	70°C	2	M.W	-
2	NaH	DMF	R.T.	O.N.	Stirring	-
3	-	DMF	60°C	72	Stirring	-
4	Triethylamine	DMF	70°C	2	M.W	-
5	I <sub>2</sub>	CH <sub>3</sub> CN	reflux	6	Stirring	-

Pheophorbide a amine and compound 2 were at 1 equivalent in all tested conditions.

DMF: dimethylformamide

M.W: microwave

O.N: overnight

### 3.3 Cholesterol – BODIPY heterodimer

The first step was to modify cholesterol molecule on the free hydroxyl group to allow the binding of BODIPY. This modification was performed as described by He (2018) using NaH as base to form an alkoxide on cholesterol. Large excess of alkylating agent (1,4 dibromobutane) was used in anhydrous THF in reflux for 48 hours, giving 16% of yield of compound 7 [19]. In parallel, BODIPY synthesis was performed following the methodology described by Liu (2008) and Barba-Bon (2014), providing BODIPY molecule with a free hydroxyl group with 15 % of yield of compound 8 [18,26]. The compounds were characterized by <sup>1</sup>H NMR and compared with the literature.

The final step was the heterodimer synthesis. The reaction was based on classic nucleophilic attack from BODIPY free hydroxyl group on bromide from cholesterol alkylation (compound 8). Table 5 summarizes the attempted conditions:

**Table 5:** Attempted conditions for Cholesterol – Bodipy heterodimer formation

Reaction	Base	Solvent	Temp	Time (h)	Method	Yield (%)
1	NaOH	DMF	R.T.	5	Stirring	-
2	K <sub>2</sub> CO <sub>3</sub>	THF	40 – 50°C	16	Stirring	-
3	NaH	THF	40 – 50°C	O.N	Stirring	-
4	K <sub>2</sub> CO <sub>3</sub>	DMF	70°C	O.N	Stirring	-
5	K <sub>2</sub> CO <sub>3</sub>	DMF	70°C	0.5	Microwave	trace
6	K <sub>2</sub> CO <sub>3</sub>	DMF	70°C	1.5	Microwave	7%
7	K <sub>2</sub> CO <sub>3</sub>	DMF	70°C	1	Microwave	7%
8	K <sub>2</sub> CO <sub>3</sub>	DMF	100°C	1	Microwave	4%
9	K <sub>2</sub> CO <sub>3</sub>	DMF	100°C	1	Microwave	7%

Compound 7 and 8 were at 1 equivalent in all tested conditions.

DMF: dimethylformamide

THF: tetrahydrofuran

O.N: overnight

The employment of microwave reactor was crucial for synthesis success. The entry 9 was chosen due the yield and reproducibility. Characterization was performed by <sup>1</sup>H NMR, <sup>13</sup>C NMR and mass spectrometry. The product (compound 9) presented signals from both building blocks. To prove that was not a mixture of compounds, mass spectroscopy was performed and was consistent to the heterodimer mass. The theoretical monoisotopic mass for positive mode was [M+H]<sup>+</sup> 781.56579 Da and 781.56464 Da was found. The figure 9 shows the <sup>1</sup>H NMR superposition of product and building blocks.

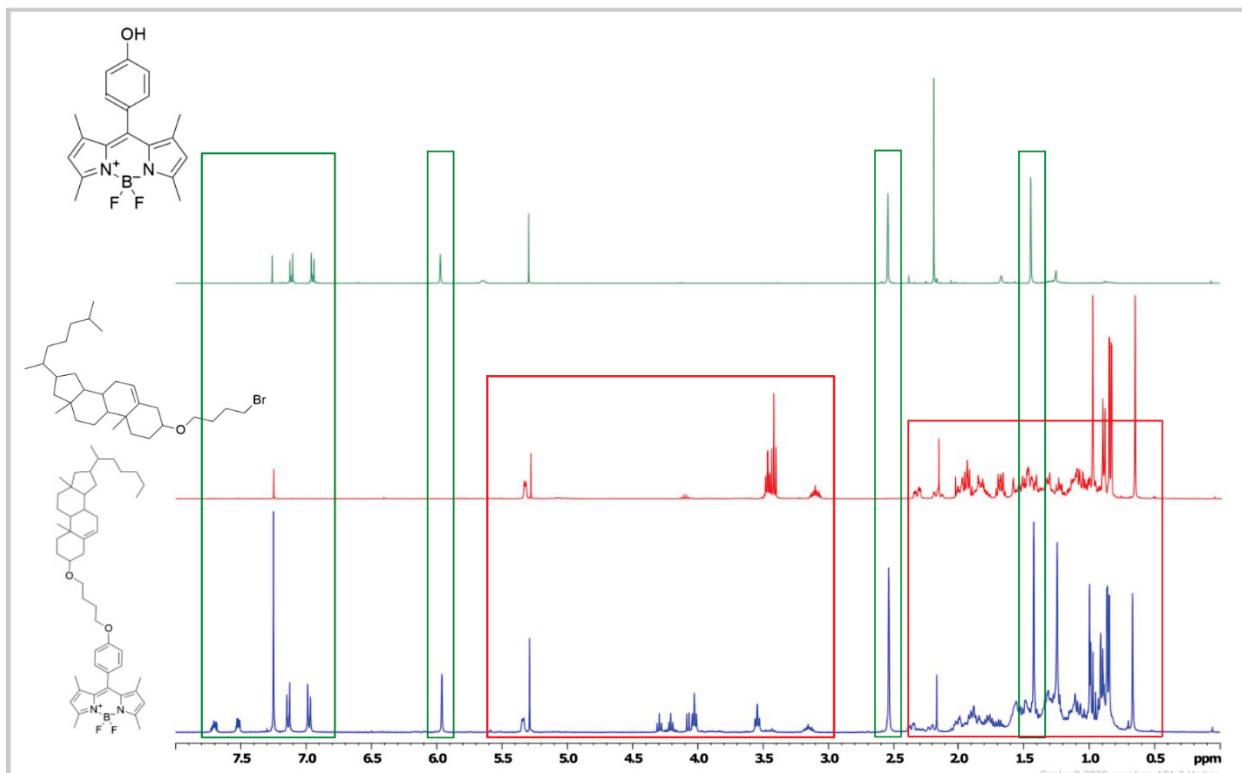


**Figure 9:** Comparison of the  $^1\text{H}$  NMR spectra from BODIPY, Cholesterol and heterodimer. The green boxes indicate the signals from BODIPY and red boxes the signals from alkylated cholesterol.

### 3.4 Cholesterol – Chalcone heterodimer

The synthesis of a heterodimer containing cholesterol and an ABCG2 inhibitor was proposed, in this case a chalcone derivative. This synthetic approach took advantage of chalcone 1 and compound 8 synthesis. Table 6 presents the attempted reactions for this heterodimer.

**Table 6:** Attempted conditions for Cholesterol – chalcone heterodimer formation.

Reaction	Base	Temp	Time (h)	Method	Yield (%)
1	NaH	R.T	O.N	Stirring	-
2	NaH	60°C	O.N	Stirring	-
3	$\text{K}_2\text{CO}_3$ /triethylamine	70°C	1	M.W	10
4*	$\text{K}_2\text{CO}_3$ /triethylamine	70°C	1	M.W	3
5	$\text{K}_2\text{CO}_3$ /triethylamine	70°C	2	M.W	7

Compound 7 and compound 1 were at 1 equivalent in all tested conditions.

Solvent: Dimethylformamide

O.N: overnight

M.W: Microwave

\*Reaction carried out with  $\text{MgSO}_4$ .

The reaction was completed at low yield (10% maximum) which made the characterization challenging. The  $^1\text{H}$  NMR presented signals from both building blocks, but those signals were split on final molecule in different proportions. Two hypotheses were considered: (i) the formation of two similar products on different proportions or (ii) the molecule behaved as a rotamer with conformations energetically different. Mass

spectroscopy revealed only one monoisotopic mass that corresponded to heterodimer calculated mass (calculated  $[M+H]^+$  748.52994, found 748.52881). In this case, the hypothesis of two products did not explain the split pattern of signals since no side reactions were found.

To verify the rotamer hypothesis,  $^1\text{H}$  NMR were performed at 25°C and 70°C and two signals were followed (singlet 3.92 ppm, 6H from chalcone and singlet 0.67 ppm, 3H from cholesterol). The signals proportion varied with the temperature and were more similar at 70°C. This shows that temperature helped the molecule to surpass energetically unfavorable conformations, reflecting on signals proportion. It is hypothesized that the increase of temperature above 70°C on this heterodimer would let the signals even more similar or merging then into one signal, meaning that the conformation energetic barrier was surpassed. Further works should explore this feature. Figure 10 presents the rotamer hypothesis and figure 11 presents the discussed  $^1\text{H}$  NMR signals pattern.

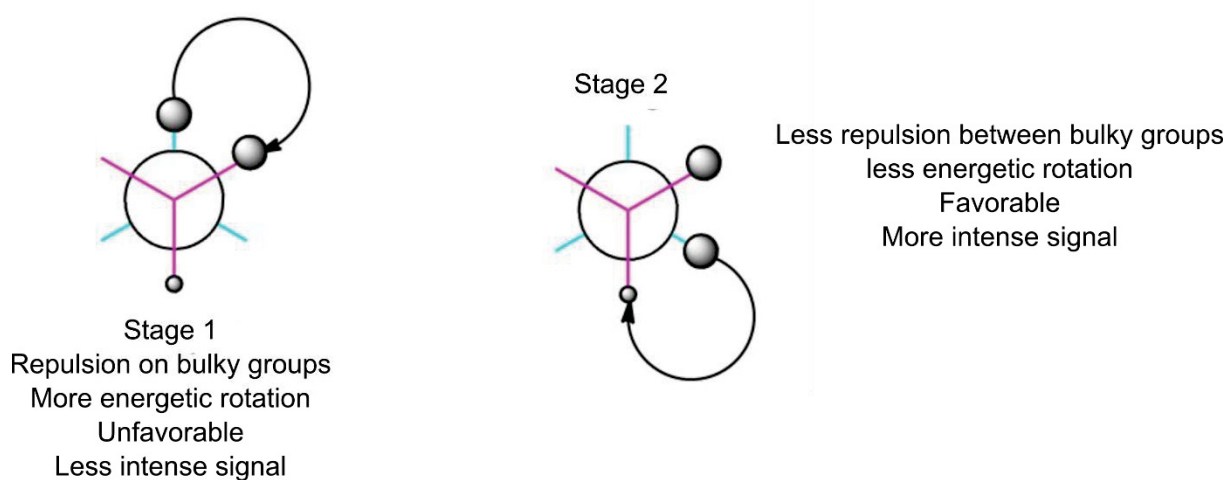


**Figure 10:** Energetic rotamer hypothesis.

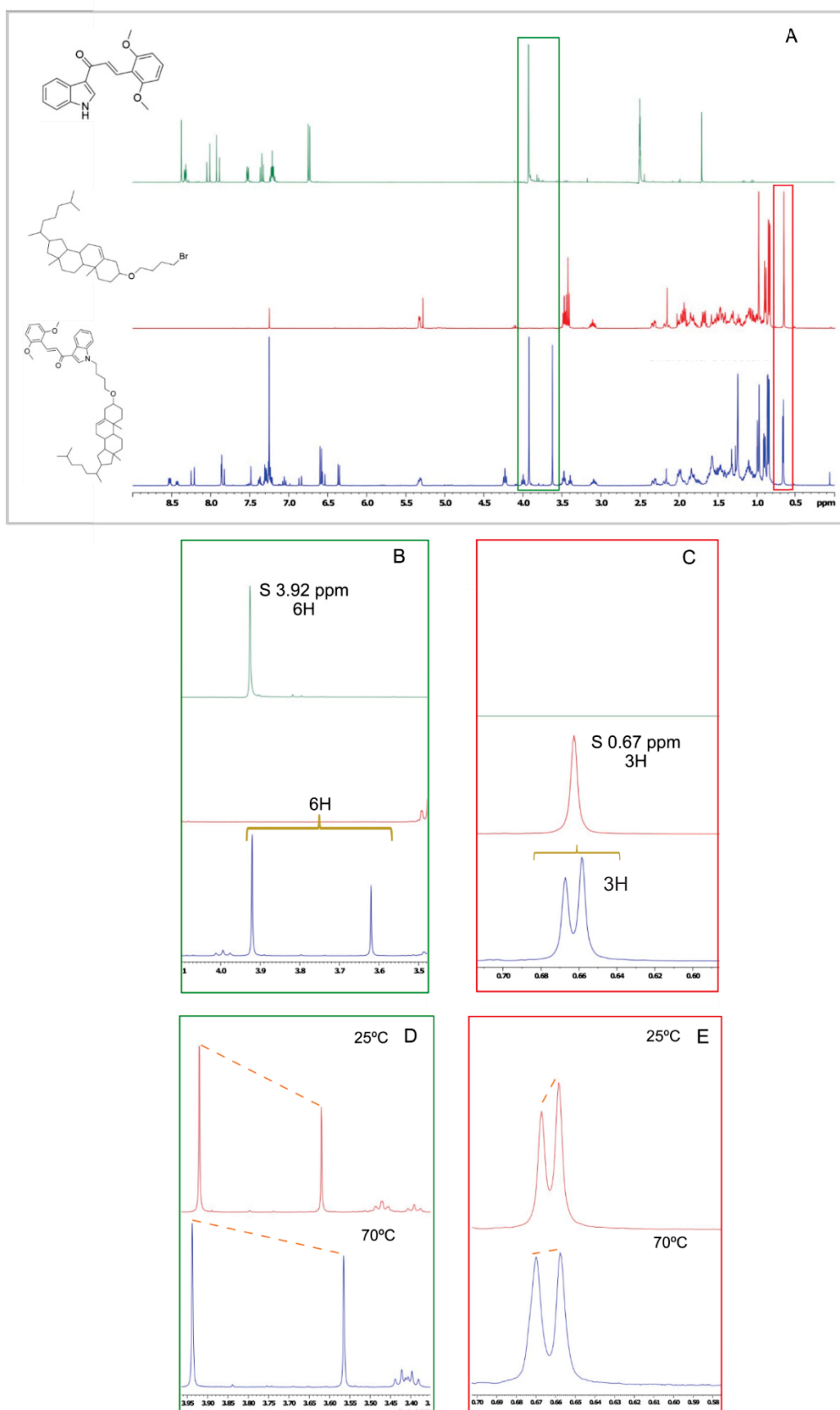


**Figure 11:** (A) Comparison of the  $^1\text{H}$  NMR spectra from chalcone (1), cholesterol (7) and heterodimer. Split pattern on signals from chalcone moiety (B) and cholesterol moiety (C). Effect on split pattern with temperature increase on chalcone singlet moiety (D) and cholesterol singlet moiety (E).

### 3.5 Biological evaluation of cholesterol and heterodimers on ABCG2

#### 3.5.1 Cholesterol effect on drug transport ABCG2-mediated

Cholesterol affects the ATPase activity of ABCG2 [10,11]. To verify the influence of cholesterol on ABCG2 transport activity, the efflux of mitoxantrone and hoechst 33342 was evaluated in HEK293-ABCG2 cells in presence of cholesterol (50  $\mu\text{M}$ ) or absence. The efflux was followed by flow cytometry and the results suggest that cholesterol did not affect the transport of ABCG2 substrates (Fig 12).

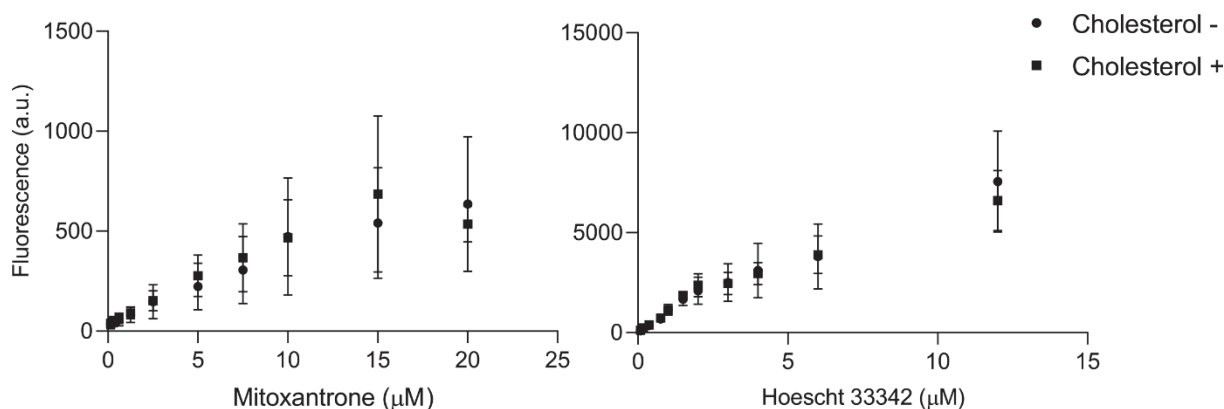


**Figure 12:** Efflux profile of mitoxantrone and hoechst 33342 in the presence or absence of cholesterol (50  $\mu\text{M}$ ). The data represent three independent experiments with Mean and SD.

#### 3.5.2 BODIPY – cholesterol

Considering that ABCG2 transport some steroid compounds, we synthesized the BODIPY – cholesterol heterodimer for track the cholesterol in cell-based models. First, to identify the intracellular accumulation of BODIPY by flow cytometry, a range of BODIPY concentrations were used in HEK293 wild type cells. A flow cytometer equipped with 3 lasers and 12 filters of fluorescence was used. Table 7 summarizes the flow cytometer set of lasers/filters used and the selected optical system.

**Table 7:** Raw data of BODIPY fluorescence screening.

Laser	BODIPY											
	Ultraviolet		Violet						Blue			
	Filter	450 - 50	670 - 30	450 - 50	525 - 50	610 - 20	670 - 30	710 - 50	780 - 60	530 - 30	575 - 25	610 - 20
Control	13	6	34	23	4	23	4	28	<b>33</b>	19	33	36
0.25 $\mu\text{M}$	12	8	31	230	8	25	4	27	<b>3182</b>	502	308	83
0.5 $\mu\text{M}$	19	12	37	482	15	36	6	36	<b>7054</b>	1078	626	150
1.0 $\mu\text{M}$	14	21	35	958	27	66	13	53	<b>14701</b>	2293	1296	286
2.0 $\mu\text{M}$	13	24	33	1745	45	61	11	47	<b>26446</b>	4192	2374	468
4.0 $\mu\text{M}$	11	44	30	3167	78	98	16	62	<b>47790</b>	7809	4492	889

As shown in table 7, the blue laser and the 530 – 30 filter showed the most intense fluorescence signal. The lowest concentration (0.25  $\mu\text{M}$ ) used was enough to identify an intense signal of fluorescence, when compared to the control condition, without BODIPY. The next step was the identification of the best concentration of BODIPY-cholesterol heterodimer using the 530 – 30 filter. A large range of concentrations was essayed (0.25 to 40  $\mu\text{M}$ ), since the chemical modification of BODIPY can change the fluorescence pattern. As shown in figure 13, for both

compounds, BODIPY and BODIPY – cholesterol heterodimer, the intracellular accumulation was dependent of the concentration.

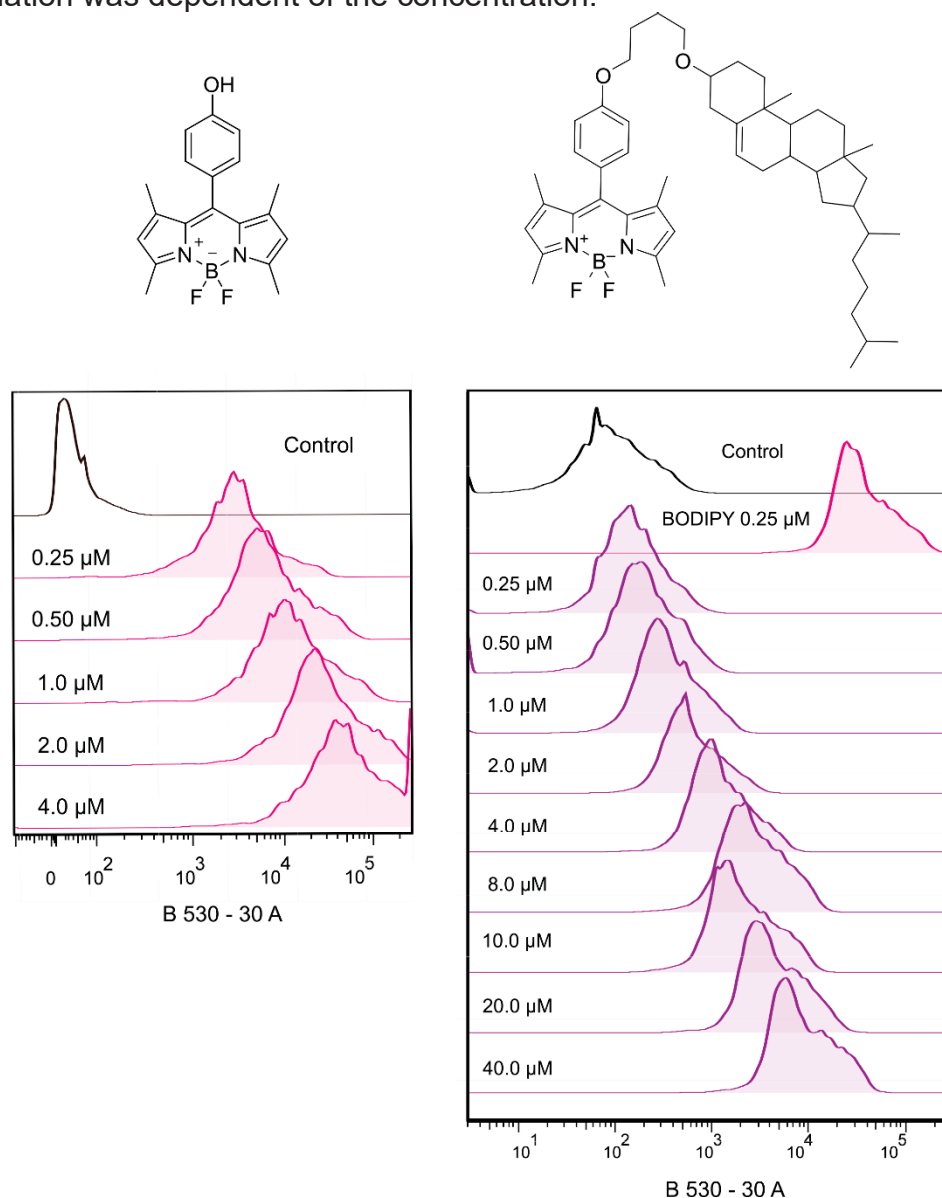


**Figure 13:** Fluorescence shift according to concentrations used for BODIPY and BODIPY – cholesterol using Blue laser and filter 530-30. The data represent one experiment.

Based on this data, the concentration of 8  $\mu\text{M}$  of BODIPY-cholesterol heterodimer was chosen for the investigation of a possible transport of cholesterol mediated by ABCG2. The effect was evaluated after 30 minutes and 24 hours of incubation, due the large size of this molecule. The preliminary data suggests that BODIPY-cholesterol heterodimer was not transported by ABCG2. This result suggest that cholesterol is not transported by ABCG2 (Fig. 14). Additional experiments in different periods need to be performed to confirm this effect.

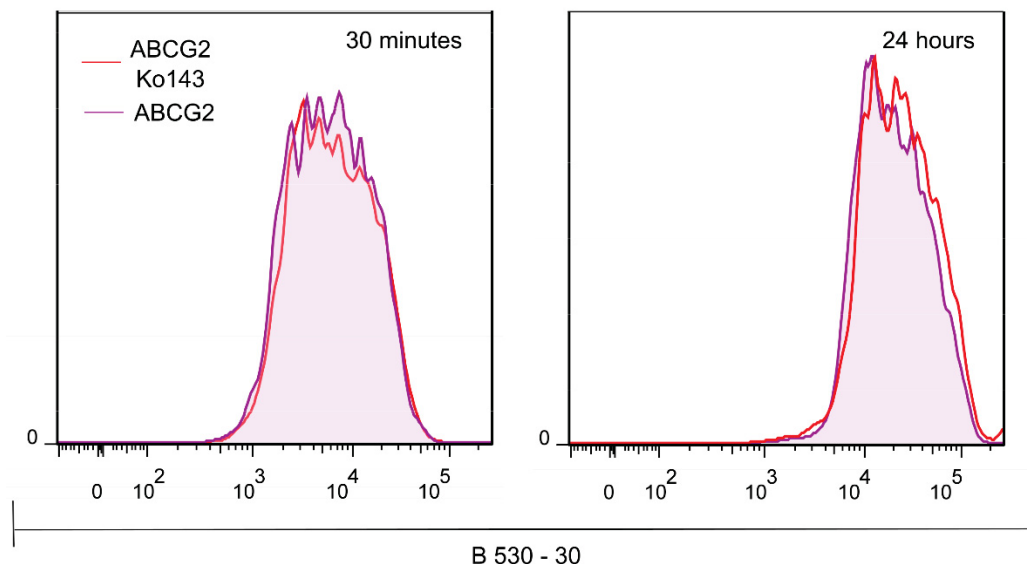


**Figure 14:** Histograms overlay of HEK293-ABCG2 (with Ko143 – red, without Ko143 – purple) treated with BODIPY-cholesterol using Blue laser and filter 530-30. The data represent one experiment.

### 3.5.3 Chalcone – cholesterol

Additionally, the effect of cholesterol on the inhibitory potency of ABCG2 inhibitors was investigated. To pursue this investigation, a chalcone – cholesterol heterodimer was synthesized and tested. Chalcone 1 alone and chalcone 1 + cholesterol were used as experimental control. As shown in figure 15, cholesterol itself did not influence inhibition profile of chalcone 1, even at high concentration, but the covalent binding between chalcone and cholesterol abrogated the inhibition potency of chalcone 1.

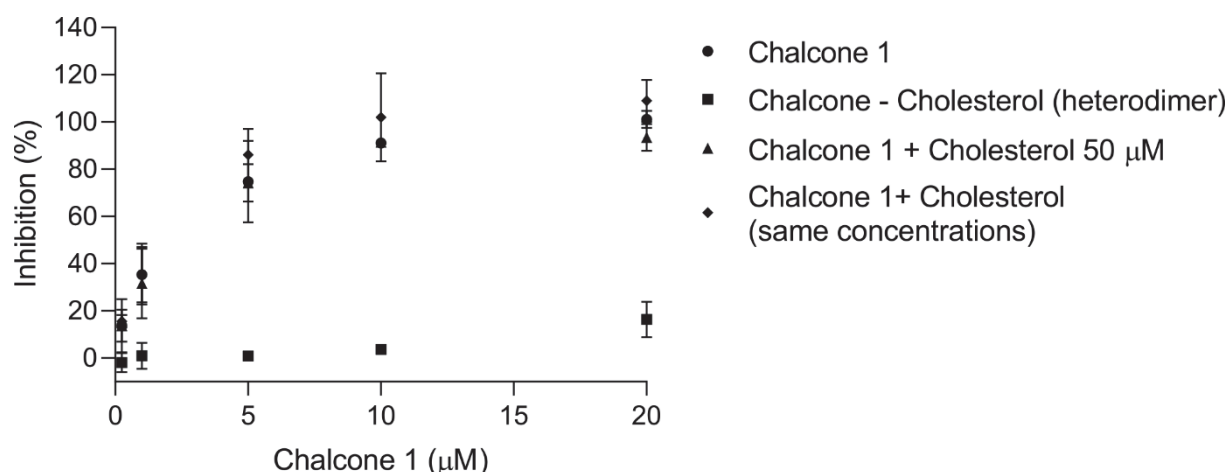


**Figure 15:** Influence of cholesterol in Chalcone 1 inhibition profile.

We concluded that the synthesis of heterodimers containing cholesterol is useless for ABCG2 inhibitors and suggest three hypotheses to explain this data: (i) the heterodimer prevents the chalcone binding on ABCG2 due steric hindrance, (ii) cholesterol is transported by ABCG2 carrying chalcone 1 out of cell, and (iii) cholesterol carried randomly the chalcone 1 to plasmatic membrane preventing the binding on

ABCG2. This research is on exploratory phase and those hypotheses must be tested in future works.

#### 4. DISCUSSION

This chapter presented the synthesis of heterodimers targeting ABCG2 transporter. Two heterodimers were successfully synthesized (BODIPY – cholesterol and chalcone – cholesterol), however, two were suspended at the final reaction step (chalcone – porphyrin 4B and chalcone – pheophorbide a). A total of 10 molecules were synthesized between intermediates and final molecules.

The BODIPY – cholesterol heterodimer was used for investigations related with a possible transport of cholesterol mediated by ABCG2. This heterodimer showed a high fluorescence signal using the blue laser and filter 530 – 30. Regarding the ABCG2 efflux, the preliminary data shows that BODIPY-cholesterol heterodimer is not transported by ABCG2. The chalcone – cholesterol heterodimer was also tested on ABCG2. The covalent coupling of cholesterol on chalcone molecule decreased the inhibition potency of chalcone alone.

In summary, the synthesis of heterodimers with cholesterol was promising. In contrast, heterodimers containing porphyrins were difficult to obtain. The preliminary results suggest that heterodimers containing cholesterol can be useful for investigations of cholesterol transport mediated by ABCG2, but useless for improve the inhibitory effect of know ABCG2 inhibitors.

#### 5. REFERENCES

- [1] R.W. Robey, K. Steadman, O. Polgar, K. Morisaki, M. Blayney, P. Mistry, S.E. Bates, Pheophorbide a Is a Specific Probe for ABCG2 Function and Inhibition, *Cancer Res.* 64 (2004) 1242–1246. <https://doi.org/10.1158/0008-5472.CAN-03-3298>.
- [2] R.G.W. Jinadasa, X. Hu, M.G.H. Vicente, K.M. Smith, Syntheses and Cellular Investigations of 173-, 152-, and 131-Amino Acid Derivatives of Chlorin e6, *J. Med. Chem.* 54 (2011) 7464–7476. <https://doi.org/10.1021/jm2005139>.
- [3] I. Yoon, J.Z. Li, Y.K. Shim, Advance in photosensitizers and light delivery for photodynamic therapy., *Clin. Endosc.* 46 (2013) 7–23. <https://doi.org/10.5946/ce.2013.46.1.7>.
- [4] L.B. Josefsen, R.W. Boyle, Photodynamic therapy and the development of metal-based photosensitizers, *Met. Based. Drugs.* 2008 (2008). <https://doi.org/10.1155/2008/276109>.
- [5] M.P. Uliana, L. Pires, S. Pratavieira, T.J. Brocksom, K.T. de Oliveira, V.S. Bagnato, C. Kurachi, Photobiological characteristics of chlorophyll a derivatives as microbial PDT agents, *Photochem. Photobiol. Sci.* 13 (2014) 1137–1145. <https://doi.org/10.1039/C3PP50376C>.
- [6] E. Desuzinges-Mandon, O. Arnaud, L. Martinez, F. Huché, A. Di Pietro, P. Falson, ABCG2 transports and transfers heme to albumin through its large extracellular loop, *J. Biol. Chem.* 285 (2010) 33123–33133. <https://doi.org/10.1074/jbc.M110.139170>.
- [7] G. Valdameri, C. Gauthier, R. Terreux, R. Kachadourian, B.J. Day, S.M.B. Winnischofer, M.E.M. Rocha, V. Frachet, X. Ronot, A. Di Pietro, A. Boumendjel, Investigation of Chalcones as Selective Inhibitors of the Breast Cancer Resistance Protein: Critical Role of Methoxylation in both Inhibition Potency and Cytotoxicity, *J. Med. Chem.* 55 (2012) 3193–3200. <https://doi.org/10.1021/jm2016528>.
- [8] C.H. Storch, R. Eehalt, W.E. Haefeli, J. Weiss, Localization of the Human Breast Cancer Resistance Protein (BCRP/ABCG2) in Lipid Rafts/Caveolae and Modulation of Its Activity by Cholesterol in Vitro, *J. Pharmacol. Exp. Ther.* 323 (2007) 257–264. <https://doi.org/10.1124/jpet.107.122994>.
- [9] J.T. Szilagyi, A.M. Vetrano, J.D. Laskin, L.M. Aleksunes, Localization of the placental BCRP/ABCG2 transporter to lipid rafts: Role for cholesterol in mediating efflux activity., *Placenta.* 55 (2017) 29–36. <https://doi.org/10.1016/j.placenta.2017.04.006>.
- [10] Á. Telbisz, M. Müller, C. Özvegy-Laczka, L. Homolya, L. Szente, A. Váradi, B. Sarkadi,



- Membrane cholesterol selectively modulates the activity of the human ABCG2 multidrug transporter, *Biochim. Biophys. Acta - Biomembr.* 1768 (2007) 2698–2713.  
<https://doi.org/https://doi.org/10.1016/j.bbamem.2007.06.026>.
- [11] Á. Pál, D. Méhn, É. Molnár, S. Gedey, P. Mészáros, T. Nagy, H. Glavinas, T. Janáky, O. von Richter, G. Báthori, L. Szente, P. Krajcsi, Cholesterol Potentiates ABCG2 Activity in a Heterologous Expression System: Improved in Vitro Model to Study Function of Human ABCG2, *J. Pharmacol. Exp. Ther.* 321 (2007) 1085 LP – 1094.  
<https://doi.org/10.1124/jpet.106.119289>.
- [12] C. Scharenberg, N. Mannowetz, R.W. Robey, C. Brendel, P. Repges, T. Sahrhage, T. Jähn, G. Wennemuth, ABCG2 is expressed in late spermatogenesis and is associated with the acrosome., *Biochem. Biophys. Res. Commun.* 378 (2009) 302–307.  
<https://doi.org/10.1016/j.bbrc.2008.11.058>.
- [13] N. Wang, D. Lan, W. Chen, F. Matsuura, A.R. Tall, ATP-binding cassette transporters G1 and G4 mediate cellular cholesterol efflux to high-density lipoproteins, *Proc. Natl. Acad. Sci.* 101 (2004) 9774–9779. <https://doi.org/10.1073/pnas.0403506101>.
- [14] N.C. Bernecic, M. Zhang, B.M. Gadella, J.F.H.M. Brouwers, J.W.A. Jansen, G.J.A. Arkesteijn, S.P. de Graaf, T. Leahy, BODIPY-cholesterol can be reliably used to monitor cholesterol efflux from capacitating mammalian spermatozoa, *Sci. Rep.* 9 (2019) 9804.  
<https://doi.org/10.1038/s41598-019-45831-7>.
- [15] Y. Kimura, A. Kodan, M. Matsuo, K. Ueda, Cholesterol fill-in model: mechanism for substrate recognition by ABC proteins., *J. Bioenerg. Biomembr.* 39 (2007) 447–452.  
<https://doi.org/10.1007/s10863-007-9109-7>.
- [16] V. Martel-Frchet, M. Kadri, A. Boumendjel, X. Ronot, Structural requirement of arylindolylpropenones as anti-bladder carcinoma cells agents, *Bioorg. Med. Chem.* 19 (2011) 6143–6148. <https://doi.org/https://doi.org/10.1016/j.bmc.2011.08.015>.
- [17] H. You, H.-E. Yoon, P.-H. Jeong, H. Ko, J.-H. Yoon, Y.-C. Kim, Pheophorbide-a conjugates with cancer-targeting moieties for targeted photodynamic cancer therapy, *Bioorg. Med. Chem.* 23 (2015) 1453–1462. <https://doi.org/https://doi.org/10.1016/j.bmc.2015.02.014>.
- [18] J.-Y. Liu, H.-S. Yeung, W. Xu, X. Li, D.K.P. Ng, Highly Efficient Energy Transfer in Subphthalocyanine–BODIPY Conjugates, *Org. Lett.* 10 (2008) 5421–5424.  
<https://doi.org/10.1021/ol8023677>.
- [19] L. He, Y. Jiang, K. Liu, V. Gomez-Murcia, X. Ma, A. Torrecillas, Q. Chen, X. Zhu, E. Lesnefsky, J.C. Gomez-Fernandez, B. Xu, S. Zhang, Insights into the Impact of a Membrane-Anchoring Moiety on the Biological Activities of Bivalent Compounds As Potential Neuroprotectants for Alzheimer's Disease, *J. Med. Chem.* 61 (2018) 777–790.  
<https://doi.org/10.1021/acs.jmedchem.7b01284>.
- [20] L.D. Guanaes, M.M. Guimarães, D.R.B. Ducatti, M.E.R. Duarte, S.M.W. Barreira, M.D. Nosedá, A.G. Gonçalves, Synthesis and photophysical evaluation of meso-phenyl-1,4-dihydropyridine and pyridine-porphyrin hybrids, *Chem. Heterocycl. Compd.* In press (2021).
- [21] A.M. Slomp, S.M.W. Barreira, L.Z.B. Carrenho, C.C. Vandresen, I.F. Zatonni, S.M.S. Ló, J.C.C. Dallagnol, D.R.B. Ducatti, A. Orsato, M.E.R. Duarte, M.D. Nosedá, M.F. Otuki, A.G. Gonçalves, Photodynamic effect of meso-(aryl)porphyrins and meso-(1-methyl-4-pyridinium)porphyrins on HaCaT keratinocytes, *Bioorganic Med. Chem. Lett.* 27 (2017) 156–161.  
<https://doi.org/10.1016/j.bmcl.2016.11.094>.
- [22] C.C. Vandresen, A.G. Gonçalves, D.R.B. Ducatti, F.S. Murakami, M.D. Nosedá, M.E.R. Duarte, S.M.W. Barreira, In vitro photodynamic inactivation of conidia of the phytopathogenic fungus *Colletotrichum graminicola* with cationic porphyrins., *Photochem. Photobiol. Sci. Off. J. Eur. Photochem. Assoc. Eur. Soc. Photobiol.* 15 (2016) 673–681.  
<https://doi.org/10.1039/c5pp00372e>.
- [23] V. V Klimov, Discovery of pheophytin function in the photosynthetic energy conversion as the primary electron acceptor of Photosystem II, *Photosynth. Res.* 76 (2003) 247–253.  
<https://doi.org/10.1023/A:1024990408747>.
- [24] E. Valeur, M. Bradley, Amide bond formation: beyond the myth of coupling reagents, *Chem. Soc. Rev.* 38 (2009) 606–631. <https://doi.org/10.1039/B701677H>.
- [25] Y. Kiso, H. Isawa, K. Kitagawa, T. Akita, Suppressing Effect of Thioanisole on a Side Reaction during the Acidolytic Cleavage of Protecting Groups of Tyrosine, *Chem. Pharm. Bull. (Tokyo)*. 26 (1978) 2562–2564. <https://doi.org/10.1248/cpb.26.2562>.
- [26] A. Barba-Bon, A.M. Costero, S. Gil, A. Harriman, F. Sancenón, Highly Selective Detection of Nerve-Agent Simulants with BODIPY Dyes, *Chem. – A Eur. J.* 20 (2014) 6339–6347.  
<https://doi.org/https://doi.org/10.1002/chem.201304475>.

## CHAPTER 3 - MULTIPLEXED FLOW CYTOMETRIC APPROACH FOR DETECTION OF ANTI-SARS-COV-2 IGG, IGM AND IGA USING BEADS COVALENTLY COUPLED TO THE NUCLEOCAPSID PROTEIN

This chapter was based on two articles, the first submitted for publication in the journal “Letters on Applied Microbiology”, and the second published in Portuguese in a Brazilian journal: “Revista Brasileira de Análises Clínicas”.

Ingrid Fatima Zattoni<sup>1</sup>, Luciano F. Huergo<sup>2</sup>, Edileusa C. M. Gerhardt<sup>3</sup>, Jeanine M. Nardin<sup>4</sup>, Alexia Marques Fernandes dos Santos<sup>4</sup>, Fabiane Gomes de Moraes Rego<sup>5</sup>, Geraldo Picheth<sup>5</sup>, Vivian Rotuno Moure<sup>#,1,5</sup>, Glaucio Valdameri<sup>#,1,5</sup>.

<sup>1</sup>Pharmaceutical Sciences Graduate Program, Laboratory of Cancer Drug Resistance, Federal University of Paraná, 80210-170, Curitiba, PR, Brazil. <sup>2</sup>Setor Litoral, Federal University of Paraná, 83260-000, Matinhos, PR, Brazil. <sup>3</sup>Department of Biochemistry and Molecular Biology, Federal University of Paraná, 80060-000, Curitiba, PR, Brazil.

<sup>4</sup>Hospital Erasto Gaertner, 81520-060, Curitiba, PR, Brazil. <sup>5</sup>Department of Clinical Analysis, Federal University of Paraná, 80210-170 Curitiba, PR, Brazil.

#Correspondence and requests for materials should be addressed to Vivian Rotuno Moure (email: vivian.moure@ufpr.br) and Glaucio Valdameri (email: gvaldameri@ufpr.br). Phone +55 41 33604078 and +55 41 991332283.

Ingrid Fatima Zattoni<sup>1</sup>; Geraldo Picheth<sup>1,2</sup>; Fabiane Gomes de Moraes Rego<sup>1,2</sup>; Mauren Isfer Anghebem<sup>2,3</sup>; Vivian Rotuno Moure<sup>\*1,2</sup>; Glaucio Valdameri<sup>\*1,2</sup>

<sup>1</sup> Programa de Pós-graduação em Ciências Farmacêuticas (PPGCF), Universidade Federal do Paraná (UFPR), Curitiba, Paraná, Brasil.

<sup>2</sup> Departamento de Análises Clínicas, Universidade Federal do Paraná (UFPR), Curitiba, Paraná, Brasil.

<sup>3</sup> Escola de Ciências da Vida, Pontifícia Universidade Católica do Paraná (PUCPR), Curitiba, Paraná, Brasil.

\*Autores correspondentes: vivian.moure@ufpr.br e gvaldameri@ufpr.br

### SIGNIFICANCE AND IMPACT OF THE STUDY

The immunological detection of different antibodies isotypes of COVID-19 may give some answers about disease severity and vaccine response. In this manner, this chapter describes a new immunological method that allow the detection of IgA, IgM and IgG at the same time by flow cytometry, providing accurate information about patient's immune responses. This method can be easily adapted for detection of antibodies against new emerging infections in the future.

### 1. INTRODUCTION

The first case of the novel coronavirus, SARS-CoV-2, which causes a disease known as COVID-19, was reported to World Health Organization (WHO) on December 31, 2019. Then, on 11 March 2020, WHO declared COVID-19 a pandemic. The course of the COVID-19 pandemic is a consequence of the rapid spread of this virus and, more recently, the emergency of novel variants. The value of diagnostic alternatives in the management of COVID-19 is high [1].

High transmission combined with virus aggressiveness of COVID-19 enhanced the hospitalizations, particularly on Intensive Care Units (ICU), collapsing the health systems in many countries. The identification of infected is a way to contain COVID-19 expansion and is essential for action plans development. In this context, the development of rapid and sensitive tests at low cost is fundamental to help to control the pandemic process (2).

The RT-qPCR (Real time reverse transcription polymerase chain reaction) is the gold standard for diagnosis. However, the detection of antibodies is also relevant to monitor the immunological response and seroconversion, particularly on a mass vaccination context (3).

Immunological methods must be applied during the epidemic process of coronavirus. The sensitivity of molecular diagnosis decreases after one week of symptom's breakthrough due the reduction of viral particles on respiratory tract. This lack of sensitivity can cause false negatives in patients with active infection (4). Thus, the understanding of immune response to SARS-CoV-2 infection is critical, especially in discrimination of disease severity and vaccine efficacy.

### 1.1 Immunological characteristics of SARS-CoV-2 infection

SARS-CoV-2 virus is formed by a set of proteins: Nucleocapsid (N), Membrane (M) Viral envelope (E) and Spike (S) proteins. Nucleocapsid protein is responsible for RNA packing, forming an helicoidal structure that binds to Membrane protein. Envelope and Spike proteins interact with each other, forming the viral envelope. This structure binds to Membrane proteins. The entrance of SARS-CoV-2 virus on host cell is mediated by Spike protein due to interaction with Angiotensin-converting enzyme 2 (ACE2). The interaction occurs specifically on Receptor binding domain (RBD) sequence, located on S1 subunit on Spike protein (5,6).

The RBD domain is considered the best target for therapies and neutralizing antibodies, so, the detection of anti-Spike neutralizing antibodies can be useful to identify recovered candidates for convalescence serum treatment. The Nucleocapsid protein is also very immunogenic and is commonly used to identify antibodies on patients' serum (5).

The classic immune response to virus involves the production of IgM as first antibody followed by IgA and IgG (7). The immune response for COVID-19 is not fully characterized. The literature shows that IgM may be produced firstly (7) but there are also some reports affirming that IgM and IgG are produced simultaneously. This least information is in accordance with the immune response for others coronavirus (9).

The seroconversion to IgM and IgG occurs 1 to 3 weeks after symptomatic infection in 50% of patients, however, the viral load may not decline (11, 12, 13). It is known that seroconversion for IgG and IgM can occur simultaneously or sequentially [2] with a median day of seroconversion of 13 days post symptom onset for both IgG and IgM [3]. The order of immunoglobulin appearance is variable (3).

The isotype IgA forms have gained attention in COVID-19 [4]. The identification of IgA on COVID-19 infection may give clinically useful information. IgA are produced on mucus surface, the detection of this class of immunoglobulin may reflect the immunological response on mucus (10). In this context, IgA can perform protective function against SARS-CoV-2 on respiratory tract, the main entrance for the virus (14). The secretory form would primarily act at the virus entry site [5] and the circulating IgA has been revealed as neutralizing antibody and correlated with disease severity [6,7]. IgA seroconversion appears as early as IgG and IgM [8], or slightly earlier than IgG and IgM [2,9].

The construction of serological profile is relevant for COVID-19 epidemiology and to determine the immune status of asymptomatic patients (3,13). Those multiple antibody isotypes target viral proteins, including spike and its receptor-binding (RBD), subunit 1 (S1) and subunit 2 (S2), and nucleocapsid (or nucleoprotein) [10,11]. Several studies described the detection of SARS-CoV-2-specific IgG and IgM [2,3,12–19],

while the detection of SARS-CoV-2-specific IgA has been less reported [8,9,14,20–22].

Most methods developed for COVID-19 immunological testing are based on immunoenzymatic and immunochromatographic tests, due to low cost and easy adaptation as a way to overcome infrastructural limitations (15). Nonetheless, those methods present some limitations such as poor application on high throughput scales and inconsistent results (16,17,18).

## 1.2 COVID-19 antibody detection methods

Serological tests can be performed using commercially available methodologies with different approaches: immunoenzymatic, fluoroenzymatic, chemiluminescence and chromatographic immunoassays. These assays can detect IgM and IgG and present high sensitivity during three weeks after symptoms breakthrough (3,12). The specificity is considered high for both above mentioned immunoglobulins (superior to 95%) but for IgA detection the specificity is near to 84% (EUROIMMUN anti-SARSCoV-2 ELISA) (19). The need of new methodologies for COVID-19 immunology is emergent.

Flow cytometry is gaining interest for COVID-19 identification/monitoring and is emerging as an alternative tool (18,20,21,22,23). This technique can analyze multiple parameters in a single cell or particle in biological samples like blood and serum. Due to the capacity to analyze individualized cells or beads with specific fluorescent probes, flow cytometry is widely used with fluorochromes-conjugated antibodies to search for specific cellular antigens. Because of its flexibility and the consolidated use of flow cytometry for diagnoses purposes, it is predictable and imperative the development of immunological flow cytometry-based diagnosis for COVID-19. The strategies based on flow cytometry can be divided in two categories: Cell based systems and Cell free systems.

## 1.3 Cell based systems

The cell-based system methods consist on cell transfections with plasmids containing viral protein gene, allowing protein expression on cell membrane. In five studies, the spike protein was overexpressed on the surface of cells, allowing the detection of antibodies in patient samples using fluorescent secondary anti-antibodies [23–27] This technique was used on HEK293T cell lines to express native Spike protein, then, cells were used to track immunoglobulins from patient serum. After the recognition of Spike protein by patient's antibodies, a second step was performed with incubation of fluorescent secondary antibody, allowing flow cytometry detection. Jurkat cells were also used as "support" for protein spike expression with the advantage that these cells are cultivated in suspension, making the assay easier (22,23).

In general, cell-based methods using flow cytometry as detection system were efficient for antibodies detection on serum and superior to ELISA based assays. They showed high sensitivity/specificity and decreased the limit of detection compared to ELISA (18). The expression of whole Spike protein allowed the recognition of antibodies with different epitopes, not only the S1 chain or RBD domain like some commercial kits (20). One disadvantage of this method is the infrastructure required for cell culture and the standardization/execution of transient transfection that presents high variability on protein expression and can directly influence the results.

## 1.4 Cell free systems

One alternative to cell-based systems is the use of beads or microspheres for protein immobilization. Beads are polymeric spheres with a chemically modified surface that allows antigen/antibody conjugation. Beads work as solid support for analyte capture on a liquid matrix (25). After incubation with samples, the fluorescent secondary antibody is added to the system, forming a sandwich that will be detected by flow cytometry. The output signal is directly proportional to fluorescent antibody binding and analyte concentration (26, 27). The complex biotin-streptavidin is also used on binding assays, improving sensitivity. In this case, the captured analyte or secondary antibody must be biotinylated, allowing the use of streptavidin as fluorochrome (28).

Commercially available beads usually have intrinsic fluorescence and may vary in size and fluorescence intensity. This variability of characteristics allows the creation of personalized analytic panels with multiparametric analysis; this system is known as multiplex. Using beads with different characteristics enables to bind many types of antigens/antibodies of interest to evaluate parameters such as the presence of different classes of immunoglobulins and inflammatory mediators related to immunological response (25,27).

This cell free system is being used for the development of flow cytometry-based test for COVID-19 diagnosis. Egia-Mendikute et al and Fong et al (16,18) used streptavidin functionalized beads to bind on biotinylated antigens (S1 Spike, RBD and Nucleocapsid proteins). Beads were incubated with serum and later marked with fluorescent anti-IgM and anti-IgG secondary antibodies. To Egia-Mendikute et al (18), the combination of three antigens created a more specific and faster test for antibody detection and decrease the limit of detection when compared to ELISA-based assays. Fong et al (16) showed that beads tests were superior to immunochromatographic tests due to the easiness of interpretation (weakly positive results on immunochromatographic tests can lead to erroneous results) and quantitative results, allowing seroconversion tracking.

Another possibility for beads-based assays is the evaluation of neutralizing antibodies. The RBD sequence is responsible for the interaction with ACE2, allowing the entrance on cell host. The conjugation of RBD sequence on beads and incubation with biotinylated ACE2 permits the evaluation of neutralizing antibodies competition for RBD sequence. In the absence of neutralizing antibodies, beads are fluorescent due to the complex formation RBD-ACE2-Biotin-Streptavidin. In the presence of neutralizing antibodies, there is competition between ACE2 and neutralizing antibodies for RBD sequence. The Streptavidin fluorescence decrease because the complex formation is interrupted meaning that the highest neutralizing antibodies titer, the lower is the streptavidin fluorescence (30).

Here, we reported the production of cytometric bead array (CBA) functional beads covalently linked to SARS-CoV-2 nucleocapsid protein, which allowed accurate multiplexed detection of IgG, IgM and IgA isotypes using flow cytometry.

## 2. MATERIALS AND METHODS

### 2.1 Chemicals and antibodies

The cytometric bead array (CBA) polystyrene beads (cat n° 560037), coupling buffer BD™ (cat n° 51-9004756), storage buffer BD™ (cat n° 51-9004758) and wash buffer BD™ (cat n° 51-9003798) were purchased from BD Biosciences. Bovine serum

albumin (BSA, A8022), 4-(N-Maleimidomethyl)cyclohexane-1-carboxylic acid 3-sulfo-N-hydroxysuccinimide ester sodium salt - sulfo-SMCC (M6035), N-ethylmaleimide (E3876) and dithiothreitol (DTT, 10197777001) were purchased from Sigma-Aldrich. Phosphate buffer saline (PBS) 10x pH 7.2 (70013-032) was purchased from Gibco. Antibodies brilliant ultraviolet (BUV395) mouse anti-human IgG (cat n° 564229), brilliant blue (BB515) mouse anti-human IgM (cat n° 564622), biotin mouse anti-human IgA1/IgA2 (cat n° 555884) and brilliant violet (BV421) streptavidin (cat n° 563259) were purchased from BD Biosciences.

## 2.2 Antigen preparation and beads conjugation

Expression and purification of recombinant SARS-CoV-2 nucleocapsid protein was performed as described previously [16]. The coupling reaction was performed as described by the manufacturer with modifications. Initially, beads and antigen were prepared. CBA E5 beads were resuspended by vortex for 30 seconds. Then 75  $\mu\text{L}$  of E5 beads were collected and sonicated for 60 seconds. After that, 1.9  $\mu\text{L}$  of DTT 1  $\text{mol.L}^{-1}$  was added, mixed with vortex and placed on horizontal shaker for 1 hour at room temperature. Then, 1 mL of coupling buffer BD™ was added, mixed, centrifuged at 2000xg for 3 minutes and the supernatant discarded. This washing step was repeated three times. Finally, the CBA beads were resuspended in coupling buffer to next step. In parallel, 90  $\mu\text{g}$  of protein in PBS (1x) was mixed with 2  $\mu\text{L}$  of Sulfo-SMCC 2  $\text{mg.mL}^{-1}$ . The mixture was placed on horizontal shaker for 1 hour at room temperature (25 °C).

The maleimide-activated nucleocapsid protein was transferred to the tube containing the prepared beads. The components were mixed in vortex and incubated under agitation for 1 hour at room temperature. After this period, 2  $\mu\text{L}$  of N-ethylmaleimide 2  $\text{mg.mL}^{-1}$  were added and kept under agitation for 15 minutes at room temperature. Then, 1 mL of storage buffer BD™ was added, mixed, centrifuged at 2000xg for 3 minutes and the supernatant discarded. This washing step was repeated three times. After this, the conjugated beads were resuspended in 500  $\mu\text{L}$  of storage buffer and kept at 4°C. The functionalized beads were stable for, at least, 2 months.

## 2.3 Samples

Human serum and EDTA-plasma were collected at Hospital Erasto Gaertner (HEG), a cancer reference center where both oncological and non-oncological COVID-19 positive patients have been admitted. This study was approved by the Ethics Committee of HEG (CEP/HEG: 31592620.4.1001.0098). The samples consisted of 10 pre-pandemic, considered as COVID-19 negative or control, and 26 COVID-19 positive, being 18 from oncologic patients and 8 from non-oncologic patients. COVID-19 positive samples were diagnosed by the detection of SARS-CoV-2 RNA using RT-PCR from nasopharyngeal sample swabs by two independent laboratories. COVID-19 positive samples were collected 14 days after hospitalization, with varied time of the appearance of first symptoms (14 to 31 days).

## 2.4 Staining and analysis

A suspension of conjugated beads was prepared following the proportion of 1  $\mu\text{L}$  of stock suspension of conjugated beads to 50  $\mu\text{L}$  of wash buffer BD™. Then, 50  $\mu\text{L}$  of diluted beads were mixed with 50  $\mu\text{L}$  serum or EDTA-plasma (pure or diluted with

PBS 1x containing BSA 0.5%) and incubated at room temperature for 90 minutes. Then, beads were centrifuged at 4000xg for 5 minutes. The supernatant was removed and 300  $\mu$ L of PBS/BSA 0.5% was added and mixed with vortex followed by centrifugation at 4000xg for 5 minutes (this step was performed twice). After that, 50  $\mu$ L of diluted anti-human antibody was added and incubated for 90 minutes (the antibody range used was 1:100; 1:200, 1:300, 1:400, 1:500, 1:1000, 1:2000, 1:3000 and 1:5000). After this time, beads were centrifuged at 4000xg for 5 minutes and washed twice with 300  $\mu$ L of PBS/BSA 0.5%. For IgG and IgM detection, the samples were resuspended in PBS and analyzed by flow cytometry using UV450/50 filter for IgG and B530/30 filter for IgM. For IgA analysis, a further incubation was performed with 50  $\mu$ L of streptavidin 1:100 for 90 minutes at room temperature (25 °C). The samples were centrifuged and washed twice with PBS/BSA 0.5%, resuspended in PBS and analyzed by flow cytometry using V450/50 filter.

For multiplex analysis, diluted beads were incubated with serum 1:1000 for 90 minutes and washed as previously described. Then a single solution was made with IgG (1:100), IgM (1:100) and IgA (1:1000). A volume of 50  $\mu$ L of antibody mixture was incubated with beads for 90 minutes and washed. After that, the incubation with streptavidin (1:100) was performed for 90 minutes and washed. The beads were resuspended in PBS and analyzed using a BD FACS Celesta™ equipped with 3 lasers (355nm, 405nm and 488nm) using UV450/50, V450/50 and B530/30 filters. The data were expressed as the percentage of positive fluorescent beads (PPFB), as previously described[28]. Statistical analysis based on receiver operating characteristic (ROC) curve was used to determine cutoff, sensibility, specificity and area under curve (AUC) using MedCalc v.7.12.7.2.0 (MedCal Software bvba).

### 3. RESULTS AND DISCUSSION

#### 3.1 Strategy at a glance

Cytometric bead array (CBA) is called functional beads by the producer and compatible with flow cytometry. These fluorescent beads have been widely used to investigate antigens in serum samples. There are several commercially available beads which are covalently covered by antibodies recognizing specific targets. The detection of the analyte using flow cytometry is performed using a fluorochrome-conjugated secondary antibody. Despite this well-established approach, the application of these CBA beads to covalently bind antigens and investigate the antibodies is poorly studied [29]. In this work, thiol groups of the commercial fluorescent polystyrene naked CBA beads were reduced to the active sulfhydryl form by DTT. The recombinant 6xHis-tagged SARS-CoV-2 nucleocapsid protein solubilized on PBS was covalently bound to CBA beads by sulfo-SMCC chemistry (Figure. 1A). These functionalized beads were named as CBA-N. CBA-N was further used as proof of concept to investigate the presence of IgG, IgM and IgA isotypes in COVID-19 positive serum samples. To allow antibodies detection, specific anti-human IgG and IgM conjugated with BD Horizon BUV395 and BD Horizon BB515 fluorochromes, respectively, were used. Biotinylated anti-human IgA1/IgA2 and streptavidin conjugated with BD Horizon BV421 was used as a second-step reagent to improve the sensitivity of IgA detection (Figure. 1B).

The prepared CBA-N was homogeneously distributed with a diameter size of 7.5  $\mu$ m, which allowed recognition by flow cytometry according to the forward (FSC) and side scatter (SSC) parameters and using a specific gate (Figure. 1C). All fluorochromes were rationally chosen to attenuate the spillover of fluorescence in a

multiplex system, since each fluorochrome is excited by a different laser. This combination of fluorochromes was optimized for a flow cytometer equipped with at least three lasers, including a 355, 405 and 488 nm lasers. As shown in Figure. 1C, the fluorescence was recorded simultaneously using three different channels.

To achieve the best standardization for multiplexed detection of IgG, IgM and IgA response to SARS-CoV-2 infection, the conditions for each antibody response were optimized.

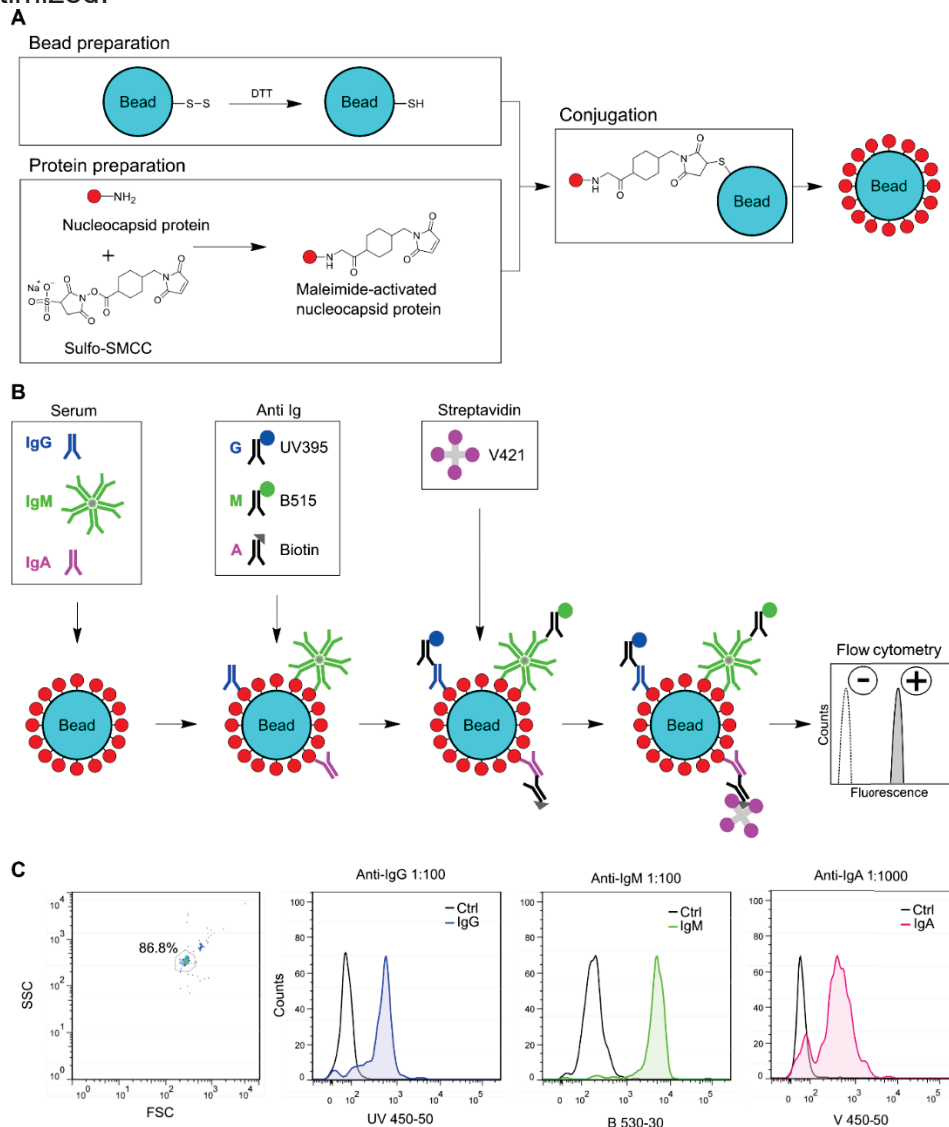


**Figure 1:** Rational strategy overview. **(A)** Fluorescent polystyrene beads of 7.5  $\mu\text{m}$  reduced by DTT. SARS-CoV-2 nucleocapsid protein solubilized in PBS covalently bound to beads surface by sulfo-SMCC chemistry to originate functionalized beads named as CBA-N. **(B)** Schematic representation of the multiplex assay. **(C)** Gate selection based on bead size. Representative histograms of COVID-19 positive samples.

### 3.2 Optimization of conditions

Negative samples were obtained before the pandemic and were called as control (Ctrl). COVID-19 positive samples were obtained of patients from an oncological hospital (HEG) at Curitiba after 14 days of hospitalization, which correspond to approximately 19 days after the symptom onset (Figure. S1). These patients were diagnosed with COVID-19 by RT-PCR positive results from two independent laboratories (data not shown), and most samples are from oncologic



patients. For standardization of antibody response, we used a mixture of, at least three, negative and positive samples.

The data were expressed as the percentage of positive fluorescent beads (PPFB) (Figure. S2). As shown in Figure. 2A, a serum dilution curve revealed that the discrimination of positive vs negative IgG samples was achieved at a serum dilution of 1000-fold. After setting the appropriate serum dilution, a range of fluorochrome conjugate (anti-IgG UV395) dilutions were evaluated. The data showed that the best results were obtained using the anti-IgG diluted 100-fold (Figure. 2B). The same rational strategy was carried out for IgM and IgA detection. The IgM detection was only able to discriminate between COVID-19 positive and negative samples when a serum dilution of 1000-fold was applied (Figure. 2C). For IgM detection, the optimized combination was with serum diluted 1000-fold and the anti-IgM B515 diluted 100-fold (Figure. 2C and D). IgA detection presented a different pattern, probably because the biotin-streptavidin system used. As shown in Figure. 2E, the best serum dilutions were between 10 and 100-fold. However, the serum 1000-fold dilution was also able to discriminate between negative and positive samples. Envisioning a multiplexed antibody detection, we decided to use 1000-fold serum dilution for the evaluation of anti-IgA curve. The anti-IgA showed similar results with secondary antibody used at dilution between 100 to 1000-fold (Figure. 2F). In addition, the anti-IgA dilution result was confirmed using the serum 10-fold diluted (Figure. S3).

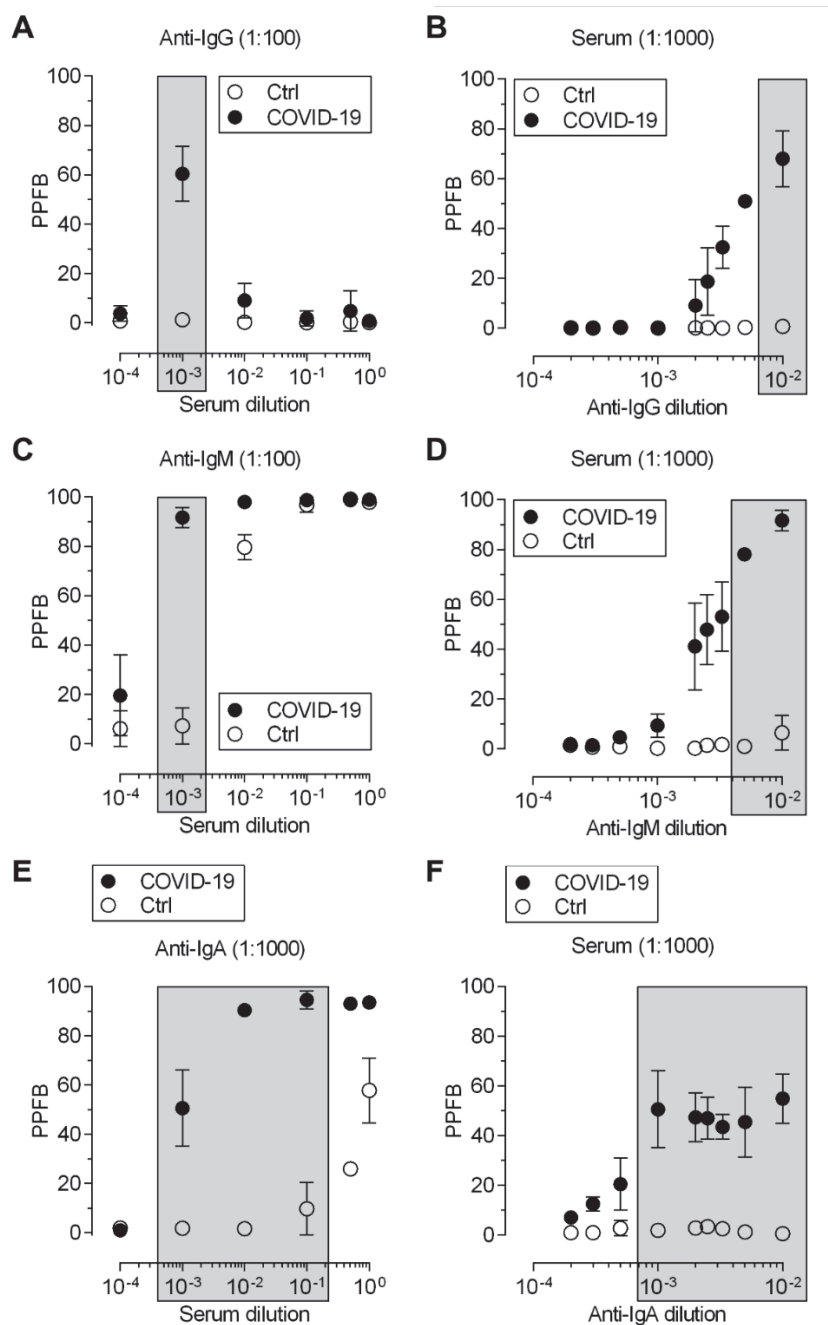


**Figure 2:** Serum and antibody dilution. Determination of Percentage of Positive Fluorescent Beads (PPFB) by flow cytometry using CBA-N beads. **(A)** Serum dilution using anti-IgG diluted 100-fold. **(B)** Anti-IgG dilution using serum diluted 1000-fold. **(C)** Serum dilution using anti-IgM diluted 100-fold. **(D)** Anti-IgM dilution using serum diluted 1000-fold. **(E)** Serum dilution using anti-IgA diluted 1000-fold. **(F)** Anti-IgA dilution using serum diluted 1000-fold. A mix of three samples were used. Data are representative of at least two independent experiments and values are expressed in mean  $\pm$  SD.

An estimation of analytical coefficient of variation (CVa) for imprecision (inter-assay;  $n=12$ ) was calculated using PPFB (%) values from serum pools of controls (mean  $2.0 \pm 2.0$ ) and COVID-19 positive (IgG, IgM and IgA combined; mean  $69.7 \pm 19.2$ ) samples, showing a CVa values of 100% and 27.5%, respectively.

### 3.3 Proof of concept

After characterization of the optimized conditions for single antibody isotype detection using dilution of serum and secondary antibodies, double and triple staining were performed. The results demonstrated the absence of fluorescence spillover (Figure. S4), confirming the feasibility of the experimental design for multiplex detection. The combination of lasers UV355 nm, V405 nm and blue 488 nm with UV395, V421 and B515 fluorochromes, allowed discriminating negative vs positive samples for the simultaneous detection of IgG, IgA and IgM, respectively, without any fluorescence compensation, as represented by the histograms (Figure. S4). Three independent beads preparations were tested, showing similar results (data not shown).

Finally, the multiplexed approach was used to evaluate a panel of negative ( $n=10$ ) and COVID-19 positive ( $n=26$ ) samples (Figure. 3, S5 and S6). ROC-established cutoff was used for discrimination of negative and COVID-19 positive samples. The specificity of 100% was achieved for all isotypes. The sensitivity was 88.5% for the detection of IgG, 92.3% for IgM and 96.2% for IgA. The area under the ROC curve was calculated as 0.946, 0.950 and 0.962 for IgG, IgM and IgA, respectively (Figure. 3 and Table S1). Venn diagram analysis showed that 22/26 presented IgG, IgM and IgA, 1/26 presented only IgG and IgA, and 2/26 presented only IgM and IgA. None of the positive samples presented only IgG and IgM, and 1/26 did not present any of the antibodies studied (Figure. 3D).

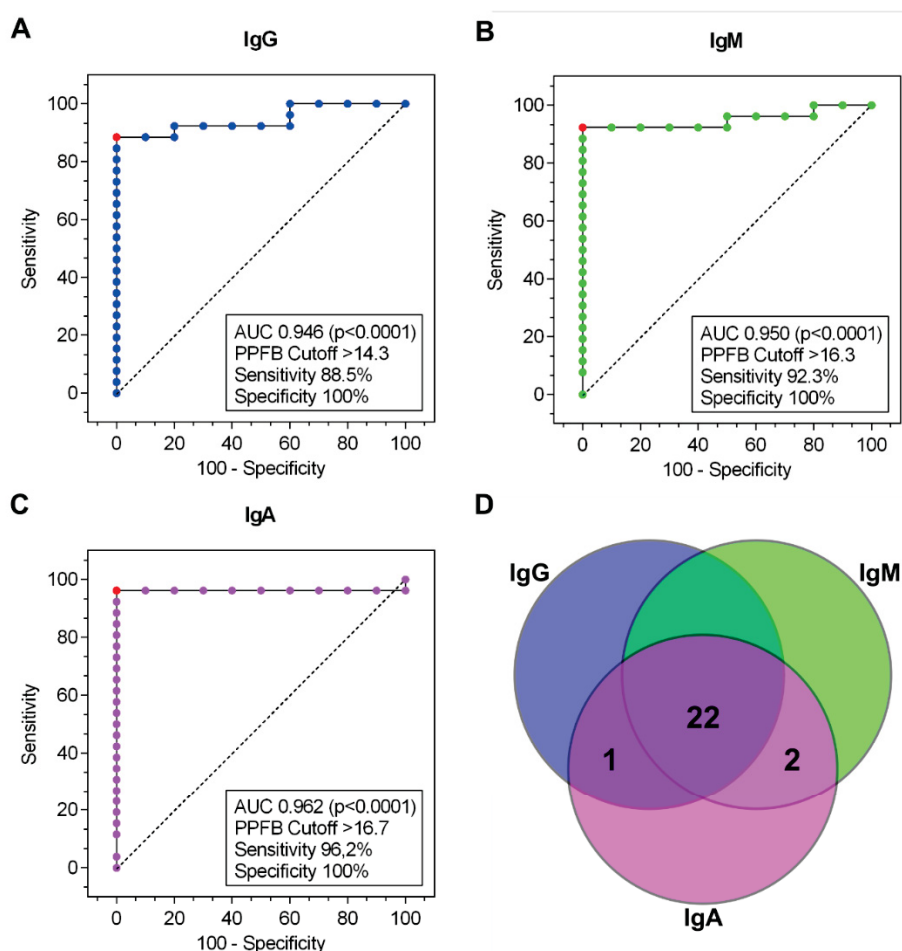


**Figure 3:** Receiver operating characteristic (ROC) curves and Venn diagram. COVID-19 negative controls ( $n=10$ ) and positive ( $n=26$ ). ROC curve for (A) IgG. (B) IgM. (C) IgA. AUC, area under de curve; PPFB, percentage of positive fluorescent beads (%); red point, highest Youden index (cutoff). (D) Venn diagram of COVID-19 positive samples simultaneously compared with the detection of IgG, IgM and IgA. The statistical calculations were performed using MedCalc v.7.12.7.2.0 (MedCal Software bvba).

Flow cytometry is described as an important analytical tool for immunological assays. Commercially available CBA functional beads are widely used for the evaluation of multiple analytes in a single sample. For instance, several papers have described the use of CBA bound to specific antibodies for the detection and quantification of a large variety of human cytokines [29] using a non-competing secondary antibody for detection. The application of flow cytometry in COVID-19 has exploited the use of cell-based assays for detection of IgM, IgA, and IgG subclasses against the SARS-CoV-2 S protein. However, most of these studies targeted a single antibody detection [23–27]. To the best of our knowledge there is only two studies employing a cell-free flow cytometric approach to evaluate the humoral immune response [19,30]. In both cases, the authors used fluorescent beads coated with streptavidin which allow the binding on biotinylated SARS-CoV-2 antigens to detect antibodies. Egia-Mendikute et al. [19] showed a simultaneous detection of IgG and IgM against SARS-CoV-2 antigens. Unexpectedly, the authors detected IgG against nucleocapsid protein in controls pre-pandemic samples [19], which is in sharp contrast to the literature [7,16,18,21]. As reported by Dogan et al. [30], the binding of each antigen to a different fluorescent bead allowed the singleplex detection of multiple antibody isotypes IgG, IgG1-4, IgM and IgA. However, the use of all secondary antibodies conjugated to phycoerythrin unmet the inherent advantage of flow cytometry for simultaneous serum antibody detection. Furthermore, it has been recognized that the detection of one antibody isotype alone has a limited value for COVID-19 diagnosis and monitoring [31]. Therefore, the need of multiplex detection of anti-SARS-CoV-2 IgG, IgM and IgA remains challenging.

In our study, the binding of SARS-CoV-2 nucleocapsid protein to CBA functional beads was covalent (Figure. 1), which offers advantages of more robust surface, higher density of epitopes and orientation to maximize epitopes exposing and complementary binding [32]. We provided a proof of concept of a cell-free multiplex assay based on flow cytometry for immunological diagnosis of COVID-19 (Figure. 1). The novel method allowed accurate discrimination between COVID-19 positive samples and pre-pandemic negative controls using standardized conditions (Figure. 2 and 3). Specificity of 100% and sensitivity of 88.5, 92.3 and 96.2% for IgG, IgM and IgA, respectively, were determined (Figure. 3 and Table S1). The results of our method for IgG and IgM showed both sensitivity and specificity similar to the FDA-approved tests (sensitivity 61-98% and specificity 90-100%) [32]. The detection of IgA showed increased sensitivity and specificity in comparison to a commercial test based on ELISA (Euroimmun™, 82.9% and 82.2%) [34]. Interestingly, the combined IgG, IgM and IgA analysis improved the serological diagnosis. Most of the RT-PCR positive samples presented the three antibody isotypes and, at least, two antibody isotypes were detected from 25/26 (Figure. 3D and S6). It should be considered that the small number of samples may affect the statistical analysis. Hence, a large cohort will be necessary to confirm the results.

A special strength of the present study is the availability of a large repertoire of combinations of multiple antigens covalent bound to each set of fluorescent CBA beads, which allows detection of unique optical signatures using conventional flow cytometers.

#### **4. FINAL REMARKS**

The detection of new cases of SARS-CoV-2 in the actual pandemic context is vital for viral propagation contention, specially with the emergence of new variants with

higher infectant potential. On the other hand, mass vaccination still demands tests for collective immune tracking.

Flow cytometry is a consolidated technique on diagnosis and is a tool capable of high throughput screening with high reliability. Many tests with polymeric and cellular matrices for antibodies research were developed but there are still possibilities for technological development. The bead-based strategy allows the conjugation of different proteins to search for many antigens/antibodies simultaneously, enhancing the possibilities with many diagnostic advantages.

The multiplexed flow cytometric-based tool presented here provided a blueprint for rapid development of antibody evaluation to others emerging infections. In summary, our data present the first flow cytometric bead-based that offers a cost-effective alternative to multiplex determination of IgG, IgM and IgA response in COVID-19, as a proof concept for further studies.

## Acknowledgments

We thank Andréa Teixeira-Carvalho for the discussion about CBA covalent immobilization. This work was supported by CNPq (grant number 400953/2016-1) and Coordenação de Aperfeiçoamento de Pessoal de Nível Superior – Brasil (CAPES) (Finance code 001).

## 5. REFERENCES

- [1] B. Hu, H. Guo, P. Zhou, Z.-L. Shi, Characteristics of SARS-CoV-2 and COVID-19, *Nat. Rev. Microbiol.* 19 (2021) 141–154. <https://doi.org/10.1038/s41579-020-00459-7>.
- [2] H.Q. Yu, B.Q. Sun, Z.F. Fang, J.C. Zhao, X.Y. Liu, Y.M. Li, X.Z. Sun, H.F. Liang, B. Zhong, Z.F. Huang, P.Y. Zheng, L.F. Tian, H.Q. Qu, D.C. Liu, E.Y. Wang, X.J. Xiao, S.Y. Li, F. Ye, L. Guan, D.S. Hu, H. Hakonarson, Z.G. Liu, N.S. Zhong, Distinct features of SARS-CoV-2-specific IgA response in COVID-19 patients, *Eur. Respir. J.* (2020). <https://doi.org/10.1183/13993003.01526-2020>.
- [3] Q.X. Long, B.Z. Liu, H.J. Deng, G.C. Wu, K. Deng, Y.K. Chen, P. Liao, J.F. Qiu, Y. Lin, X.F. Cai, D.Q. Wang, Y. Hu, J.H. Ren, N. Tang, Y.Y. Xu, L.H. Yu, Z. Mo, F. Gong, X.L. Zhang, W.G. Tian, L. Hu, X.X. Zhang, J.L. Xiang, H.X. Du, H.W. Liu, C.H. Lang, X.H. Luo, S.B. Wu, X.P. Cui, Z. Zhou, M.M. Zhu, J. Wang, C.J. Xue, X.F. Li, L. Wang, Z.J. Li, K. Wang, C.C. Niu, Q.J. Yang, X.J. Tang, Y. Zhang, X.M. Liu, J.J. Li, D.C. Zhang, F. Zhang, P. Liu, J. Yuan, Q. Li, J.L. Hu, J. Chen, A.L. Huang, Antibody responses to SARS-CoV-2 in patients with COVID-19, *Nat. Med.* (2020). <https://doi.org/10.1038/s41591-020-0897-1>.
- [4] M.W. Russell, Z. Moldoveanu, P.L. Ogra, J. Mestecky, Mucosal Immunity in COVID-19: A Neglected but Critical Aspect of SARS-CoV-2 Infection, *Front. Immunol.* 11 (2020) 3221. <https://doi.org/10.3389/fimmu.2020.611337>.
- [5] Y.X. Chao, O. Röttschke, E.-K. Tan, The role of IgA in COVID-19, *Brain. Behav. Immun.* 87 (2020) 182–183. <https://doi.org/10.1016/j.bbi.2020.05.057>.
- [6] W. Zeng, H. Ma, C. Ding, Y. Yang, Y. Sun, X. Huang, W. He, Y. Xiang, Y. Gao, T. Jin, Characterization of SARS-CoV-2-specific antibodies in COVID-19 patients reveals highly potent neutralizing IgA, *Signal Transduct. Target. Ther.* (2021). <https://doi.org/10.1038/s41392-021-00478-7>.
- [7] A.N. Grossberg, L.A. Koza, A. Ledreux, C. Prusmack, H.K. Krishnamurthy, V. Jayaraman, A.-C. Granholm, D.A. Linseman, A multiplex chemiluminescent immunoassay for serological profiling of COVID-19-positive symptomatic and asymptomatic patients, *Nat. Commun.* 12 (2021) 740. <https://doi.org/10.1038/s41467-021-21040-7>.
- [8] M. Norman, T. Gilboa, A.F. Ogata, A.M. Maley, L. Cohen, E.L. Busch, R. Lazarovits, C.P. Mao, Y. Cai, J. Zhang, J.E. Feldman, B.M. Hauser, T.M. Caradonna, B. Chen, A.G. Schmidt, G. Alter, R.C. Charles, E.T. Ryan, D.R. Walt, Ultrasensitive high-resolution profiling of early seroconversion in patients with COVID-19, *Nat. Biomed. Eng.* (2020). <https://doi.org/10.1038/s41551-020-00611-x>.
- [9] A. Padoan, L. Sciacovelli, D. Basso, D. Negrini, S. Zuin, C. Cosma, D. Faggian, P. Matricardi,

- M. Plebani, IgA-Ab response to spike glycoprotein of SARS-CoV-2 in patients with COVID-19: A longitudinal study, *Clin. Chim. Acta.* 507 (2020) 164–166.  
<https://doi.org/https://doi.org/10.1016/j.cca.2020.04.026>.
- [10] B. Meyer, C. Drosten, M.A. Müller, Serological assays for emerging coronaviruses: Challenges and pitfalls, *Virus Res.* (2014). <https://doi.org/10.1016/j.virusres.2014.03.018>.
- [11] F.Y. Chang, H.C. Chen, P.J. Chen, M.S. Ho, S.L. Hsieh, J.C. Lin, F.T. Liu, H.K. Sytwu, Immunologic aspects of characteristics, diagnosis, and treatment of coronavirus disease 2019 (COVID-19), *J. Biomed. Sci.* 27 (2020) 72. <https://doi.org/10.1186/s12929-020-00663-w>.
- [12] A. Petherick, Developing antibody tests for SARS-CoV-2, *Lancet* (London, England). (2020). [https://doi.org/10.1016/S0140-6736\(20\)30788-1](https://doi.org/10.1016/S0140-6736(20)30788-1).
- [13] S.K. Vashist, In Vitro Diagnostic Assays for COVID-19: Recent Advances and Emerging Trends, *Diagnostics.* 10 (2020) 2–7. <https://doi.org/10.3390/diagnostics10040202>.
- [14] N.M.A. Okba, M.A. Müller, W. Li, C. Wang, C.H. Geurtsvankessel, V.M. Corman, M.M. Lamers, R.S. Sikkema, E. De Bruin, F.D. Chandler, Y. Yazdanpanah, Q. Le Hingrat, D. Descamps, N. Houhou-Fidouh, C.B.E.M. Reusken, B.J. Bosch, C. Drosten, M.P.G. Koopmans, B.L. Haagmans, Severe Acute Respiratory Syndrome Coronavirus 2-Specific Antibody Responses in Coronavirus Disease Patients, *Emerg. Infect. Dis.* (2020). <https://doi.org/10.3201/eid2607.200841>.
- [15] A. Hachim, N. Kavian, C.A. Cohen, A.W.H. Chin, D.K.W. Chu, C.K.P. Mok, O.T.Y. Tsang, Y.C. Yeung, R.A.P.M. Perera, L.L.M. Poon, J.S.M. Peiris, S.A. Valkenburg, ORF8 and ORF3b antibodies are accurate serological markers of early and late SARS-CoV-2 infection, *Nat. Immunol.* (2020). <https://doi.org/10.1038/s41590-020-0773-7>.
- [16] L.F. Huergo, K.A. Selim, M.S. Conzentino, E.C.M. Gerhardt, A.R.S. Santos, B. Wagner, J.T. Alford, N. Deobald, F.O. Pedrosa, E.M. de Souza, M.B. Nogueira, S.M. Raboni, D. Souto, F.G.M. Rego, D.L. Zanette, M.N. Aoki, J.M. Nardin, B. Fornazari, H.M.P. Morales, V.A. Borges, A. Nelde, J.S. Walz, M. Becker, N. Schneiderhan-Marra, U. Rothbauer, R.A. Reis, K. Forchhammer, Magnetic Bead-Based Immunoassay Allows Rapid, Inexpensive, and Quantitative Detection of Human SARS-CoV-2 Antibodies, *ACS Sensors.* (2021). <https://doi.org/10.1021/acssensors.0c02544>.
- [17] R.R. de Assis, A. Jain, R. Nakajima, A. Jasinskis, J. Felgner, J.M. Obiero, P.J. Norris, M. Stone, G. Simmons, A. Bagri, J. Irsch, M. Schreiber, A. Buser, A. Holbro, M. Battegay, P. Hosimer, C. Noesen, O. Adenaiye, S. Tai, F. Hong, D.K. Milton, D.H. Davies, P. Contestable, L.M. Corash, M.P. Busch, P.L. Felgner, S. Khan, Analysis of SARS-CoV-2 antibodies in COVID-19 convalescent blood using a coronavirus antigen microarray, *Nat. Commun.* (2021). <https://doi.org/10.1038/s41467-020-20095-2>.
- [18] J. Mariën, A. Ceulemans, J. Michiels, L. Heyndrickx, K. Kerkhof, N. Foque, M.-A. Widdowson, L. Mortgat, E. Duysburgh, I. Desombere, H. Jansens, M. Van Esbroeck, K.K. Ariën, Evaluating SARS-CoV-2 spike and nucleocapsid proteins as targets for antibody detection in severe and mild COVID-19 cases using a Luminex bead-based assay, *J. Virol. Methods.* 288 (2021) 114025. <https://doi.org/https://doi.org/10.1016/j.jviromet.2020.114025>.
- [19] L. Egia-Mendikute, A. Bosch, E. Prieto-Fernández, S.Y. Lee, B. Jiménez-Lasheras, A. García del Río, A. Antoñana-Vildosola, C. Bruzzone, M. Bizkarguenaga, N. Embade, R. Gil-Redondo, M.L. Martínez-Chantar, M. López-Hoyos, N.G.A. Abrescia, J.M. Mato, Ó. Millet, A. Palazón, Sensitive detection of SARS-CoV-2 seroconversion by flow cytometry reveals the presence of nucleoprotein-reactive antibodies in unexposed individuals, *Commun. Biol.* 4 (2021) 486. <https://doi.org/10.1038/s42003-021-02011-6>.
- [20] G.M.N. Behrens, A. Cossmann, M. V. Stankov, T. Witte, D. Ernst, C. Happle, A. Jablonka, Perceived versus proven SARS-CoV-2-specific immune responses in health-care professionals, *Infection.* (2020). <https://doi.org/10.1007/s15010-020-01461-0>.
- [21] A. Munitz, L. Edry-Botzer, M. Itan, R. Tur-Kaspa, D. Dicker, D. Marcoviciu, M.G. Goren, M. Mor, S. Lev, T. Gottesman, K. Muhsen, D. Cohen, M. Stein, U. Qimron, N.T. Freund, Y. Wine, M. Gerlic, Rapid seroconversion and persistent functional IgG antibodies in severe COVID-19 patients correlates with an IL-12p70 and IL-33 signature, *Sci. Rep.* (2021). <https://doi.org/10.1038/s41598-021-83019-0>.
- [22] D. Sterlin, A. Mathian, M. Miyara, A. Mohr, F. Anna, L. Claër, P. Quentric, J. Fadlallah, H. Devilliers, P. Ghillani, C. Gunn, R. Hockett, S. Mudumba, A. Guihot, C.E. Luyt, J. Mayaux, A. Beurton, S. Fourati, T. Bruel, O. Schwartz, J.M. Lacorte, H. Yssel, C. Parizot, K. Dorgham, P. Charneau, Z. Amoura, G. Gorochov, IgA dominates the early neutralizing antibody response to SARS-CoV-2, *Sci. Transl. Med.* 13 (2021). <https://doi.org/10.1126/scitranslmed.abd2223>.
- [23] D. Lapuente, C. Maier, P. Irrgang, J. Hübner, S. Peter, M. Hoffmann, A. Ensser, K. Ziegler,

- T.H. Winkler, A.E. Kremer, P. Steininger, K. Korn, F. Neipel, M. Tenbusch, Rapid response flow cytometric assay for the detection of antibody responses to SARS-CoV-2, 2 (2020).
- [24] C. Simard, J. Richard, R. Bazin, A. Finzi, P. Trepanier, Standardization of a flow cytometry SARS-CoV-2 serologic test., *MedRxiv*. (2021).
- [25] L. Horndler, P. Delgado, D. Abia, I. Balabanov, P. Martínez-Fleta, G. Cornish, M.A. Llamas, S. Serrano-Villar, F. Sánchez-Madrid, M. Fresno, H.M. van Santen, B. Alarcón, Flow cytometry multiplexed method for the detection of neutralizing human antibodies to the native SARS-CoV-2 spike protein, *EMBO Mol. Med.* 13 (2021) e13549. <https://doi.org/https://doi.org/10.15252/emmm.202013549>.
- [26] Y.S. Goh, J.-M. Chavatte, A. Lim Jieling, B. Lee, P.X. Hor, S.N. Amrun, C.Y.-P. Lee, R.S.-L. Chee, B. Wang, C.Y. Lee, E.Z.X. Ngoh, C.-I. Wang, B.E. Young, P.A. Tambyah, S. Kalimuddin, S. Pada, S.-Y. Tan, L.J. Sun, M.I.-C. Chen, Y.-S. Leo, D.C. Lye, L.F.P. Ng, R.T.P. Lin, L. Renia, Sensitive detection of total anti-Spike antibodies and isotype switching in asymptomatic and symptomatic individuals with COVID-19, *Cell Reports Med.* 2 (2021) 100193. <https://doi.org/https://doi.org/10.1016/j.xcrm.2021.100193>.
- [27] S.P. Anand, J. Prévost, J. Richard, J. Perreault, T. Tremblay, M. Drouin, M.J. Fournier, A. Lewin, R. Bazin, A. Finzi, High-throughput detection of antibodies targeting the SARS-CoV-2 Spike in longitudinal convalescent plasma samples, *Transfusion.* 61 (2021) 1377–1382. <https://doi.org/10.1111/trf.16318>.
- [28] H. Gama Ker, R. Dian de Oliveira Aguiar-Soares, B. Mendes Roatt, N. das Dores Moreira, W. Coura-Vital, C. Martins Carneiro, A. Teixeira-Carvalho, O. Assis Martins-Filho, R. Cordeiro Giunchetti, D. da Silveira-Lemos, A. Barbosa Reis, Effect of the preservative and temperature conditions on the stability of *Leishmania infantum* promastigotes antigens applied in a flow cytometry diagnostic method for canine visceral leishmaniasis, *Diagn. Microbiol. Infect. Dis.* 76 (2013) 470–476. <https://doi.org/10.1016/j.diagmicrobio.2013.04.007>.
- [29] E. Morgan, R. Varro, H. Sepulveda, J.A. Ember, J. Apgar, J. Wilson, L. Lowe, R. Chen, L. Shivraj, A. Agadir, R. Campos, D. Ernst, A. Gaur, Cytometric bead array: a multiplexed assay platform with applications in various areas of biology, *Clin. Immunol.* 110 (2004) 252–266. <https://doi.org/https://doi.org/10.1016/j.clim.2003.11.017>.
- [30] M. Dogan, L. Kozhaya, L. Placek, C. Gunter, M. Yigit, R. Hardy, M. Plassmeyer, P. Coatney, K. Lillard, Z. Bukhari, M. Kleinberg, C. Hayes, M. Arditi, E. Klapper, N. Merin, B.T.T. Liang, R. Gupta, O. Alpan, D. Unutmaz, SARS-CoV-2 specific antibody and neutralization assays reveal the wide range of the humoral immune response to virus, *Commun. Biol.* 4 (2021) 1–13. <https://doi.org/10.1038/s42003-021-01649-6>.
- [31] P. Escribano, A. Álvarez-Uría, R. Alonso, P. Catalán, L. Alcalá, P. Muñoz, J. Guinea, Detection of SARS-CoV-2 antibodies is insufficient for the diagnosis of active or cured COVID-19, *Sci. Rep.* 10 (2020) 1–7. <https://doi.org/10.1038/s41598-020-76914-5>.
- [32] N.G. Welch, J.A. Scoble, B.W. Muir, P.J. Pigram, Orientation and characterization of immobilized antibodies for improved immunoassays (Review)., *Biointerphases.* 12 (2017) 02D301. <https://doi.org/10.1116/1.4978435>.
- [33] B. Sen-Crowe, M. McKenney, A. Elkbuli, COVID-19 laboratory testing issues and capacities as we transition to surveillance testing and contact tracing, *Am. J. Emerg. Med.* 40 (2021) 217–219. <https://doi.org/10.1016/j.ajem.2020.05.071>.
- [34] G. Cota, M.L. Freire, C.S. de Souza, M.J. Pedras, J.W. Saliba, V. Faria, L.L. Alves, A. Rabello, D.M. Avelar, Diagnostic performance of commercially available COVID-19 serology tests in Brazil, *Int. J. Infect. Dis.* 101 (2020) 382–390. <https://doi.org/10.1016/j.ijid.2020.10.008>.

## THESIS CONCLUSION

One of the goals of this thesis was the identification of new inhibitors of ABCG2 based on porphyrin scaffold. Among a set of porphyrins, porphyrin **4B** was the most promising, since selectively inhibited ABCG2 activity. This compound was not transported by ABCG2 and successfully chemosensitized resistant cancer cell lines. These results can guide *in vivo* experiments and the synthesis of a second generation of porphyrinic inhibitors for improve some features, as the therapeutic ratio. Other goal was the synthesis and biological evaluation of heterodimers targeting ABCG2. The tested conditions used during the synthesis process may serve as a guide for new synthetic approaches and conditions optimization. BODIPY – cholesterol heterodimer seems to be promising to investigate the role of cholesterol on ABCG2, as a possible transport of cholesterol mediated by ABCG2. Unfortunately, the strategy of heterodimers containing cholesterol was useless since cholesterol abrogated the chalcone inhibitory effect.

The unprecedented COVID-19 pandemic started during the development of this thesis. In Brazil, more than 95% of the scientific production is generated by public universities. Considering this pivot role of universities, an additional goal was added in this thesis, targeting the development of a multiplex flow cytometric bead-based method for detection of antibodies against SARS-CoV-2 infection. The proposed method showed high specificity and sensitivity and can be applied to better understand the immunological response on COVID-19 disease. This method can be easily improved using other antigens, allowing the simultaneous detection of antibodies against different diseases.

## REFERENCES

- [1] Y.A. Luqmani, Mechanisms of Drug Resistance in Cancer Chemotherapy, *Med. Princ. Pract.* 14(suppl 1 (2005) 35–48. <https://doi.org/10.1159/000086183>.
- [2] K. Bukowski, M. Kciuk, R. Kontek, Mechanisms of Multidrug Resistance in Cancer Chemotherapy, *Int. J. Mol. Sci.* 21 (2020). <https://doi.org/10.3390/ijms21093233>.
- [3] Q. Wu, Z. Yang, Y. Nie, Y. Shi, D. Fan, Multi-drug resistance in cancer chemotherapeutics: Mechanisms and lab approaches, *Cancer Lett.* 347 (2014) 159–166. <https://doi.org/https://doi.org/10.1016/j.canlet.2014.03.013>.
- [4] S.M. Simon, M. Schindler, Cell biological mechanisms of multidrug resistance in tumors, *Proc. Natl. Acad. Sci.* 91 (1994) 3497 LP – 3504. <https://doi.org/10.1073/pnas.91.9.3497>.
- [5] M. Dean, The genetics of ATP-binding cassette transporters., *Methods Enzymol.* 400 (2005) 409–429. [https://doi.org/10.1016/S0076-6879\(05\)00024-8](https://doi.org/10.1016/S0076-6879(05)00024-8).
- [6] M. Dean, A. Rzhetsky, R. Allikmets, The human ATP-binding cassette (ABC) transporter superfamily, *Genome Res.* 11 (2001) 1156–1166. <https://doi.org/10.1101/gr.184901>.
- [7] M.M. Gottesman, I. Pastan, Biochemistry of Multidrug Resistance mediated by the Multidrug transporter, *Annu. Rev. Biochem.* 62 (1993) 385–427.
- [8] R.W. Robey, S. Shukla, E.M. Finley, R.K. Oldham, D. Barnett, S. V Ambudkar, T. Fojo, S.E. Bates, Inhibition of P-glycoprotein (ABCB1)- and multidrug resistance-associated protein 1 (ABCC1)-mediated transport by the orally administered inhibitor, CBT-1((R))., *Biochem. Pharmacol.* 75 (2008) 1302–1312. <https://doi.org/10.1016/j.bcp.2007.12.001>.
- [9] I.S. Mohammad, W. He, L. Yin, Understanding of human ATP binding cassette superfamily and novel multidrug resistance modulators to overcome MDR., *Biomed. Pharmacother.* 100 (2018) 335–348. <https://doi.org/10.1016/j.biopha.2018.02.038>.
- [10] K.J. Linton, Structure and Function of ABC Transporters, *Physiology.* 22 (2007) 122–130. <https://doi.org/10.1152/physiol.00046.2006>.
- [11] I.B. Holland, ABC transporters, mechanisms and biology: an overview, *Essays Biochem.* 50 (2011) 1–17. <https://doi.org/10.1042/bse0500001>.
- [12] Y.H. Choi, A. Yu, ABC Transporters in Multidrug Resistance and Pharmacokinetics , and Strategies for Drug Development, *Curr. Pharm. Des.* 20 (2014) 793–807.



- [13] R.L. Juliano, V. Ling, A surface glycoprotein modulating drug permeability in Chinese hamster ovary cell mutants, *Biochim. Biophys. Acta - Biomembr.* 455 (1976) 152–162. [https://doi.org/https://doi.org/10.1016/0005-2736\(76\)90160-7](https://doi.org/https://doi.org/10.1016/0005-2736(76)90160-7).
- [14] S.P.C. Cole, G. Bhardwaj, J.H. Gerlach, J.E. Mackie, C.E. Grant, K.C. Almquist, A.J. Stewart, E.U. Kurz, A.M. V Duncan, R.G. Deeley, Overexpression of a Transporter Gene in a Multidrug-Resistant Human Lung Cancer Cell Line, *Science* (80-. ). 258 (1992) 1650–1654. <https://doi.org/10.1126/science.1360704>.
- [15] K. Natarajan, Y. Xie, M.R. Baer, D.D. Ross, Role of breast cancer resistance protein (BCRP/ABCG2) in cancer drug resistance, *Biochem. Pharmacol.* 83 (2012) 1084–1103. <https://doi.org/https://doi.org/10.1016/j.bcp.2012.01.002>.
- [16] L.A. Doyle, W. Yang, L. V Abruzzo, T. Krogmann, Y. Gao, A.K. Rishi, D.D. Ross, A multidrug resistance transporter from human MCF-7 breast cancer cells., *Proc. Natl. Acad. Sci. U. S. A.* 95 (1998) 15665–15670. <https://doi.org/10.1073/pnas.95.26.15665>.
- [17] K. Miyake, L. Mickley, T. Litman, Z. Zhan, R. Robey, B. Cristensen, M. Brangi, L. Greenberger, M. Dean, T. Fojo, S.E. Bates, Molecular Cloning of cDNAs Which Are Highly Overexpressed in Mitoxantrone-resistant Cells, *Cancer Res.* 59 (1999) 8–13. <http://cancerres.aacrjournals.org/content/59/1/8.abstract>.
- [18] R. Allikmets, L.M. Schriml, A. Hutchinson, V. Romano-Spica, M. Dean, A human placenta-specific ATP-binding cassette gene (ABCP) on chromosome 4q22 that is involved in multidrug resistance., *Cancer Res.* 58 (1998) 5337–5339.
- [19] M.M. Gottesman, S. V Ambudkar, D. Xia, Structure of a multidrug transporter, *Nat. Biotechnol.* 27 (2009) 546–547. <https://doi.org/10.1038/nbt0609-546>.
- [20] J.-P. Becker, G. Depret, F. Van Bambeke, P.M. Tulkens, M. Prévost, Molecular models of human P-glycoprotein in two different catalytic states., *BMC Struct. Biol.* 9 (2009) 3. <https://doi.org/10.1186/1472-6807-9-3>.
- [21] T.J. Altstadt, C.R. Fairchild, J. Golik, K.A. Johnston, J.F. Kadow, F.Y. Lee, B.H. Long, W.C. Rose, D.M. Vyas, H. Wong, M.-J. Wu, M.D. Wittman, Synthesis and Antitumor Activity of Novel C-7 Paclitaxel Ethers: Discovery of BMS-184476, *J. Med. Chem.* 44 (2001) 4577–4583. <https://doi.org/10.1021/jm0102607>.
- [22] M. Distefano, G. Scambia, C. Ferlini, C. Gaggini, R. De Vincenzo, A. Riva, E. Bombardelli, I. Ojima, A. Fattorossi, P.B. Panici, S. Mancuso, Anti-proliferative activity of a new class of taxanes (14 $\beta$ -hydroxy-10-deacetylbaaccatin III derivatives) on multidrug-resistance-positive human cancer cells, *Int. J. Cancer.* 72 (1997) 844–850. [https://doi.org/https://doi.org/10.1002/\(SICI\)1097-0215\(19970904\)72:5<844::AID-IJC22>3.0.CO;2-7](https://doi.org/https://doi.org/10.1002/(SICI)1097-0215(19970904)72:5<844::AID-IJC22>3.0.CO;2-7).
- [23] M. Shionoya, T. Jimbo, M. Kitagawa, T. Soga, A. Tohgo, DJ-927, a novel oral taxane, overcomes P-glycoprotein-mediated multidrug resistance in vitro and in vivo, *Cancer Sci.* 94 (2003) 459–466. <https://doi.org/https://doi.org/10.1111/j.1349-7006.2003.tb01465.x>.
- [24] H. Glavinas, P. Krajcsi, J. Cserepes, B. Sarkadi, The Role of ABC Transporters in Drug Resistance , *Metabolism and Toxicity, Curr. Drug Deliv.* 1 (2004) 27–42.
- [25] G. Szakács, M.D. Hall, M.M. Gottesman, A. Boumendjel, R. Kachadourian, B.J. Day, H. Cortay-Baubichon, A. Di Pietro, Targeting the Achilles Heel of Multidrug-Resistant Cancer by Exploiting the Fitness Cost of Resistance Gergely Szaka c, (2014).
- [26] W. Szybaski, V. Bryson, Genetic studies on microbial cross resistance to toxic agents. I. Cross resistance of *Escherichia coli* to fifteen antibiotics, *J. Bacteriol.* 64 (1952) 489–499. <https://doi.org/10.1128/jb.64.4.489-499.1952>.
- [27] N.T. Bech-Hansen, J.E. Till, V. Ling, Pleiotropic phenotype of colchicine-resistant CHO cells: cross-resistance and collateral sensitivity., *J. Cell. Physiol.* 88 (1976) 23–31. <https://doi.org/10.1002/jcp.1040880104>.
- [28] J.R. Warr, D.J. Flanagan, M. Anderson, Mutants of Chinese hamster ovary cells with altered sensitivity to taxol and benzimidazole carbamates, *Cell Biol. Int. Rep.* 6 (1982) 455–460. [https://doi.org/https://doi.org/10.1016/0309-1651\(82\)90117-5](https://doi.org/https://doi.org/10.1016/0309-1651(82)90117-5).
- [29] J.R. Warr, F. Brewer, M. Anderson, J. Fergusson, Verapamil hypersensitivity of vincristine resistant Chinese hamster ovary cell lines., *Cell Biol. Int. Rep.* 10 (1986) 389–399. [https://doi.org/10.1016/0309-1651\(86\)90011-1](https://doi.org/10.1016/0309-1651(86)90011-1).
- [30] J.R. Warr, M. Anderson, J. Fergusson, Properties of verapamil-hypersensitive multidrug-resistant Chinese hamster ovary cells., *Cancer Res.* 48 (1988) 4477–4483.
- [31] D.F. Cano-Gauci, J.R. Riordan, Action of calcium antagonists on multidrug resistant cells. Specific cytotoxicity independent of increased cancer drug accumulation., *Biochem. Pharmacol.* 36 (1987) 2115–2123. [https://doi.org/10.1016/0006-2952\(87\)90139-0](https://doi.org/10.1016/0006-2952(87)90139-0).
- [32] J. Karwatsky, M.C. Lincoln, E. Georges, A Mechanism for P-Glycoprotein-Mediated Apoptosis As

- Revealed by Verapamil Hypersensitivity, *Biochemistry*. 42 (2003) 12163–12173. <https://doi.org/10.1021/bi034149+>.
- [33] V. Kuete, P.D. Tchakam, B. Wiench, B. Ngameni, H.K. Wabo, M.F. Tala, M.L. Moungang, B.T. Ngadjui, T. Murayama, T. Efferth, Cytotoxicity and modes of action of four naturally occurring benzophenones: 2,2',5,6'-tetrahydroxybenzophenone, guttiferone E, isogarcinol and isoxanthochymol., *Phytomedicine*. 20 (2013) 528–536. <https://doi.org/10.1016/j.phymed.2013.02.003>.
- [34] S.M. Jackson, I. Manolaridis, J. Kowal, M. Zechner, N.M.I. Taylor, M. Bause, S. Bauer, R. Bartholomaeus, G. Bernhardt, B. Koenig, A. Buschauer, H. Stahlberg, K.H. Altmann, K.P. Locher, Structural basis of small-molecule inhibition of human multidrug transporter ABCG2, *Nat. Struct. Mol. Biol.* 25 (2018) 333–340. <https://doi.org/10.1038/s41594-018-0049-1>.
- [35] D. Peña-Solórzano, S.A. Stark, B. König, C.A. Sierra, C. Ochoa-Puentes, ABCG2/BCRP: Specific and Nonspecific Modulators, *Med. Res. Rev.* 37 (2017) 987–1050. <https://doi.org/https://doi.org/10.1002/med.21428>.
- [36] M. de Bruin, K. Miyake, T. Litman, R. Robey, S.E. Bates, Reversal of resistance by GF120918 in cell lines expressing the ABC half-transporter, MXR, *Cancer Lett.* 146 (1999) 117–126. [https://doi.org/https://doi.org/10.1016/S0304-3835\(99\)00182-2](https://doi.org/https://doi.org/10.1016/S0304-3835(99)00182-2).
- [37] L.D. Weidner, S.S. Zoghbi, S. Lu, S. Shukla, S. V. Ambudkar, V.W. Pike, J. Mulder, M.M. Gottesman, R.B. Innis, M.D. Hall, The inhibitor Ko143 is not specific for ABCG2, *J. Pharmacol. Exp. Ther.* 354 (2015) 384–393. <https://doi.org/10.1124/jpet.115.225482>.
- [38] J.D. Allen, A. van Loevezijn, J.M. Lakhai, M. van der Valk, O. van Tellingen, G. Reid, J.H.M. Schellens, G.-J. Koomen, A.H. Schinkel, Potent and Specific Inhibition of the Breast Cancer Resistance Protein Multidrug Transporter *in Vitro* and in Mouse Intestine by a Novel Analogue of Fumitremorgin C 1 This work was supported in part by grant NKI 97-1433 from the Dutch Cancer Socie, *Mol. Cancer Ther.* 1 (2002) 417 LP – 425. <http://mct.aacrjournals.org/content/1/6/417.abstract>.
- [39] Y.A. Gandhi, M.E. Morris, Structure–Activity Relationships and Quantitative Structure–Activity Relationships for Breast Cancer Resistance Protein (ABCG2), *AAPS J.* 11 (2009) 541. <https://doi.org/10.1208/s12248-009-9132-1>.
- [40] J.S. Shim, J.O. Liu, Recent Advances in Drug Repositioning for the Discovery of New Anticancer Drugs, *Int J Biol Sci.* 10 (2014) 654–663. <https://doi.org/10.7150/ijbs.9224>.
- [41] Y. Zhang, A. Gupta, H. Wang, L. Zhou, R.R. Vethanayagam, J.D. Unadkat, Q. Mao, BCRP Transports Dipyridamole and is Inhibited by Calcium Channel Blockers, *Pharm. Res.* 22 (2005) 2023–2034. <https://doi.org/10.1007/s11095-005-8384-4>.
- [42] Y. Toyoda, T. Takada, H. Suzuki, Inhibitors of Human ABCG2: From Technical Background to Recent Updates With Clinical Implications, *Front. Pharmacol.* 10 (2019) 208. <https://doi.org/10.3389/fphar.2019.00208>.
- [43] J. Weiss, W.E. Haefeli, Potential of the novel antiretroviral drug rilpivirine to modulate the expression and function of drug transporters and drug-metabolising enzymes *in vitro.*, *Int. J. Antimicrob. Agents.* 41 (2013) 484–487. <https://doi.org/10.1016/j.ijantimicag.2013.01.004>.
- [44] A. Gupta, Y. Zhang, J.D. Unadkat, Q. Mao, HIV Protease Inhibitors Are Inhibitors but Not Substrates of the Human Breast Cancer Resistance Protein (BCRP/ABCG2), *J. Pharmacol. Exp. Ther.* 310 (2004) 334 LP – 341. <https://doi.org/10.1124/jpet.104.065342>.
- [45] T.J. Raub, P-Glycoprotein Recognition of Substrates and Circumvention through Rational Drug Design, *Mol. Pharm.* 3 (2006) 3–25. <https://doi.org/10.1021/mp0500871>.
- [46] E. Nicolle, A. Boumendjel, S. Macalou, E. Genoux, A. Ahmed-Belkacem, P.A. Carrupt, A. Di Pietro, QSAR analysis and molecular modeling of ABCG2-specific inhibitors, *Adv. Drug Deliv. Rev.* 61 (2009) 34–46. <https://doi.org/10.1016/j.addr.2008.10.004>.
- [47] G. Szakács, J.K. Paterson, J.A. Ludwig, C. Booth-Genthe, M.M. Gottesman, Targeting multidrug resistance in cancer, *Nat. Rev. Drug Discov.* 5 (2006) 219–234. <https://doi.org/10.1038/nrd1984>.
- [48] A. Boumendjel, S. Macalou, A. Ahmed-Belkacem, M. Blanc, A. Di Pietro, Acridone derivatives: Design, synthesis, and inhibition of breast cancer resistance protein ABCG2, *Bioorg. Med. Chem.* 15 (2007) 2892–2897. <https://doi.org/https://doi.org/10.1016/j.bmc.2007.02.017>.
- [49] T. Hegedűs, L. Örfi, A. Seprődi, A. Váradi, B. Sarkadi, G. Kéri, Interaction of tyrosine kinase inhibitors with the human multidrug transporter proteins, MDR1 and MRP1, *Biochim. Biophys. Acta - Mol. Basis Dis.* 1587 (2002) 318–325. [https://doi.org/https://doi.org/10.1016/S0925-4439\(02\)00095-9](https://doi.org/https://doi.org/10.1016/S0925-4439(02)00095-9).
- [50] C. Özvegy-Laczka, T. Hegedűs, G. Várady, O. Ujhelly, J.D. Schuetz, A. Váradi, G. Kéri, L. Örfi, K. Németh, B. Sarkadi, High-Affinity Interaction of Tyrosine Kinase Inhibitors with the ABCG2 Multidrug Transporter, *Mol. Pharmacol.* 65 (2004) 1485 LP – 1495. <https://doi.org/10.1124/mol.65.6.1485>.
- [51] S. Zhang, X. Yang, M.E. Morris, Flavonoids Are Inhibitors of Breast Cancer Resistance Protein (ABCG2)-Mediated Transport, *Mol. Pharmacol.* 65 (2004) 1208 LP – 1216. <https://doi.org/10.1124/mol.65.5.1208>.

- [52] C.J. Henrich, R.W. Robey, K. Takada, H.R. Bokesch, S.E. Bates, S. Shukla, S. V Ambudkar, J.B. McMahon, K.R. Gustafson, Botryllamides: Natural Product Inhibitors of ABCG2, *ACS Chem. Biol.* 4 (2009) 637–647. <https://doi.org/10.1021/cb900134c>.
- [53] S. Shukla, H. Zaher, A. Hartz, B. Bauer, J.A. Ware, S. V Ambudkar, Curcumin Inhibits the Activity of ABCG2/BCRP1, a Multidrug Resistance-Linked ABC Drug Transporter in Mice, *Pharm. Res.* 26 (2009) 480–487. <https://doi.org/10.1007/s11095-008-9735-8>.
- [54] L. Homolya, T.I. Orbán, L. Csanády, B. Sarkadi, Mitoxantrone is expelled by the ABCG2 multidrug transporter directly from the plasma membrane, *Biochim. Biophys. Acta - Biomembr.* 1808 (2011) 154–163. <https://doi.org/https://doi.org/10.1016/j.bbmem.2010.07.031>.
- [55] R.W. Robey, K. Steadman, O. Polgar, K. Morisaki, M. Blayney, P. Mistry, S.E. Bates, Pheophorbide a Is a Specific Probe for ABCG2 Function and Inhibition, *Cancer Res.* 64 (2004) 1242–1246. <https://doi.org/10.1158/0008-5472.CAN-03-3298>.
- [56] G. Valdameri, L. Pereira Rangel, C. Spatafora, J. Guitton, C. Gauthier, O. Arnaud, A. Ferreira-Pereira, P. Falson, S.M.B. Winnischofer, M.E.M. Rocha, C. Tringali, A. Di Pietro, Methoxy Stilbenes as Potent, Specific, Untransported, and Noncytotoxic Inhibitors of Breast Cancer Resistance Protein, *ACS Chem. Biol.* 7 (2012) 322–330. <https://doi.org/10.1021/cb200435y>.
- [57] E. Wang, C.N. Casciano, R.P. Clement, W.W. Johnson, Cholesterol Interaction with the Daunorubicin Binding Site of P-Glycoprotein, *Biochem. Biophys. Res. Commun.* 276 (2000) 909–916. <https://doi.org/https://doi.org/10.1006/bbrc.2000.3554>.
- [58] G.P. Tegos, A.M. Evangelisti, J.J. Strouse, O. Ursu, C. Bologna, L.A. Sklar, A high throughput flow cytometric assay platform targeting transporter inhibition, *Drug Discov. Today Technol.* 12 (2014) e95–e103. <https://doi.org/https://doi.org/10.1016/j.ddtec.2014.03.010>.
- [59] F. Förster, A. Volz, G. Fricker, Compound profiling for ABCC2 (MRP2) using a fluorescent microplate assay system, *Eur. J. Pharm. Biopharm.* 69 (2008) 396–403. <https://doi.org/https://doi.org/10.1016/j.ejpb.2007.10.003>.
- [60] B. Bauer, D.S. Miller, G. Fricker, Compound Profiling for P-Glycoprotein at the Blood–Brain Barrier Using a Microplate Screening System, *Pharm. Res.* 20 (2003) 1170–1176. <https://doi.org/10.1023/A:1025040712857>.
- [61] T. Frgala, O. Kalous, R.T. Proffitt, C.P. Reynolds, A fluorescence microplate cytotoxicity assay with a 4-log dynamic range that identifies synergistic drug combinations, *Mol. Cancer Ther.* 6 (2007) 886–897. <https://doi.org/10.1158/1535-7163.MCT-04-0331>.
- [62] H. Glavinas, P. Krajcsi, J. Cserepes, B. Sarkadi, The Role of ABC Transporters in Drug Resistance, Metabolism and Toxicity, *Curr. Drug Deliv.* 1 (2004).
- [63] G. Szakács, A. Váradi, C. Özvegy-Laczka, B. Sarkadi, The role of ABC transporters in drug absorption, distribution, metabolism, excretion and toxicity (ADME–Tox), *Drug Discov. Today.* 13 (2008) 379–393. <https://doi.org/10.1016/j.drudis.2007.12.010>.
- [64] E. Ulukaya, M. Colakogullari, E.J. Wood, Interference by Anti-Cancer Chemotherapeutic Agents in the MTT-Tumor Chemosensitivity Assay, *Chemotherapy.* 50 (2004) 43–50. <https://doi.org/10.1159/000077285>.
- [65] M.C. Alley, D.A. Scudiero, A. Monks, M.L. Hursey, M.J. Czerwinski, D.L. Fine, B.J. Abbott, J.G. Mayo, R.H. Shoemaker, M.R. Boyd, Feasibility of Drug Screening with Panels of Human Tumor Cell Lines Using a Microculture Tetrazolium Assay, *Cancer Res.* 48 (1988) 589–601. <https://cancerres.aacrjournals.org/content/48/3/589>.
- [66] H. Mueller, M.U. Kassack, M. Wiese, Comparison of the Usefulness of the MTT, ATP, and Calcein Assays to Predict the Potency of Cytotoxic Agents in Various Human Cancer Cell Lines, *J. Biomol. Screen.* 9 (2004) 506–515. <https://doi.org/10.1177/1087057104265386>.
- [67] R. Sen, K. Natarajan, J. Bhullar, S. Shukla, H.-B. Fang, L. Cai, Z.-S. Chen, S. V Ambudkar, M.R. Baer, The Novel BCR-ABL and FLT3 Inhibitor Ponatinib Is a Potent Inhibitor of the MDR-Associated ATP-Binding Cassette Transporter ABCG2, *Mol. Cancer Ther.* 11 (2012) 2033–2044. <https://doi.org/10.1158/1535-7163.MCT-12-0302>.
- [68] M.D. Hall, M.D. Handley, M.M. Gottesman, Is resistance useless? Multidrug resistance and collateral sensitivity, *Trends Pharmacol. Sci.* 30 (2009) 546–556. <https://doi.org/https://doi.org/10.1016/j.tips.2009.07.003>.
- [69] Á. Telbisz, C. Hegedüs, C. Özvegy-Laczka, K. Goda, G. Várady, Z. Takáts, E. Szabó, B.P. Sorrentino, A. Váradi, B. Sarkadi, Antibody binding shift assay for rapid screening of drug interactions with the human ABCG2 multidrug transporter, *Eur. J. Pharm. Sci.* 45 (2012) 101–109. <https://doi.org/https://doi.org/10.1016/j.ejps.2011.10.021>.
- [70] N.M.I. Taylor, I. Manolaridis, S.M. Jackson, J. Kowal, H. Stahlberg, K.P. Locher, Structure of the human multidrug transporter ABCG2., *Nature.* 546 (2017) 504–509. <https://doi.org/10.1038/nature22345>.

- [71] M. Murakami, S. Ohnuma, M. Fukuda, E.E. Chufan, K. Kudoh, K. Kanehara, N. Sugisawa, M. Ishida, T. Naitoh, H. Shibata, Y. Iwabuchi, S. V Ambudkar, M. Unno, Synthetic Analogs of Curcumin Modulate the Function of Multidrug Resistance-Linked ATP-Binding Cassette Transporter ABCG2, *Drug Metab. Dispos.* 45 (2017) 1166–1177. <https://doi.org/10.1124/dmd.117.076000>.
- [72] P.-R. Ding, A.K. Tiwari, S. Ohnuma, J.W.K.K. Lee, X. An, C.-L. Dai, Q.-S. Lu, S. Singh, D.-H. Yang, T.T. Talele, S. V Ambudkar, Z.-S. Chen, The Phosphodiesterase-5 Inhibitor Vardenafil Is a Potent Inhibitor of ABCB1/P-Glycoprotein Transporter, *PLoS One.* 6 (2011) e19329. <https://doi.org/10.1371/journal.pone.0019329>.
- [73] A. Pozza, J.M. Préz-Victoria, A. Di Pietro, Overexpression of homogeneous and active ABCG2 in insect cells, *Protein Expr. Purif.* 63 (2009) 75–83. <https://doi.org/https://doi.org/10.1016/j.pep.2008.09.021>.
- [74] S. V Ambudkar, Drug-stimulatable ATPase activity in crude membranes of human MDR1-transfected mammalian cells, in: *ABC Transp. Biochem. Cell. Mol. Asp.*, Academic Press, 1998: pp. 504–514. [https://doi.org/https://doi.org/10.1016/S0076-6879\(98\)92039-0](https://doi.org/https://doi.org/10.1016/S0076-6879(98)92039-0).
- [75] I.F. Zattoni, T. Kronenberger, D.H. Kita, L.D. Guanaes, M.M. Guimarães, L. de O. Prado, M. Ziasch, L.C. Vesga, F.G. de M. Rego, G. Picheth, M.B. Gonçalves, M.D. Nosedá, D.R.B. Ducatti, A. Poso, R.W. Robey, S. V Ambudkar, V.R. Moure, A.G. Gonçalves, G. Valdameri, A new porphyrin as selective-based inhibitor of breast cancer resistance protein (BCRP/ABCG2), *Chem. Biol. Interact.* In press (2021).
- [76] G.J. Gozzi, Z. Bouaziz, E. Winter, N. Daflon-Yunes, M. Honorat, N. Guragossian, C. Marminon, G. Valdameri, A. Bollacke, J. Guillon, N. Pinaud, M. Marchivie, S.M. Cadena, J. Jose, M. Le Borgne, A. Di Pietro, Phenolic indeno[1,2-b]indoles as ABCG2-selective potent and non-toxic inhibitors stimulating basal ATPase activity., *Drug Des. Devel. Ther.* 9 (2015) 3481–3495. <https://doi.org/10.2147/DDDT.S84982>.
- [77] S. Lusvardi, S. V Ambudkar, ATP-dependent thermostabilization of human P-glycoprotein (ABCB1) is blocked by modulators, *Biochem. J.* 476 (2019) 3737–3750. <https://doi.org/10.1042/BCJ20190736>.
- [78] D.H. Kita, N. Guragossian, I.F. Zattoni, V.R. Moure, F.G. de M. Rego, S. Lusvardi, T. Moulenat, B. Belhani, G. Picheth, S. Bouacida, Z. Bouaziz, C. Marminon, M. Berredjem, J. Jose, M.B. Gonçalves, S. V Ambudkar, G. Valdameri, M. Le Borgne, Mechanistic basis of breast cancer resistance protein inhibition by new indeno[1,2-b]indoles, *Sci. Rep.* 11 (2021) 1788. <https://doi.org/10.1038/s41598-020-79892-w>.
- [79] A. Wadood, N. Ahmed, L. Shah, A. Ahmad, H. Hassan, S. Shams, In-silico drug design: An approach which revolutionised the drug discovery process, *Drug Des. Deliv.* 1 (2013).
- [80] A. Ganesan, M.L. Coote, K. Barakat, Molecular dynamics-driven drug discovery: leaping forward with confidence, *Drug Discov. Today.* 22 (2017) 249–269. <https://doi.org/https://doi.org/10.1016/j.drudis.2016.11.001>.
- [81] G.F. Ecker, T. Stockner, P. Chiba, Computational models for prediction of interactions with ABC-transporters, *Drug Discov. Today.* 13 (2008) 311–317. <https://doi.org/https://doi.org/10.1016/j.drudis.2007.12.012>.
- [82] B.J. Orlando, M. Liao, ABCG2 transports anticancer drugs via a closed-to-open switch, *Nat. Commun.* 11 (2020) 1–11. <https://doi.org/10.1038/s41467-020-16155-2>.
- [83] J. Kowal, D. Ni, S.M. Jackson, I. Manolaridis, H. Stahlberg, K.P. Locher, Structural Basis of Drug Recognition by the Multidrug Transporter ABCG2, *J. Mol. Biol.* 433 (2021) 166980. <https://doi.org/https://doi.org/10.1016/j.jmb.2021.166980>.
- [84] H. Miyata, T. Takada, Y. Toyoda, H. Matsuo, K. Ichida, H. Suzuki, Identification of Febuxostat as a New Strong ABCG2 Inhibitor: Potential Applications and Risks in Clinical Situations, *Front. Pharmacol.* 7 (2016) 518. <https://doi.org/10.3389/fphar.2016.00518>.
- [85] A. Ahmed-Belkacem, A. Pozza, F. Muñoz-Martínez, S.E. Bates, S. Castanys, F. Gamarro, A. Di Pietro, J.M. Pérez-Victoria, Flavonoid structure-activity studies identify 6-prenylchrysin and tectochrysin as potent and specific inhibitors of breast cancer resistance protein ABCG2., *Cancer Res.* 65 (2005) 4852–4860. <https://doi.org/10.1158/0008-5472.CAN-04-1817>.
- [86] G. Valdameri, C. Gauthier, R. Terreux, R. Kachadourian, B.J. Day, S.M. Winnischofer, M.E. Rocha, V. Frachet, X. Ronot, A. Di Pietro, A. Boumendjel, Investigation of chalcones as selective inhibitors of the breast cancer resistance protein: critical role of methoxylation in both inhibition potency and cytotoxicity, *J Med Chem.* 55 (2012) 3193–3200. <https://doi.org/10.1021/jm2016528>.
- [87] M. Nishiyama, T. Kuga, Central Effects of the Neurotropic Mycotoxin Fumitremorgin A in the Rabbit (I) Effects on the Spinal Cord, *Jpn. J. Pharmacol.* 50 (1989) 167–173. [https://doi.org/https://doi.org/10.1016/S0021-5198\(19\)42469-4](https://doi.org/https://doi.org/10.1016/S0021-5198(19)42469-4).
- [88] G. Valdameri, C. Gauthier, R. Terreux, R. Kachadourian, B.J. Day, S.M.B. Winnischofer, M.E.M. Rocha, V. Frachet, X. Ronot, A. Di Pietro, A. Boumendjel, Investigation of Chalcones as Selective Inhibitors of the Breast Cancer Resistance Protein: Critical Role of Methoxylation in both Inhibition

- Potency and Cytotoxicity, *J. Med. Chem.* 55 (2012) 3193–3200. <https://doi.org/10.1021/jm2016528>.
- [89] G. Valdameri, E. Genoux-Bastide, B. Peres, C. Gauthier, J. Guitton, R. Terreux, S.M.B. Winnischofer, M.E.M. Rocha, A. Boumendjel, A. Di Pietro, Substituted chromones as highly-potent nontoxic inhibitors, specific for the breast cancer resistance protein., *J. Med. Chem.* (2011). <https://doi.org/10.1021/jm201404w>.
- [90] M.M. Honorat, L.L. Payen, J.J. Guitton, C. Gauthier, C. Bouard, F. Lecerf-Schmidt, B. Peres, R.R. Terreux, H.H. Gervot, C. Rioufol, A.A. Boumendjel, A. Puisieux, A. di Pietro, MBL-II-141, a hormone derivative, enhances irinotecan (CPT-11) anticancer efficiency in ABCG2-positive xenografts, *Oncotarget*. 5 (2014) 11957–11970.
- [91] A. Tamaki, C. Ierano, G. Szakacs, R.W. Robey, S.E. Bates, The controversial role of ABC transporters in clinical oncology, *Essays Biochem.* 50 (2011) 209–232. <https://doi.org/10.1042/bse0500209>.
- [92] A. Pick, M. Wiese, Tyrosine Kinase Inhibitors Influence ABCG2 Expression in EGFR-Positive MDCK BCRP Cells via the PI3K/Akt Signaling Pathway, *ChemMedChem*. 7 (2012) 650–662. <https://doi.org/https://doi.org/10.1002/cmdc.201100543>.
- [93] C. Özvegy-Laczka, G. Várady, G. Köblös, O. Ujhelly, J. Cervenak, J.D. Schuetz, B.P. Sorrentino, G.J. Koomen, A. Váradi, K. Németh, B. Sarkadi, Function-dependent conformational changes of the ABCG2 multidrug transporter modify its interaction with a monoclonal antibody on the cell surface, *J. Biol. Chem.* 280 (2005) 4219–4227. <https://doi.org/10.1074/jbc.M411338200>.
- [94] C. Özvegy, T. Litman, G. Szakács, Z. Nagy, S. Bates, A. Váradi, B. Sarkadi, Functional Characterization of the Human Multidrug Transporter, ABCG2, Expressed in Insect Cells, *Biochem. Biophys. Res. Commun.* 285 (2001) 111–117. <https://doi.org/https://doi.org/10.1006/bbrc.2001.5130>.
- [95] K.F.K. Ejendal, N.K. Diop, L.C. Schweiger, C.A. Hrycyna, The nature of amino acid 482 of human ABCG2 affects substrate transport and ATP hydrolysis but not substrate binding, *Protein Sci.* 15 (2006) 1597–1607. <https://doi.org/https://doi.org/10.1110/ps.051998406>.
- [96] L.C. Vesga, T. Kronenberger, A.K. Tonduru, D.H. Kita, I.F. Zattoni, C.C. Bernal, A.R.R. Bohórquez, S.C. Mendez-Sánchez, S. V Ambudkar, G. Valdameri, A. Poso, Tetrahydroquinoline/4,5-dihydroisoxazole molecular hybrids as novel inhibitors of Breast Cancer Resistance Protein (BCRP/ABCG2)., *ChemMedChem*. (2021). <https://doi.org/10.1002/cmdc.202100188>.
- [97] F. Antoni, M. Bause, M. Scholler, S. Bauer, S.A. Stark, S.M. Jackson, I. Manolaridis, K.P. Locher, B. König, A. Buschauer, G. Bernhardt, Tariquidar-related triazoles as potent, selective and stable inhibitors of ABCG2 (BCRP), *Eur. J. Med. Chem.* 191 (2020) 1–16. <https://doi.org/10.1016/j.ejmech.2020.112133>.
- [98] B. Poller, D. Iusuf, R.W. Sparidans, E. Wagenaar, J.H. Beijnen, A.H. Schinkel, Differential Impact of P-Glycoprotein (ABCB1) and Breast Cancer Resistance Protein (ABCG2) on Axitinib Brain Accumulation and Oral Plasma Pharmacokinetics, *Drug Metab. Dispos.* 39 (2011) 729–735. <https://doi.org/10.1124/dmd.110.037317>.
- [99] W. Li, H. Zhang, Y.G. Assaraf, K. Zhao, X. Xu, J. Xie, D.-H.H. Yang, Z.-S.S. Chen, Overcoming ABC transporter-mediated multidrug resistance: Molecular mechanisms and novel therapeutic drug strategies, *Drug Resist. Updat.* 27 (2016) 14–29. <https://doi.org/https://doi.org/10.1016/j.drug.2016.05.001>.
- [100] S.M. Stefan, Multi-target ABC transporter modulators: what next and where to go?, *Future Med. Chem.* 11 (2019) 2353–2358. <https://doi.org/10.4155/fmc-2019-0185>.
- [101] R. Allikmets, L.M. Schriml, A. Hutchinson, V. Romano-Spica, M. Dean, A human placenta-specific ATP-binding cassette gene (ABCP) on chromosome 4q22 that is involved in multidrug resistance, *Cancer Res.* 58 (1998) 5337–5339.
- [102] R.W. Robey, K.K.K. To, O. Polgar, M. Dohse, P. Fetsch, M. Dean, S.E. Bates, ABCG2: A perspective, *Adv. Drug Deliv. Rev.* 61 (2009) 3–13. <https://doi.org/10.1016/j.addr.2008.11.003>.
- [103] D. Hira, T. Terada, BCRP/ABCG2 and high-alert medications: Biochemical, pharmacokinetic, pharmacogenetic, and clinical implications, *Biochem. Pharmacol.* 147 (2018) 201–210. <https://doi.org/10.1016/j.bcp.2017.10.004>.
- [104] T. Litman, M. Brangi, E. Hudson, P. Fetsch, A. Abati, D.D. Ross, K. Miyake, J.H. Resau, S.E. Bates, The multidrug-resistant phenotype associated with overexpression of the new ABC half-transporter, MXR (ABCG2), *J. Cell Sci.* 113 (2000) 2011–2021. <https://doi.org/10.1242/jcs.113.11.2011>.
- [105] E.L. Volk, K.M. Farley, Y. Wu, F. Li, R.W. Robey, E. Schneider, Overexpression of Wild-Type Breast Cancer Resistance Protein Mediates Methotrexate Resistance, *Cancer Res.* 62 (2002) 5035–5040.
- [106] K. Nakatomi, M. Yoshikawa, M. Oka, Y. Ikegami, S. Hayasaka, K. Sano, K. Shiozawa, S. Kawabata, H. Soda, T. Ishikawa, S. Tanabe, S. Kohno, Transport of 7-Ethyl-10-hydroxycamptothecin (SN-38) by Breast Cancer Resistance Protein ABCG2 in Human Lung Cancer Cells, *Biochem. Biophys. Res. Commun.* 288 (2001) 827–832. <https://doi.org/https://doi.org/10.1006/bbrc.2001.5850>.
- [107] R.W. Robey, K. Steadman, O. Polgar, K. Morisaki, M. Blayney, P. Mistry, S.E. Bates, Pheophorbide a Is a Specific Probe for ABCG2 Function and Inhibition, *Cancer Res.* 64 (2004) 1242–1246.

- <https://doi.org/10.1158/0008-5472.CAN-03-3298>.
- [108] S. Zhou, J.D. Schuetz, K.D. Bunting, A.M. Colapietro, J. Sampath, J.J. Morris, I. Lagutina, G.C. Grosveld, M. Osawa, H. Nakauchi, B.P. Sorrentino, The ABC transporter Bcrp1/ABCG2 is expressed in a wide variety of stem cells and is a molecular determinant of the side-population phenotype., *Nat. Med.* 7 (2001) 1028–1034. <https://doi.org/10.1038/nm0901-1028>.
- [109] L. Yang, P. Shi, G. Zhao, J. Xu, W. Peng, J. Zhang, G. Zhang, X. Wang, Z. Dong, F. Chen, H. Cui, Targeting cancer stem cell pathways for cancer therapy, *Signal Transduct. Target. Ther.* 5 (2020) 8. <https://doi.org/10.1038/s41392-020-0110-5>.
- [110] M.A. Goodell, K. Brose, G. Paradis, A.S. Conner, R.C. Mulligan, Isolation and functional properties of murine hematopoietic stem cells that are replicating in vivo., *J. Exp. Med.* 183 (1996) 1797–1806. <https://doi.org/10.1084/jem.183.4.1797>.
- [111] J. Zhao, Cancer stem cells and chemoresistance: The smartest survives the raid, *Pharmacol. Ther.* 160 (2016) 145–158. <https://doi.org/https://doi.org/10.1016/j.pharmthera.2016.02.008>.
- [112] E. Desuzinges-Mandon, O. Arnaud, L. Martinez, F. Huché, A. Di Pietro, P. Falson, ABCG2 transports and transfers heme to albumin through its large extracellular loop, *J. Biol. Chem.* 285 (2010) 33123–33133. <https://doi.org/10.1074/jbc.M110.139170>.
- [113] P. Wang, M. Sachar, J. Lu, A.I. Shehu, J. Zhu, J. Chen, K. Liu, K.E. Anderson, W. Xie, F.J. Gonzalez, C.D. Klaassen, X. Ma, The essential role of the transporter ABCG2 in the pathophysiology of erythropoietic protoporphyria, *Sci. Adv.* 5 (2019) 1–9. <https://doi.org/10.1126/sciadv.aaw6127>.
- [114] J.W. Jonker, M. Buitelaar, E. Wagenaar, M.A. Van der Valk, G.L. Scheffer, R.J. Scheper, T. Plösch, F. Kuipers, R.P.J. Oude Elferink, H. Rosing, J.H. Beijnen, A.H. Schinkel, T. Plosch, F. Kuipers, R.P.J.O. Elferink, H. Rosing, J.H. Beijnen, A.H. Schinkel, The breast cancer resistance protein protects against a major chlorophyll-derived dietary phototoxin and protoporphyria, *Proc. Natl. Acad. Sci. U. S. A.* 99 (2002) 15649–15654. <https://doi.org/10.1073/pnas.202607599>.
- [115] R.W. Robey, K. Steadman, O. Polgar, S.E. Bates, ABCG2-mediated transport of photosensitizers: Potential impact on photodynamic therapy, *Cancer Biol. Ther.* 4 (2005) 187–194. <https://doi.org/10.4161/cbt.4.2.1440>.
- [116] J. Usuda, Y. Tsunoda, S. Ichinose, T. Ishizumi, K. Ohtani, Lung Cancer Breast cancer resistant protein (BCRP) is a molecular determinant of the outcome of photodynamic therapy (PDT) for centrally located early lung cancer, 67 (2010) 198–204. <https://doi.org/10.1016/j.lungcan.2009.04.002>.
- [117] N. Kawai, Y. Hirohashi, Y. Ebihara, T. Saito, A. Murai, T. Saito, T. Shirosaki, T. Kubo, M. Nakatsugawa, T. Kanaseki, T. Tsukahara, T. Shichinohe, L. Li, S. Hirano, T. Torigoe, ABCG2 expression is related to low 5-ALA photodynamic diagnosis (PDD) efficacy and cancer stem cell phenotype, and suppression of ABCG2 improves the efficacy of PDD, *PLoS One.* 14 (2019) 1–15. <https://doi.org/10.1371/journal.pone.0216503>.
- [118] Z.Y. Xu, K. Wang, X.Q. Li, S. Chen, J.M. Deng, Y. Cheng, Z.G. Wang, The ABCG2 transporter is a key molecular determinant of the efficacy of sonodynamic therapy with Photofrin in glioma stem-like cells, *Ultrasonics.* 53 (2013) 232–238. <https://doi.org/10.1016/j.ultras.2012.06.005>.
- [119] J. Usuda, S. Ichinose, T. Ishizumi, K. Ohtani, T. Inoue, S. Maehara, K. Imai, K. Shima, T. Ohira, H. Kato, N. Ikeda, S. Ichinose, T. Ishizumi, K. Ohtani, T. Inoue, S. Maehara, Molecular determinants of photodynamic therapy for lung cancers, *Lasers Surg. Med.* 599 (2011) 591–599. <https://doi.org/10.1002/lsm.21097>.
- [120] L.N. Eadie, T.P. Hughes, D.L. White, Interaction of the Efflux Transporters ABCB1 and ABCG2 With Imatinib, Nilotinib, and Dasatinib, *Clin. Pharmacol. Ther.* 95 (2014) 294–306. <https://doi.org/10.1038/clpt.2013.208>.
- [121] S. Shukla, A.P. Skoumbourdis, M.J. Walsh, A.M.S. Hartz, K.L. Fung, C. Wu, M.M. Gottesman, C.J. Thomas, S. V. Ambudkar, Synthesis and Characterization of a BODIPY Conjugate of the BCR-ABL Kinase Inhibitor Tasigna (Nilotinib): Evidence for Transport of Tasigna and Its Fluorescent Derivative by ABC Drug Transporters, *Mol. Pharm.* (2011) 1292–1302. <https://doi.org/10.1021/mp2001022>.
- [122] Y. Inoue, T. Morita, M. Onozuka, K.-I. Saito, K. Sano, K. Hanada, M. Kondo, Y. Nakamura, T. Kishino, H. Nakagawa, Y. Ikegami, Impact of Q141K on the Transport of Epidermal Growth Factor Receptor Tyrosine Kinase Inhibitors by ABCG2., *Cells.* 8 (2019) 1–12. <https://doi.org/10.3390/cells8070763>.
- [123] P. Breedveld, D. Pluim, G. Cipriani, F. Dahlhaus, M.A.J. van Eijndhoven, C.J.F. de Wolf, A. Kuil, J.H. Beijnen, G.L. Scheffer, G. Jansen, P. Borst, J.H.M. Schellens, The Effect of Low pH on Breast Cancer Resistance Protein (ABCG2)-Mediated Transport of Methotrexate, 7-Hydroxymethotrexate, Methotrexate Diglutamate, Folic Acid, Mitoxantrone, Topotecan, and Resveratrol in In Vitro Drug Transport Models, *Mol. Pharmacol.* 71 (2007) 240 LP – 249. <https://doi.org/10.1124/mol.106.028167>.
- [124] H.C. Cooray, T. Janvilisri, H.W. van Veen, S.B. Hladky, M.A. Barrand, Interaction of the breast cancer resistance protein with plant polyphenols., *Biochem. Biophys. Res. Commun.* 317 (2004) 269–275. <https://doi.org/10.1016/j.bbrc.2004.03.040>.

- [125] P. Kannan, S. Telu, S. Shukla, S. V. Ambudkar, V.W. Pike, C. Halldin, M.M. Gottesman, R.B. Innis, M.D. Hall, The “specific” P-glycoprotein inhibitor tariquidar is also a substrate and an inhibitor for Breast Cancer Resistance Protein (BCRP/ABCG2), *ACS Chem. Neurosci.* 2 (2011) 82–89. <https://doi.org/10.1021/cn100078a>.
- [126] S. Bauer, C. Ochoa-Puentes, Q. Sun, M. Bause, G. Bernhardt, B. König, A. Buschauer, Quinoline carboxamide-type ABCG2 modulators: Indole and quinoline moieties as anilide replacements, *ChemMedChem.* 8 (2013) 1773–1778. <https://doi.org/10.1002/cmdc.201300319>.
- [127] C. Ochoa-Puentes, S. Bauer, M. Kühnle, G.G. Bernhardt, A. Buschauer, B. König, M. Kühnle, G.G. Bernhardt, A. Buschauer, B. König, Benzanilide-biphenyl replacement: A bioisosteric approach to quinoline carboxamide-type ABCG2 modulators, *ACS Med. Chem. Lett.* 4 (2013) 393–396. <https://doi.org/10.1021/ml4000832>.
- [128] A. Pick, W. Klinkhammer, M. Wiese, Specific inhibitors of the breast cancer resistance protein (BCRP), *ChemMedChem.* 5 (2010) 1498–1505. <https://doi.org/10.1002/cmdc.201000216>.
- [129] M. Kühnle, M. Egger, C. Müller, A. Mahringer, G. Bernhardt, G. Fricker, B. König, A. Buschauer, Potent and selective inhibitors of breast cancer resistance protein (ABCG2) derived from the p-glycoprotein (ABCB1) modulator tariquidar, *J. Med. Chem.* 52 (2009) 1190–1197. <https://doi.org/10.1021/jm8013822>.
- [130] C.O. Puentes, P. Höcherl, M. Kühnle, S. Bauer, K. Bürger, G. Bernhardt, A. Buschauer, B. König, Solid phase synthesis of tariquidar-related modulators of ABC transporters preferring breast cancer resistance protein (ABCG2), *Bioorganic Med. Chem. Lett.* 21 (2011) 3654–3657. <https://doi.org/10.1016/j.bmcl.2011.04.094>.
- [131] J.C.C. Dallagnol, D.R.B. Ducatti, S.M.W. Barreira, M.D. Nosedá, M.E.R. Duarte, A.G. Gonçalves, Synthesis of porphyrin glycoconjugates bearing thiourea, thiocarbamate and carbamate connecting groups: Influence of the linker on chemical and photophysical properties, *Dye. Pigment.* 107 (2014) 69–80. <https://doi.org/10.1016/j.dyepig.2014.03.029>.
- [132] A.M. Slomp, S.M.W. Barreira, L.Z.B. Carrenho, C.C. Vandresen, I.F. Zattoni, S.M.S. Ló, J.C.C. Dallagnol, D.R.B. Ducatti, A. Orsato, M.E.R. Duarte, M.D. Nosedá, M.F. Otuki, A.G. Gonçalves, Photodynamic effect of meso - (aryl) porphyrins and meso - (1-methyl-4-pyridinium) porphyrins on HaCaT keratinocytes, *Bioorg. Med. Chem. Lett.* 27 (2017) 156–161. <https://doi.org/10.1016/j.bmcl.2016.11.094>.
- [133] S.M.S. Ló, D.R.B. Ducatti, M.E.R. Duarte, S.M.W. Barreira, M.D. Nosedá, A.G. Gonçalves, Synthesis of meso-tetraarylporphyrins using SeO<sub>2</sub> as oxidant, *Tetrahedron Lett.* 52 (2011) 1441–1443. <https://doi.org/10.1016/j.tetlet.2011.01.044>.
- [134] C.M.A. Alonso, M.G.P.M.S. Neves, A.C. Tomé, A.M.S. Silva, J.A.S. Cavaleiro, Reaction of (2-amino-5,10,15,20-tetraphenylporphyrinato)nickel(II) with quinones, *Tetrahedron.* 61 (2005) 11866–11872. <https://doi.org/https://doi.org/10.1016/j.tet.2005.09.080>.
- [135] L.D. Guanaes, M.M. Guimarães, D.R.B. Ducatti, M.E.R. Duarte, S.M.W. Barreira, M.D. Nosedá, A.G. Gonçalves, Synthesis and photophysical evaluation of meso-phenyl-1,4-dihydropyridine and pyridine-porphyrin hybrids, *Chem. Heterocycl. Compd.* In press (2021).
- [136] S. V Ambudkar, Drug-stimulatable ATPase activity in crude membranes of human MDR1-transfected mammalian cells., *Methods Enzymol.* 292 (1998) 504–514. [https://doi.org/10.1016/s0076-6879\(98\)92039-0](https://doi.org/10.1016/s0076-6879(98)92039-0).
- [137] M.K. Krapf, J. Gallus, S. Vahdati, M. Wiese, New Inhibitors of Breast Cancer Resistance Protein (ABCG2) Containing a 2,4-Disubstituted Pyridopyrimidine Scaffold, *J. Med. Chem.* 61 (2018) 3389–3408. <https://doi.org/10.1021/acs.jmedchem.7b01012>.
- [138] G.M. Sastry, M. Adzhigirey, T. Day, R. Annabhimoju, W. Sherman, Protein and ligand preparation: parameters, protocols, and influence on virtual screening enrichments., *J. Comput. Aided. Mol. Des.* 27 (2013) 221–234. <https://doi.org/10.1007/s10822-013-9644-8>.
- [139] M.P. Jacobson, D.L. Pincus, C.S. Rapp, T.J.F. Day, B. Honig, D.E. Shaw, R.A. Friesner, A hierarchical approach to all-atom protein loop prediction., *Proteins.* 55 (2004) 351–367. <https://doi.org/10.1002/prot.10613>.
- [140] J.C. Shelley, A. Cholleti, L.L. Frye, J.R. Greenwood, M.R. Timlin, M. Uchimaya, Epik: a software program for pK<sub>a</sub> prediction and protonation state generation for drug-like molecules., *J. Comput. Aided. Mol. Des.* 21 (2007) 681–691. <https://doi.org/10.1007/s10822-007-9133-z>.
- [141] K. Roos, C. Wu, W. Damm, M. Reboul, J.M. Stevenson, C. Lu, M.K. Dahlgren, S. Mondal, W. Chen, L. Wang, R. Abel, R.A. Friesner, E.D. Harder, OPLS3e: Extending Force Field Coverage for Drug-Like Small Molecules, *J. Chem. Theory Comput.* 15 (2019) 1863–1874. <https://doi.org/10.1021/acs.jctc.8b01026>.
- [142] R.A. Friesner, J.L. Banks, R.B. Murphy, T.A. Halgren, J.J. Klicic, D.T. Mainz, M.P. Repasky, E.H. Knoll, M. Shelley, J.K. Perry, D.E. Shaw, P. Francis, P.S. Shenkin, Glide: A New Approach for Rapid,

- Accurate Docking and Scoring. 1. Method and Assessment of Docking Accuracy, *J. Med. Chem.* 47 (2004) 1739–1749. <https://doi.org/10.1021/jm0306430>.
- [143] T.A. Halgren, R.B. Murphy, R.A. Friesner, H.S. Beard, L.L. Frye, W.T. Pollard, J.L. Banks, Glide: a new approach for rapid, accurate docking and scoring. 2. Enrichment factors in database screening., *J. Med. Chem.* 47 (2004) 1750–1759. <https://doi.org/10.1021/jm030644s>.
- [144] W. Sherman, T. Day, M.P. Jacobson, R.A. Friesner, R. Farid, Novel Procedure for Modeling Ligand/Receptor Induced Fit Effects, *J. Med. Chem.* 49 (2006) 534–553. <https://doi.org/10.1021/jm050540c>.
- [145] K.J. Bowers, E. Chow, H. Xu, R.O. Dror, M.P. Eastwood, B.A. Gregersen, J.L. Klepeis, I. Kolossvary, M.A. Moraes, F.D. Sacerdoti, J.K. Salmon, Y. Shan, D.E. Shaw, Scalable Algorithms for Molecular Dynamics Simulations on Commodity Clusters, in: *Proc. 2006 ACM/IEEE Conf. Supercomput.*, Association for Computing Machinery, New York, NY, USA, 2006: pp. 84–es. <https://doi.org/10.1145/1188455.1188544>.
- [146] E. Harder, W. Damm, J. Maple, C. Wu, M. Reboul, J.Y. Xiang, L. Wang, D. Lupyan, M.K. Dahlgren, J.L. Knight, J.W. Kaus, D.S. Cerutti, G. Krilov, W.L. Jorgensen, R. Abel, R.A. Friesner, OPLS3: A Force Field Providing Broad Coverage of Drug-like Small Molecules and Proteins, *J. Chem. Theory Comput.* 12 (2016) 281–296. <https://doi.org/10.1021/acs.jctc.5b00864>.
- [147] H. Glavinas, E. Kis, Á. Pál, R. Kovács, M. Jani, E. Vági, É. Molnár, S. Bánsághi, Z. Kele, T. Janáky, G. Báthori, O. von Richter, G.-J.J. Koomen, P. Krajcsi, ABCG2 (Breast Cancer Resistance Protein/Mitoxantrone Resistance-Associated Protein) ATPase Assay: A Useful Tool to Detect Drug-Transporter Interactions, *Drug Metab. Dispos.* 35 (2007) 1533–1542. <https://doi.org/10.1124/dmd.106.014605>.
- [148] P. Müller, S.A. Abdel, W. Zimmermann, R. Wittig, H. Stepp, S.A. Abdel Gaber, W. Zimmermann, R. Wittig, H. Stepp, ABCG2 influence on the efficiency of photodynamic therapy in glioblastoma cells, *J. Photochem. Photobiol. B Biol.* 210 (2020) 111963. <https://doi.org/10.1016/j.jphotobiol.2020.111963>.
- [149] J.H. Kim, J.M. Park, Y.J. Roh, I.W. Kim, T. Hasan, M.G. Choi, Enhanced efficacy of photodynamic therapy by inhibiting ABCG2 in colon cancers, *BMC Cancer.* 15 (2015) 1–9. <https://doi.org/10.1186/s12885-015-1514-4>.
- [150] N. Ji, Y. Yang, Z. Lei, C. Cai, J. Wang, P. Gupta, Ulixertinib ( BVD-523 ) antagonizes ABCB1- and ABCG2-mediated chemotherapeutic drug resistance, *Biochem. Pharmacol.* 158 (2018) 274–285. <https://doi.org/10.1016/j.bcp.2018.10.028>.
- [151] S. Kraege, K. Stefan, S.C. Köhler, M. Wiese, Optimization of Acryloylphenylcarboxamides as Inhibitors of ABCG2 and Comparison with Acryloylphenylcarboxylates, *ChemMedChem.* 11 (2016) 2547–2558. <https://doi.org/10.1002/cmdc.201600455>.
- [152] F. Zeng, F. Wang, Z. Zheng, Z. Chen, K.K. Wah To, H. Zhang, Q. Han, L. Fu, Rociletinib (CO-1686) enhanced the efficacy of chemotherapeutic agents in ABCG2-overexpressing cancer cells in vitro and in vivo, *Acta Pharm. Sin. B.* 10 (2020) 799–811. <https://doi.org/https://doi.org/10.1016/j.apsb.2020.01.008>.
- [153] C.J. Henrich, R.W. Robey, H.R. Bokesch, S.E. Bates, S. Shukla, S. V. Ambudkar, M. Dean, J.B. McMahon, New inhibitors of ABCG2 identified by high-throughput screening, *Mol. Cancer Ther.* 6 (2007) 3271–3278. <https://doi.org/10.1158/1535-7163.MCT-07-0352>.
- [154] N. Khunweeraphong, T. Stockner, K. Kuchler, The structure of the human ABC transporter ABCG2 reveals a novel mechanism for drug extrusion, *Sci. Rep.* 7 (2017) 13767. <https://doi.org/10.1038/s41598-017-11794-w>.
- [155] M. Miwa, S. Tsukahara, E. Ishikawa, S. Asada, Y. Imai, Y. Sugimoto, Single amino acid substitutions in the transmembrane domains of breast cancer resistance protein (BCRP) alter cross resistance patterns in transfectants., *Int. J. Cancer.* 107 (2003) 757–763. <https://doi.org/10.1002/ijc.11484>.
- [156] N. Khunweeraphong, K. Kuchler, The first intracellular loop is essential for the catalytic cycle of the human ABCG2 multidrug resistance transporter, *FEBS Lett.* 594 (2020) 4059–4075. <https://doi.org/10.1002/1873-3468.13994>.
- [157] I. Manolaridis, S.M. Jackson, N.M.I. Taylor, J. Kowal, H. Stahlberg, K.P. Locher, Cryo-EM structures of a human ABCG2 mutant trapped in ATP-bound and substrate-bound states, *Nature.* 563 (2018) 426–430. <https://doi.org/10.1038/s41586-018-0680-3>.
- [158] M.L.H. Vlaming, J.S. Lagas, A.H. Schinkel, Physiological and pharmacological roles of ABCG2 (BCRP): Recent findings in *Abcg2* knockout mice, *Adv. Drug Deliv. Rev.* 61 (2009) 14–25. <https://doi.org/https://doi.org/10.1016/j.addr.2008.08.007>.
- [159] E. Teodori, S. Dei, C. Martelli, S. Scapecchi, F. Gualtieri, The Functions and Structure of ABC Transporters: Implications for the Design of New Inhibitors of Pgp and MRP1 to Control Multidrug Resistance (MDR), *Curr. Drug Targets.* 7 (2006) 893–909. <https://doi.org/10.2174/138945006777709520>.
- [160] J.W. Jonker, J.W. Smit, R.F. Brinkhuis, M. Maliepaard, J.H. Beijnen, J.H. Schellens, A.H. Schinkel,



- Role of breast cancer resistance protein in the bioavailability and fetal penetration of topotecan., *J. Natl. Cancer Inst.* 92 (2000) 1651–1656. <https://doi.org/10.1093/jnci/92.20.1651>.
- [161] C.M.F. Kruijtzter, J.H. Beijnen, H. Rosing, W.W. ten Bokkel Huinink, M. Schot, R.C. Jewell, E.M. Paul, J.H.M. Schellens, Increased oral bioavailability of topotecan in combination with the breast cancer resistance protein and P-glycoprotein inhibitor GF120918., *J. Clin. Oncol. Off. J. Am. Soc. Clin. Oncol.* 20 (2002) 2943–2950. <https://doi.org/10.1200/JCO.2002.12.116>.
- [162] R.G.W. Jinadasa, X. Hu, M.G.H. Vicente, K.M. Smith, Syntheses and Cellular Investigations of 173-, 152-, and 131-Amino Acid Derivatives of Chlorin e6, *J. Med. Chem.* 54 (2011) 7464–7476. <https://doi.org/10.1021/jm2005139>.
- [163] I. Yoon, J.Z. Li, Y.K. Shim, Advance in photosensitizers and light delivery for photodynamic therapy., *Clin. Endosc.* 46 (2013) 7–23. <https://doi.org/10.5946/ce.2013.46.1.7>.
- [164] L.B. Josefsen, R.W. Boyle, Photodynamic therapy and the development of metal-based photosensitisers, *Met. Based. Drugs.* 2008 (2008). <https://doi.org/10.1155/2008/276109>.
- [165] M.P. Uliana, L. Pires, S. Pratavieira, T.J. Brocksom, K.T. de Oliveira, V.S. Bagnato, C. Kurachi, Photobiological characteristics of chlorophyll a derivatives as microbial PDT agents, *Photochem. Photobiol. Sci.* 13 (2014) 1137–1145. <https://doi.org/10.1039/C3PP50376C>.
- [166] C.H. Storch, R. Ehehalt, W.E. Haefeli, J. Weiss, Localization of the Human Breast Cancer Resistance Protein (BCRP/ABCG2) in Lipid Rafts/Caveolae and Modulation of Its Activity by Cholesterol in Vitro, *J. Pharmacol. Exp. Ther.* 323 (2007) 257–264. <https://doi.org/10.1124/jpet.107.122994>.
- [167] J.T. Szilagy, A.M. Vetrano, J.D. Laskin, L.M. Aleksunes, Localization of the placental BCRP/ABCG2 transporter to lipid rafts: Role for cholesterol in mediating efflux activity., *Placenta.* 55 (2017) 29–36. <https://doi.org/10.1016/j.placenta.2017.04.006>.
- [168] Á. Telbisz, M. Müller, C. Özvegy-Laczka, L. Homolya, L. Szente, A. Váradi, B. Sarkadi, Membrane cholesterol selectively modulates the activity of the human ABCG2 multidrug transporter, *Biochim. Biophys. Acta - Biomembr.* 1768 (2007) 2698–2713. <https://doi.org/https://doi.org/10.1016/j.bbmem.2007.06.026>.
- [169] Á. Pál, D. Méhn, É. Molnár, S. Gedey, P. Mészáros, T. Nagy, H. Glavinas, T. Janáky, O. von Richter, G. Báthori, L. Szente, P. Krajcsi, Cholesterol Potentiates ABCG2 Activity in a Heterologous Expression System: Improved in Vitro Model to Study Function of Human ABCG2, *J. Pharmacol. Exp. Ther.* 321 (2007) 1085 LP – 1094. <https://doi.org/10.1124/jpet.106.119289>.
- [170] C. Scharenberg, N. Mannowetz, R.W. Robey, C. Brendel, P. Repges, T. Sahrhage, T. Jähn, G. Wennemuth, ABCG2 is expressed in late spermatogenesis and is associated with the acrosome., *Biochem. Biophys. Res. Commun.* 378 (2009) 302–307. <https://doi.org/10.1016/j.bbrc.2008.11.058>.
- [171] N. Wang, D. Lan, W. Chen, F. Matsuura, A.R. Tall, ATP-binding cassette transporters G1 and G4 mediate cellular cholesterol efflux to high-density lipoproteins, *Proc. Natl. Acad. Sci.* 101 (2004) 9774–9779. <https://doi.org/10.1073/pnas.0403506101>.
- [172] N.C. Bernecic, M. Zhang, B.M. Gadella, J.F.H.M. Brouwers, J.W.A. Jansen, G.J.A. Arkesteijn, S.P. de Graaf, T. Leahy, BODIPY-cholesterol can be reliably used to monitor cholesterol efflux from capacitating mammalian spermatozoa, *Sci. Rep.* 9 (2019) 9804. <https://doi.org/10.1038/s41598-019-45831-7>.
- [173] Y. Kimura, A. Kodan, M. Matsuo, K. Ueda, Cholesterol fill-in model: mechanism for substrate recognition by ABC proteins., *J. Bioenerg. Biomembr.* 39 (2007) 447–452. <https://doi.org/10.1007/s10863-007-9109-7>.
- [174] V. Martel-Frchet, M. Kadri, A. Boumendjel, X. Ronot, Structural requirement of arylindolylpropenones as anti-bladder carcinoma cells agents, *Bioorg. Med. Chem.* 19 (2011) 6143–6148. <https://doi.org/https://doi.org/10.1016/j.bmc.2011.08.015>.
- [175] H. You, H.-E. Yoon, P.-H. Jeong, H. Ko, J.-H. Yoon, Y.-C. Kim, Pheophorbide-a conjugates with cancer-targeting moieties for targeted photodynamic cancer therapy, *Bioorg. Med. Chem.* 23 (2015) 1453–1462. <https://doi.org/https://doi.org/10.1016/j.bmc.2015.02.014>.
- [176] J.-Y. Liu, H.-S. Yeung, W. Xu, X. Li, D.K.P. Ng, Highly Efficient Energy Transfer in Subphthalocyanine–BODIPY Conjugates, *Org. Lett.* 10 (2008) 5421–5424. <https://doi.org/10.1021/ol8023677>.
- [177] L. He, Y. Jiang, K. Liu, V. Gomez-Murcia, X. Ma, A. Torrecillas, Q. Chen, X. Zhu, E. Lesnefsky, J.C. Gomez-Fernandez, B. Xu, S. Zhang, Insights into the Impact of a Membrane-Anchoring Moiety on the Biological Activities of Bivalent Compounds As Potential Neuroprotectants for Alzheimer’s Disease, *J. Med. Chem.* 61 (2018) 777–790. <https://doi.org/10.1021/acs.jmedchem.7b01284>.
- [178] A.M. Slomp, S.M.W. Barreira, L.Z.B. Carrenho, C.C. Vandresen, I.F. Zattoni, S.M.S. Ló, J.C.C. Dallagnol, D.R.B. Ducatti, A. Orsato, M.E.R. Duarte, M.D. Nosedá, M.F. Otuki, A.G. Gonçalves, Photodynamic effect of meso-(aryl)porphyrins and meso-(1-methyl-4-pyridinium)porphyrins on HaCaT keratinocytes, *Bioorganic Med. Chem. Lett.* 27 (2017) 156–161.

- <https://doi.org/10.1016/j.bmcl.2016.11.094>.
- [179] C.C. Vandresen, A.G. Gonçalves, D.R.B. Ducatti, F.S. Murakami, M.D. Nosedá, M.E.R. Duarte, S.M.W. Barreira, In vitro photodynamic inactivation of conidia of the phytopathogenic fungus *Colletotrichum graminicola* with cationic porphyrins., *Photochem. Photobiol. Sci. Off. J. Eur. Photochem. Assoc. Eur. Soc. Photobiol.* 15 (2016) 673–681. <https://doi.org/10.1039/c5pp00372e>.
- [180] V. V Klimov, Discovery of pheophytin function in the photosynthetic energy conversion as the primary electron acceptor of Photosystem II, *Photosynth. Res.* 76 (2003) 247–253. <https://doi.org/10.1023/A:1024990408747>.
- [181] E. Valeur, M. Bradley, Amide bond formation: beyond the myth of coupling reagents, *Chem. Soc. Rev.* 38 (2009) 606–631. <https://doi.org/10.1039/B701677H>.
- [182] Y. Kiso, H. Isawa, K. Kitagawa, T. Akita, Suppressing Effect of Thioanisole on a Side Reaction during the Acidolytic Cleavage of Protecting Groups of Tyrosine, *Chem. Pharm. Bull. (Tokyo)*. 26 (1978) 2562–2564. <https://doi.org/10.1248/cpb.26.2562>.
- [183] A. Barba-Bon, A.M. Costero, S. Gil, A. Harriman, F. Sancenón, Highly Selective Detection of Nerve-Agent Simulants with BODIPY Dyes, *Chem. – A Eur. J.* 20 (2014) 6339–6347. <https://doi.org/https://doi.org/10.1002/chem.201304475>.
- [184] B. Hu, H. Guo, P. Zhou, Z.-L. Shi, Characteristics of SARS-CoV-2 and COVID-19, *Nat. Rev. Microbiol.* 19 (2021) 141–154. <https://doi.org/10.1038/s41579-020-00459-7>.
- [185] H.Q. Yu, B.Q. Sun, Z.F. Fang, J.C. Zhao, X.Y. Liu, Y.M. Li, X.Z. Sun, H.F. Liang, B. Zhong, Z.F. Huang, P.Y. Zheng, L.F. Tian, H.Q. Qu, D.C. Liu, E.Y. Wang, X.J. Xiao, S.Y. Li, F. Ye, L. Guan, D.S. Hu, H. Hakonarson, Z.G. Liu, N.S. Zhong, Distinct features of SARS-CoV-2-specific IgA response in COVID-19 patients, *Eur. Respir. J.* (2020). <https://doi.org/10.1183/13993003.01526-2020>.
- [186] Q.X. Long, B.Z. Liu, H.J. Deng, G.C. Wu, K. Deng, Y.K. Chen, P. Liao, J.F. Qiu, Y. Lin, X.F. Cai, D.Q. Wang, Y. Hu, J.H. Ren, N. Tang, Y.Y. Xu, L.H. Yu, Z. Mo, F. Gong, X.L. Zhang, W.G. Tian, L. Hu, X.X. Zhang, J.L. Xiang, H.X. Du, H.W. Liu, C.H. Lang, X.H. Luo, S.B. Wu, X.P. Cui, Z. Zhou, M.M. Zhu, J. Wang, C.J. Xue, X.F. Li, L. Wang, Z.J. Li, K. Wang, C.C. Niu, Q.J. Yang, X.J. Tang, Y. Zhang, X.M. Liu, J.J. Li, D.C. Zhang, F. Zhang, P. Liu, J. Yuan, Q. Li, J.L. Hu, J. Chen, A.L. Huang, Antibody responses to SARS-CoV-2 in patients with COVID-19, *Nat. Med.* (2020). <https://doi.org/10.1038/s41591-020-0897-1>.
- [187] M.W. Russell, Z. Moldoveanu, P.L. Ogra, J. Mestecky, Mucosal Immunity in COVID-19: A Neglected but Critical Aspect of SARS-CoV-2 Infection, *Front. Immunol.* 11 (2020) 3221. <https://doi.org/10.3389/fimmu.2020.611337>.
- [188] Y.X. Chao, O. Röttschke, E.-K. Tan, The role of IgA in COVID-19, *Brain. Behav. Immun.* 87 (2020) 182–183. <https://doi.org/10.1016/j.bbi.2020.05.057>.
- [189] W. Zeng, H. Ma, C. Ding, Y. Yang, Y. Sun, X. Huang, W. He, Y. Xiang, Y. Gao, T. Jin, Characterization of SARS-CoV-2-specific antibodies in COVID-19 patients reveals highly potent neutralizing IgA, *Signal Transduct. Target. Ther.* (2021). <https://doi.org/10.1038/s41392-021-00478-7>.
- [190] A.N. Grossberg, L.A. Koza, A. Ledreux, C. Prusmack, H.K. Krishnamurthy, V. Jayaraman, A.-C. Granholm, D.A. Linseman, A multiplex chemiluminescent immunoassay for serological profiling of COVID-19-positive symptomatic and asymptomatic patients, *Nat. Commun.* 12 (2021) 740. <https://doi.org/10.1038/s41467-021-21040-7>.
- [191] M. Norman, T. Gilboa, A.F. Ogata, A.M. Maley, L. Cohen, E.L. Busch, R. Lazarovits, C.P. Mao, Y. Cai, J. Zhang, J.E. Feldman, B.M. Hauser, T.M. Caradonna, B. Chen, A.G. Schmidt, G. Alter, R.C. Charles, E.T. Ryan, D.R. Walt, Ultrasensitive high-resolution profiling of early seroconversion in patients with COVID-19, *Nat. Biomed. Eng.* (2020). <https://doi.org/10.1038/s41551-020-00611-x>.
- [192] A. Padoan, L. Sciacovelli, D. Basso, D. Negrini, S. Zuin, C. Cosma, D. Faggian, P. Matricardi, M. Plebani, IgA-Ab response to spike glycoprotein of SARS-CoV-2 in patients with COVID-19: A longitudinal study, *Clin. Chim. Acta.* 507 (2020) 164–166. <https://doi.org/https://doi.org/10.1016/j.cca.2020.04.026>.
- [193] B. Meyer, C. Drosten, M.A. Müller, Serological assays for emerging coronaviruses: Challenges and pitfalls, *Virus Res.* (2014). <https://doi.org/10.1016/j.virusres.2014.03.018>.
- [194] F.Y. Chang, H.C. Chen, P.J. Chen, M.S. Ho, S.L. Hsieh, J.C. Lin, F.T. Liu, H.K. Sytwu, Immunologic aspects of characteristics, diagnosis, and treatment of coronavirus disease 2019 (COVID-19), *J. Biomed. Sci.* 27 (2020) 72. <https://doi.org/10.1186/s12929-020-00663-w>.
- [195] A. Petherick, Developing antibody tests for SARS-CoV-2, *Lancet (London, England)*. (2020). [https://doi.org/10.1016/S0140-6736\(20\)30788-1](https://doi.org/10.1016/S0140-6736(20)30788-1).
- [196] S.K. Vashist, In Vitro Diagnostic Assays for COVID-19: Recent Advances and Emerging Trends, *Diagnostics*. 10 (2020) 2–7. <https://doi.org/10.3390/diagnostics10040202>.
- [197] N.M.A. Okba, M.A. Müller, W. Li, C. Wang, C.H. Geurtsvankessel, V.M. Corman, M.M. Lamers, R.S. Sikkema, E. De Bruin, F.D. Chandler, Y. Yazdanpanah, Q. Le Hingrat, D. Descamps, N. Houhou-

- Fidouh, C.B.E.M. Reusken, B.J. Bosch, C. Drosten, M.P.G. Koopmans, B.L. Haagmans, Severe Acute Respiratory Syndrome Coronavirus 2-Specific Antibody Responses in Coronavirus Disease Patients, *Emerg. Infect. Dis.* (2020). <https://doi.org/10.3201/eid2607.200841>.
- [198] A. Hachim, N. Kavian, C.A. Cohen, A.W.H. Chin, D.K.W. Chu, C.K.P. Mok, O.T.Y. Tsang, Y.C. Yeung, R.A.P.M. Perera, L.L.M. Poon, J.S.M. Peiris, S.A. Valkenburg, ORF8 and ORF3b antibodies are accurate serological markers of early and late SARS-CoV-2 infection, *Nat. Immunol.* (2020). <https://doi.org/10.1038/s41590-020-0773-7>.
- [199] L.F. Huergo, K.A. Selim, M.S. Conzentino, E.C.M. Gerhardt, A.R.S. Santos, B. Wagner, J.T. Alford, N. Deobald, F.O. Pedrosa, E.M. de Souza, M.B. Nogueira, S.M. Raboni, D. Souto, F.G.M. Rego, D.L. Zanette, M.N. Aoki, J.M. Nardin, B. Fornazari, H.M.P. Morales, V.A. Borges, A. Nelde, J.S. Walz, M. Becker, N. Schneiderhan-Marra, U. Rothbauer, R.A. Reis, K. Forchhammer, Magnetic Bead-Based Immunoassay Allows Rapid, Inexpensive, and Quantitative Detection of Human SARS-CoV-2 Antibodies, *ACS Sensors.* (2021). <https://doi.org/10.1021/acssensors.0c02544>.
- [200] R.R. de Assis, A. Jain, R. Nakajima, A. Jasinskas, J. Felgner, J.M. Obiero, P.J. Norris, M. Stone, G. Simmons, A. Bagri, J. Irsch, M. Schreiber, A. Buser, A. Holbro, M. Battegay, P. Hosimer, C. Noesen, O. Adenaiye, S. Tai, F. Hong, D.K. Milton, D.H. Davies, P. Contestable, L.M. Corash, M.P. Busch, P.L. Felgner, S. Khan, Analysis of SARS-CoV-2 antibodies in COVID-19 convalescent blood using a coronavirus antigen microarray, *Nat. Commun.* (2021). <https://doi.org/10.1038/s41467-020-20095-2>.
- [201] J. Mariën, A. Ceulemans, J. Michiels, L. Heyndrickx, K. Kerkhof, N. Foque, M.-A. Widdowson, L. Mortgat, E. Duysburgh, I. Desombere, H. Jansens, M. Van Esbroeck, K.K. Ariën, Evaluating SARS-CoV-2 spike and nucleocapsid proteins as targets for antibody detection in severe and mild COVID-19 cases using a Luminex bead-based assay, *J. Virol. Methods.* 288 (2021) 114025. <https://doi.org/https://doi.org/10.1016/j.jviromet.2020.114025>.
- [202] L. Egia-Mendikute, A. Bosch, E. Prieto-Fernández, S.Y. Lee, B. Jiménez-Lasheras, A. García del Río, A. Antoñana-Vildosola, C. Bruzzone, M. Bizkarguenaga, N. Embade, R. Gil-Redondo, M.L. Martínez-Chantar, M. López-Hoyos, N.G.A. Abrescia, J.M. Mato, Ó. Millet, A. Palazón, Sensitive detection of SARS-CoV-2 seroconversion by flow cytometry reveals the presence of nucleoprotein-reactive antibodies in unexposed individuals, *Commun. Biol.* 4 (2021) 486. <https://doi.org/10.1038/s42003-021-02011-6>.
- [203] G.M.N. Behrens, A. Cossmann, M. V. Stankov, T. Witte, D. Ernst, C. Happle, A. Jablonka, Perceived versus proven SARS-CoV-2-specific immune responses in health-care professionals, *Infection.* (2020). <https://doi.org/10.1007/s15010-020-01461-0>.
- [204] A. Munitz, L. Edry-Botzer, M. Itan, R. Tur-Kaspa, D. Dicker, D. Marcoviciu, M.G. Goren, M. Mor, S. Lev, T. Gottesman, K. Muhsen, D. Cohen, M. Stein, U. Qimron, N.T. Freund, Y. Wine, M. Gerlic, Rapid seroconversion and persistent functional IgG antibodies in severe COVID-19 patients correlates with an IL-12p70 and IL-33 signature, *Sci. Rep.* (2021). <https://doi.org/10.1038/s41598-021-83019-0>.
- [205] D. Sterlin, A. Mathian, M. Miyara, A. Mohr, F. Anna, L. Claër, P. Quentric, J. Fadlallah, H. Devilliers, P. Ghillani, C. Gunn, R. Hockett, S. Mudumba, A. Guihot, C.E. Luyt, J. Mayaux, A. Beurton, S. Fourati, T. Bruel, O. Schwartz, J.M. Lacorte, H. Yssel, C. Parizot, K. Dorgham, P. Charneau, Z. Amoura, G. Gorochov, IgA dominates the early neutralizing antibody response to SARS-CoV-2, *Sci. Transl. Med.* 13 (2021). <https://doi.org/10.1126/scitranslmed.abd2223>.
- [206] D. Lapuente, C. Maier, P. Irrgang, J. Hübner, S. Peter, M. Hoffmann, A. Ensser, K. Ziegler, T.H. Winkler, A.E. Kremer, P. Steininger, K. Korn, F. Neipel, M. Tenbusch, Rapid response flow cytometric assay for the detection of antibody responses to SARS-CoV-2, 2 (2020).
- [207] C. Simard, J. Richard, R. Bazin, A. Finzi, P. Trepanier, Standardization of a flow cytometry SARS-CoV-2 serologic test., *MedRxiv.* (2021).
- [208] L. Horndler, P. Delgado, D. Abia, I. Balabanov, P. Martínez-Fleta, G. Cornish, M.A. Llamas, S. Serrano-Villar, F. Sánchez-Madrid, M. Fresno, H.M. van Santen, B. Alarcón, Flow cytometry multiplexed method for the detection of neutralizing human antibodies to the native SARS-CoV-2 spike protein, *EMBO Mol. Med.* 13 (2021) e13549. <https://doi.org/https://doi.org/10.15252/emmm.202013549>.
- [209] Y.S. Goh, J.-M. Chavatte, A. Lim Jieling, B. Lee, P.X. Hor, S.N. Amrun, C.Y.-P. Lee, R.S.-L. Chee, B. Wang, C.Y. Lee, E.Z.X. Ngoh, C.-I. Wang, B.E. Young, P.A. Tambyah, S. Kalimuddin, S. Pada, S.-Y. Tan, L.J. Sun, M.I.-C. Chen, Y.-S. Leo, D.C. Lye, L.F.P. Ng, R.T.P. Lin, L. Renia, Sensitive detection of total anti-Spike antibodies and isotype switching in asymptomatic and symptomatic individuals with COVID-19, *Cell Reports Med.* 2 (2021) 100193. <https://doi.org/https://doi.org/10.1016/j.xcrm.2021.100193>.
- [210] S.P. Anand, J. Prévost, J. Richard, J. Perreault, T. Tremblay, M. Drouin, M.J. Fournier, A. Lewin, R. Bazin, A. Finzi, High-throughput detection of antibodies targeting the SARS-CoV-2 Spike in longitudinal convalescent plasma samples, *Transfusion.* 61 (2021) 1377–1382. <https://doi.org/10.1111/trf.16318>.

- [211] H. Gama Ker, R. Dian de Oliveira Aguiar-Soares, B. Mendes Roatt, N. das Dores Moreira, W. Coura-Vital, C. Martins Carneiro, A. Teixeira-Carvalho, O. Assis Martins-Filho, R. Cordeiro Giunchetti, D. da Silveira-Lemos, A. Barbosa Reis, Effect of the preservative and temperature conditions on the stability of *Leishmania infantum* promastigotes antigens applied in a flow cytometry diagnostic method for canine visceral leishmaniasis, *Diagn. Microbiol. Infect. Dis.* 76 (2013) 470–476. <https://doi.org/10.1016/j.diagmicrobio.2013.04.007>.
- [212] E. Morgan, R. Varro, H. Sepulveda, J.A. Ember, J. Apgar, J. Wilson, L. Lowe, R. Chen, L. Shivraj, A. Agadir, R. Campos, D. Ernst, A. Gaur, Cytometric bead array: a multiplexed assay platform with applications in various areas of biology, *Clin. Immunol.* 110 (2004) 252–266. <https://doi.org/https://doi.org/10.1016/j.clim.2003.11.017>.
- [213] M. Dogan, L. Kozhaya, L. Placek, C. Gunter, M. Yigit, R. Hardy, M. Plassmeyer, P. Coatney, K. Lillard, Z. Bukhari, M. Kleinberg, C. Hayes, M. Arditi, E. Klapper, N. Merin, B.T.T. Liang, R. Gupta, O. Alpan, D. Unutmaz, SARS-CoV-2 specific antibody and neutralization assays reveal the wide range of the humoral immune response to virus, *Commun. Biol.* 4 (2021) 1–13. <https://doi.org/10.1038/s42003-021-01649-6>.
- [214] P. Escribano, A. Álvarez-Uría, R. Alonso, P. Catalán, L. Alcalá, P. Muñoz, J. Guinea, Detection of SARS-CoV-2 antibodies is insufficient for the diagnosis of active or cured COVID-19, *Sci. Rep.* 10 (2020) 1–7. <https://doi.org/10.1038/s41598-020-76914-5>.
- [215] N.G. Welch, J.A. Scoble, B.W. Muir, P.J. Pigram, Orientation and characterization of immobilized antibodies for improved immunoassays (Review)., *Biointerphases.* 12 (2017) 02D301. <https://doi.org/10.1116/1.4978435>.
- [216] B. Sen-Crowe, M. McKenney, A. Elkbuli, COVID-19 laboratory testing issues and capacities as we transition to surveillance testing and contact tracing, *Am. J. Emerg. Med.* 40 (2021) 217–219. <https://doi.org/10.1016/j.ajem.2020.05.071>.
- [217] G. Cota, M.L. Freire, C.S. de Souza, M.J. Pedras, J.W. Saliba, V. Faria, L.L. Alves, A. Rabello, D.M. Avelar, Diagnostic performance of commercially available COVID-19 serology tests in Brazil, *Int. J. Infect. Dis.* 101 (2020) 382–390. <https://doi.org/10.1016/j.ijid.2020.10.008>.

## PHD SCIENTIFIC PRODUCTION

International Journals		
Year	Article	Journal
2021	Zattoni I F, Kronenberger T, Kita D H, Guanaes L D, Guimarães M M, Prado, L O, Ziasch M, Vesga L C, Rego, F G M, Picheth G, Gonçalves M B, Nosedá M D, Ducatti D R B, Poso A, Robey R W, Ambudkar S V, Moure V R, Gonçalves A G, Valdameri G. <b>A new porphyrin as selective substrate-based inhibitor of breast cancer resistance protein (BCRP/ABCG2).</b>	Chemico-Biological Interactions
Submitted (under review)	Zattoni, I F, Huergo, L F, Gerhardt, E C M, Nardin, J M, Santos, A M F, Rego, F G M, Picheth G, Moure, V R, Valdameri, G. <b>Multiplexed flow cytometric approach for detection of anti-SARS-CoV-2 IgG, IgM and IgA using beads covalently coupled to the nucleocapsid protein.</b>	Letters in Applied Microbiology
Submitted (under review)	Kita, D H, Andrade, G A, Missina, J M, Postal K, Boell, V K, Santana, F S, Zattoni, I F, Zanzarini, I S, Moure, V R, Rego, F G M, Picheth, G, Souza, E M, Soares, J F, Ambudkar, S V, Nunes, G G, Valdameri, G <b>Identification of polyoxovanadates as new P-glycoprotein inhibitors: insights into the mechanism of inhibition.</b>	FEBS Letters
2021	Kita, D H; Guragossian, N; Zattoni, I F; Moure, V R; Rego, F G M; Lusvarghi, S; Moulenat, T; Belhani, b; Picheth, G; Bouacida, S; Bouaziz, Z; Marminon, C ; Berredjem, M; Jose, J; Gonçalves, M B; Ambudkar, S V; Valdameri, G; Le Borgne, M. <b>Mechanistic basis of Breast cancer resistance protein inhibition by new indenof[1,2-b]indoles.</b>	Scientific Reports
2021	Vesga, L C; Kronenberger, T; Tonduru, A K; Kita, D H; Zattoni, I F; Bernal, C C ; Bohórquez, A R R ; Mendez-Sánchez, S C; Ambudkar, S V. ; Valdameri, G; Poso, A. <b>Tetrahydroquinoline/4,5 dihydroisoxazole molecular hybrids as novel inhibitors of Breast Cancer Resistance Protein (BCRP/ABCG2).</b>	ChemMedChem
2020	Gribner, C; Moura, P F; Veiga, A; Gatto, L J; Santos, N C. S; Marques, F A; Zattoni, I; Valdameri, G; Dias, J F G; Miguel, O G; Zanin, S M W. <b>Chemical constituents of Ocotea paranaensis(Lauraceae) essential oil and their antioxidant, anticancer and antimicrobial properties.</b>	Boletín Latinoamericano y del Caribe de Plantas Medicinales y Aromáticas
Brazilian Journals		
Year	Article	Journal
2021	Zattoni, I F; Picheth, G; Rego, F G M; Anghebem, M I; Moure, V R; Valdameri, G. <b>Uso da citometria de fluxo no diagnóstico sorológico da COVID-19</b>	Revista Brasileira de Análises Clínicas
Patents application		
Year	Patent	Institution
2021	Zattoni, I. F; Guanaes, L. D; Kita, D H; Valdameri, G; Gonçalves, A G; Moure, V R; Nosedá, M. D. <b>Porfirina 4B como inibidor específico do transportador ABCG2.</b>	Instituto Nacional da Propriedade Industrial - Brazil
2021	Valdameri, G; Postal, K; Missina, J. M; Soares, J. F; Nunes, G. G; Souza, E. M; Moure, V R; Zattoni, I. F; Andrade, G. A; Kita, D. H. <b>Uso de polioxovanadatos como inibidores específicos do transportador glicoproteína P (P-gp).</b>	Instituto Nacional da Propriedade Industrial - Brazil
2020	Valdameri, G; Valdameri, V. R. M; Prado, A. L; Prado, L. O; Paz, G; Volsanki, W; Zattoni, I. F; Kita, D. H; Rego, F. G. M; Picheth, G. <b>Equipamento de irradiação homogênea de luz não coerente para aplicação de terapia fotodinâmica em diferentes propósitos em pesquisa.</b>	Instituto Nacional da Propriedade Industrial - Brazil

## SUPPLEMENTARY DATA

## CHAPTER 1 - A NEW PORPHYRIN AS SELECTIVE SUBSTRATE-BASED INHIBITOR OF BREAST CANCER RESISTANCE PROTEIN (BCRP/ABCG2)

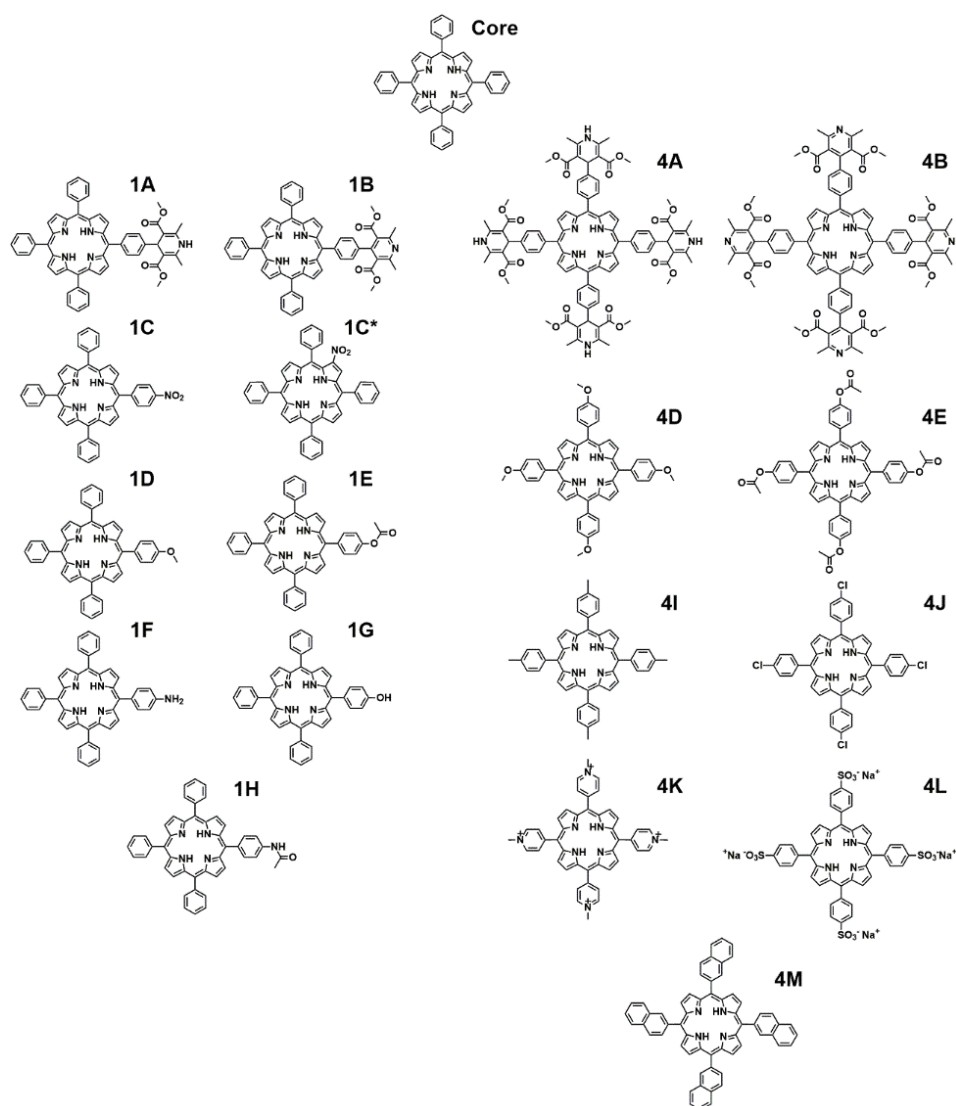


Figure S1: Chemical structure of screened porphyrins

Table S1: Chemical names of screened porphyrins

Porphyrin	Chemical nomenclature
<b>Core</b>	5,10,15,20-Tetraphenylporphyrin
<b>1A</b>	5- [4- (Dimethyl-2,6-dimethyl-1,4-dihydropyridine-3,5- dicarboxylate) -phenyl] -10,15,20-triphenyl porphyrin
<b>1B</b>	5- [4- (Dimethyl-2,6-dimethyl-3,5-pyridinedicarboxylate) - phenyl] -10,15,20- triphenyl porphyrin
<b>1C</b>	5,10,15-Triphenyl-20-(4-nitrophenyl) porphyrin
<b>1C*</b>	2-nitro-5,10,15,20-tetraphenylporphyrin
<b>1D</b>	5-(4-methoxyphenyl)-10,15,20-triphenylporphyrin
<b>1E</b>	5-(4-acetoxyphenyl)-10,15,20-triphenylporphyrin
<b>1F</b>	5-(4-aminophenyl)-10,15,20-triphenylporphyrin
<b>1G</b>	5-(4-hidroxyphenyl)-10,15,20-triphenylporphyrin

<b>1H</b>	5-(4-acetamidophenyl)-10,15,20-triphenylporphyrin
<b>4A</b>	5,10,15,20 -[Tetrakis-4-(dimethyl-2,6-dimethyl-1,4-dihydropyridine-3,5- dicarboxylate)-phenyl]-porphyrin
<b>4B</b>	5,10,15,20 - [tetrakis-4- (Dimethyl 2,6-dimethyl-3,5-pyridinedicarboxylate) - phenyl] –porphyrin
<b>4D</b>	5,10,15,20-Tetrakis(p-methoxyphenyl) porphyrin
<b>4E</b>	5,10,15,20-Tetrakis(4-acetoxyphenyl) porphyrin
<b>4I</b>	5,10,15,20-Tetrakis(4-methylphenyl) porphyrin
<b>4J</b>	5,10,15,20-Tetrakis(4-chlorophenyl) porphyrin
<b>4K</b>	5,10,15,20-Tetrakis(1-methylpyridinium-4-yl) porphyrin tetraiodide
<b>4L</b>	Tetrasodium 5,10,15,20-tetrakis(4-benzenesulfonate) porphyrin
<b>4M</b>	5,10,15,20-Tetrakis(naphthalen-2-yl) porphyrin

**Table S2:** Porphyrins fluorescence raw data.

	<b>FL-1</b>	<b>FL-2</b>	<b>FL-3</b>	<b>FL-4</b>
<b>Blank</b>	2.11	2.94	2.48	2.97
<b>Mitoxantrone</b>	2.67	1.81	75.67	139.49
<b>CORE</b>	1.95	2.79	2.48	3.37
<b>1A</b>	2.81	6.04	12.63	12.52
<b>1B</b>	2.31	3.68	5.05	13.22
<b>1C</b>	9.82	9.22	11.55	10.75
<b>1C*</b>	2.02	2.76	2.55	3.25
<b>1D</b>	6.32	6.21	6.32	5.52
<b>1E</b>	8.43	8.28	9.14	7.99
<b>1F</b>	2.67	2.09	8.74	6.82
<b>1G</b>	2.35	1.91	6.38	5.62
<b>1H</b>	9.06	9.31	22.27	15.96
<b>4A</b>	2.50	3.65	3.96	4.03
<b>4B</b>	9.91	12.86	16.4	5.94
<b>4D</b>	6.21	8.13	<b>103.66</b>	54.74
<b>4E</b>	5.00	5.05	10.55	11.34
<b>4I</b>	2.39	1.84	1.78	1.01
<b>4J</b>	8.43	7.7	7.17	4.74
<b>4K</b>	2.67	2.19	10.65	4.78
<b>4L</b>	3.11	2.41	21.29	19.11
<b>4M</b>	3.28	3.11	3.16	3.43

Cells were submitted to 24 hours of treatment at 5  $\mu\text{M}$  of each porphyrin. Fluorescence detection was performed by flow cytometry using 488 and 635 nm lasers for excitation and 4 channels for detection: FL-1 (530/30), FL-2 (585/42), FL-3 (670 LP) and FL-4 (661/16). 4D was the most fluorescent porphyrin and was used as probe for the accumulation assay. Mitoxantrone (at 10  $\mu\text{M}$ ) for 30 minutes was used as positive control.

**Table S3:** Concentration-dependent chemosensitization of ABCG2 overexpressing and parental (wild-type) cell lines.

	SN-38 ( $\mu\text{M}$ )	Wild type ( $\pm\text{SD}$ )	ABCG2 ( $\pm\text{SD}$ )	ABCG2 + 4B ( $\pm\text{SD}$ )
HEK293	0.0001	104.82 ( $\pm 6.78$ )	101.27 ( $\pm 11.74$ )	89.22 ( $\pm 12.39$ )
	0.001	91.58 ( $\pm 10.51$ )	100.57 ( $\pm 9.21$ )	86.20 ( $\pm 13.41$ )
	0.005	45.96 ( $\pm 13.72$ )	99.19 ( $\pm 3.41$ )	60.50 ( $\pm 18.97$ )
	0.01	52.47 ( $\pm 16.46$ )	94.49 ( $\pm 15.60$ )	57.92 ( $\pm 11.81$ )
	0.05	38.31 ( $\pm 15.63$ )	61.18 ( $\pm 14.34$ )	48.00 ( $\pm 11.42$ )
	0.1	35.19 ( $\pm 12.14$ )	52.32 ( $\pm 12.39$ )	41.50 ( $\pm 5.86$ )
	0.5	25.90 ( $\pm 10.30$ )	51.81 ( $\pm 16.66$ )	33.45 ( $\pm 10.46$ )
	1	29.05 ( $\pm 10.54$ )	36.11 ( $\pm 8.87$ )	31.81 ( $\pm 6.28$ )
	10	21.22 ( $\pm 6.62$ )	29.17 ( $\pm 8.99$ )	27.44 ( $\pm 5.74$ )
	20	15.72 ( $\pm 8.59$ )	16.22 ( $\pm 4.57$ )	23.52 ( $\pm 8.82$ )
H460	0.5	69.77 ( $\pm 4.42$ )	92.53 ( $\pm 7.03$ )	62.90 ( $\pm 9.71$ )
	5.0	36.73 ( $\pm 5.78$ )	72.18 ( $\pm 0.86$ )	32.08 ( $\pm 5.31$ )

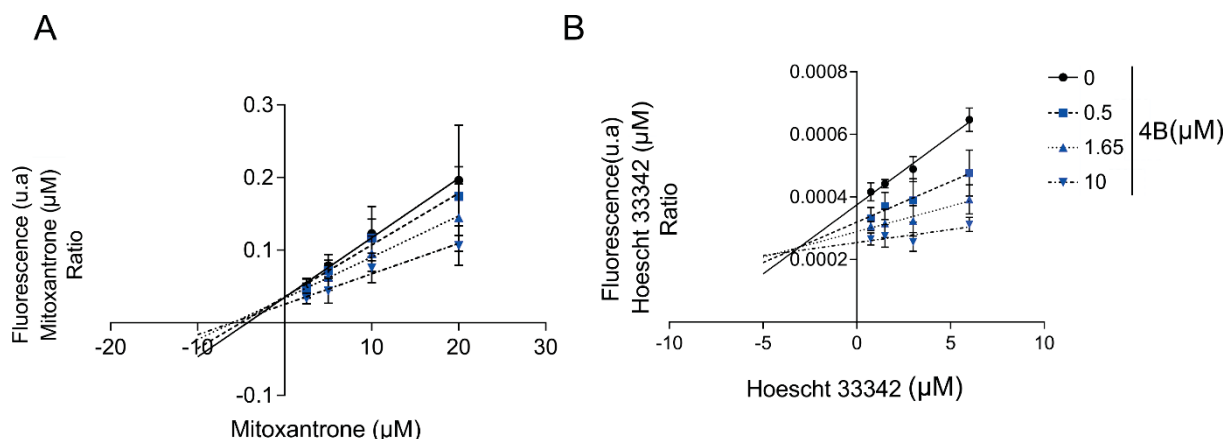


**Figure S2:** (A) Type of inhibition using mitoxantrone as substrate (B) Type of inhibition using hoechst 33342 as substrate. Data were linearized by the Hanes-Woolf method. The data represent at least two independent experiments.

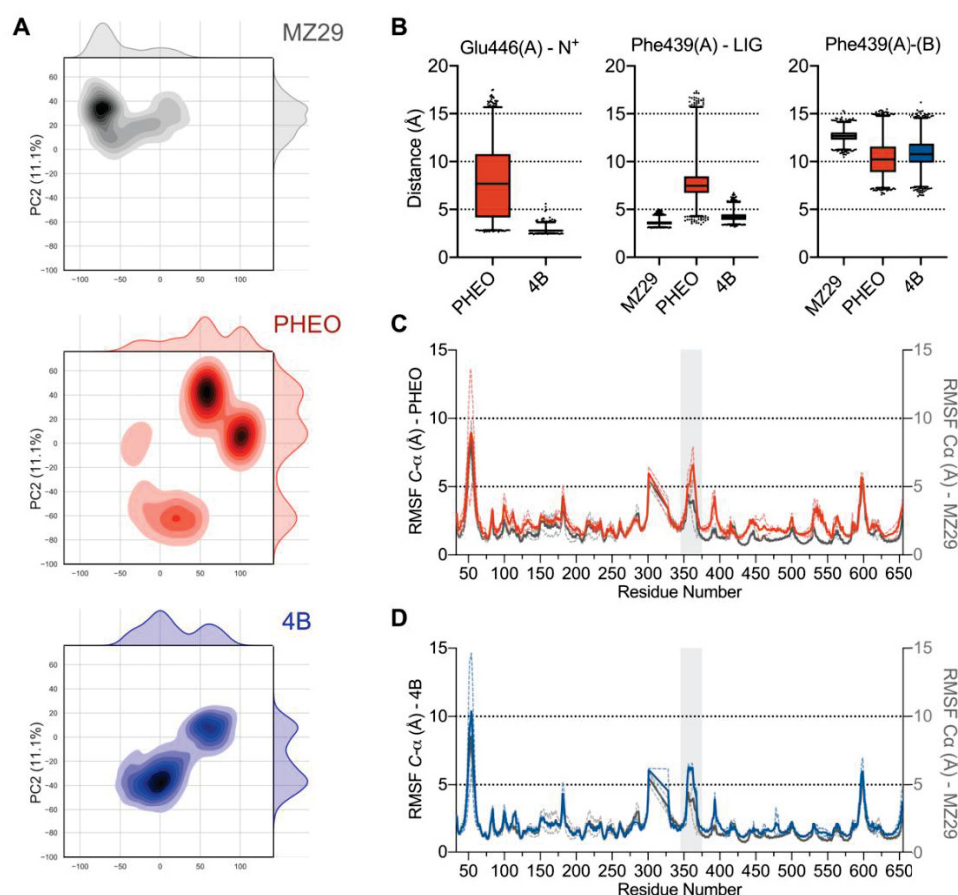


**Figure S3:** (A) Principal component analyses of ABCG2's backbone atoms revealing a single major conformation for simulations with the co-crystallized ligand MZ29 (grey) three major conformational populations for the substrate PHEO (red) and two for the inhibitor **4B** (blue). (B) distance between the centre of mass of relevant residues and the closes atom from the ligand. Average residue fluctuations obtained from the root mean square deviation fluctuations (RMSF) of the ABCG2's backbone atoms calculated in relation to the initial simulation frame in comparison to simulations with the co-crystallized ligand, for each inhibitor as described in the labels. Each dark-colored line represents the average distance of the three independent (1  $\mu$ s) simulations and the respective light-coloured dashed line represent the observed standard deviation, for PHEO (C) and **4B** (D). Gray lines are the average for the simulations with co-crystallized original ligand MZ29, previously reported elsewhere. Shaded region (residues 350-375) represents the loop connecting the NBD to the TM domain, which has higher fluctuation in simulations with our ligands in comparison to MZ29, even after equilibration.



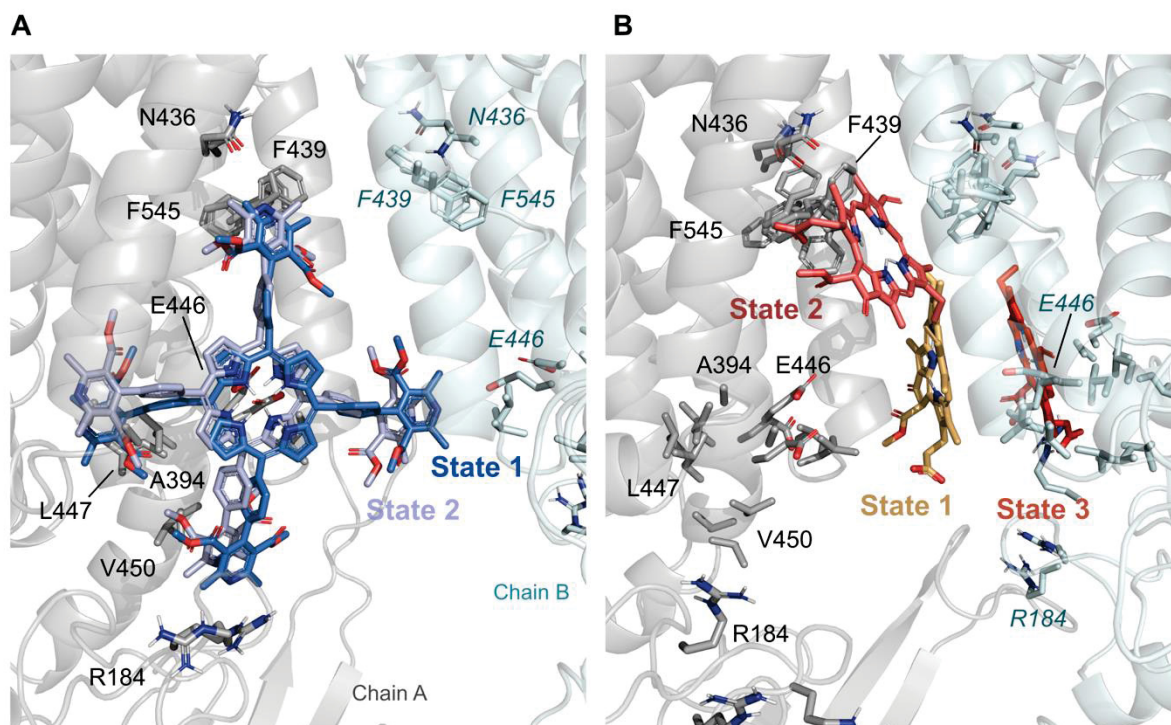


**Figure S4:** Representative snapshots from the MD simulations for each of the compounds: **4B** (A) and PHEO (B).

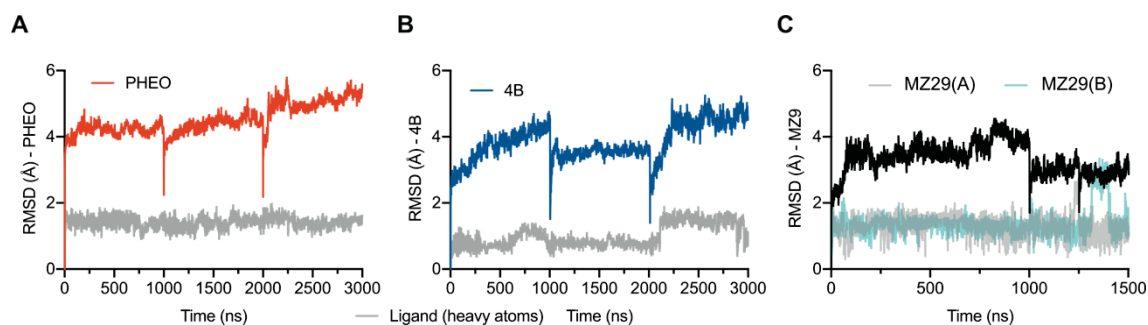
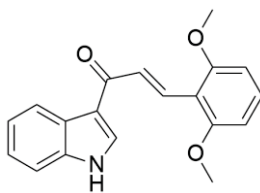


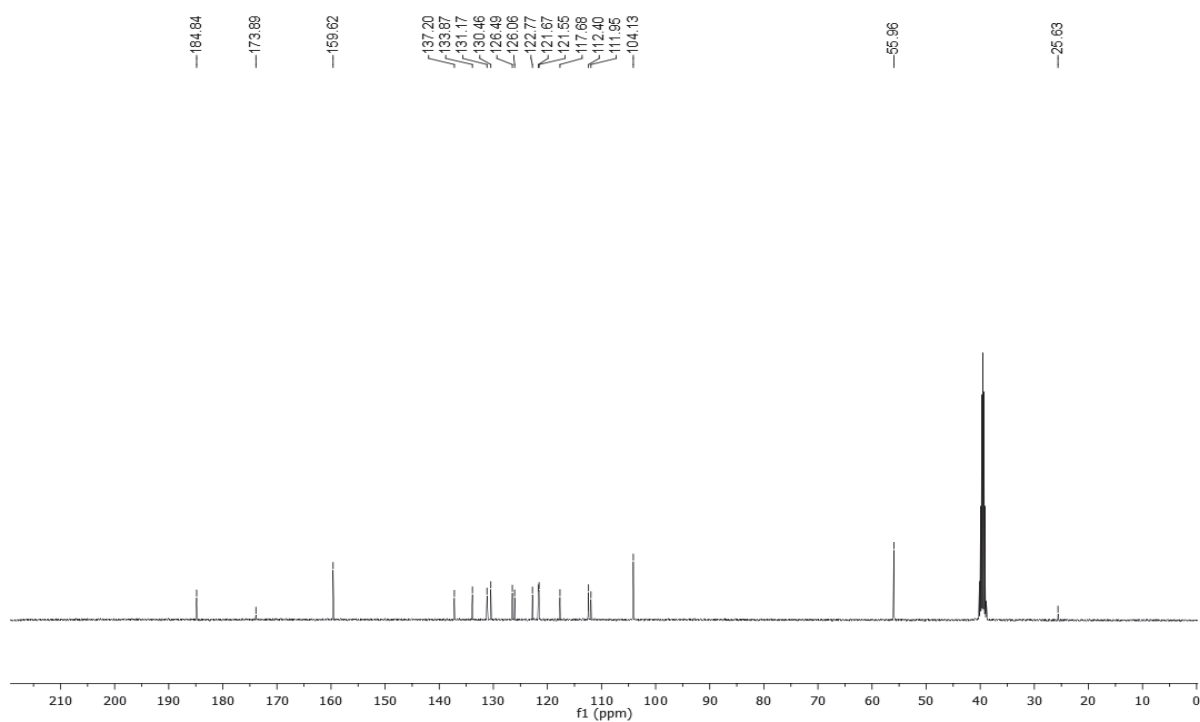
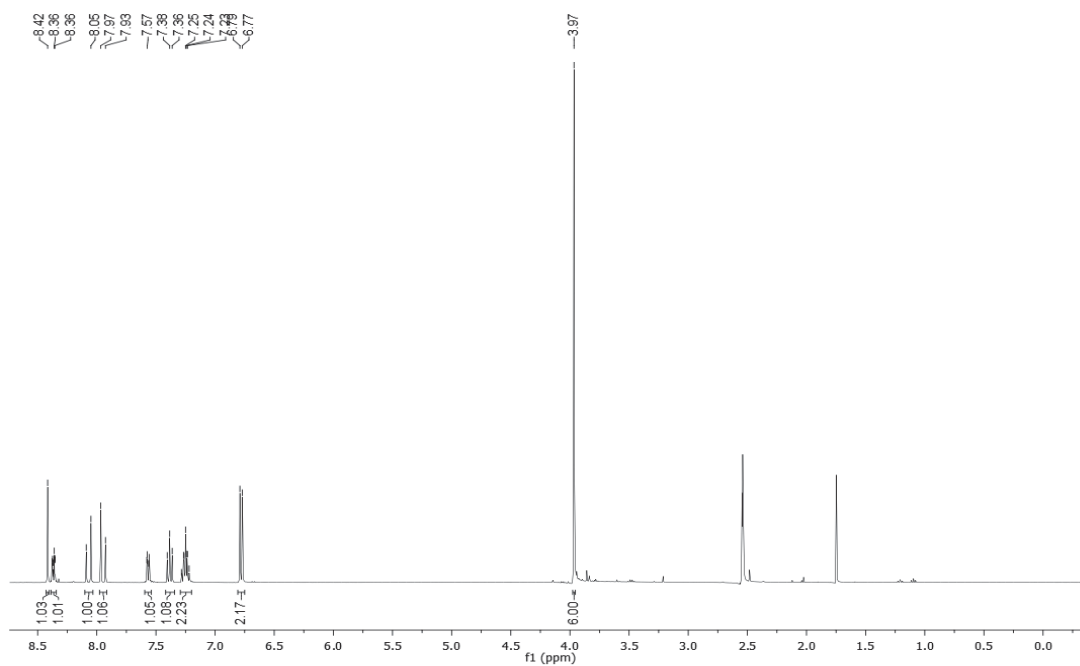
**Figure S5:** Representative picture of root-mean-square deviation (RMSD) values of protein backbone for our two protein-ligand complexes, observed along a total simulation time of 3  $\mu$ s, for each. Colored lines represent the RMSD of ABCG2's backbone atoms along the simulation time related to the initial time frame with each ABCG2 inhibitor, while grey lines represent the ligand fluctuation normalized by the local protein fluctuation. (A) PHEO, (B) **4B** and the co-crystallized ligand MZ29 (C).

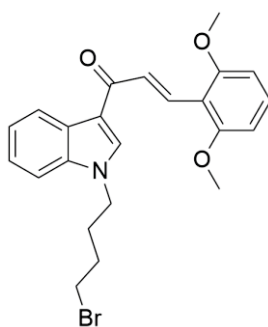
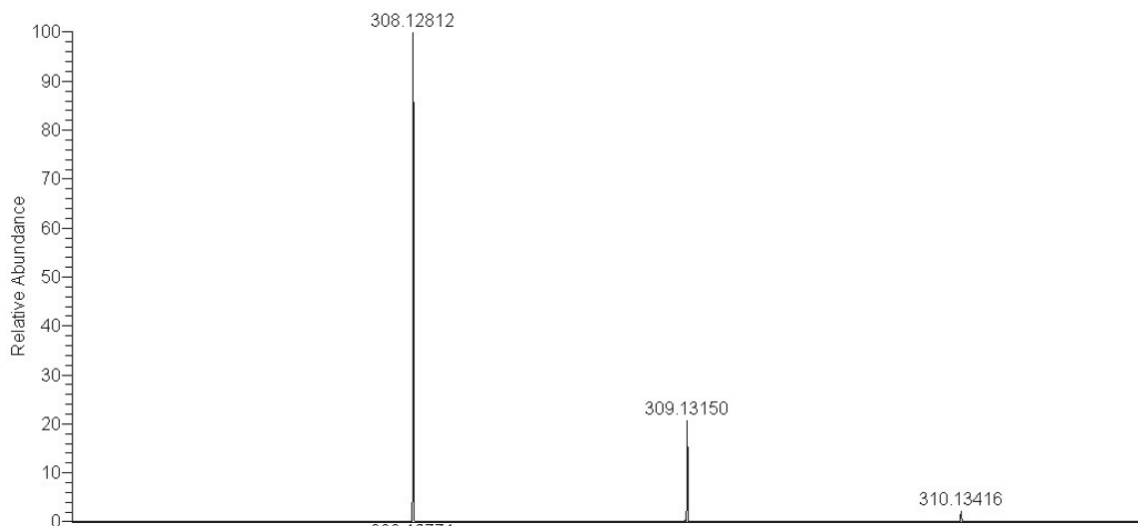
## CHAPTER 2 - SYNTHESIS AND BIOLOGICAL EVALUATION OF HETERODIMERS ON ABCG2 ACTIVITY



CHALCONE (1)

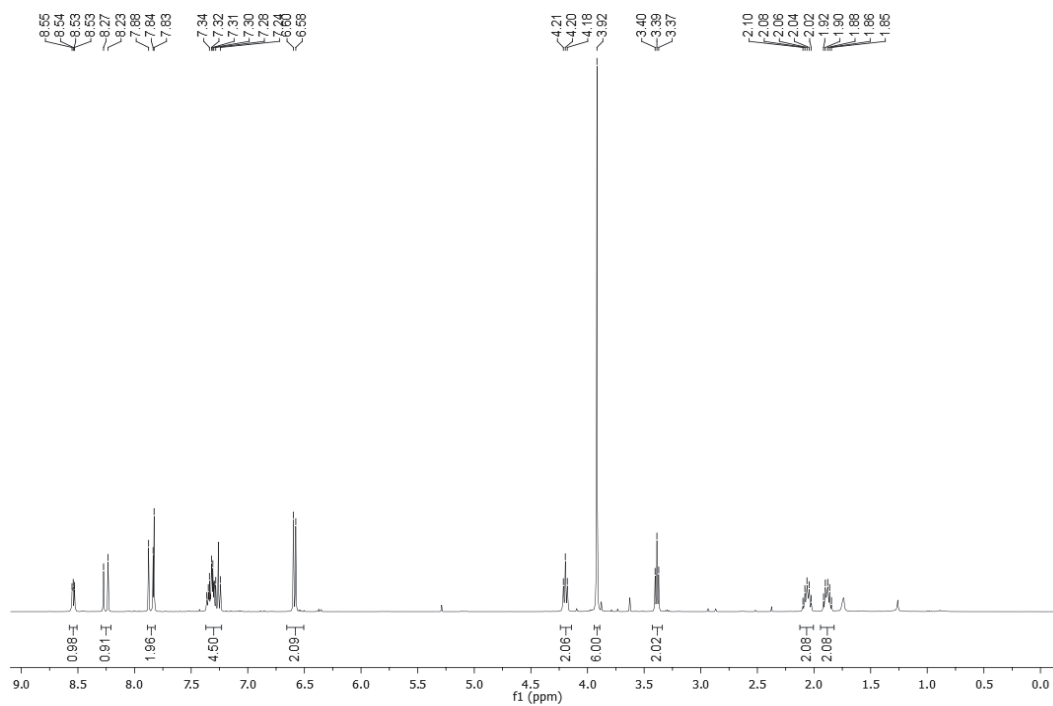
IUPAC: (E)-3-(2,6-dimethoxyphenyl)-1-(1H-indol-3-yl)prop-2-en-1-one

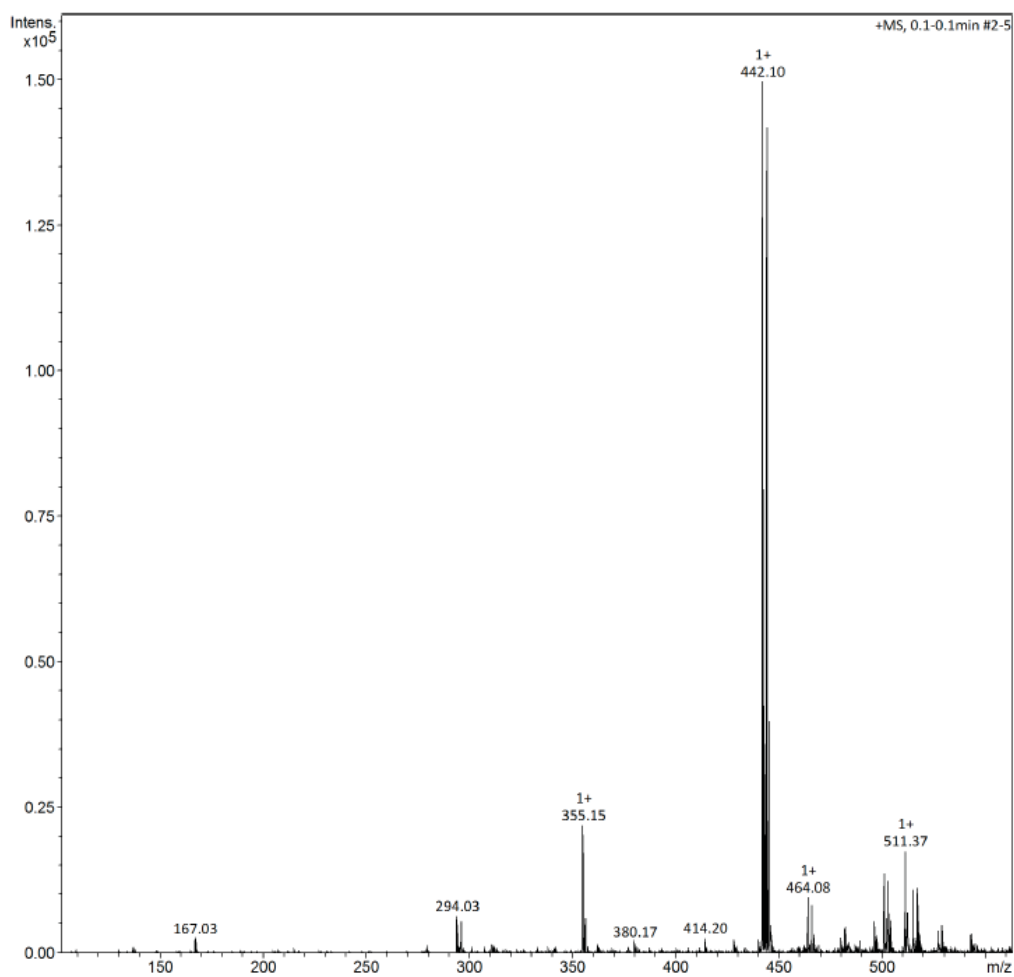
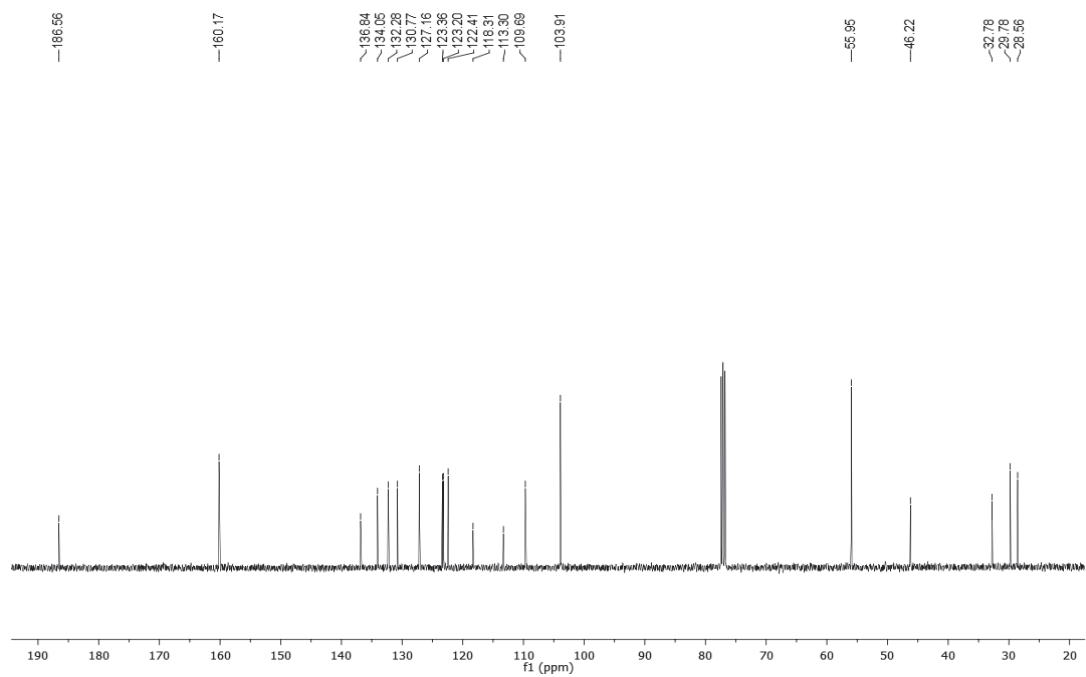


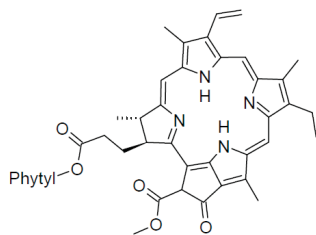


### CHALCONE (2)

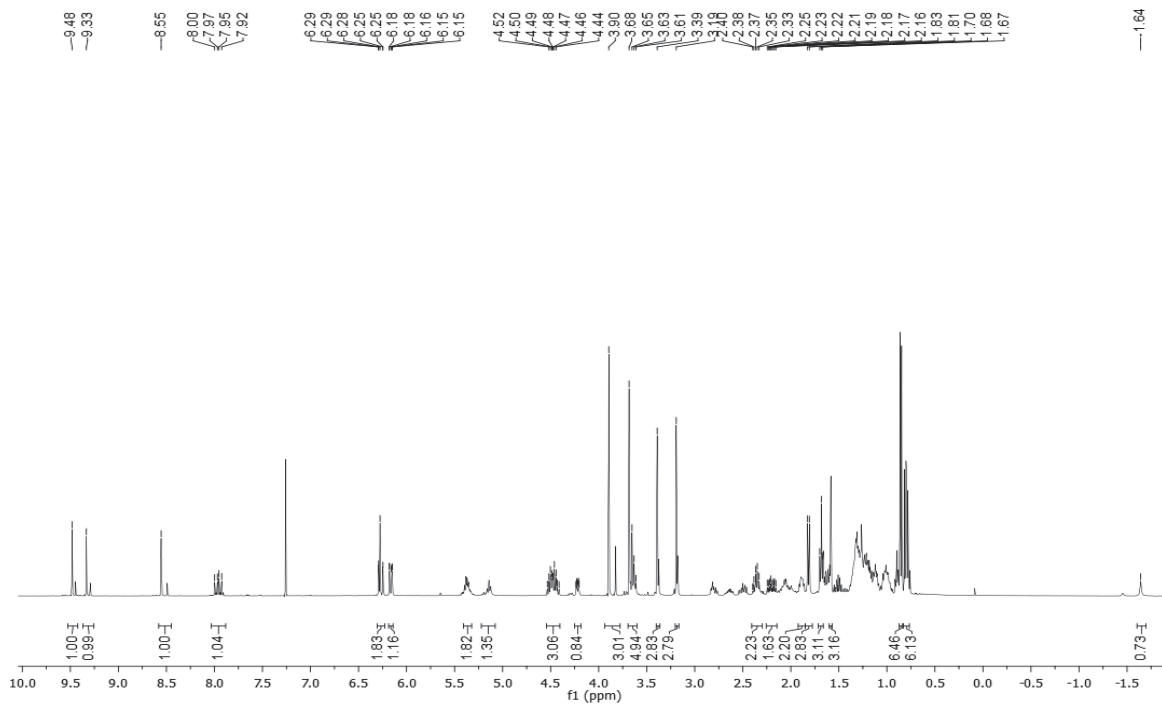
IUPAC: (E)-1-(1-(4-bromobutyl)-1H-indol-3-yl)-3-(2,6-dimethoxyphenyl)prop-2-en-1-one



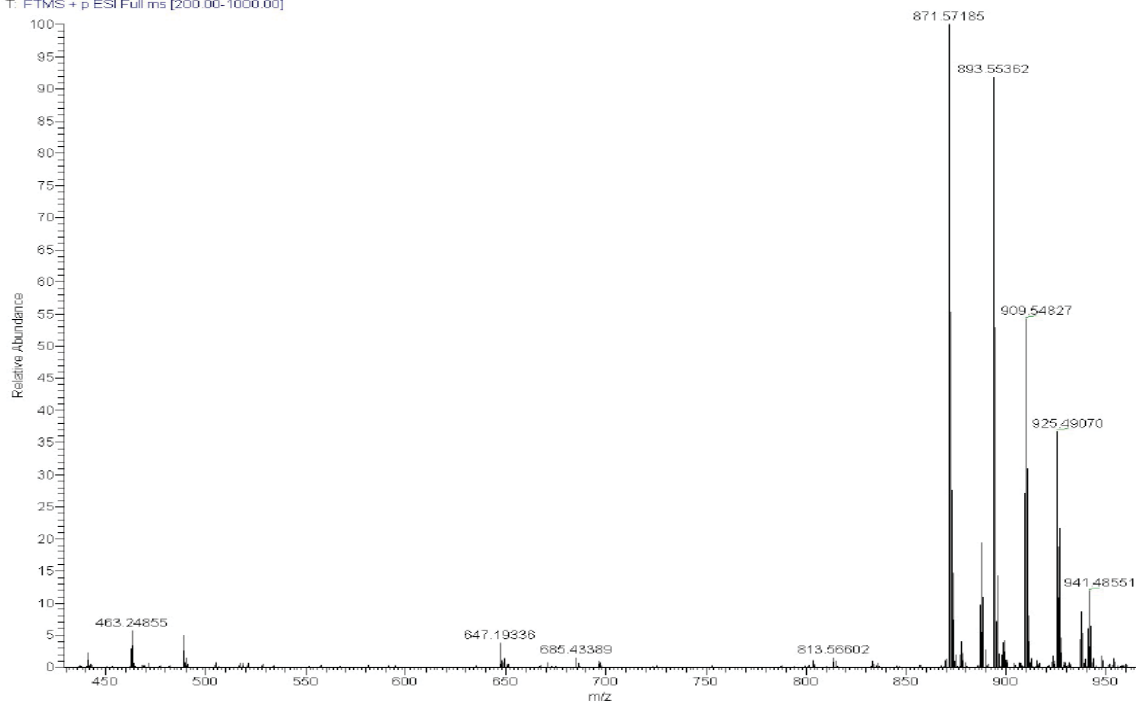


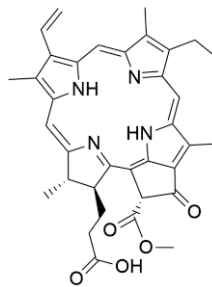


### PHEOPHYTIN (3)

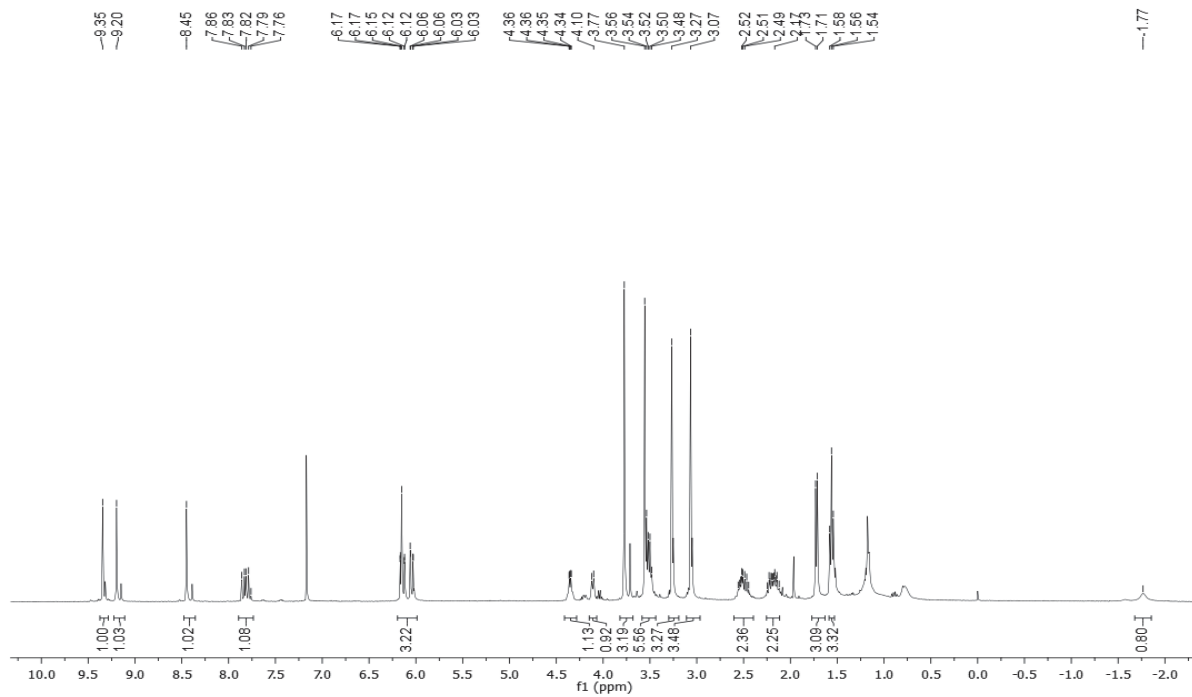


01P61G #10.22 RT: 0.26-0.58 AV: 13 NL: 4.78E6  
T: FTMS + p ESI Full ms [200.00-1000.00]

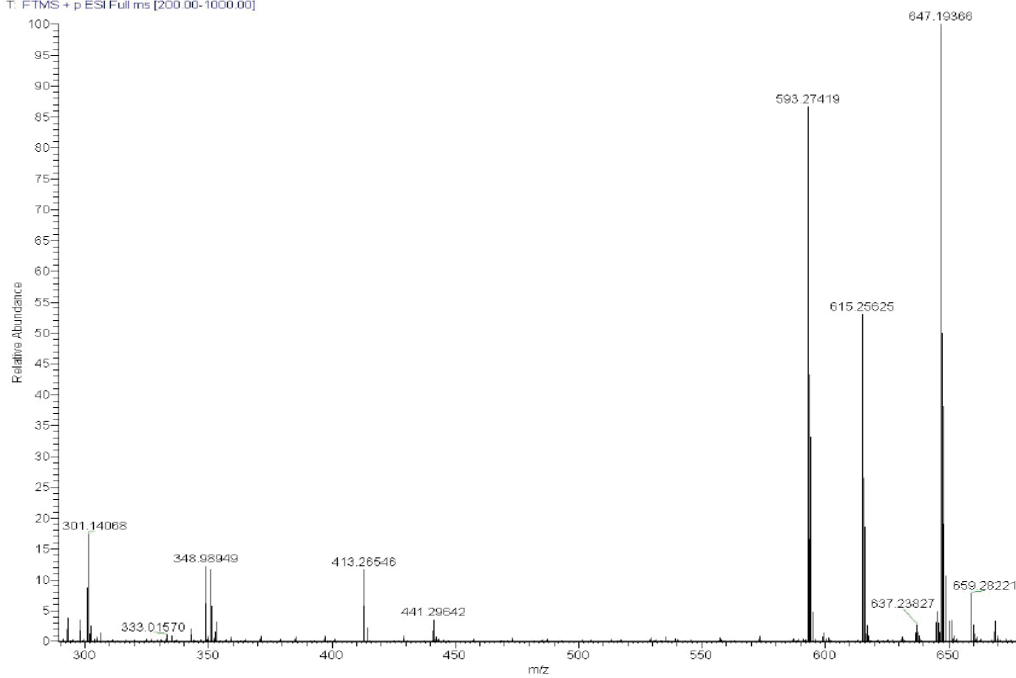


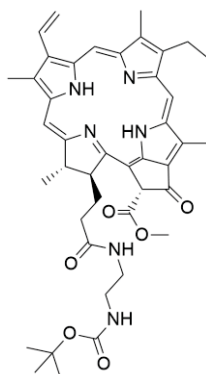


### PHEOPHORBIDE A (4)

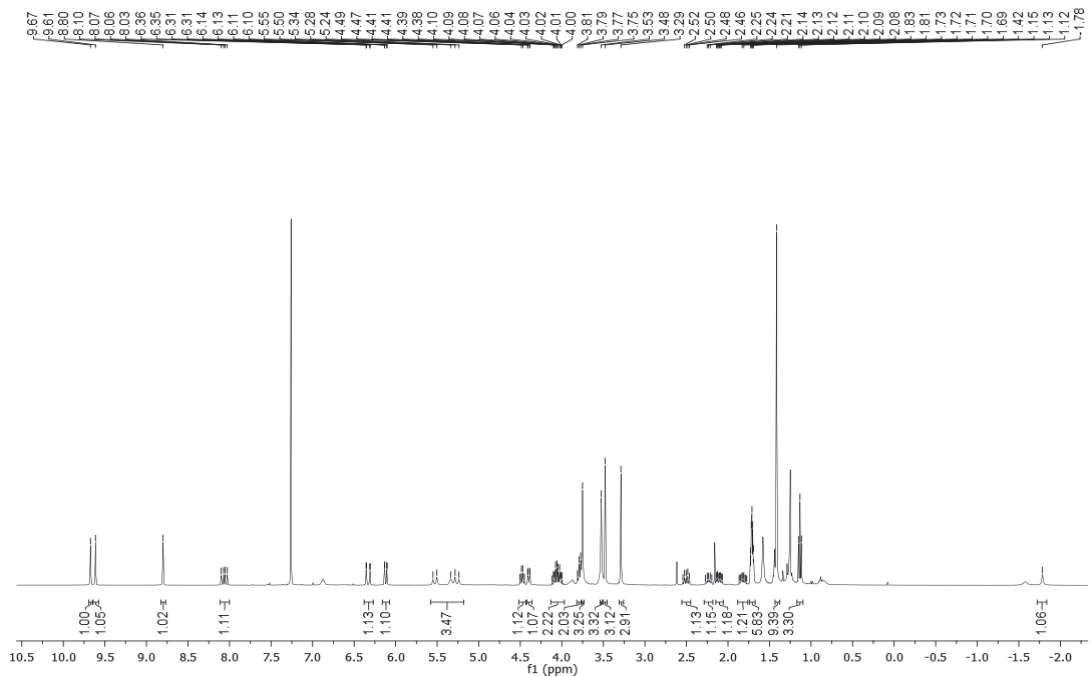


01P61H#12:26 RT: 0.30-0.68 AV: 15 NL: 8.38E6  
T: FTMS + p ESI Full ms [200.00-1000.00]

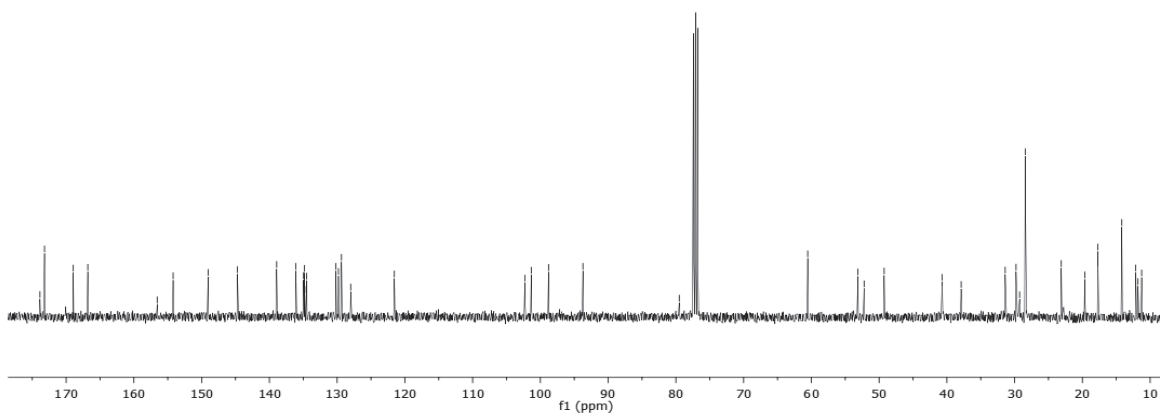


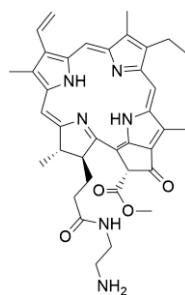
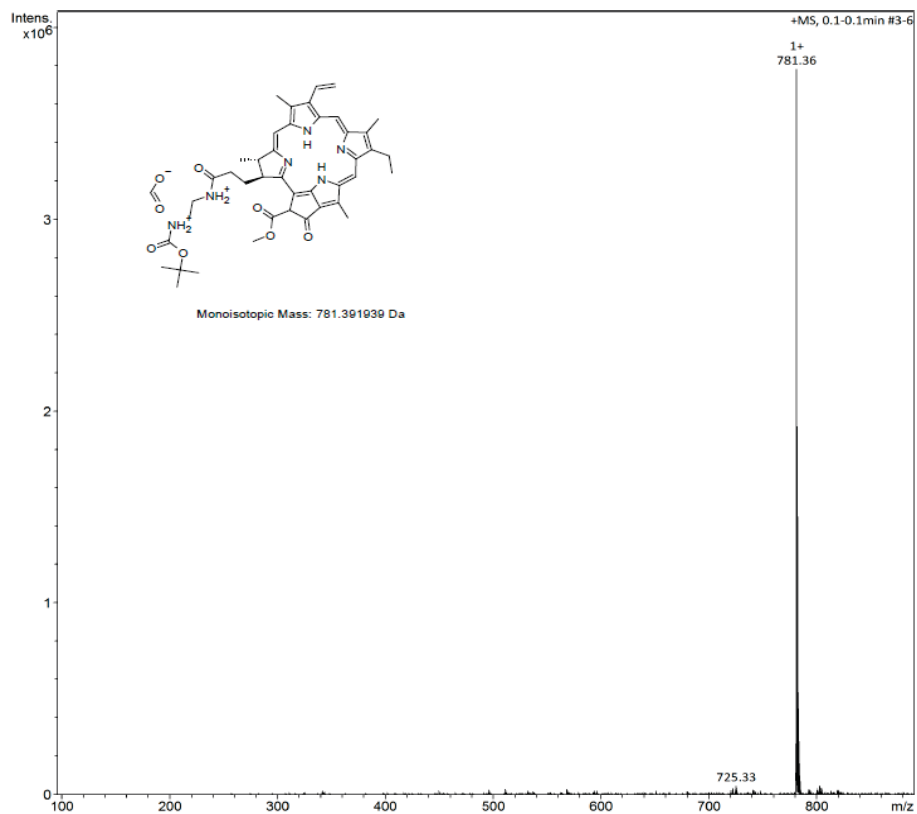


PHEOPHORBIDE AMIDE (5)

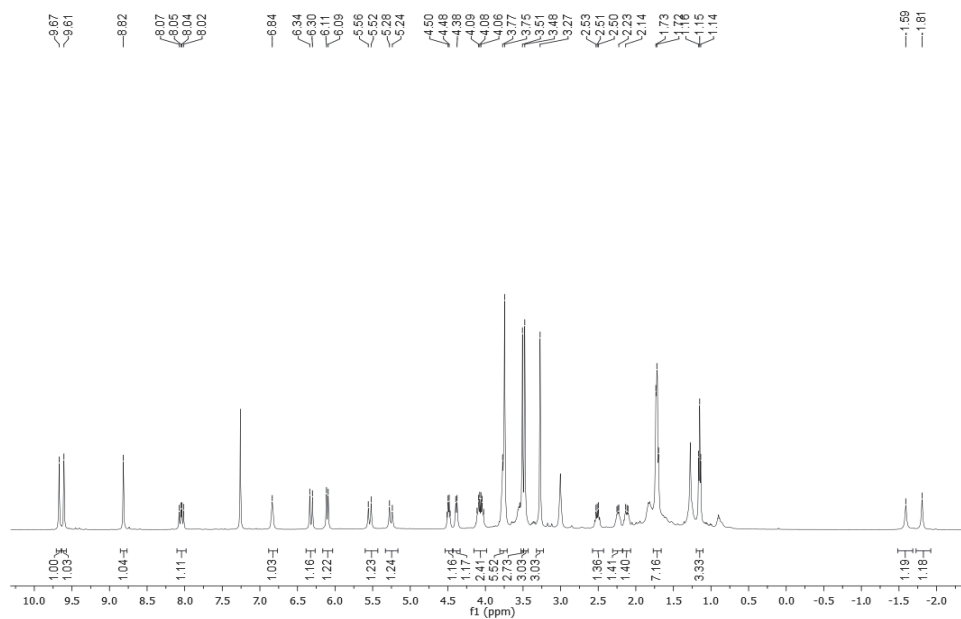


- 173.86
- 173.19
- 168.94
- 166.80
- 156.55
- 154.21
- 149.04
- 144.70
- 138.92
- 136.06
- 134.95
- 134.81
- 134.51
- 130.16
- 128.81
- 128.55
- 102.29
- 101.35
- 98.79
- 93.72
- 79.50
- 60.54
- 53.14
- 52.22
- 48.26
- 40.89
- 37.89
- 31.39
- 29.70
- 28.27
- 28.42
- 23.12
- 19.65
- 17.73
- 14.18
- 12.13
- 11.80
- 11.25

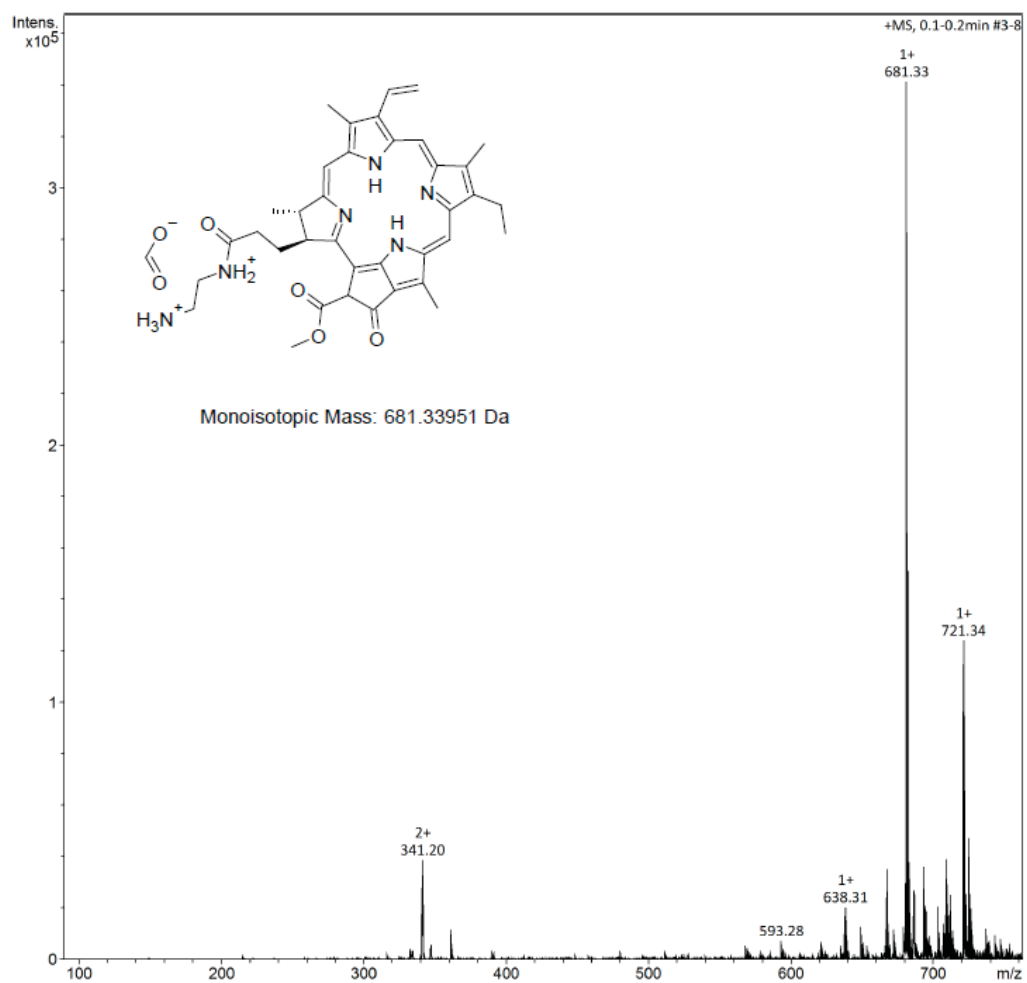
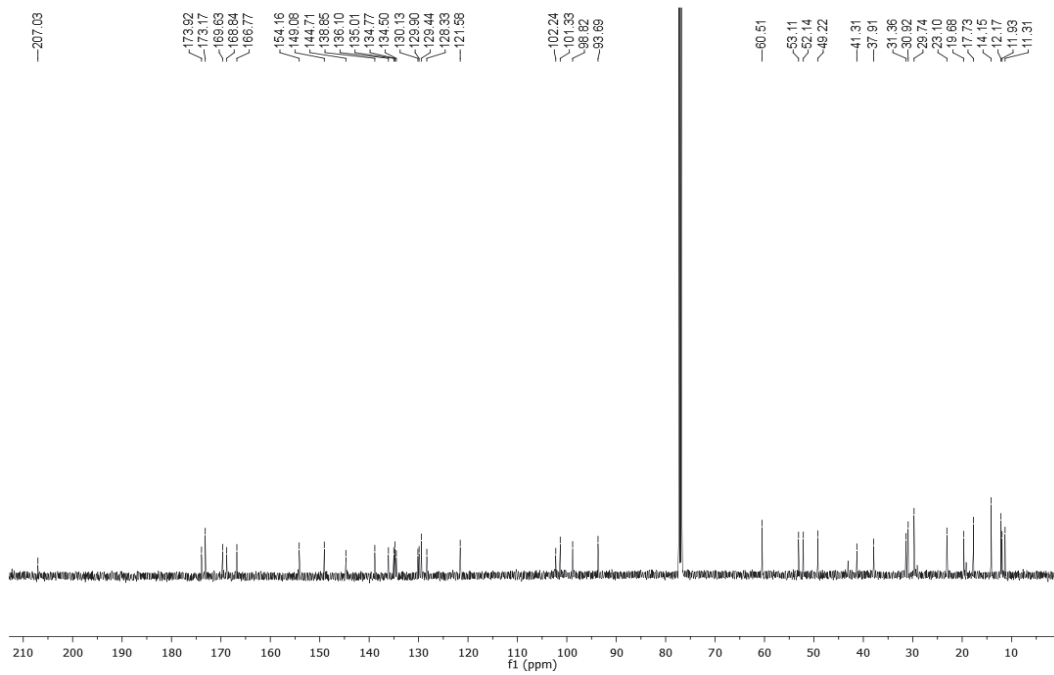


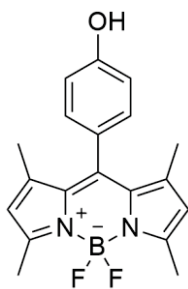


### PHEOPHORBIDE AMINE DEPROTECTED (6)



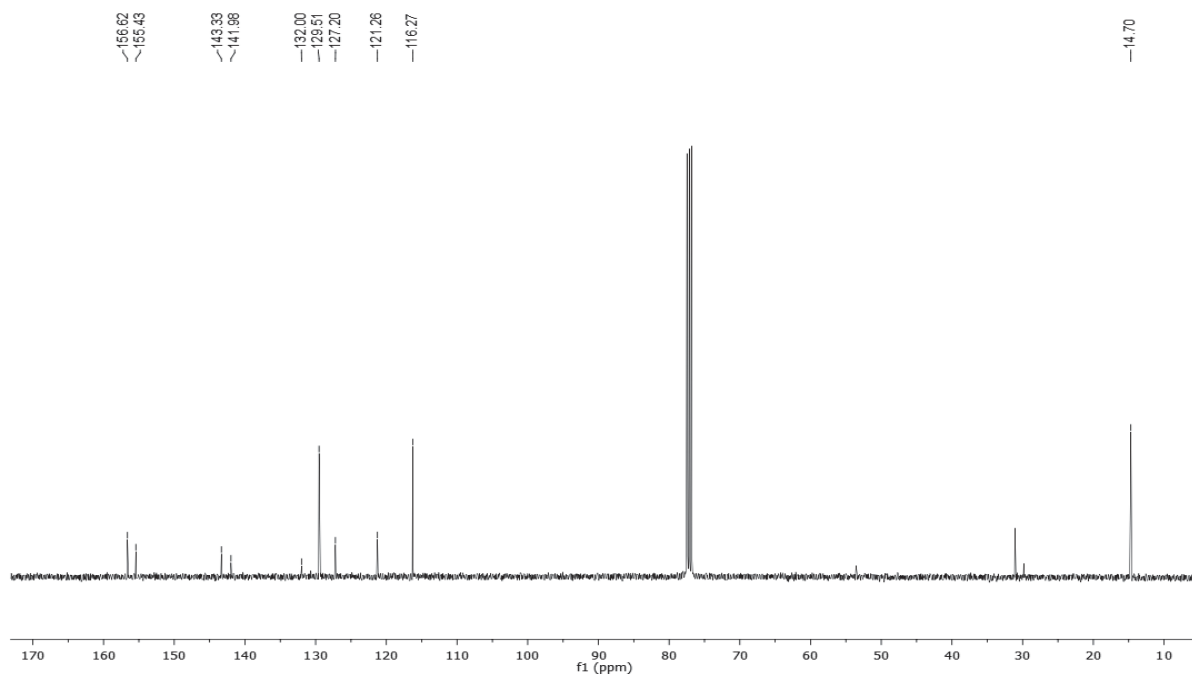
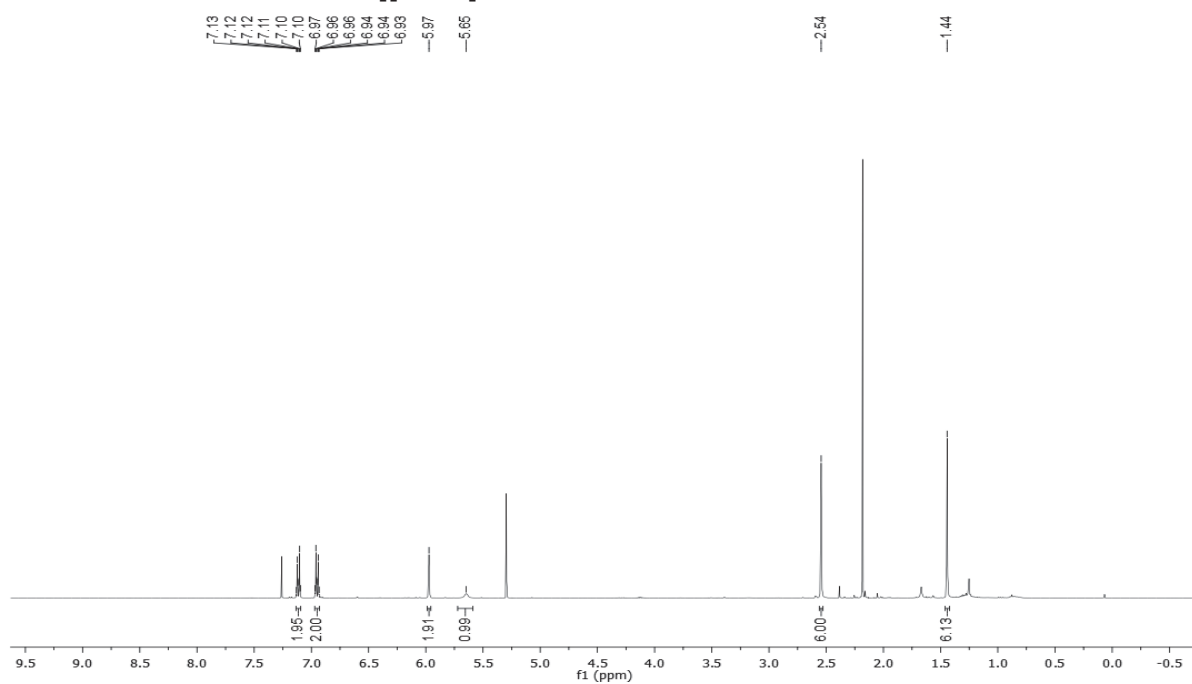


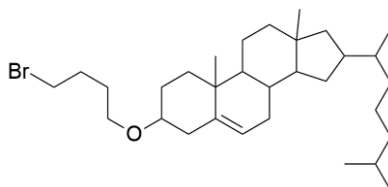




BODIPY (7)

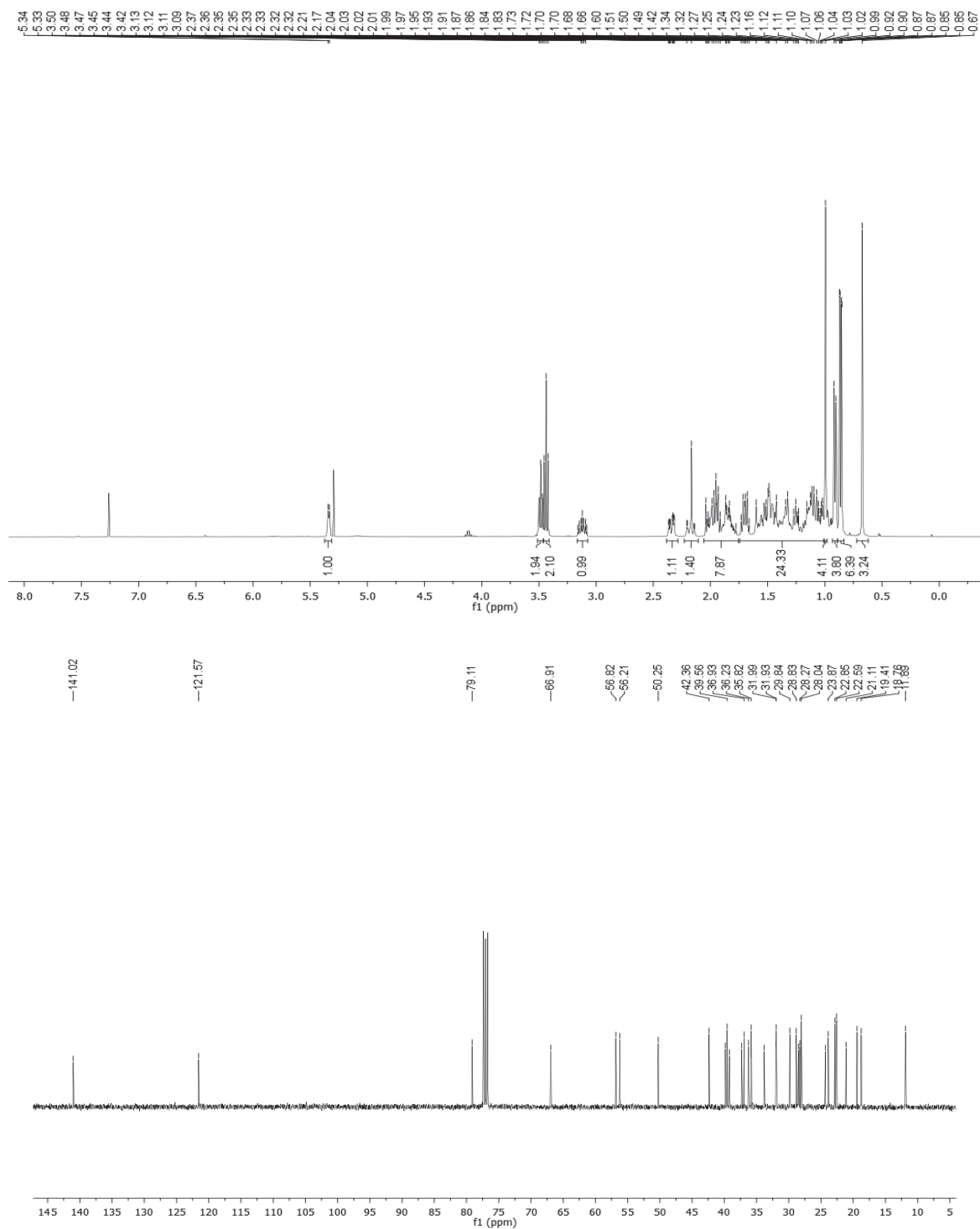
IUPAC: 5,5-difluoro-10-(4-hydroxyphenyl)-1,3,7,9-tetramethyl-5H-dipyrrolo[1,2-c:2',1'-f][1,3,2]diazaborinin-4-ium-5-uide

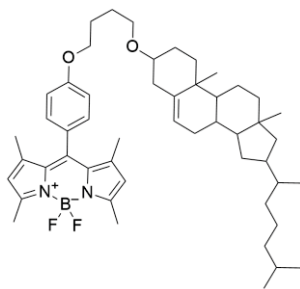




CHOLESTEROL – BR (8)

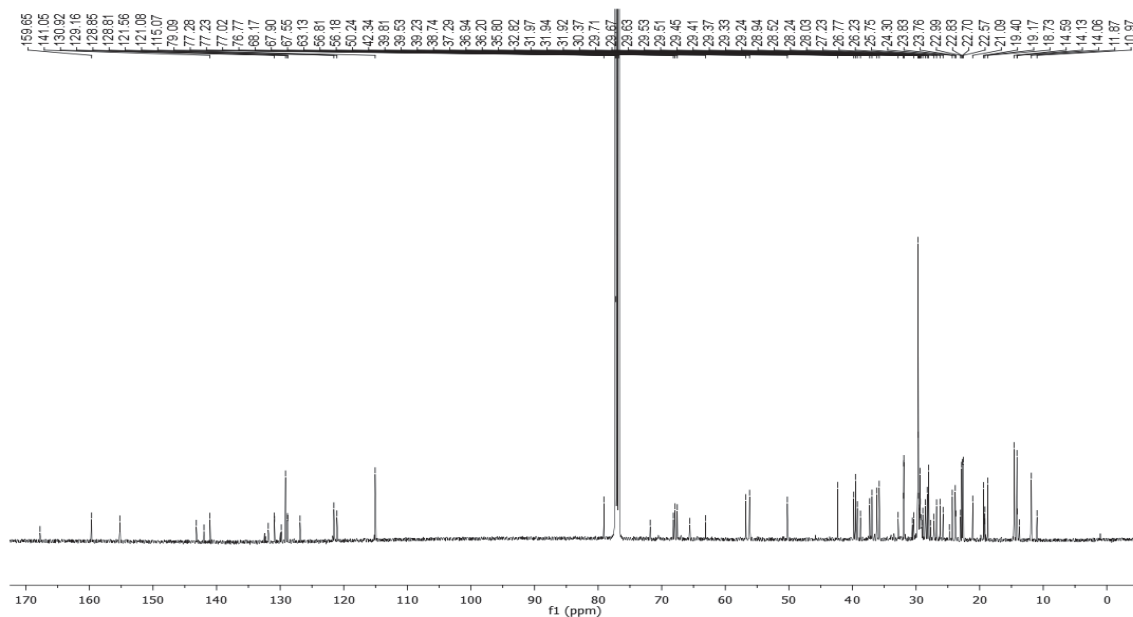
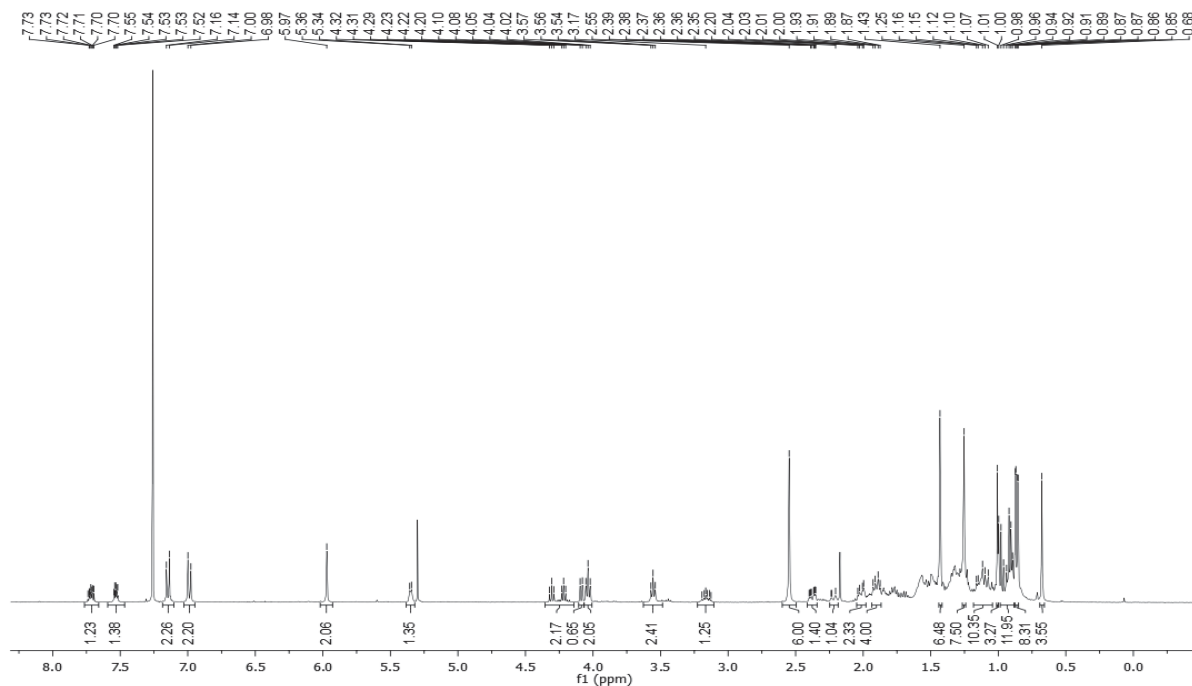
IUPAC: 3-(4-bromobutoxy)-10,13-dimethyl-16-(6-methylheptan-2-yl)-2,3,4,7,8,9,10,11,12,13,14,15,16,17-tetradecahydro-1H-cyclopenta[a]phenanthrene

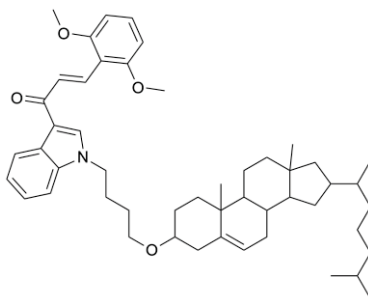
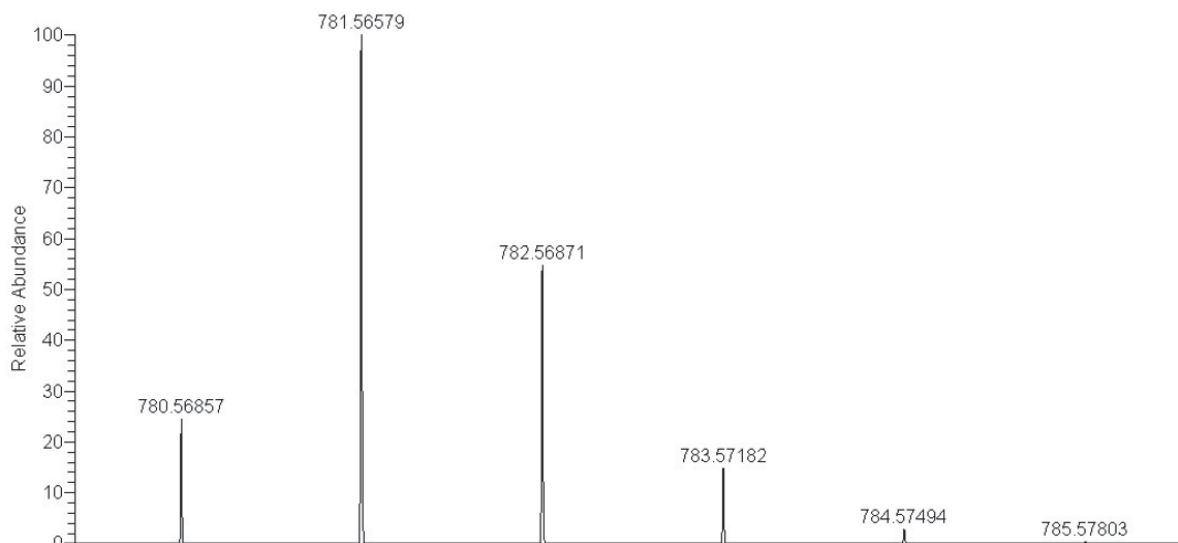




### CHOLESTEROL – BODIPY (9)

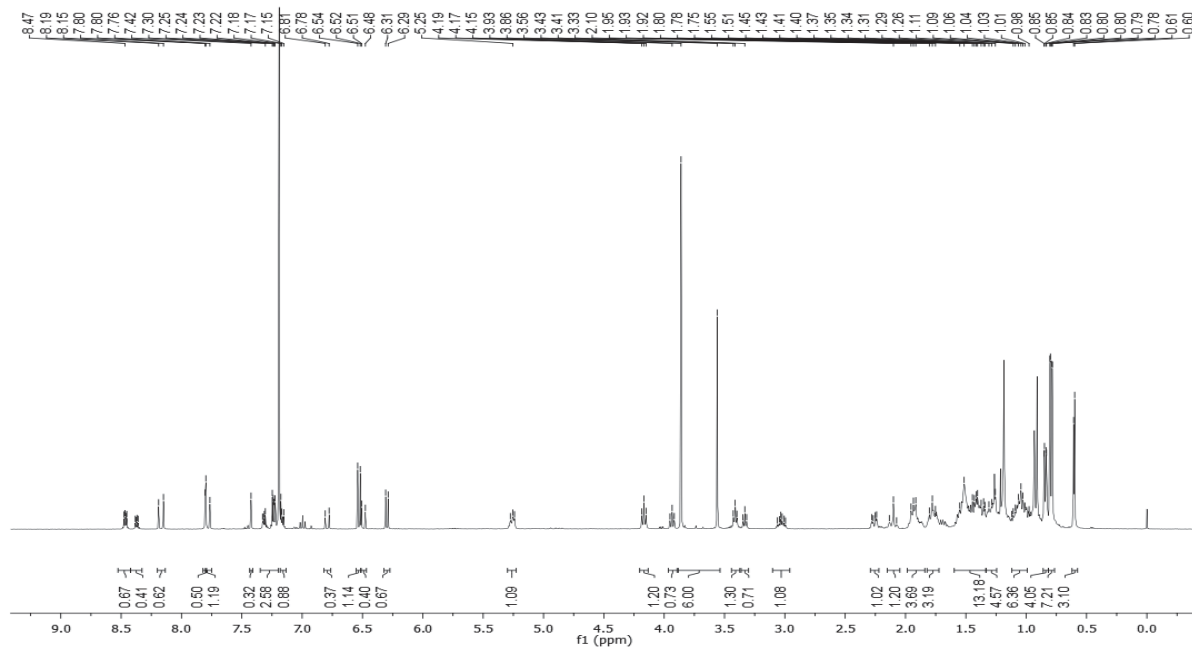
IUPAC: 10-(4-(4-((10,13-dimethyl-16-(6-methylheptan-2-yl)-2,3,4,7,8,9,10,11,12,13,14,15,16,17-tetradecahydro-1H-cyclopenta[a]phenanthren-3-yl)oxy)butoxy)phenyl)-5,5-difluoro-1,3,7,9-tetramethyl-5H-dipyrrolo[1,2-c:2',1'-f][1,3,2]diazaborin-4-ium-5-uide

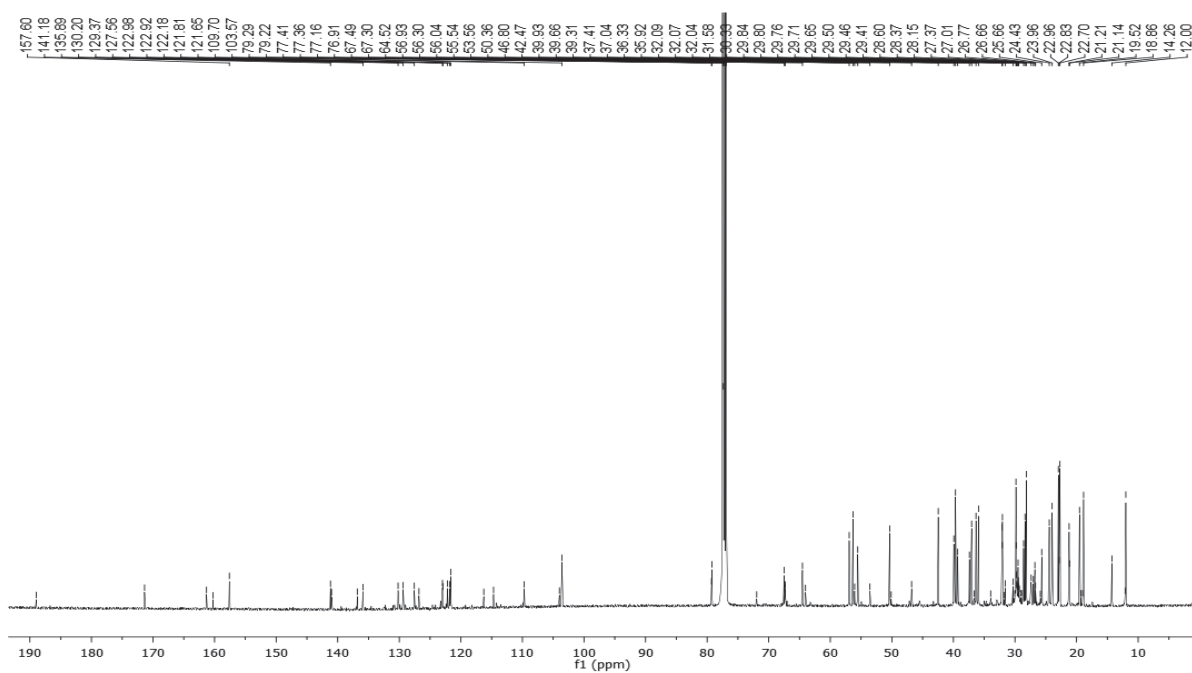




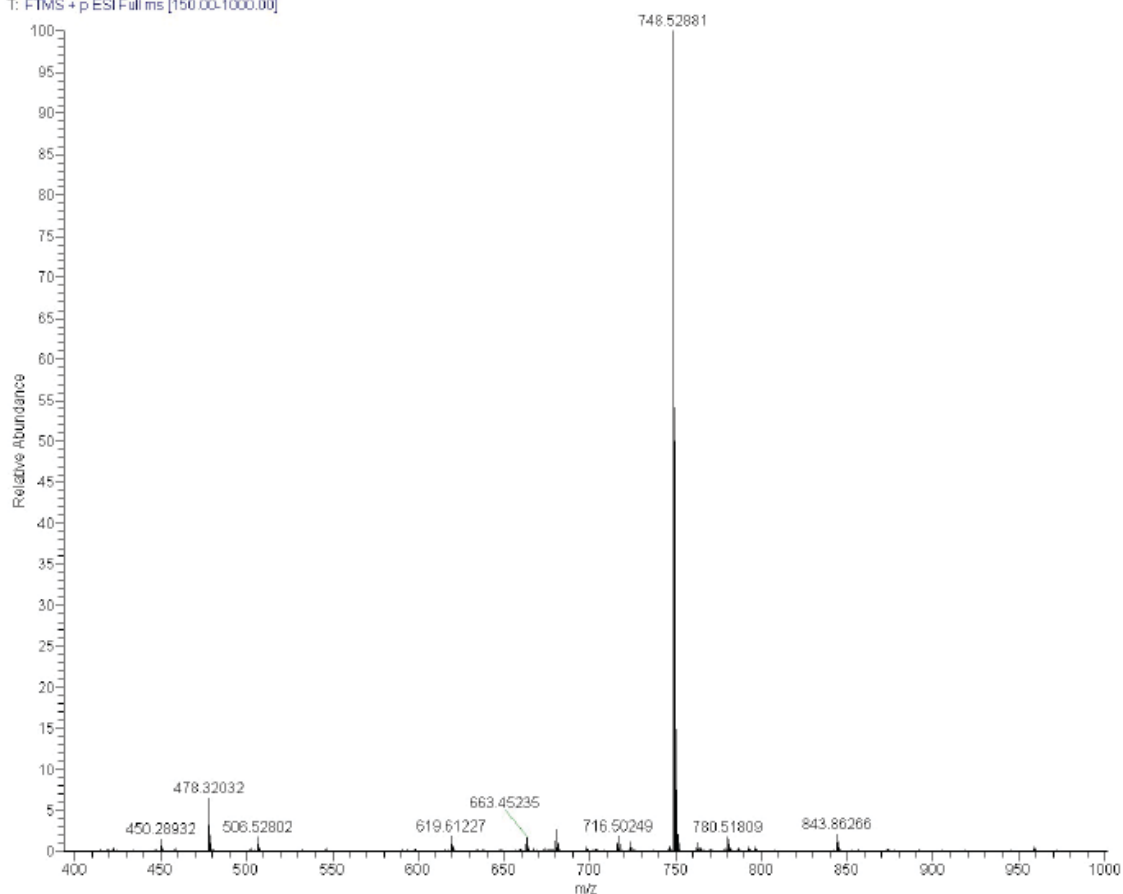
### CHALCONE – CHOLESTEROL (10)

IUPAC: (E)-3-(2,6-dimethoxyphenyl)-1-(1-(4-((10,13-dimethyl-16-(6-methylheptan-2-yl)-2,3,4,7,8,9,10,11,12,13,14,15,16,17-tetradecahydro-1H-cyclopenta[a]phenanthren-3-yl)oxy)butyl)-1H-indol-3-yl)prop-2-en-1-one





01P09C #18-37 RT: 0.50-1.02 AV: 20 NL: 1.84E7  
T: FTMS + p ESI Full ms [150.00-1000.00]



### CHAPTER 3 - MULTIPLEXED FLOW CYTOMETRIC APPROACH FOR DETECTION OF ANTI-SARS-COV-2 IGG, IGM AND IGA USING BEADS COVALENTLY COUPLED TO THE NUCLEOCAPSID PROTEIN

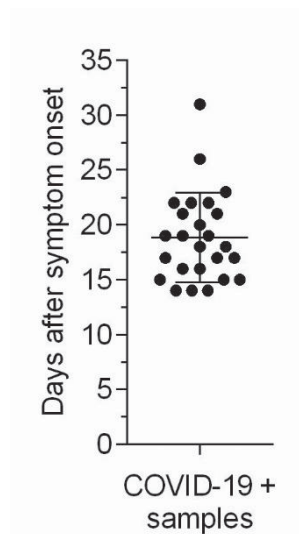


**Figure S1:** Representation of symptoms onset for the COVID-19 positive samples ( $n=26$ ) used in this work. Samples were collected from patients after 14 days of hospitalization.

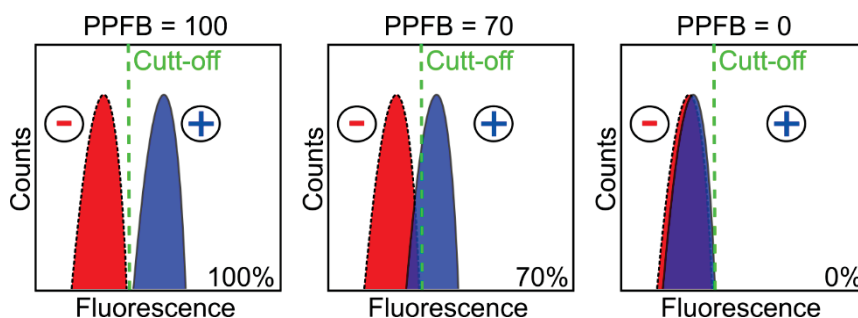


**Figure S2:** Representative image of the determination of Percentage of Positive Fluorescent Beads (PPFB).

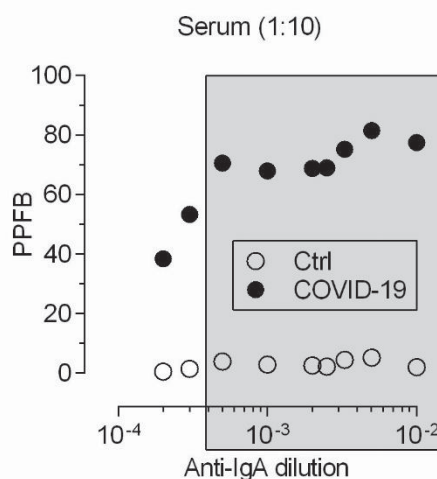


**Figure S3:** Determination of Percentage of Positive Fluorescent Beads (PPFB) by flow cytometry using CBA-N beads. Anti-IgA dilution using serum 10-fold diluted.

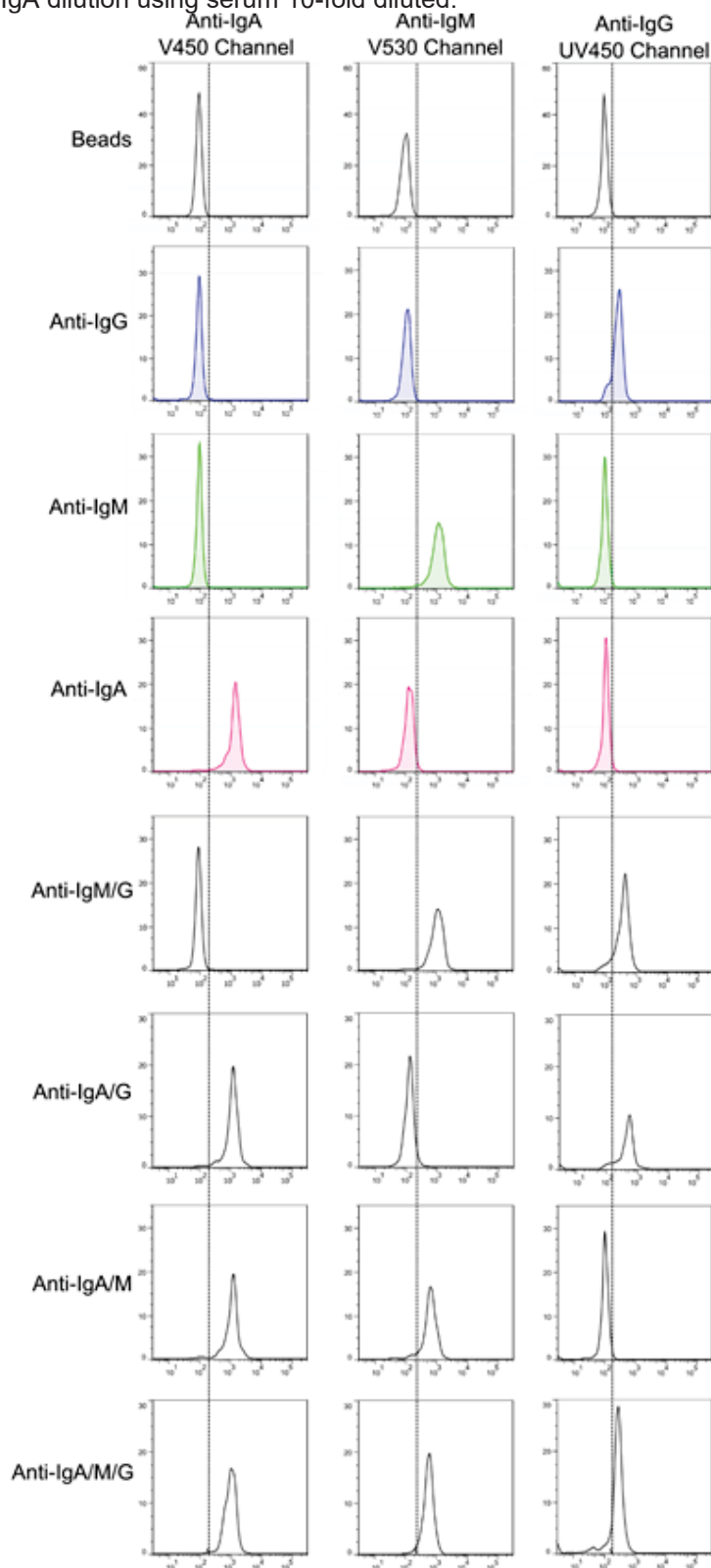


**Figure S4:** Representative histograms of single, double and triple staining for positive COVID-19 samples.



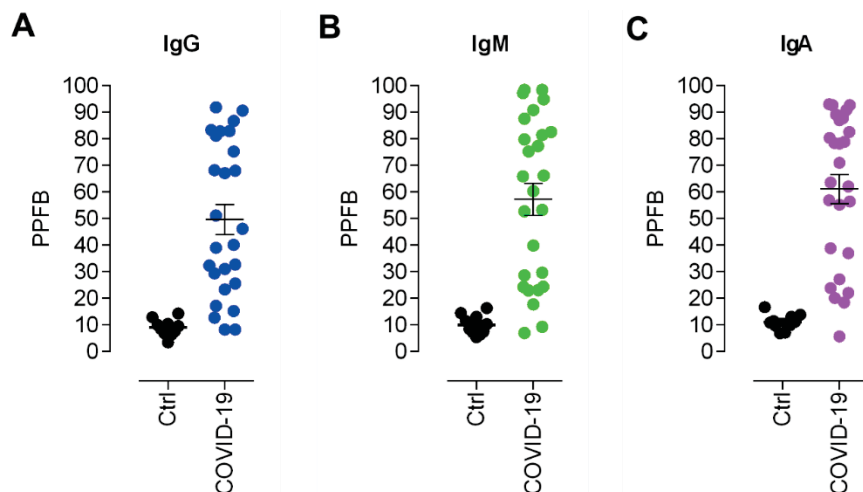


**Figure S5:** Simultaneous identification of IgG, IgM and IgA using the multiplex approach. Control (Ctrl, negative COVID-19;  $n=10$ ) and COVID-19 positive ( $n=26$ ) samples were analyzed. Determination of Percentage of Positive Fluorescent Beads (PPFB) by flow cytometry using CBA-N beads. (A) IgG. (B) IgM. (C) IgA.

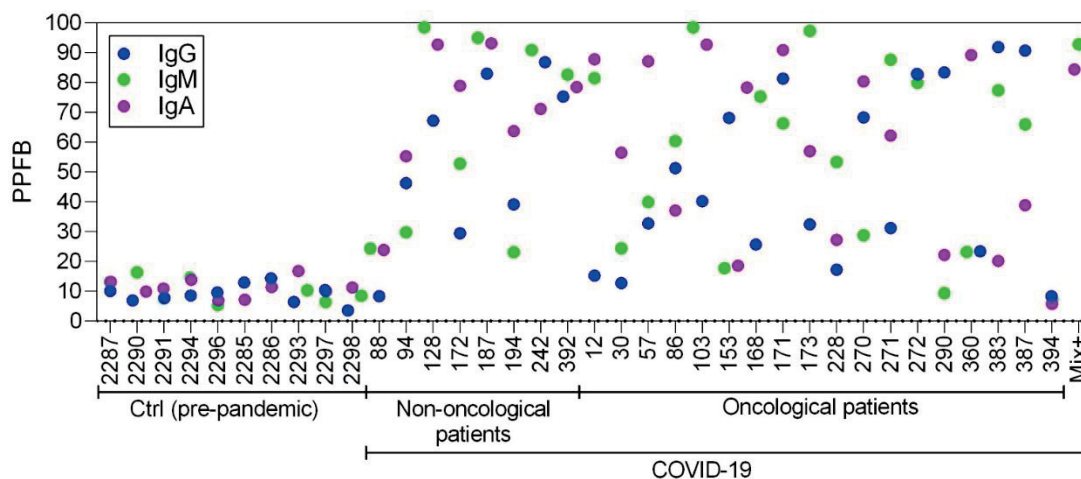


**Figure S6:** Antibodies profile of each sample. Determination of Percentage of Positive Fluorescent Beads (PPFB) using the multiplex approach based on flow cytometry.

**Table S1:** ROC curve analysis using MedCalc.

Parameters	IgG	IgM	IgA
AUC (P-value)	0.946 (<0.0001)	0.950 (<0.0001)	0.962 (<0.0001)
Youden index J (95%CI)	0.885 (0.73-0.96)	0.923 (0.77-1.0)	0.962 (0.79-1.0)
Association criterion (95%CI)	>14.3 (>12.9 to >14.3)	>16.3 (>14.5 to >16.3)	>16.7 (>13.8 to >16.7)
Sensitivity, % (95%CI)	88.5 (69.8-97.6)	92.3 (74.9-99.1)	96.2 (80.4-99.9)
Specificity, % (95%CI)	100.0 (69.2-100.0)	100.0 (69.2-100.0)	100.0 (69.2-100.0)
Accuracy, % (95%CI)	91.7 (77.5-98.3)	94.4 (81.3-99.3)	97.2 (85.5-99.9)
Positive Predictive value, % (95%CI)	100.0	100.0	100.0
Negative Predictive value, % (95%CI)	76.9 (53.5-90.6)	83.3 (56.9-94.0)	90.9 (59.4-98.6)